AD_____

Award Number: W81XWH-10-2-0162

TITLE: Spectroscopic Biomarkers for Monitoring Wound Healing and Infection in Combat Wounds

PRINCIPAL INVESTIGATOR: Eric Elster

CONTRACTING ORGANIZATION: The Geneva Foundation
Tacoma, WA 98402

REPORT DATE: October 2011

TYPE OF REPORT: Annual

PREPARED FOR: U.S. Army Medical Research and Materiel Command
Fort Detrick, Maryland 21702-5012

DISTRIBUTION STATEMENT: Approved for Public Release;
Distribution Unlimited

REPORT DOCUMENTATION PAGE

Form Approved
OMB No. 0704-0188

1. REPORT DATE	2. REPORT TYPE	3. DATES COVERED
October 2011	Annual	30 September 2010 – 29 September 2011

4. TITLE AND SUBTITLE

Spectroscopic Biomarkers for Monitoring Wound Healing and Infection in Combat Wounds

5a. CONTRACT NUMBER

5b. GRANT NUMBER
W81XWH-10-2-0162

5c. PROGRAM ELEMENT NUMBER

6. AUTHOR(S)

Dr. Eric Elster, Dr. Nicole Crane

E-Mail: eric.elster1@med.navy.mil

5d. PROJECT NUMBER

5e. TASK NUMBER

5f. WORK UNIT NUMBER

7. PERFORMING ORGANIZATION NAME(S) AND ADDRESS(ES)

The Geneva Foundation
Tacoma, WA 98402

8. PERFORMING ORGANIZATION REPORT NUMBER

9. SPONSORING / MONITORING AGENCY NAME(S) AND ADDRESS(ES)
U.S. Army Medical Research and Materiel Command
Fort Detrick, Maryland 21702-5012

10. SPONSOR/MONITOR'S ACRONYM(S)

11. SPONSOR/MONITOR'S REPORT NUMBER(S)

12. DISTRIBUTION / AVAILABILITY STATEMENT
Approved for Public Release; Distribution Unlimited

13. SUPPLEMENTARY NOTES

14. ABSTRACT

This proposal focuses on the use of multimodal imaging and spectroscopy of post-traumatic soft tissue and bone to assess wound healing. Combining infrared (IR) imaging, near-infrared spectroscopic (NIRS) imaging, and visible reflectance spectroscopic (VRS) imaging with Raman Spectroscopy (RS) will enable the surgeon to probe the tissue with a two-dimensional, real-time approach. This assessment allows optimal determination of the viability of damaged tissue, the suitability of the tissue environment for healing, the potential for wound infection and ectopic bone formation based on the degree of tissue compromise, and development of potential objective indicators for early limb salvage versus amputation. These imaging systems are currently available and readily applicable for clinical use. Combining these technologies in a multimodal system holds great promise in permitting the surgeon to make a better objective assessment of the viability of tissues in ways that have not previously been possible.

15. SUBJECT TERMS
None provided.

16. SECURITY CLASSIFICATION OF:			17. LIMITATION OF ABSTRACT	18. NUMBER OF PAGES	19a. NAME OF RESPONSIBLE PERSON
a. REPORT	b. ABSTRACT	c. THIS PAGE			USAMRMC
U	U	U	UU	180	19b. TELEPHONE NUMBER *(include area code)*

Table of Contents

INTRODUCTION:

Casualties in Operation Iraqi Freedom (OIF) and Operation Enduring Freedom (OEF) have experienced a high rate of extremity injuries with nearly ubiquitous diffuse tissue damage and compromised local circulation often associated with overt vascular injury. These injuries include traumatic amputations, open fractures, crush injuries, burns, acute vascular disruption, blastwave-associated pressure injuries, air, thrombotic, and fat embolism, and compartment syndrome.

In the treatment of such complex traumatic injuries, improved assessment of global and regional perfusion, extent of infection, location and development of necrotic tissue, as well as location and development of early heterotopic ossification would facilitate the resuscitation and definitive treatment of these patients. Noninvasive spectroscopic methods may fulfill such a role, particularly Raman spectroscopy, infrared imaging, near-infrared spectroscopic imaging, and visible reflectance spectroscopic imaging. These technologies are capable of monitoring tissue temperature[1], perfusion[2] and associated hypoxia[3-6], collagen deposition[7-8], and development of calcified tissue[9-18].

BODY:

Aim 1 is comprised of four tasks:

a) Optimize each imaging system for focal distance, illumination source and power, and acquisition times.

Task 1a was significantly delayed because of the manufacturing of the custom LED array. The original LED array was not delivered in the desired format, as indicated by the prototype drawings. As a result, we than had to wait for an additional piece to be machined. The entire multimodal system is not assembled, but calibration of individual components has begun for all components. We are currently drafting a design for the final assembly of the system. To date, the infrared system and 3-CCD systems have been calibrated. Figure 1 demonstrates the linearity of the 3-CCD response compared to the fluorescence tissue oxygenation probe. The original 3-CCD image (Figure 1A) shows a six well plate with four wells of blood. Increasing amounts of sodium dithionite, a reducing agent, has been added to three of the wells, decreasing the concentration of HbO_2 in those wells. The individual 3-CCD channel responses are displayed (Figures 1B-C), along with the calculated response (Figure 1D). There is clearly a linear relationship between the amount of sodium dithionite added to the wells and the measured pO_2 (as measured by the fluorescence probe), as expected – Figure 1E. Finally, we demonstrate a linear relationship between the calculated response of the 3-CCD camera and the fluorescence probe measurements (Figure 1F). The visible reflectance imaging system is currently undergoing calibration along with the fluorescence oxygenation probes.

b) Collect images and Raman spectra of unaffected tissue of patients at various anatomical sites.

For Task 1b, an amendment was submitted and approved by the IRB for collection of “control” Raman spectra. We have begun enrolling patients (two to date) and anticipate completing this task in one month or less.

c) Characterize specific tissue features of normal tissue.

Once Task 1b is competed and we have collected control muscle for an additional 20 patients, Task 1c will be completed.

d) Correlate spectral parameters of normal tissue and their response with physician observations.

Once Task 1b is competed and we have collected control muscle for an additional 20 patients, Task 1c will be completed. Upon completion, we will initiate Task 1d.

Aim 2 is comprised of five tasks:

a) Correlate the presence of necrotic tissue with spectroscopic markers.

b) Correlate spectroscopic markers with wound infection.

c) Correlate spectroscopic markers with the development of heterotopic ossification.

Since submission of the proposal, we have received tissue biopsies from wounds for an additional 24 patients and Raman spectra have been collected for these patients. We have also enrolled 33 patients into the 3-CCD study, collecting 3-CCD images of wounds for all of these patients. Preliminary results for the 3-CCD study are outlined in the attached poster (A) presented recently at the Federation of Analytical Chemist and Spectroscopy Societites (FACSS) – see the Reportable Outcomes section for “Monitoring Limb Ischemia Using Non-invasive Imaging and Spectroscopic Techniques”. Briefly, the majority of the patients enrolled in the 3-CCD study to date have been normal healers, so correlation of outcome to 3-CCD data has not yet been possible. We have, however, determined the optimum conditions for obtained quality 3-CCD images and this practice has been implemented by the clinical team. White balancing the camera prior to image acquisition is critical for correcting for various illumination conditions. This step was critical for obtaining usable data consistently.

We have also collected Raman spectra of bacterial isolates for four species of bacteria found in combat wounds (MRSA, Klebsiella, Pseudomonas, and Acinetobacter). For Acinetobacter, we have collected Raman spectra of 30 unique strains. For preliminary results, please see the attached poster (B) presented recently at FACSS – see the Reportable Outcomes section for “Profiling Wound Healing with Effluent: Raman Spectroscopic Indicators of Infection”. Briefly, hierarchical clustering with very little pre-processing is able

to classify individual Acinetobacter baumannii strains into groups of relatedness (Figure 2). For instance, strains 13, 15, 23, and 26 are spectrally similar (purple spectrum) and exhibit a unique band at 978 cm^{-1} (Figure 3); these particular strains are also genetically similar and demonstrate increased virulence. We are currently working with Dr. Daniel Zurawski in the Department of Infectious Diseases at the Walter Reed Army Institute of Research to optimize Raman spectroscopic results for accurate genetic and phenotypic classification. This model will be used to classify the Raman spectra of bacteria collected from wound effluent or tissue. We have noticed a large fluorescence background that dominates some of the bacterial Raman spectra; this can make extraction of a quality Raman spectrum difficult. We are currently investigating rinsing techniques to diminish the fluorescence signal as well as the use of Raman signal enhancing substrates.

Our examination of heterotopic ossification (HO) tissue and non-HO tissue has revealed differences between normal tissue and tissue that goes on to develop HO. Briefly, preliminary results illuminate distinct differences between control muscle and muscle that eventually develops HO (Figure 4). These spectral differences can be directly attributed to protein and mineral content. Tissue that goes on to develop HO exhibits bands that are more similar to type I collagen, the matrix framework for bone; this is evidenced by a decreased 1240/1270 cm^{-1} band area ratio (BAR) and a decreased 1340/1270 cm^{-1} BAR. Additionally, examination of the mineral bands of HO tissue indicates that HO that develops quickly after injury has lower carbonate content (1070:960 cm^{-1} band area ratio) and an increased 948 cm^{-1} shoulder (945:960 cm^{-1} band area ratio), indicating a less mature HO that may not be fully mineralized (Figure 6).

d) Correlate spectral parameters and their response with physician and pathologist observations.

We have not completed enrolling patients for Task 2 and do not anticipate doing so until the following fiscal year. Upon completion of Tasks 2a-c, Task 2d will be initiated.

KEY RESEARCH ACCOMPLISHMENTS:

- The infrared system and 3-CCD systems have been calibrated.
- An amended protocol was submitted and approved by the IRB for collection of “control” Raman spectra. We have begun enrolling patients (two to date) and anticipate completing this task in one month or less.
- We have received tissue biopsies from wounds for an additional 24 patients and Raman spectra have been collected for these patients.
- We have also enrolled 33 patients into the 3-CCD study, collecting 3-CCD images

of wounds for all of these patients.

- We have also collected Raman spectra of bacterial isolates for four species of bacteria found in combat wounds (MRSA, Klebsiella, Pseudomonas, and Acinetobacter). For Acinetobacter, we have collected Raman spectra of 30 unique strains.

- We have used hierarchical clustering to classify individual Acinetobacter baumannii strains into groups of relatedness. We are currently working with Dr. Daniel Zurawski in the Department of Infectious Diseases at the Walter Reed Army Institute of Research to optimize Raman spectroscopic results for accurate genetic and phenotypic classification.

- Our examination of heterotopic ossification (HO) tissue and non-HO tissue has revealed differences between normal tissue and tissue that goes on to develop HO. These spectral differences can be directly attributed to protein and mineral content.

REPORTABLE OUTCOMES:

Poster presentations:

- Rajiv Luthra, Nicole Crane, Eric Elster. “Monitoring Limb Ischemia Using Non-invasive Imaging and Spectroscopic Techniques”. FACSS. Reno, NV: October 2-7th, 2011.
- Nicole Crane, Rajiv Luthra, Eric Elster. “Profiling Wound Healing with Effluent: Raman Spectroscopic Indicators of Infection”. FACSS. Reno, NV: October 2-7th, 2011.

Oral Presentations:

- Nicole Crane, Eric Elster. Developing a New Toolbox for Analysis of Warrior Wound Biopsies: Vibrational Spectroscopy. Photonics West BiOS. San Francisco, CA: January 22nd - 27th, 2011.
- Nicole Crane. Developing a New Toolbox for Analysis of Warrior Wounds. Biomedical Sciences and Engineering Conference. Knoxville, TN: March 17th, 2011.
- Nicole Crane. Raman Spectroscopic Studies of Heterotopic Ossification in Combat-Wounded Soldiers. Metropolitan Biophotonics Symposium. College Park, MD: April 16th, 2011.
- Nicole Crane. Vibrational Spectroscopy: A New Tool for the Analysis of Warfighter Wounds. Invited talk at Uniformed Services University of Health Sciences. Bethesda, MD: May 19th, 2011.

Manuscripts:

- B. K. Potter, J. A. Forsberg, T. A. Davis, K. N. Evans, J. S. Hawksworth, D. Tadaki, T. S. Brown, N. J. Crane, T. C. Burns, F. P. O’Brien, E. A. Elster. *Heterotopic Ossification Following Combat-Related Trauma*. J. Bone Joint Surg., 92, 74-89, 2010.
- Nicole J. Crane, Frederick P. O’Brien, Jonathan A. Forsberg, Benjamin K. Potter, Eric A. Elster. Developing a toolbox for analysis of warrior wound biopsies:

vibrational spectroscopy. *Proceedings of SPIE*, 7895-24 (2011).

- S. Phinney, N. J. Crane, F. A. Gage, A. M. Gorbach, E. A. Elster (2011). Use of Optical Imaging and Spectroscopy in Assessment of Organ Perfusion. In K. Uygun and C. Lee (eds.), *Organ Preservation and Reengineering* (pp. 137-159). Norwood, MA: Artech House.

CONCLUSION:

In this effort we have made progress in all task areas and disseminated our findings through both national presentations and publications. With regards to three of the key outcomes in wounded warriors (the development of HO, wound failure and wound infection) our efforts have begun to demonstrate success. The ability to detect soft tissue mineralization prior to phenotypic HO development has the potential to direct both surgical and pharmacologic therapy.

With regards to wound healing, we have enrolled more than 50 patients (each with multiple wounds and time points) for both Raman and 3CCD analysis and have begun obtaining control specimens from non-injured patients. As these data are analyzed along with patient outcomes we will move closer to an “optical biomarker” which can guide debridement and predict outcomes.

Finally, as both HO and wound failure are related to the presence of bioburden our efforts in determining the spectra of common flora in combat patients will not only augment our understanding of the interplay between host and response to injury but help select appropriate anti-microbial approaches. In summary, this multi-faceted approach has laid the foundation for continued advances over the ensuing years.

REFERENCES:

1. Katz, L., et al., *Infrared imaging for detection of compartment syndrome.* Academic Emergency Medicine, 2007. **14**(5): p. S41.
2. Gorbach, A., et al., *Objective, real-time, intraoperative assessment of renal perfusion using infrared imaging.* American Journal of Transplantation, 2003. **3**: p. 988-993.
3. Zuzak, K.J., et al., *Imaging hemoglobin oxygen saturation in sickle cell disease patients using noninvasive visible reflectance hyperspectral techniques: effects of nitric oxide.* American Journal of Physiology: Heart and Circulation Physiology, 2003. **285**: p. H1183-H1189.
4. Zuzak, K.J., et al., *Noninvasive determination of spatially resolved and time-resolved tissue perfusion in humans during nitric oxide inhibition and inhalation by use of a visible-reflectance hyperspectral imaging technique.* Circulation, 2001. **104**: p. 2905-2910.
5. Zuzak, K.J., et al., *Visible reflectance hyperspectral imaging: characterization of a noninvasive, in vivo system for determining tissue perfusion.* Analytical Chemistry, 2002. **74**: p. 2021-2028.
6. Khaodhiar, L., et al., *The use of medical hyperspectral technology to evaluate microcirulatory changes in diabetic foot ulcers and to predict clinical outcomes.* Diabetes Care, 2007. **30**: p. 903-910.

7. Chan, K.L., et al., *A Coordinated Approach to Cutaneous Wound Healing: Vibrational Microscopy and Molecular Biology.* J Cell Mol Med, 2008.
8. Frushour, B.G. and J.L. Koenig, *Raman scattering of collagen, gelatin, and elastin.* Biopolymers, 1975. **14**: p. 379-391.
9. Carden, A. and M.D. Morris, *Application of vibrational spectroscopy to the study of mineralized tissues.* J. Biomed. Optics, 2000. **5**(3): p. 259-268.
10. Kontoyannis, C.G. and N.V. Vagenas, *FT-Raman spectroscopy: a tool for monitoring the demineralization of bone.* Applied Spectroscopy, 2000. **54**(11): p. 1605-1609.
11. Wang, Y.-N., C. Galiotis, and D.L. Bader, *Determination of Molecular Changes in Soft Tissues Under Strain Using Laser Raman Microscopy.* Journal of Biomechanics, 2000. **33**: p. 483 - 486.
12. Carden, A., et al., *Raman imaging of bone mineral and matrix: composition and function.* Proc. SPIE, 1999. **3608**: p. 132-138.
13. Crane, N.J., et al., *Raman spectroscopic evidence for octacalcium phosphate and other transient mineral species deposited during intramembraneous mineralization.* Bone, 2006. **39**: p. 434-442.
14. Morris, M.D., et al., *Raman spectroscopy of early mineralization of normal and pathological calvaria.* Proc. SPIE, 2002. **4614**: p. 28-39.
15. Morris, M.D., et al., *Raman microscopy of de novo woven bone tissue.* Proc. SPIE, 2001. **4254**.
16. Tarnowski, C.P., M.A. Ignelzi, and M.D. Morris, *Mineralization of developing mouse calvaria as revealed by Raman microspectroscopy.* Journal of Bone and Mineral Research, 2003. **17**(6): p. 1118-1126.
17. Timlin, J., et al., *Raman Spectroscopic Imaging Markers for Fatigue-Related Microdamage in Bovine Bone.* Analytical Chemistry, 2000. **72**(10): p. 2229 - 2236.
18. Timlin, J.A., A. Carden, and M.D. Morris, *Chemical microstructure of cortical bone probed by Raman transects.* Applied Spectroscopy, 1999. **53**(11): p. 1429-1435.

APPENDICES:

Please see attached manuscript and poster pdf files.

SUPPORTING DATA:

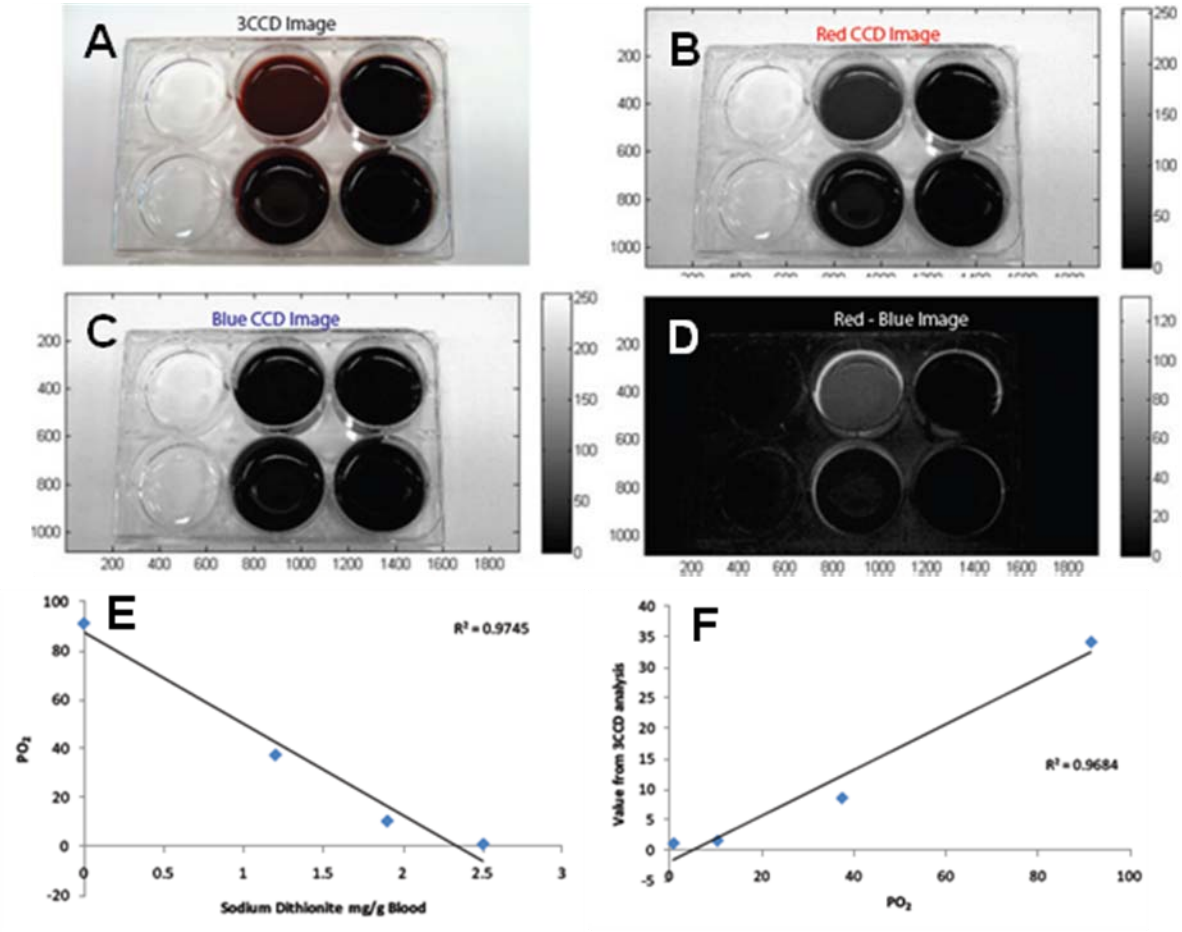

Figure 1. Displayed are the original 3-CCD image (A) and its red (B) and blue (C) channel responses, in addition to the calculated image of the red channel response minus the blue channel response (D) for wells filled with blood. There is a linear trend for pO_2 fluorescence measurements and the concentration of sodium dithionite added to the wells of blood, a surrogate for HbO_2 concentration (E). A linear relationship is also demonstrated for the calculated 3-CCD values for each well and the pO_2 fluorescence measurements (F).

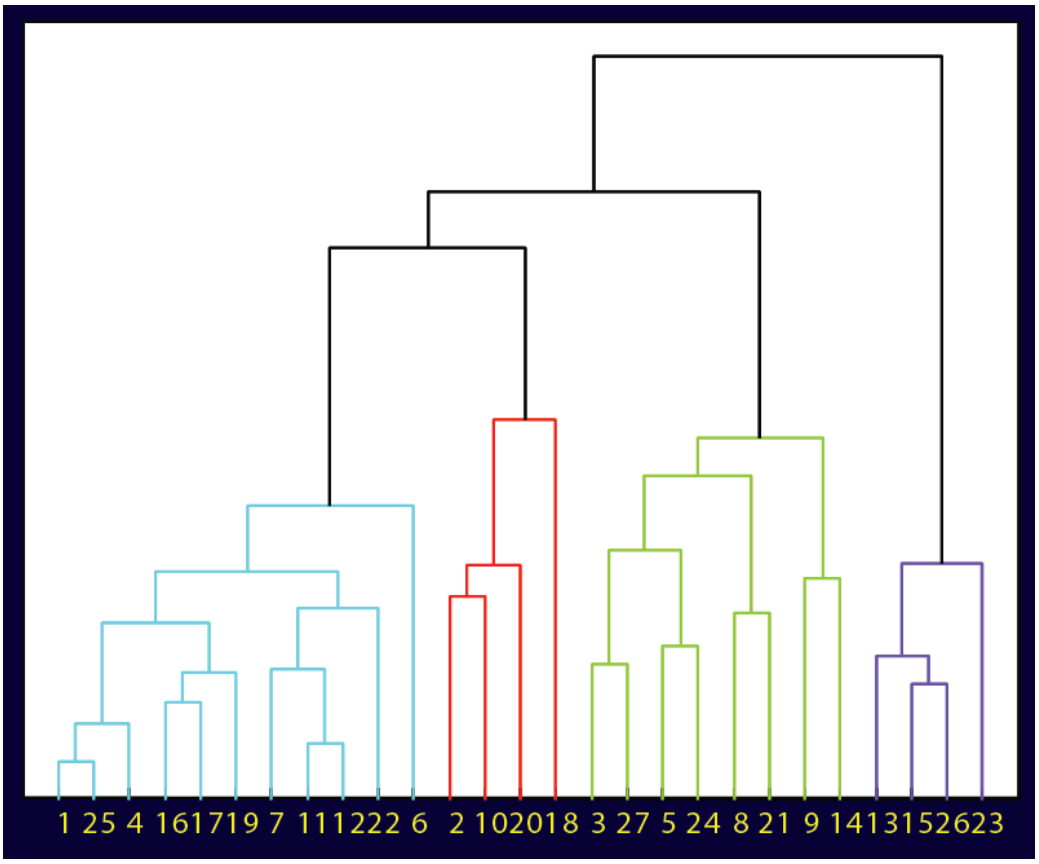

Figure 2. Hierarchical clustering of Acinetobacter baumannii strains based on Raman spectra of bacterial isolates.

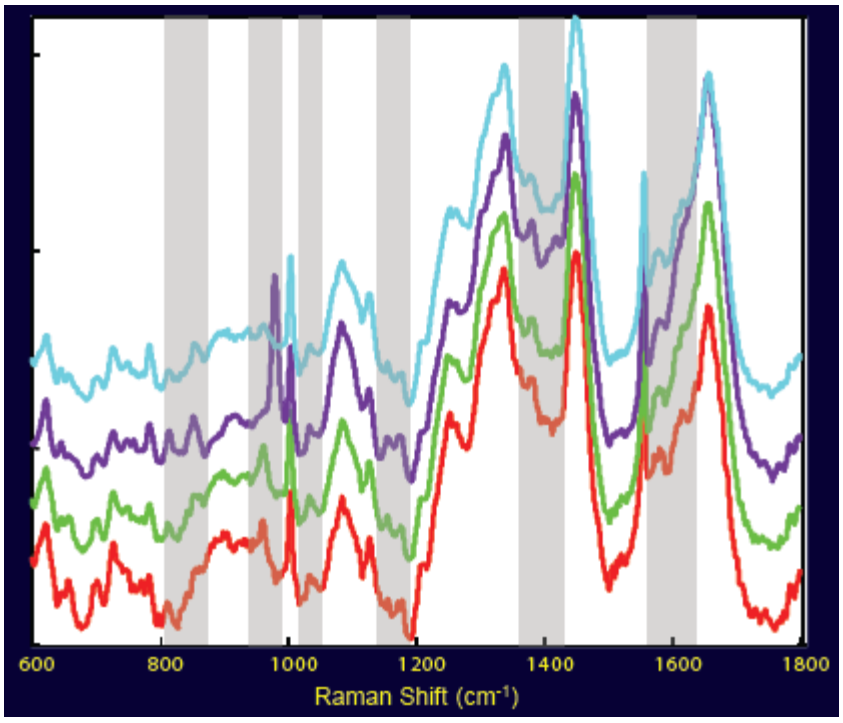

Figure 3. Average spectra of Acinetobacter baumannii classes, as determined by Raman spectroscopy.

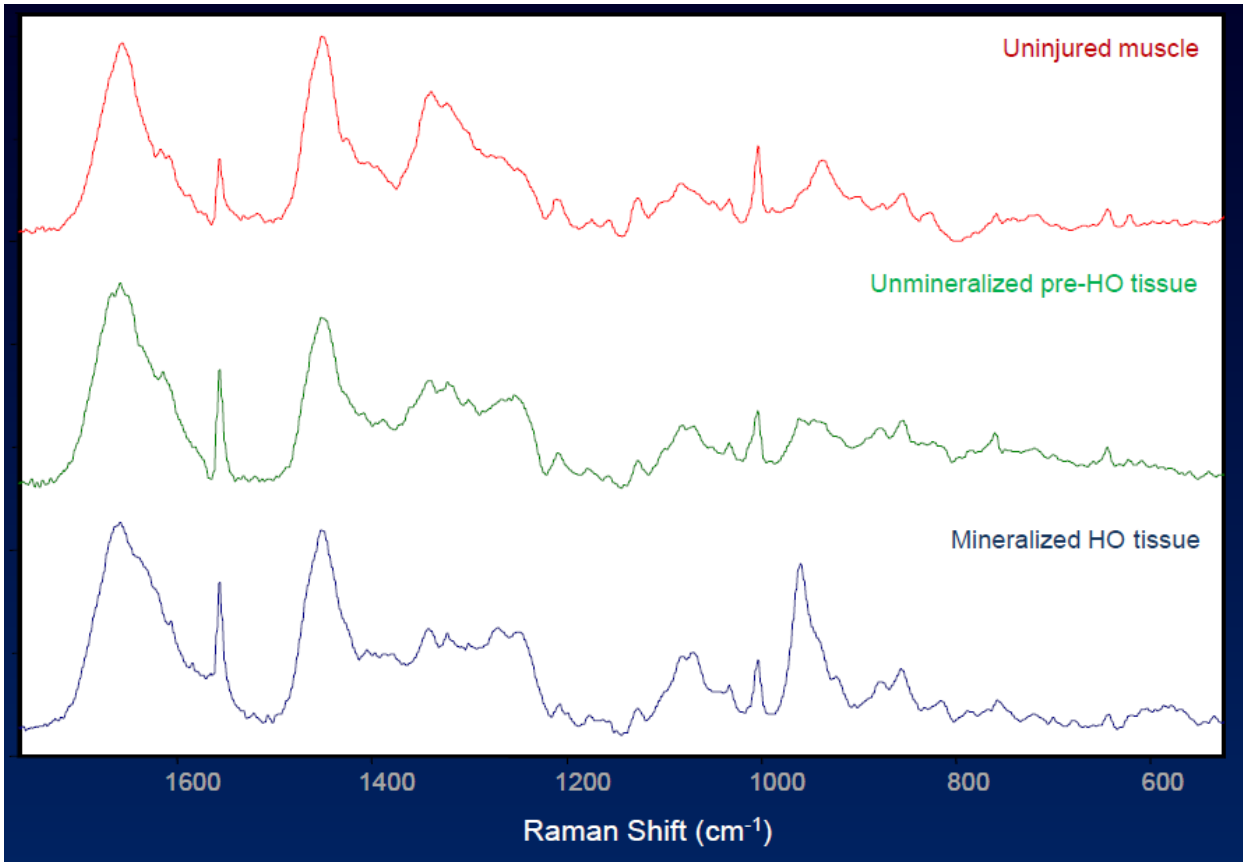

Figure 4. The Raman spectrum of uninjured muscle looks distinctly different pre-HO tissue or HO tissue.

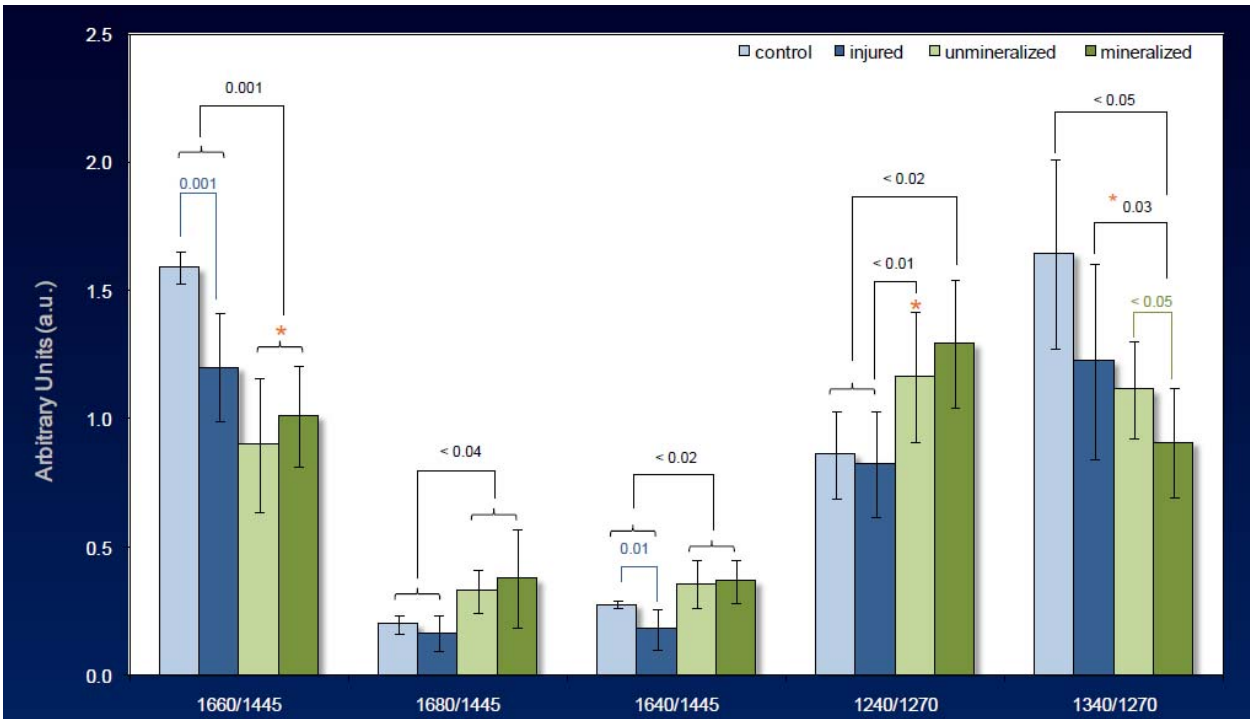

Figure 5. Comparisons of band area ratios for the Amide I and Amide III envelopes (proteins) demonstrate significant differences for HO and non-HO tissue.

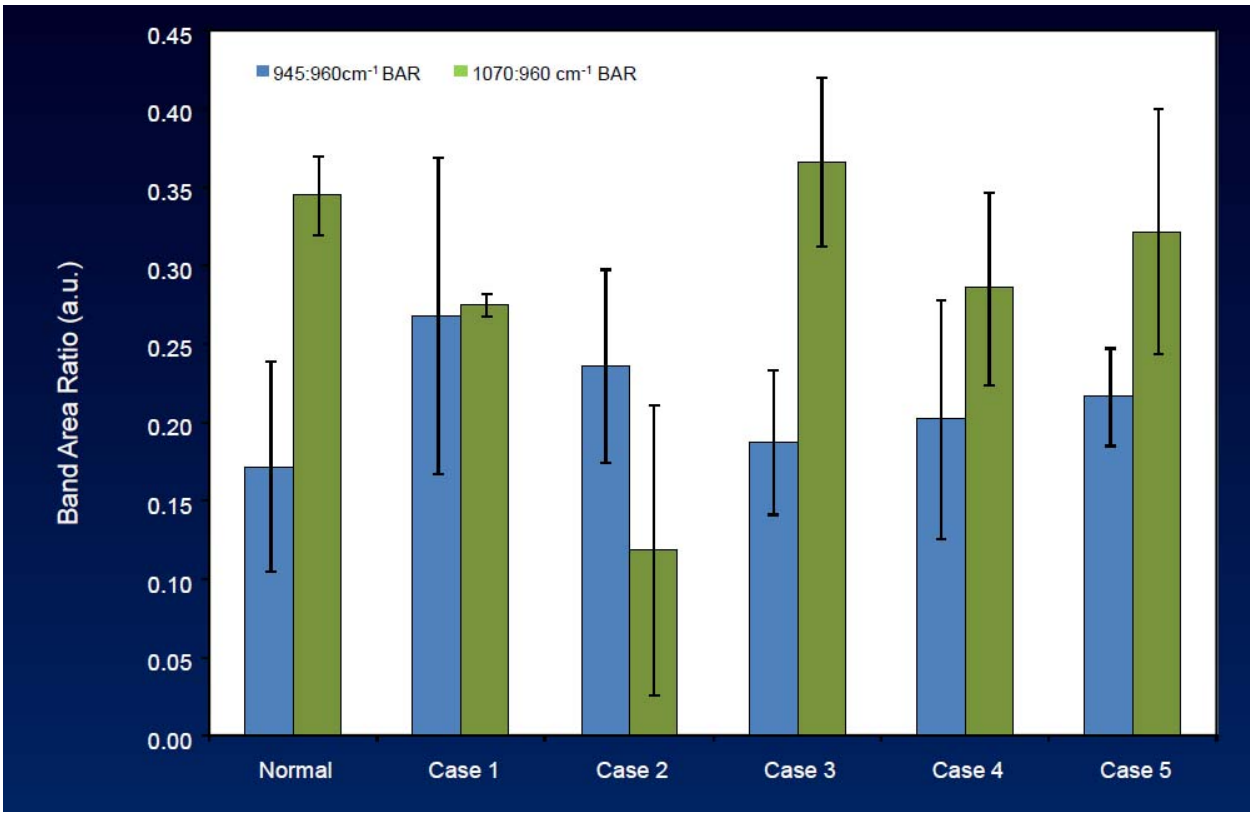

Figure 6. Comparison of the mineral bands for HO tissue also demonstrates differences that correlate with the maturity of the HO tissue.

Raman Spectroscopic Studies of Heterotopic Ossification in Combat-Wounded Soldiers

Nicole J. Crane

Naval Medical Research Center
Silver Spring, MD

Metropolitan Biophotonics Symposium
April 16th, 2011

Acute Combat Wounds

- The management of modern traumatic war wounds remains a significant challenge for clinicians.
  - Extensive osseous and soft-tissue damage caused by blasts and high-energy projectiles.
- The ensuing inflammatory response ultimately dictates the pace of wound healing and tissue regeneration.
- The timing of wound closure or definitive coverage is subjectively based.
- Despite the use and application of novel wound-specific treatment modalities, some wounds fail to close, or dehisce.
    - wound infection and subsequent biofilm formation
    - heterotopic ossification (the pathological mineralization of soft tissues)

Acute Combat Wounds

An understanding of the molecular environment of acute wounds throughout the debridement process can provide valuable insight into the mechanisms associated with the eventual wound outcome.

Acute Combat Wounds – Current Treatment

Surgical debridements are performed every 2-3 days.

- remove devitalized tissue
- decrease bacterial load

Negative pressure wound therapy (NPWT) is applied between debridements. NPWT promotes wound closure.

Wound assessment involves:

- patient's general condition
- injury location
- adequacy of perfusion
- gross appearance of the wound

Acute Combat Wounds – The Challenge

Monitor wound healing *in vivo*, i.e. monitor wound healing during surgical debridements.

- Is it the best time to close the wound?
- Is the wound developing HO?
- Is the wound infected? With what?

Develop an objective and predictive model for wound healing.

Data Collection

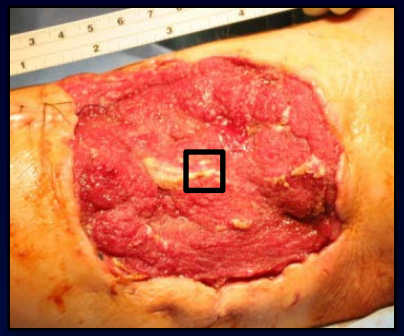

Approximately 1 cm^2 tissue biopsy is excised from the center of the wound bed.

Tissue is fixed in 10% neutral buffered formalin for storage.

Prior to spectral acquisition, samples are rinsed in 0.9% NaCl saline solution.

Examine multiple spots across the tissue.

40 accumulations, 5s spectrum

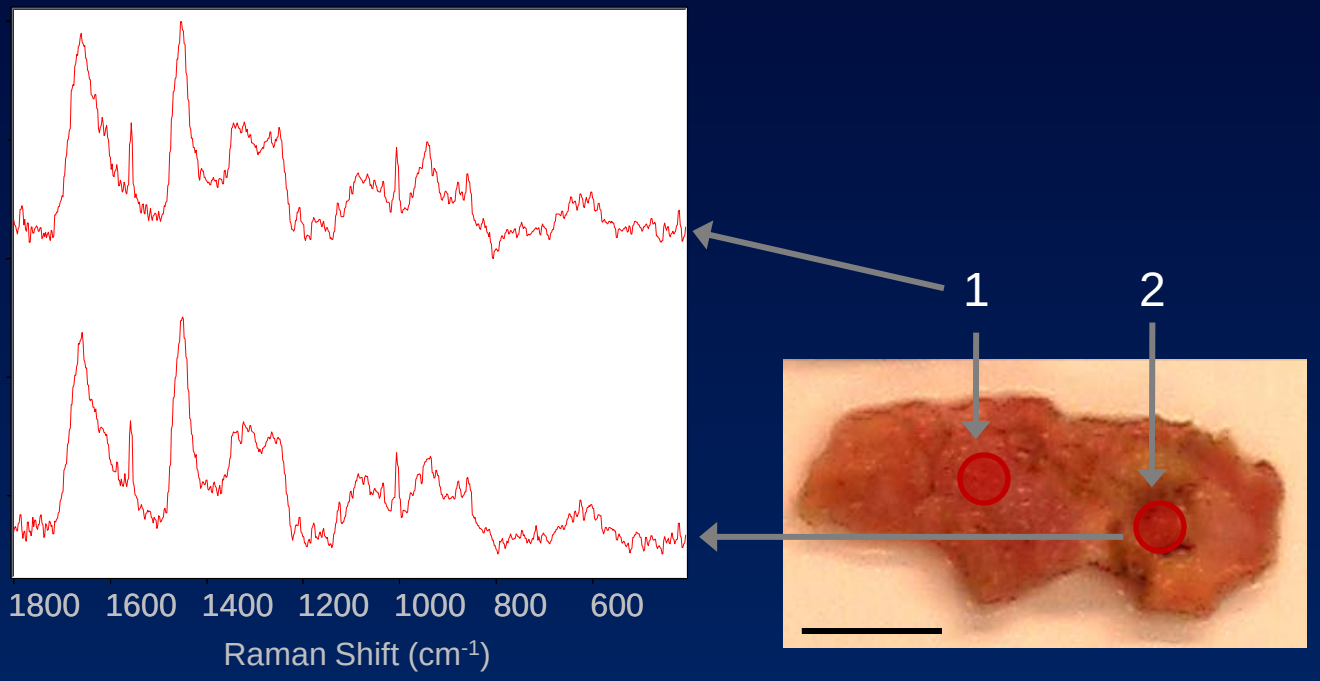

Monitoring a Wound Over Time – Normal vs. Impaired Healing

- Previous study demonstrated the potential of Raman spectroscopic analysis of wound biopsies for classification of wounds as normal or impaired healing from changes in the 1665 cm^{-1}/1445 cm^{-1} band area ratio.

Wound Rep Regen. 18(4): 409-416, 2010.

Ann Surg. 250(6):1002-7, 2009.

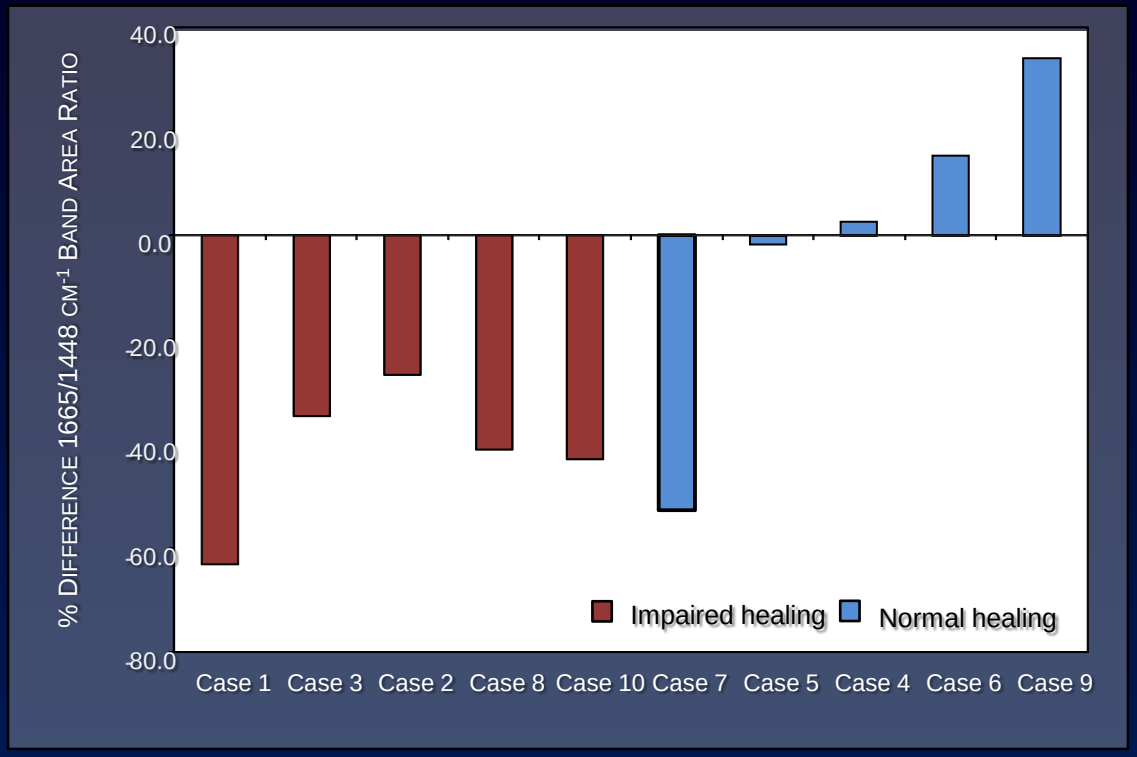

- Impaired healing wounds demonstrate a significant decrease in the 1665/1448 cm^{-1} band area ratio compared to normal healing wounds, as demonstrated by Raman spectroscopic mapping.

Monitoring a Wound Over Time – Normal vs. Impaired Healing

- Results were corroborated by altered collagen/collagenase gene expression profiles of tissue biopsies.
- Gene expression profiles confirm decreased gene expression of collagen types I and III at the first debridement and collagen type III at the final debridement in impaired wounds.

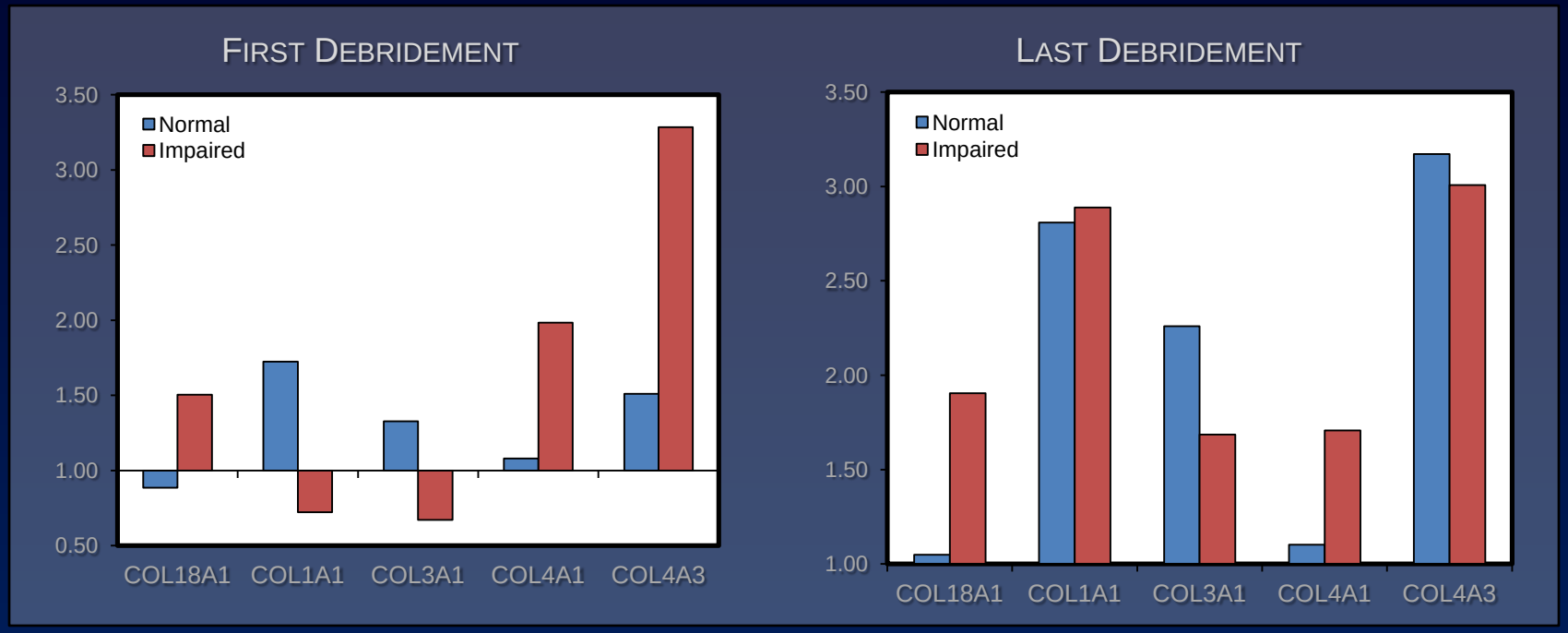

- COL18A1 mRNA expression remains elevated for impaired healing wounds at almost all time points when compared to normal healing wounds. Continued elevation of endostatin would inhibit neovascularization.

The Development of Heterotopic Ossification

Heterotopic Ossification

- Heterotopic ossification (HO) refers to the aberrant formation of mature, lamellar bone in non-osseous tissues.
- Currently, orthopaedic surgeons faced with treating mature, refractory, symptomatic HO are left with few options other than operative excision. *Potter et al. J Bone Joint Surg Am. 2007;89:476-486.*
- Following most civilian trauma, HO formation is relatively rare in the absence of head injury. Even following traumatic brain or spinal cord injury, it develops in only 20% and 11% of patients. Rates of HO formation exceed 50% only in the setting of femoral shaft fractures with concomitant head injury.

Potter et al. J Bone Joint Surg Am. (In press).

ORTHOPEDICS 2008;31(12):1237.

UPOJ 1998;11:59-66.

Heterotopic Ossification

- In a study evaluating whether the mechanism of injury (blast or non-blast) correlated with either the presence or severity of HO, we found clinically detectable HO in 63% of residual limbs. Combat-related injuries, in general, are associated with higher-than-expected prevalence of HO, when compared to civilian data.

- Some patients with HO remain entirely asymptomatic and no specific treatment is indicated. Many patients, however, develop symptoms directly attributable to their HO which persists indefinitely.

- The most common indications for HO excision in our wounded warrior population is pain with prosthesis wear.

USA Today, February 12, 2006.

Potter et al. J Bone Joint Surg Am. (In press).

Bone

- Bone is 35% organic material and 65% inorganic material

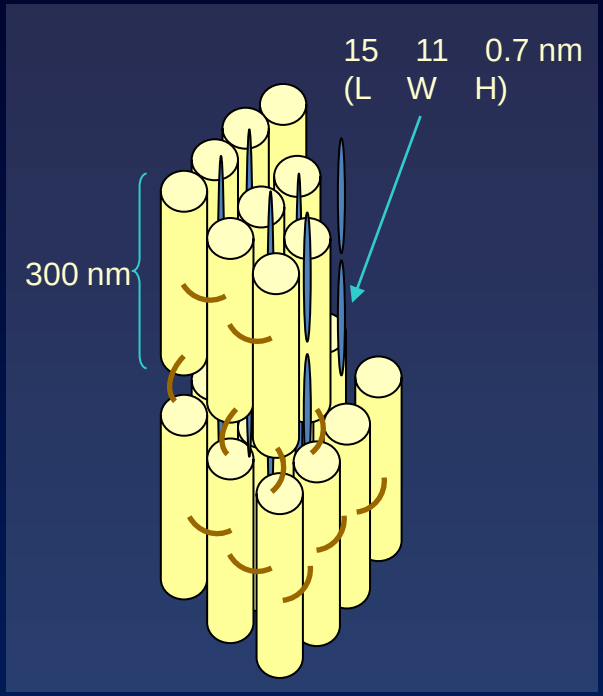

- For organic material
  - 90% of organic material is type I collagen
  - 10% noncollagenous proteins
- For inorganic material
  - commonly assumed to be some form of hydroxyapatite

$$Ca_{10}(PO_4)_2(OH)_6$$

  - more closely resembles a B-type carbonated apatite

$$Ca_{8.3\ \ 1.7}(PO_4)_{4.3}(CO_3)_1(HPO_4)_{0.7}(OH)_{0.3}$$

Raman Spectrum of Bone

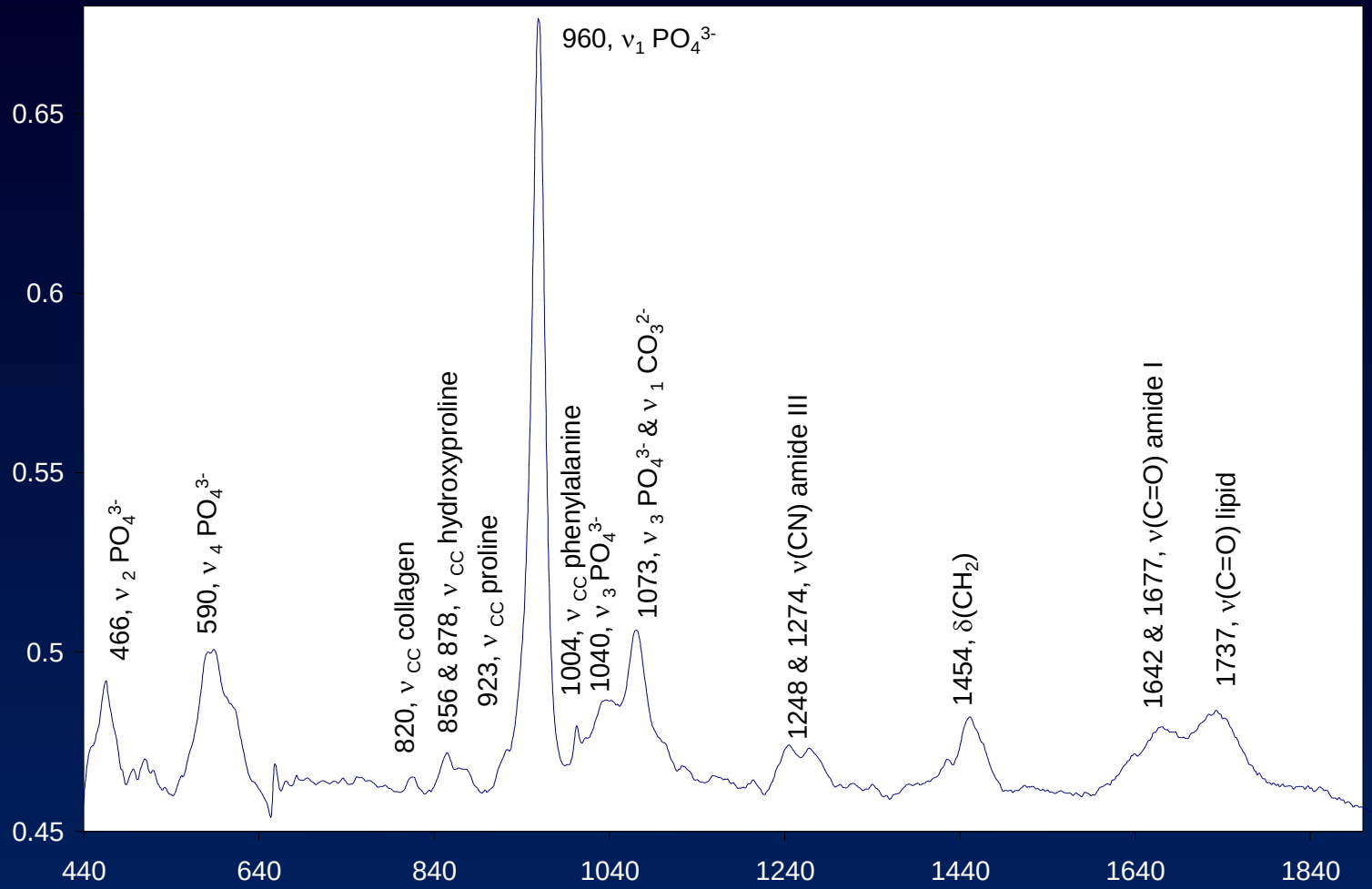

Heterotopic Ossification

- Pre-HO tissue is not necessarily obvious.

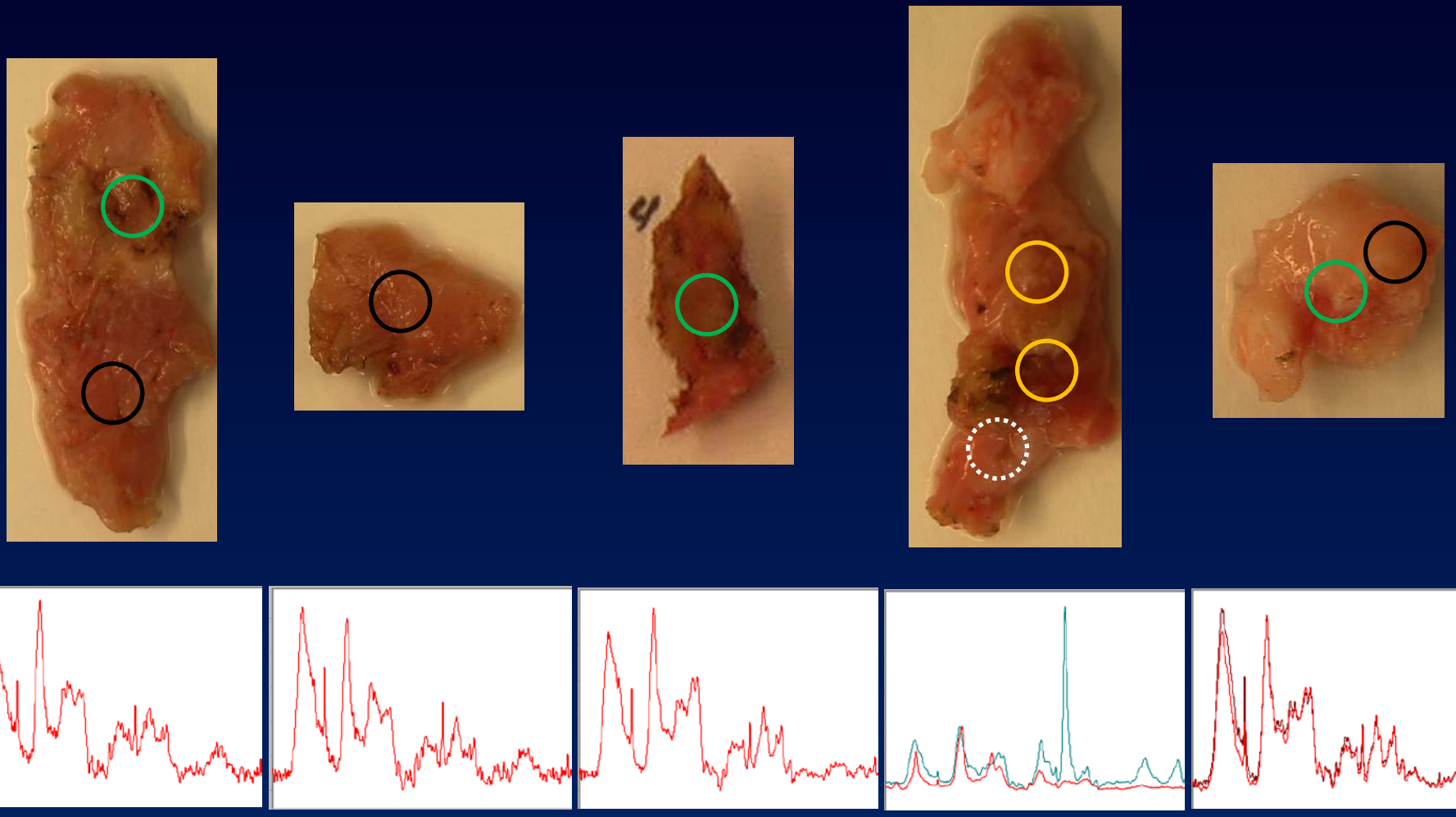

Heterotopic Ossification

- Sometimes HO tissue is incredibly obvious.

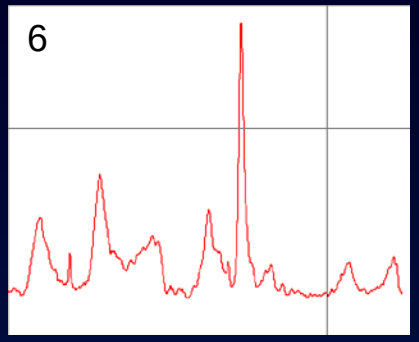

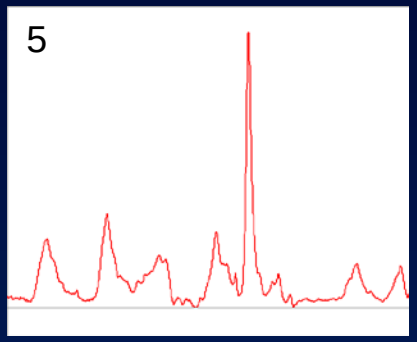

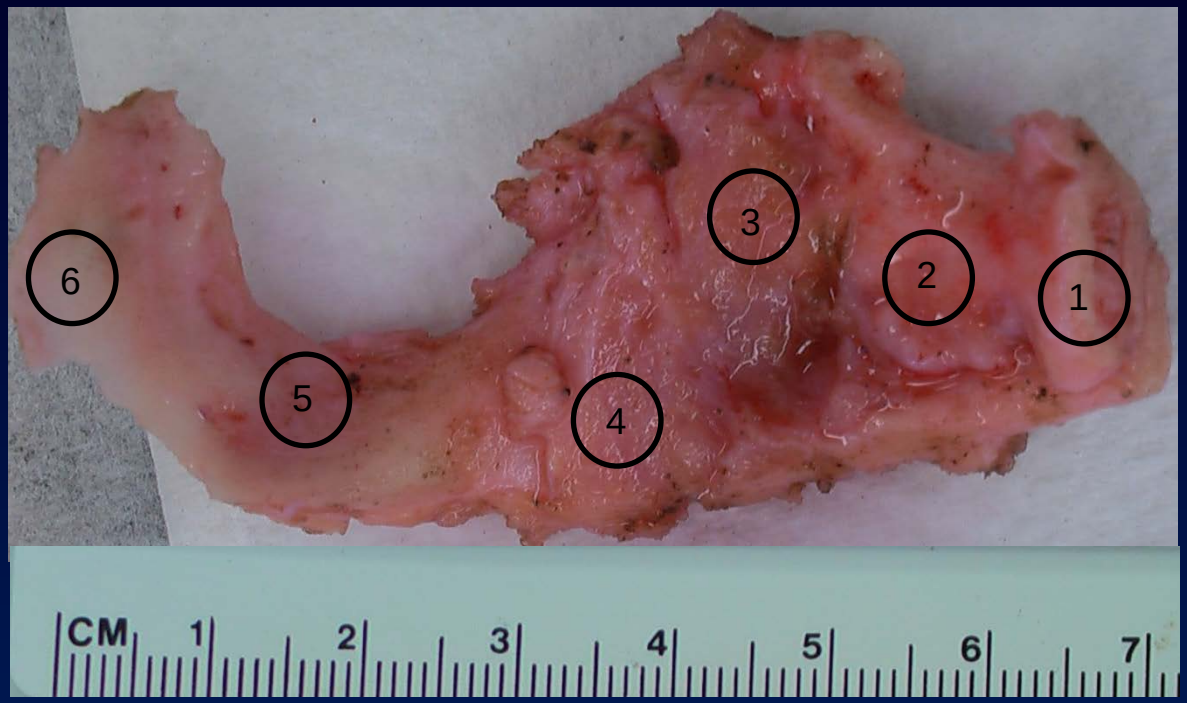

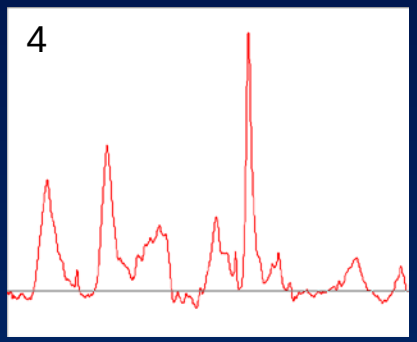

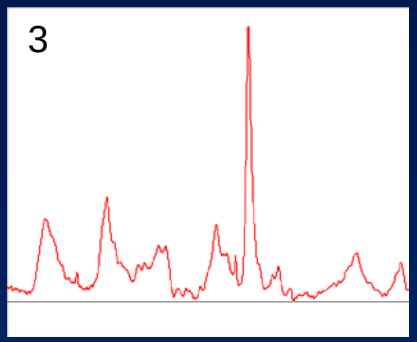

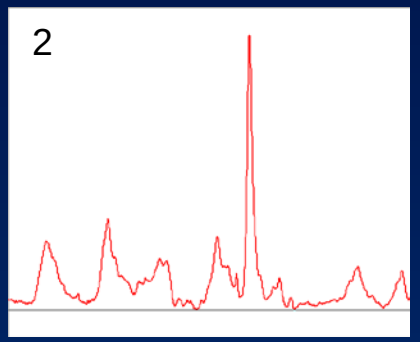

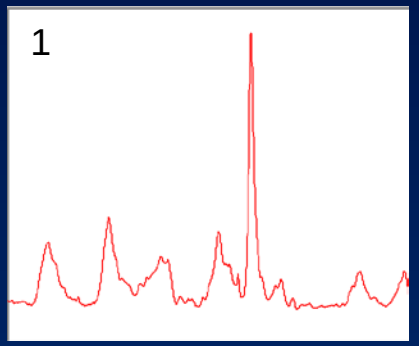

Heterotopic Ossification

Spectral comparison of muscle and collagen.

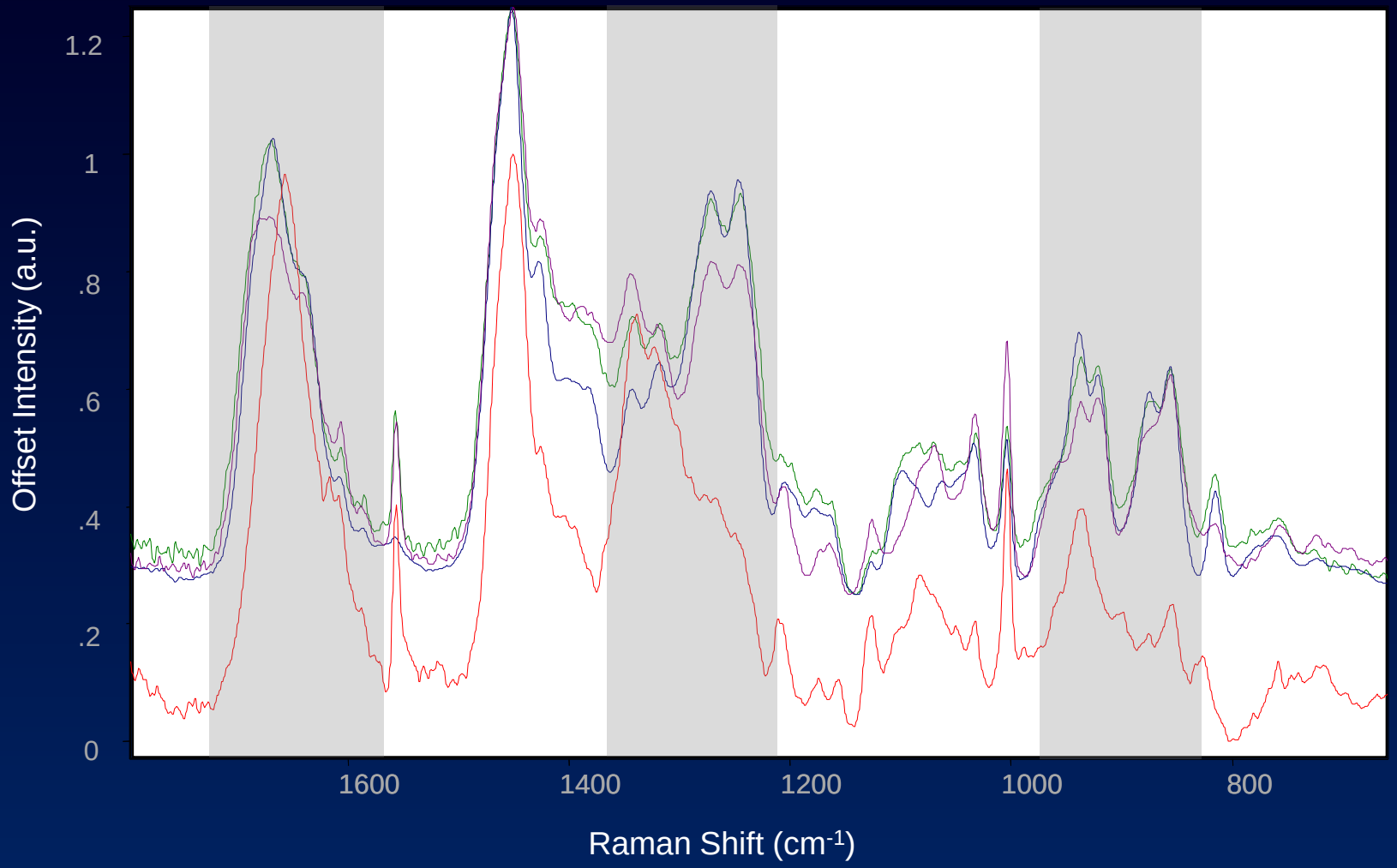

Heterotopic Ossification

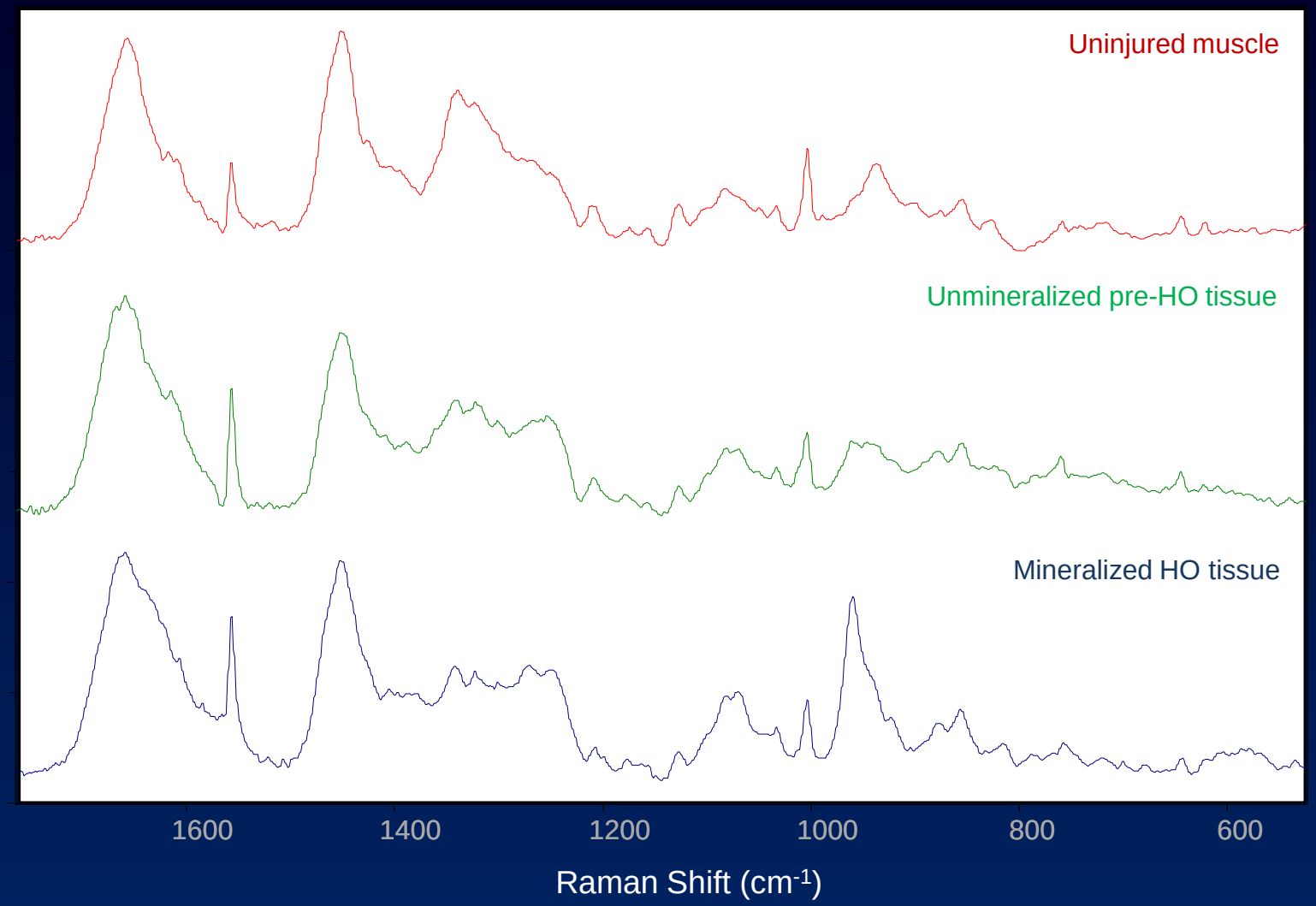

Heterotopic Ossification

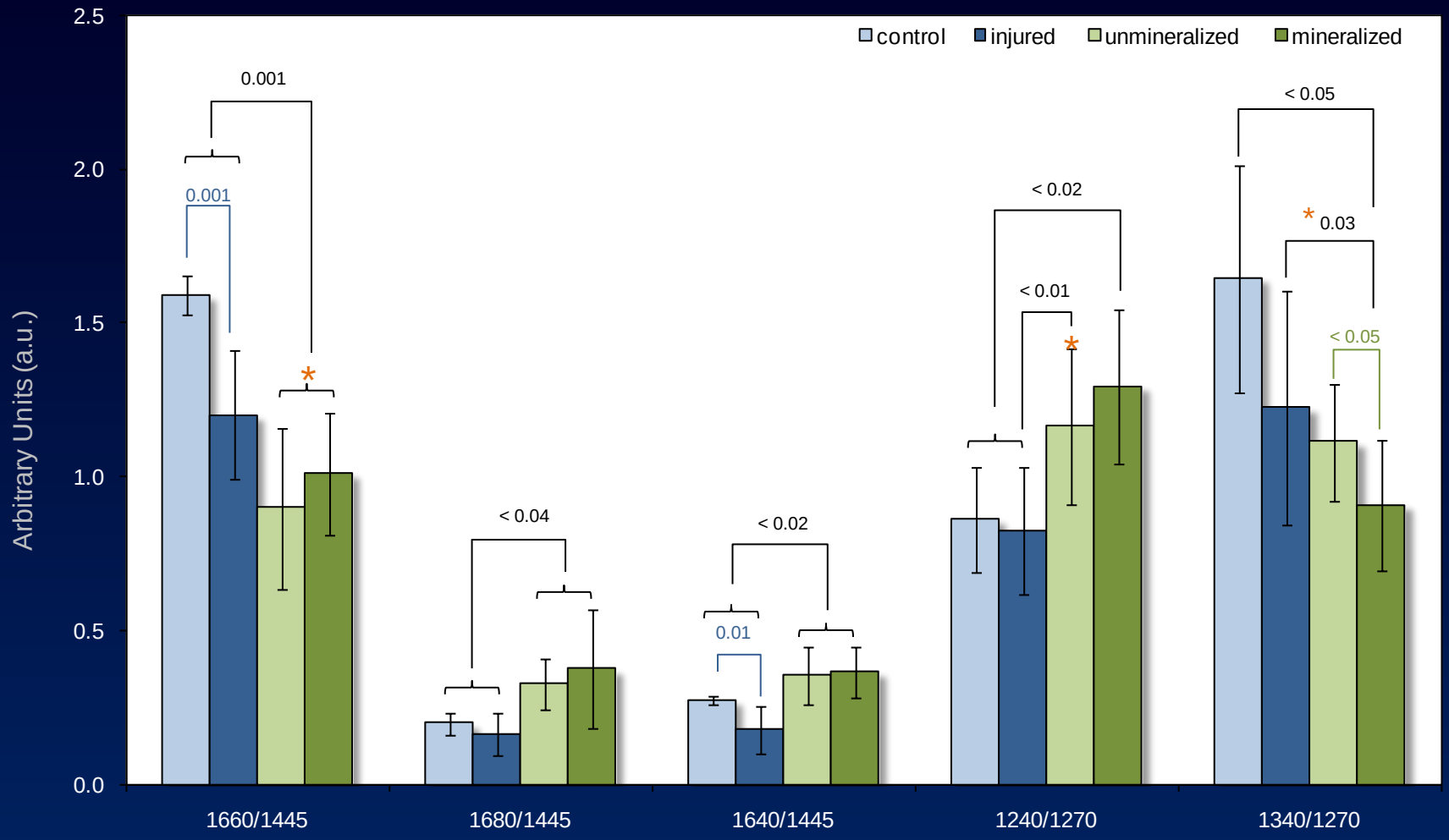

Heterotopic Ossification

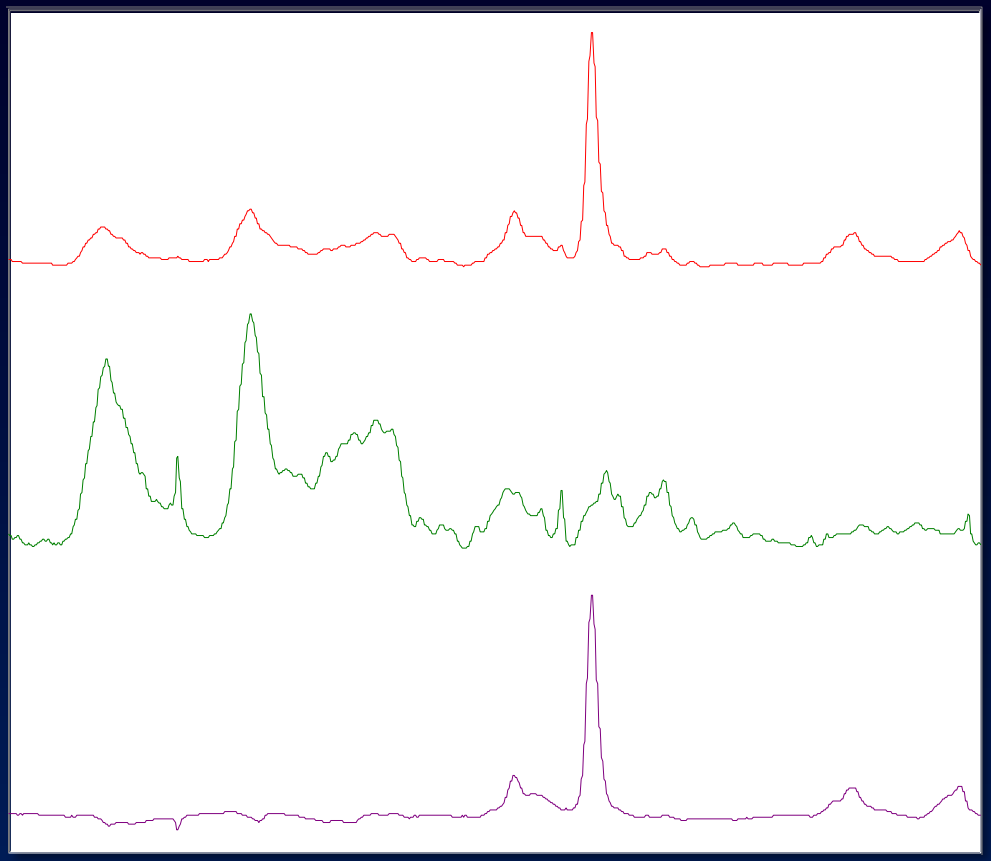

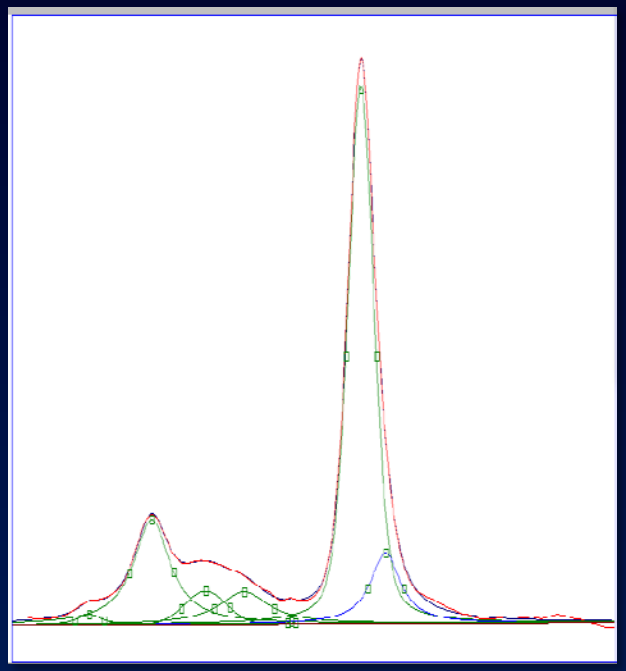

Soft tissue was subtracted from the spectrum to isolate the mineral spectrum.

Normal Bone vs. HO Bone

The adjacent femur is used as a normal bone control.

Heterotopic Ossification

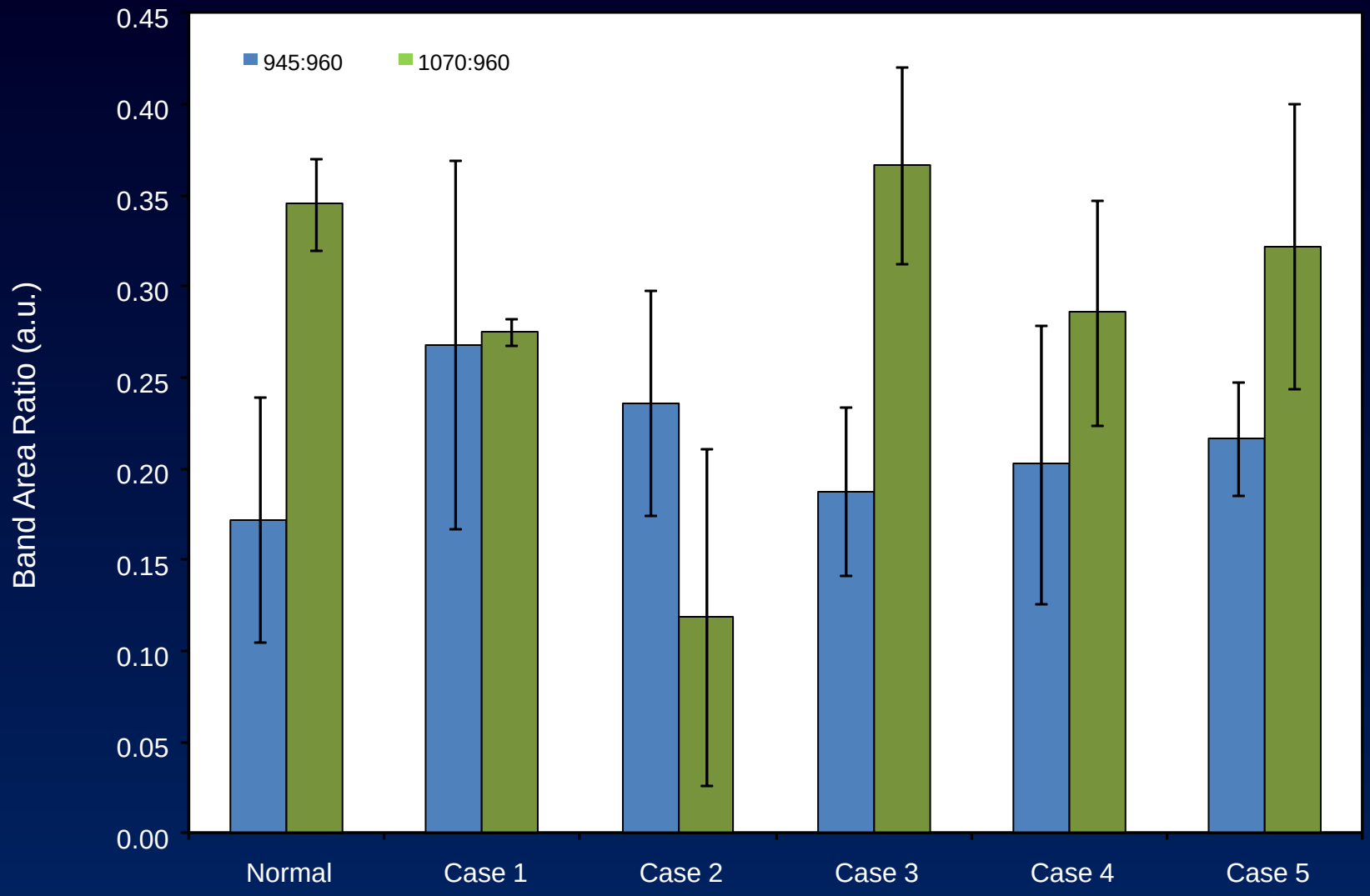

Heterotopic Ossification

- Preliminary results illuminate distinct differences between control muscle and muscle that eventually develops HO.

- HO that develops quickly after injury has lower carbonate content (1070:960 cm^{-1} band area ratio) and an increased 948 cm^{-1} shoulder (945:960 cm^{-1} band area ratio).

- We would like to be able to accurately determine which portions of the tissue are mineralizing – this has significant implications for amputation revisions. Additionally, we may be able to prevent the development of HO by accurately excising pre-HO tissue during the course of the surgical debridements.

- While we only have samples from 5 patients that developed HO, we are continuing to collect samples.

Disclaimer

- The multidisciplinary care of these patients would not have been possible without the dedicated efforts of everyone at WRAMC and NNMC. Both civilian and military personnel have rendered skilled and compassionate care for these casualties. All of our efforts are dedicated to those who have been placed in harm's way for the good of our nation.
- The views expressed in this manuscript are those of the authors and do not reflect the official policy of the Department of the Army, Department of the Navy, the Department of Defense or the United States Government.

- This effort was supported (in part) by the U.S. Navy Bureau of Medicine and Surgery under the Medical Development Program and Office of Naval Research work unit number (604771N.0933.001.A0604).

- This study was approved by the National Naval Medical Center Institutional Review Board in compliance with all Federal regulations governing the protection of human subjects.

Acknowledgements

Naval Medical Research Center

Dr. Eric Elster
Dr. Trevor Brown
Dr. Doug Tadaki
Dr. Tom Davis
Nancy Porterfield
Frederick Gage
Eric Olsen
Wesley Stepp

National Naval Medical Center

Dr. Jonathan Forsberg
Dr. Benjamin Potter

Walter Reed Army Institute of Research

Dr. Daniel Zurowski

Walter Reed Army Medical Center

Dr. Fred O'Brien

Thermo Scientific

Developing a New Toolbox for Analysis of Warrior Wound Biopsies: Vibrational Spectroscopy

Nicole J. Crane[1], Eric A. Elster[1,2,3]

[1]Naval Medical Research Center

[2]National Naval Medical Center

[3]Department of Surgery, Uniformed Services University of the Health Sciences

Photonics West BiOS – San Francisco, CA
January 22nd - 27th, 2011

Acute Combat Wounds

- The management of modern traumatic war wounds remains a significant challenge for clinicians.
  - Extensive osseous and soft-tissue damage caused by blasts and high-energy projectiles.
- The ensuing inflammatory response ultimately dictates the pace of wound healing and tissue regeneration.
- The timing of wound closure or definitive coverage is subjectively based.
- Despite the use and application of novel wound-specific treatment modalities, some wounds fail to close, or dehisce.
  - wound infection and subsequent biofilm formation
  - heterotopic ossification (the pathological mineralization of soft tissues)

Acute Combat Wounds

An understanding of the molecular environment of acute wounds throughout the debridement process can provide valuable insight into the mechanisms associated with the eventual wound outcome.

Acute Combat Wounds – Current Treatment

Surgical debridements are performed every 2-3 days.

- remove devitalized tissue
- decrease bacterial load

Negative pressure wound therapy (NPWT) is applied between debridements. NPWT promotes wound closure.

Wound assessment involves:

- patient's general condition
- injury location
- adequacy of perfusion
- gross appearance of the wound

Acute Combat Wounds – The Challenge

Monitor wound healing *in vivo*, i.e. monitor wound healing during surgical debridements.

- Is it the best time to close the wound?
- Is the wound developing HO?
- Is the wound infected? With what?

Develop an objective and predictive model for wound healing.

Data Collection

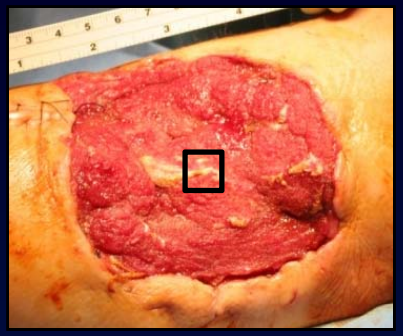

Approximately 1 cm^2 tissue biopsy is excised from the center of the wound bed.

Tissue is fixed in 10% neutral buffered formalin for storage.

Prior to spectral acquisition, samples are rinsed in 0.9% NaCl saline solution.

Examine multiple spots across the tissue.

40 accumulations, 5s spectrum

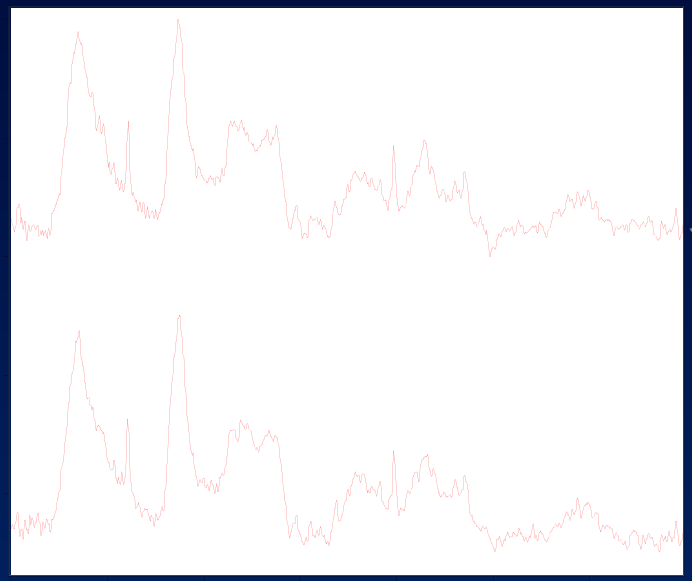

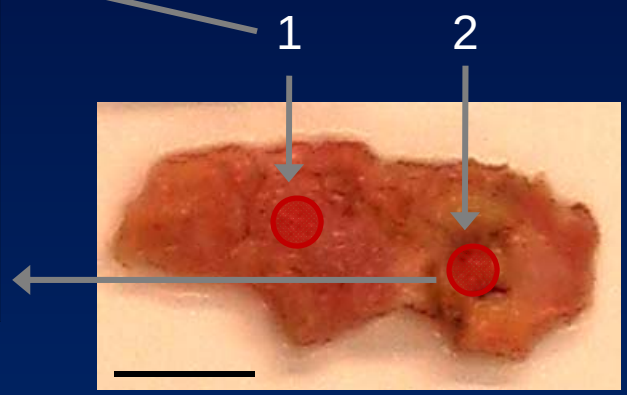

Monitoring a Wound Over Time – Normal vs. Impaired Healing

- Previous study demonstrated the potential of Raman spectroscopic analysis of wound biopsies for classification of wounds as normal or impaired healing from changes in the 1665 cm^{-1}/1445 cm^{-1} band area ratio.

Wound Rep Regen. 18(4): 409-416, 2010.

Ann Surg. 250(6):1002-7, 2009.

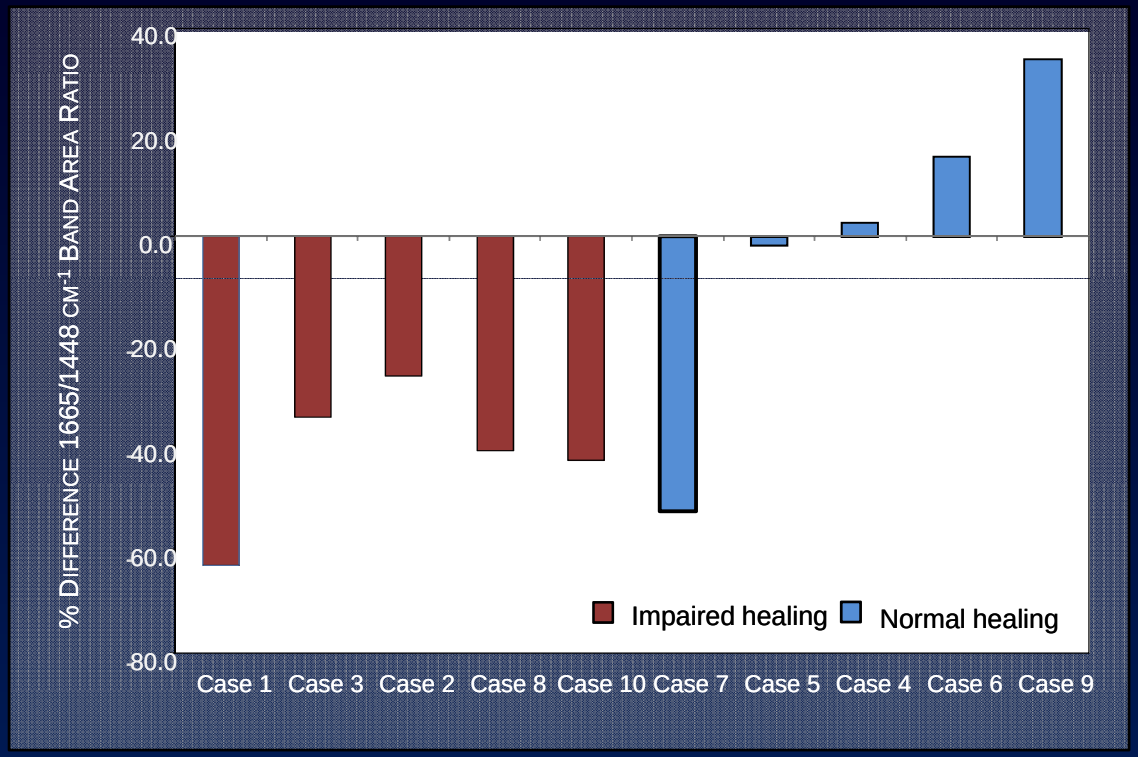

- Impaired healing wounds demonstrate a significant decrease in the 1665/1448 cm^{-1} band area ratio compared to normal healing wounds, as demonstrated by Raman spectroscopic mapping.

Monitoring a Wound Over Time – Normal vs. Impaired Healing

- Results were corroborated by altered collagen/collagenase gene expression profiles of tissue biopsies.
- Gene expression profiles confirm decreased gene expression of collagen types I and III at the first debridement and collagen type III at the final debridement in impaired wounds.

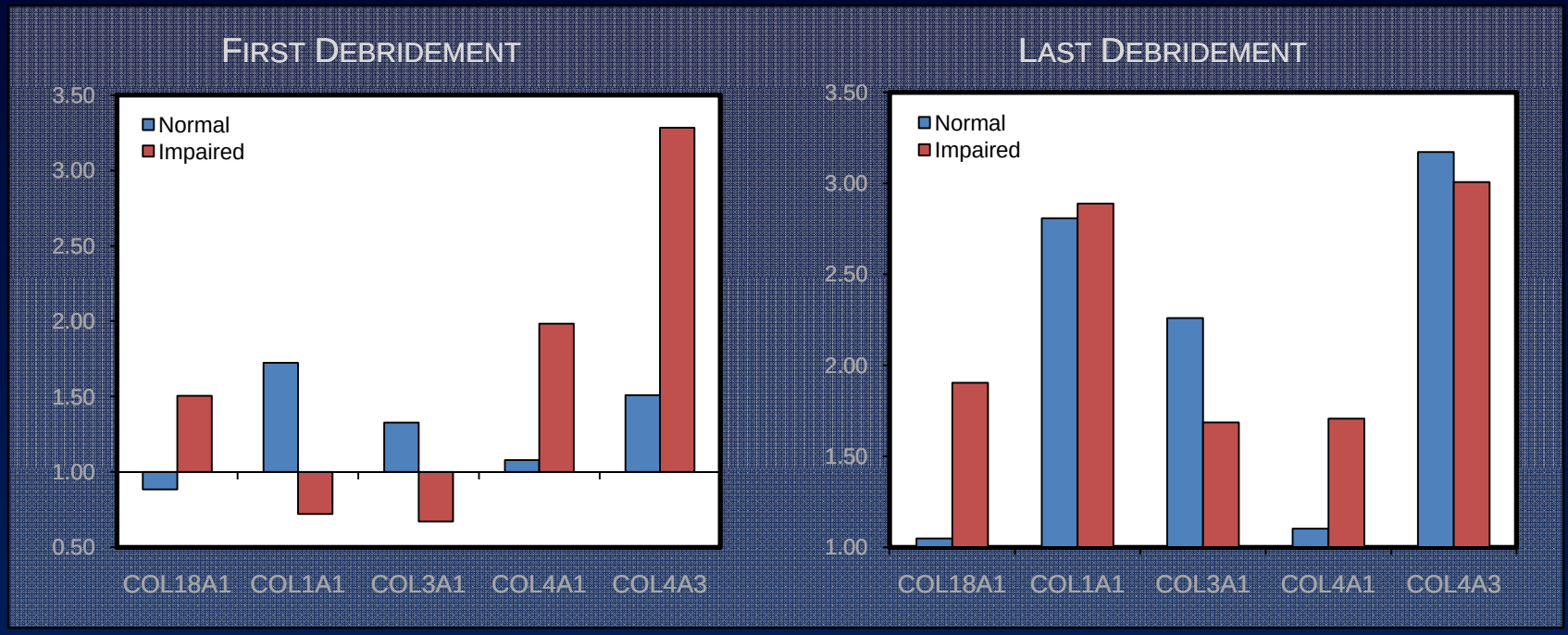

- COL18A1 mRNA expression remains elevated for impaired healing wounds at almost all time points when compared to normal healing wounds. Continued elevation of endostatin would inhibit neovascularization.

Monitoring a Wound Over Time – Normal vs. Impaired Healing

During early wound healing, type III collagen is the most abundant collagen and is gradually replaced by type I collagen.

- *delayed deposition of type III collagen* = *delayed deposition of type I collagen* = *delayed re-epithelialization*

Could this type of analysis be extended to intact wound biopsies and ultimately obviate the need for excisional wound biopsies?

Monitoring a Wound Over Time - Normal vs. Impaired Healing

Monitoring a Wound Over Time – Normal vs. Impaired Healing

First Debridement

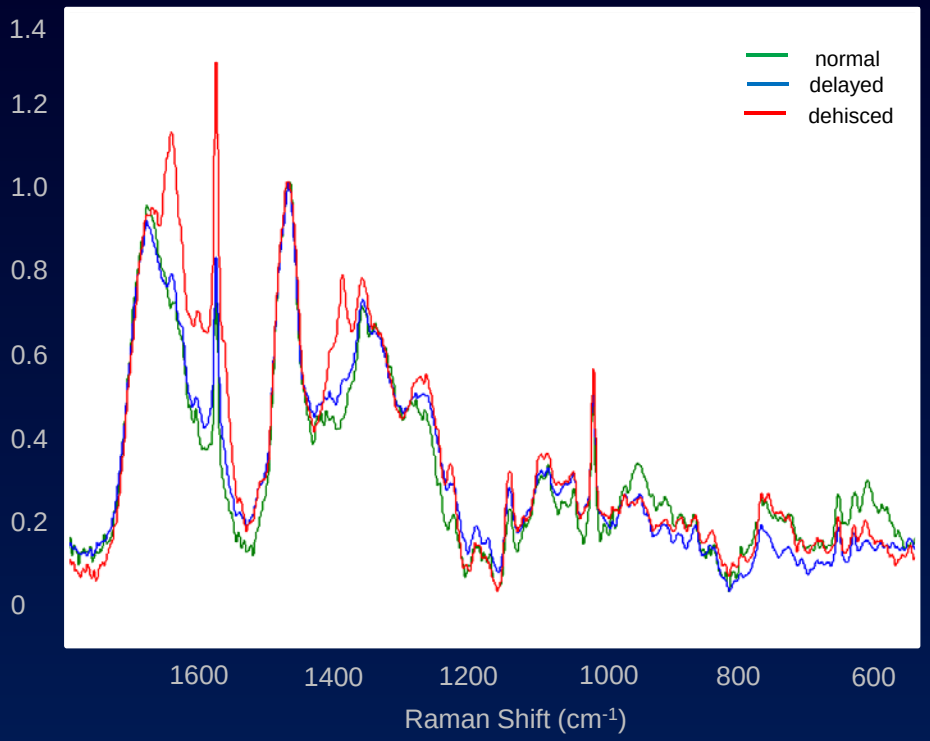

Final Debridement

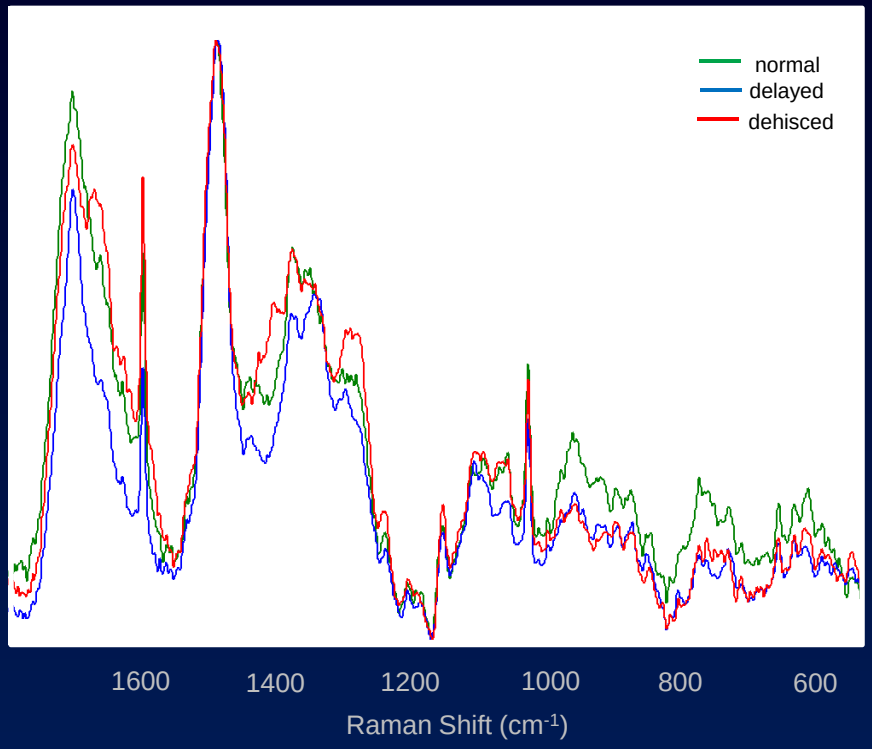

- At the first debridement, the normal and impaired healing biopsy spectra are similar.
- The first debridement the wound biopsy from the dehisced wound already exhibits spectral differences when compared to the normal and impaired healing wounds.
- At the final debridement, there appears to be a decrease in the 1665 cm^{-1}/1445 cm^{-1} band area ratio of the impaired healing wound.

Monitoring a Wound Over Time – Normal vs. Impaired Healing

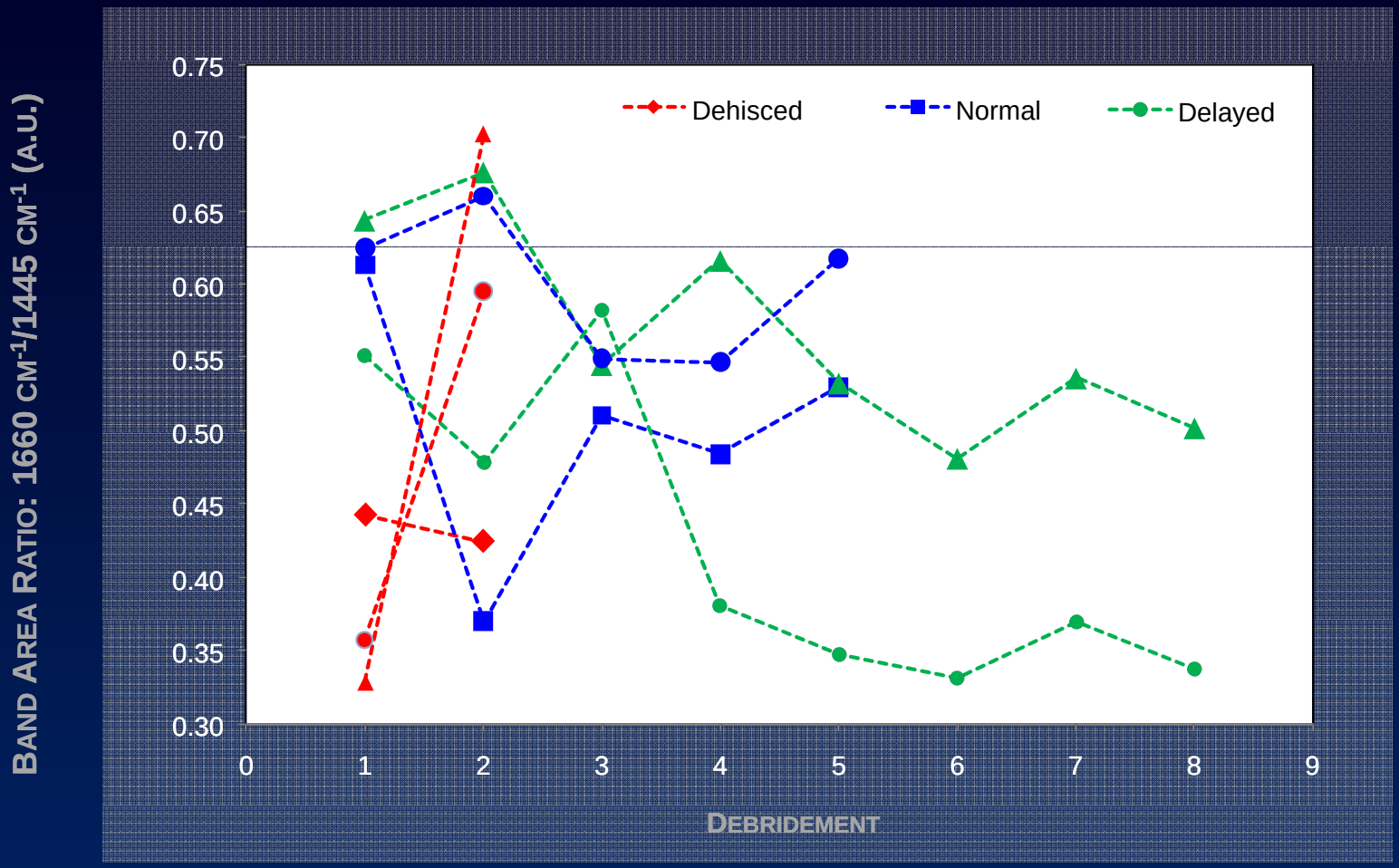

Monitoring a Wound Over Time – Normal vs. Impaired Healing

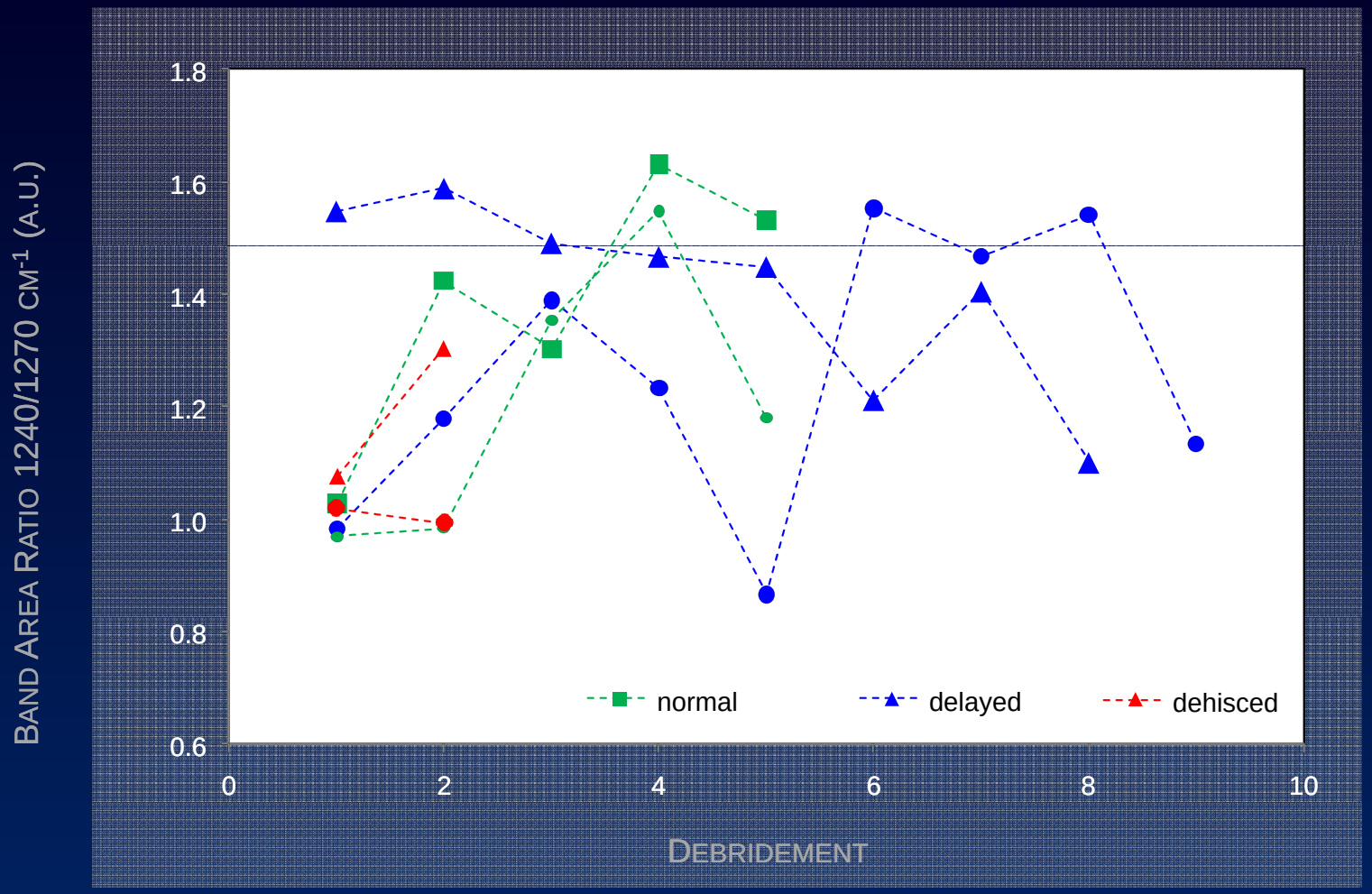

Monitoring a Wound Over Time – Normal vs. Impaired Healing

- Currently, we are building our biopsy database for Bayesian Belief Network modeling.
- We have over 200 tissue biopsies from over 50 patients.
- Peak fitting needs to be performed over the entire spectrum to determine which vibrational bands provide optimal sensitivity and specificity.
- We have an amendment submitted to the IRB for the use of Raman spectroscopy in the operating room during the surgical debridements. Note, at this time the collection of Raman spectra will not alter the course of treatment, i.e. not a clinical diagnostic.

The Development of Heterotopic Ossification

Heterotopic Ossification

- Heterotopic ossification (HO) refers to the aberrant formation of mature, lamellar bone in non-osseous tissues.
- Currently, orthopaedic surgeons faced with treating mature, refractory, symptomatic HO are left with few options other than operative excision. *Potter et al. J Bone Joint Surg Am. 2007;89:476-486.*
- Following most civilian trauma, HO formation is relatively rare in the absence of head injury. Even following traumatic brain or spinal cord injury, it develops in only 20% and 11% of patients. Rates of HO formation exceed 50% only in the setting of femoral shaft fractures with concomitant head injury.

Potter et al. J Bone Joint Surg Am. (In press).

ORTHOPEDICS 2008;31(12):1237.

UPOJ 1998;11:59-66.

Heterotopic Ossification

- In a study evaluating whether the mechanism of injury (blast or non-blast) correlated with either the presence or severity of HO, we found clinically detectable HO in 63% of residual limbs. Combat-related injuries, in general, are associated with higher-than-expected prevalence of HO, when compared to civilian data.
- Some patients with HO remain entirely asymptomatic and no specific treatment is indicated. Many patients, however, develop symptoms directly attributable to their HO which persists indefinitely.
- The most common indications for HO excision in our wounded warrior population is pain with prosthesis wear.

USA Today, February 12, 2006.

Potter et al. J Bone Joint Surg Am. (In press).

Heterotopic Ossification

- Pre-HO tissue is not necessarily obvious.

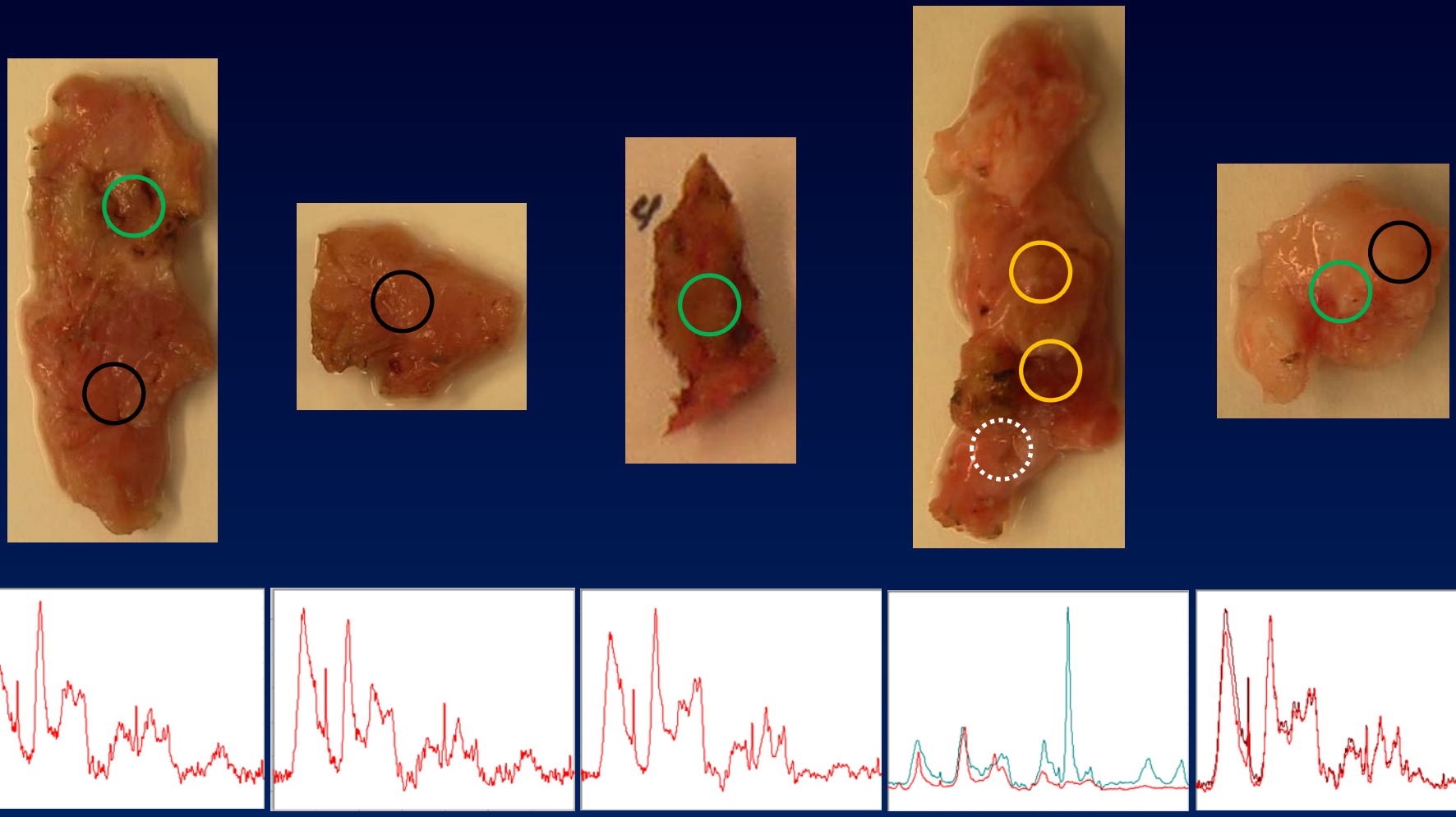

Heterotopic Ossification

- Sometimes HO tissue is incredibly obvious.

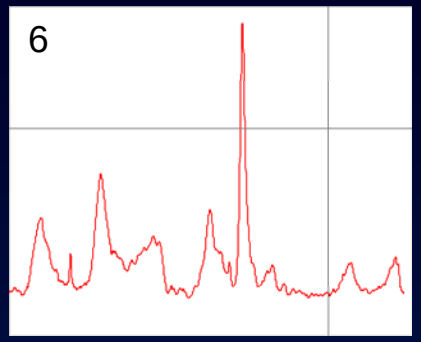

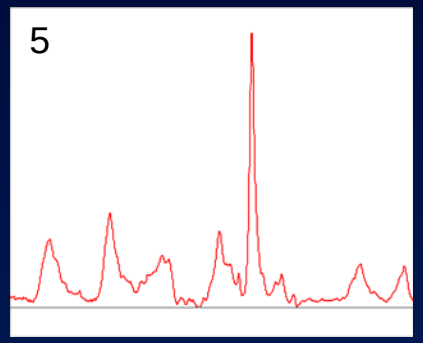

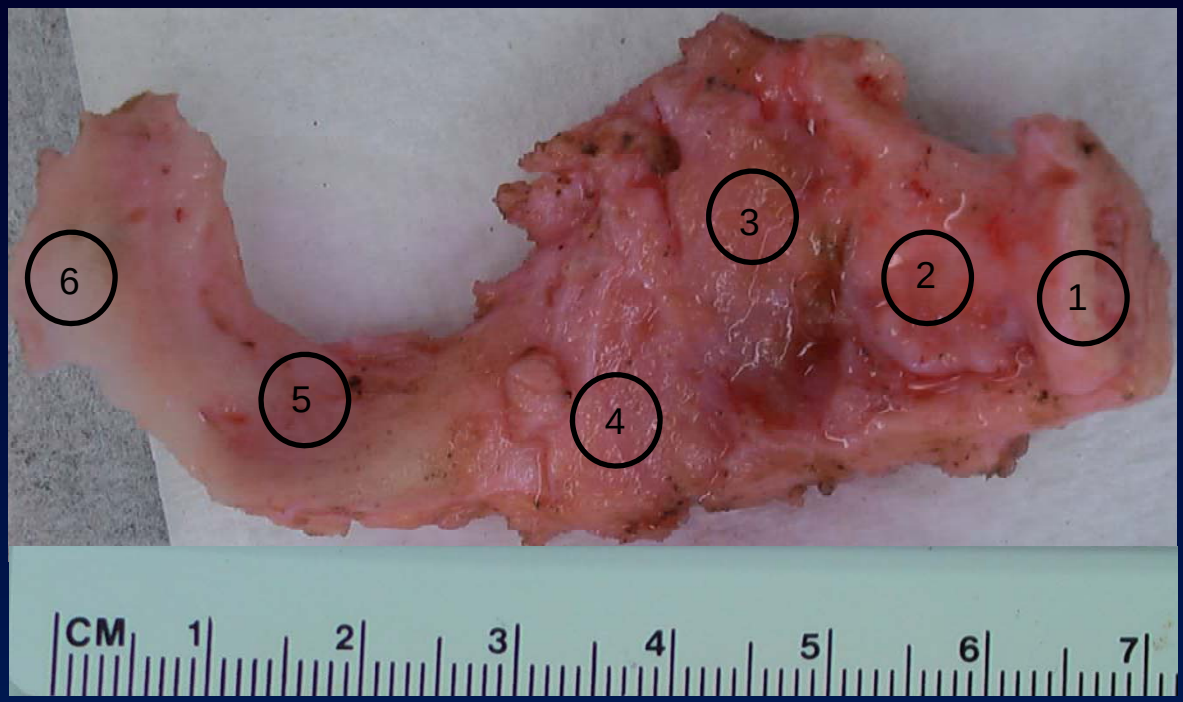

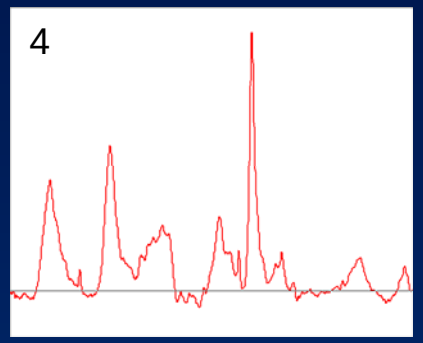

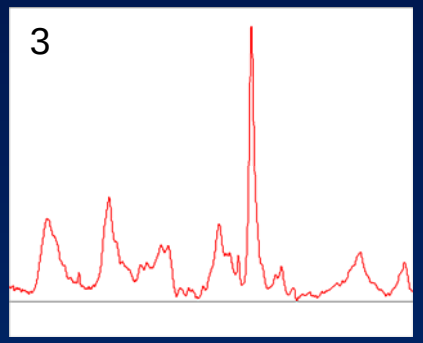

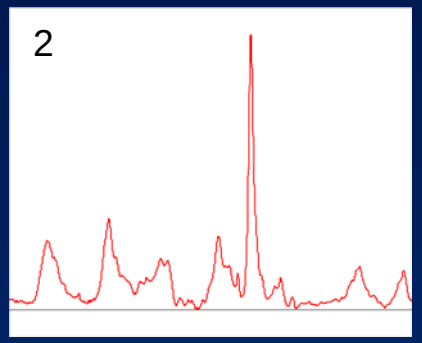

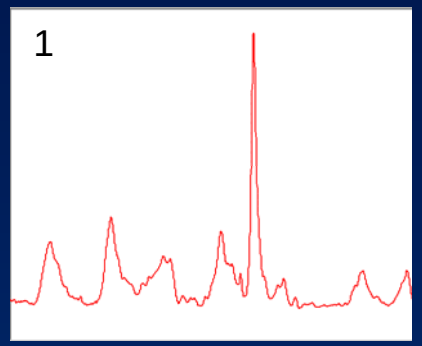

Heterotopic Ossification

Spectral comparison of muscle and collagen.

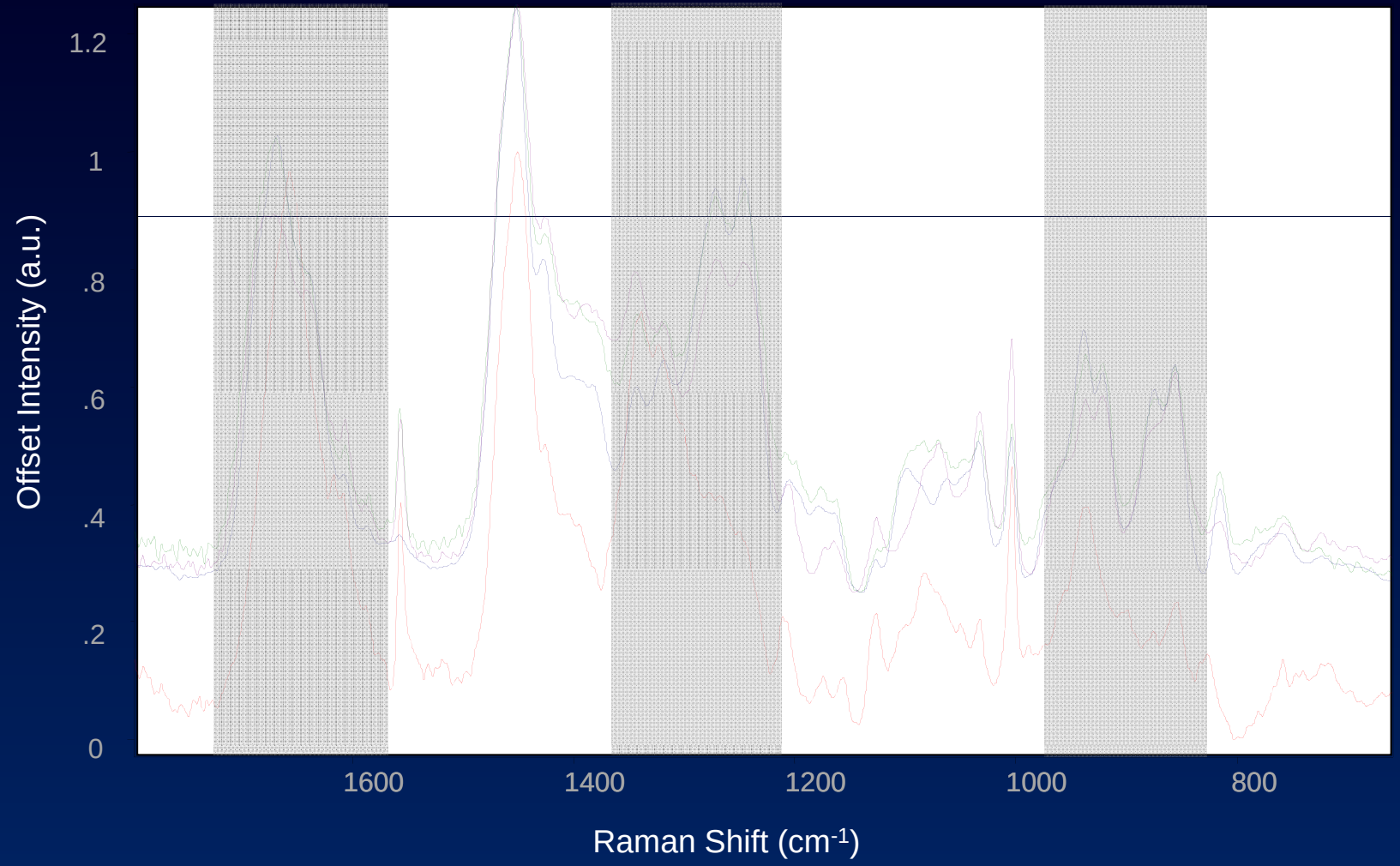

Heterotopic Ossification

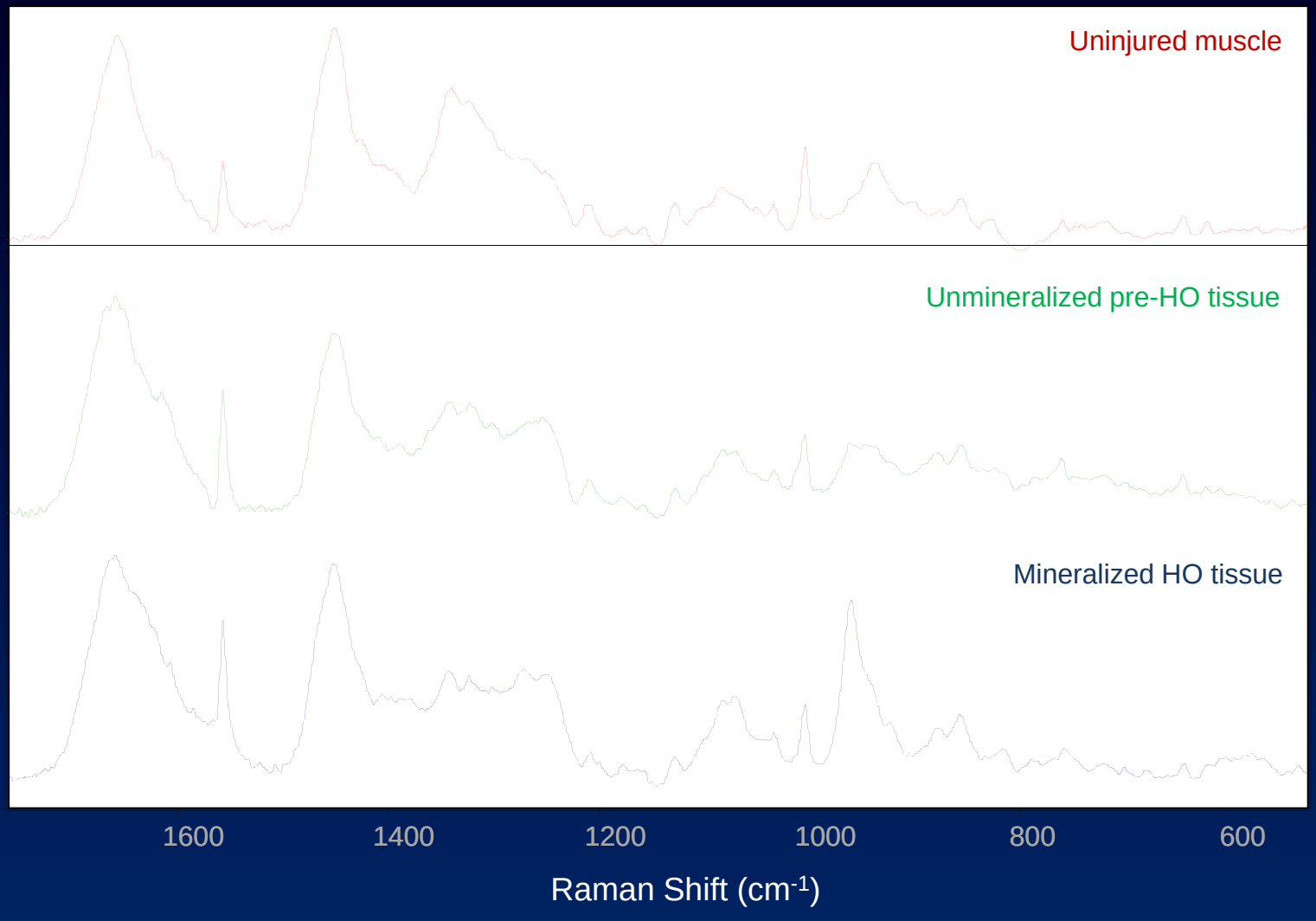

Heterotopic Ossification

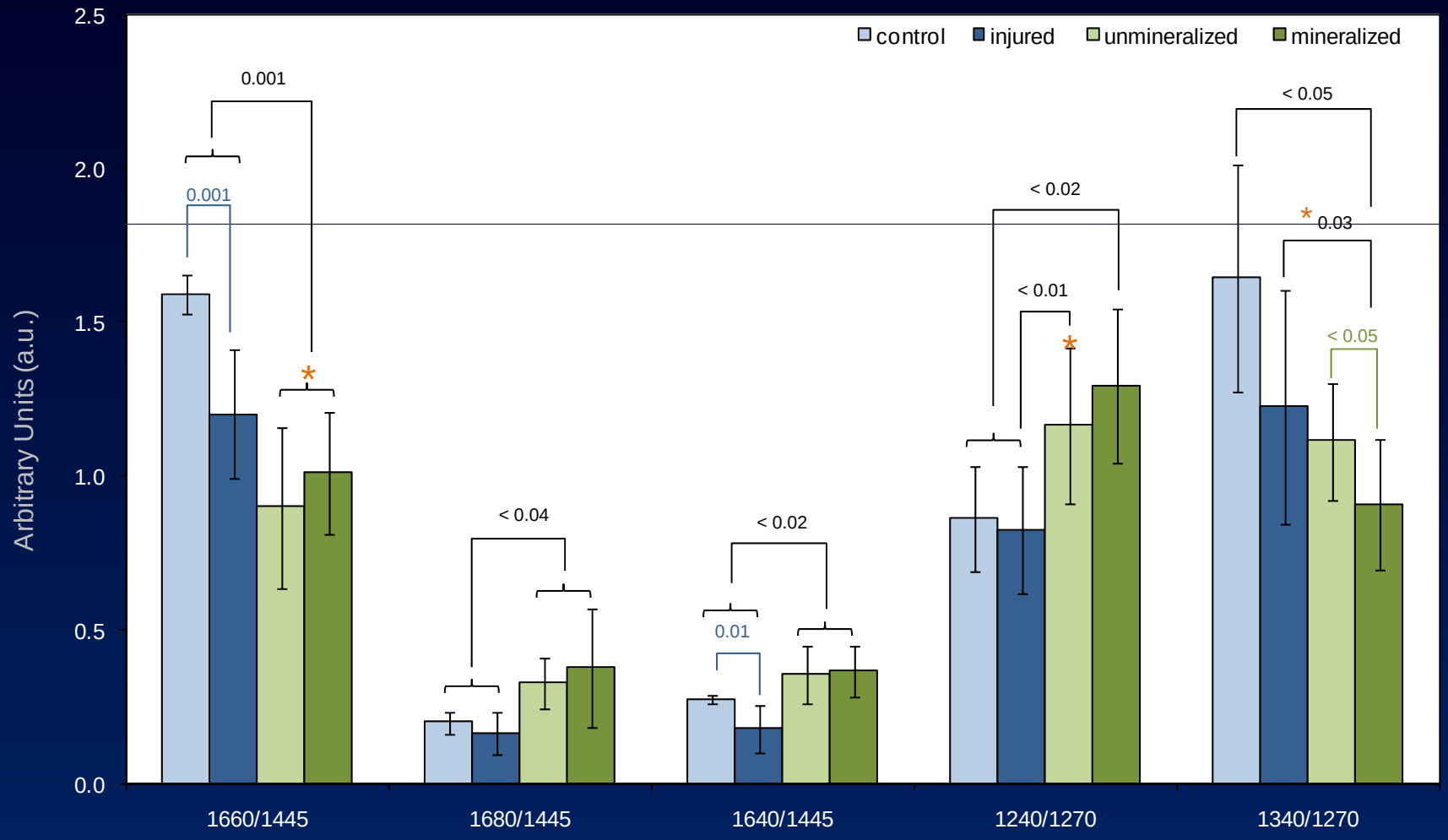

Heterotopic Ossification

- Preliminary results illuminate distinct differences between control muscle and muscle that eventually develops HO.
- We would like to be able to accurately determine which portions of the tissue are mineralizing – this has significant implications for amputation revisions. Additionally, we may be able to prevent the development of HO by accurately excising pre-HO tissue during the course of the surgical debridements.
- While we only have samples from 4 patients that developed HO, we are continuing to collect samples.
- We have not yet examined the quality of the bone formed during HO development.

FTIR Images of Wound Effluent

Wound Effluent

- Also called exudate – fluid that filters from the circulatory system into lesions or areas of inflammation.

- Complicated mixture of various fluids, cells, and proteins.
  - *Plasma, lymph fluid, white blood cells, red blood cells, dead tissue, dead cells, cytokines, chemokines, immunoglobulins, growth factors, etc.*

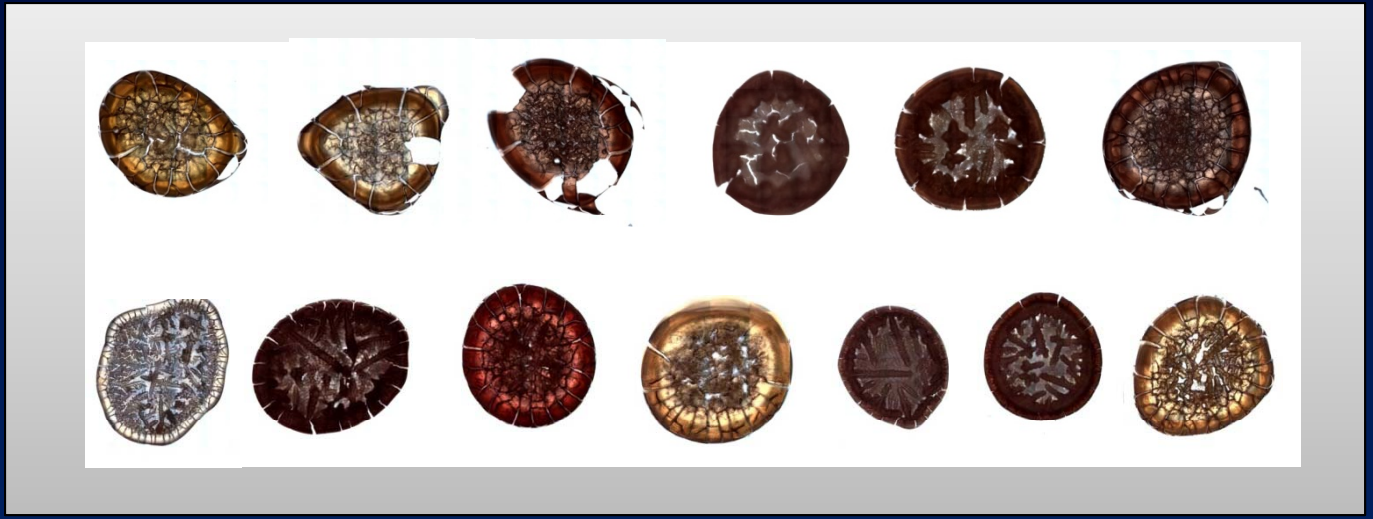

Sample Preparation

- Effluent was collected from WoundVac container
  - *Sample was centrifuged at 12,000-13,000 g*
  - *Supernatant was drawn off with pipette and passed through a 0.65 μm filter*
  - *Samples stored at -20°C*
- 4μL of effluent were deposited onto an aluminized slide and allowed to air dry
- FTIR images were acquired using the Nicolet iN10 FTIR microscope
  - Imaging Parameters:

    8 cm^{-1} spectral resolution

    4000 – 715 cm^{-1} spectral range
  - Factor analysis performed on images over truncated spectral range (1870-715 cm^{-1})

Effluent from a Normal Healing Wound, Not Colonized

high intensity

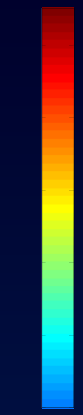

low intensity

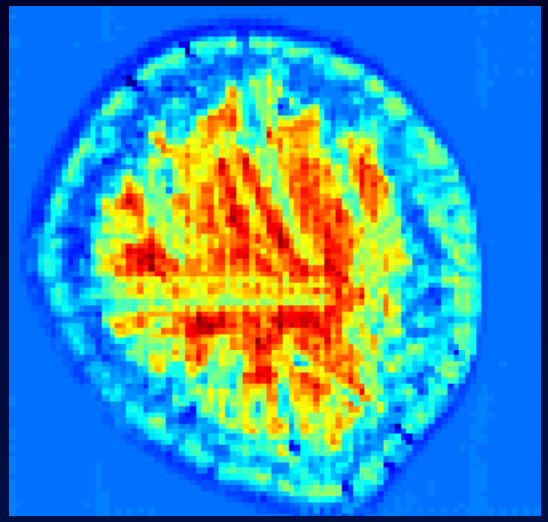

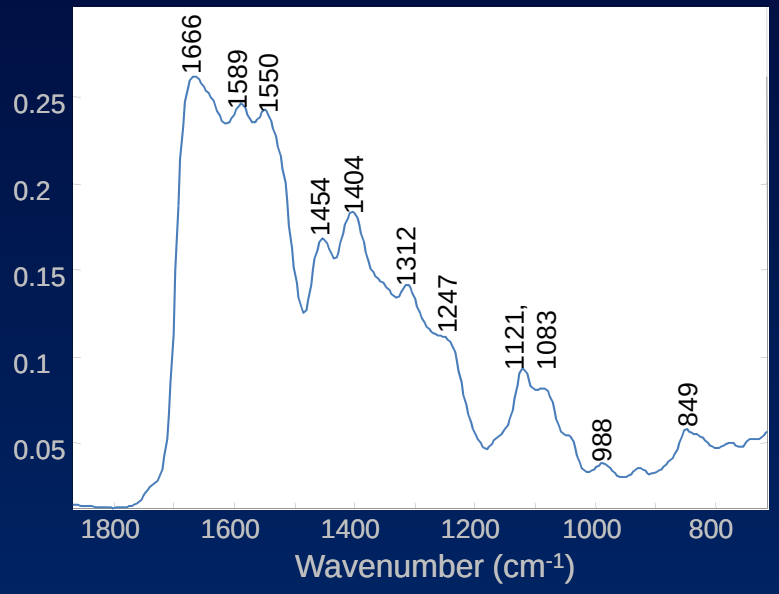

Effluent from a Dehisced Wound, Colonized with *Acinetobacter*

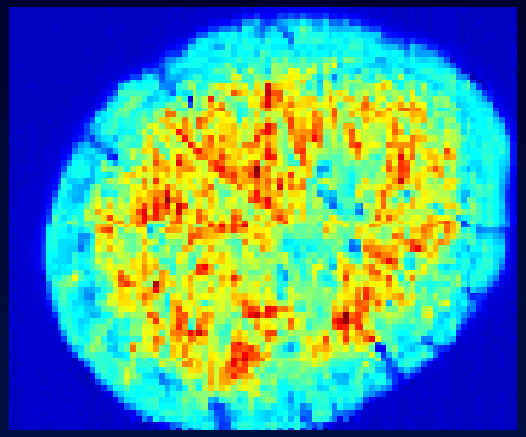

high intensity

low intensity

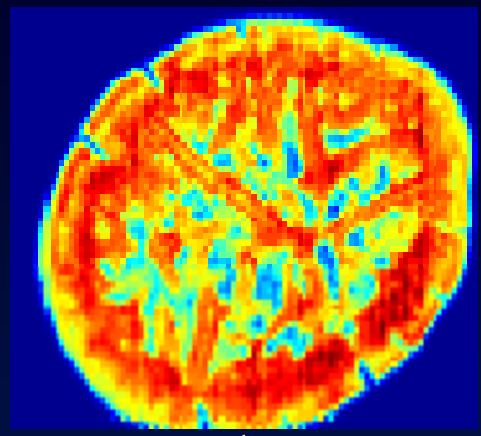

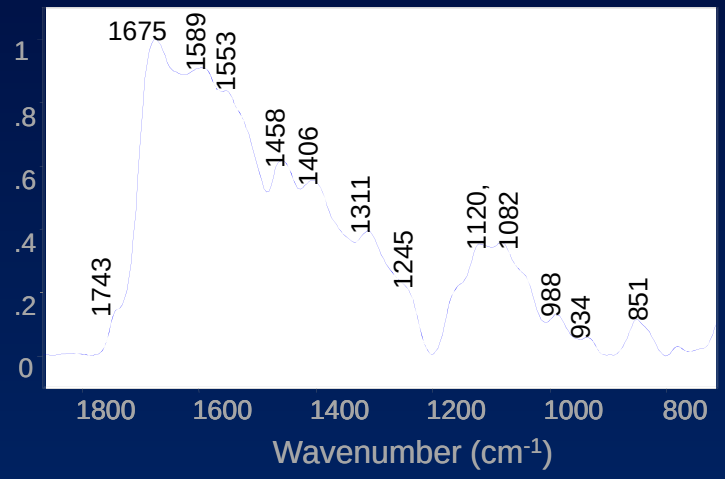

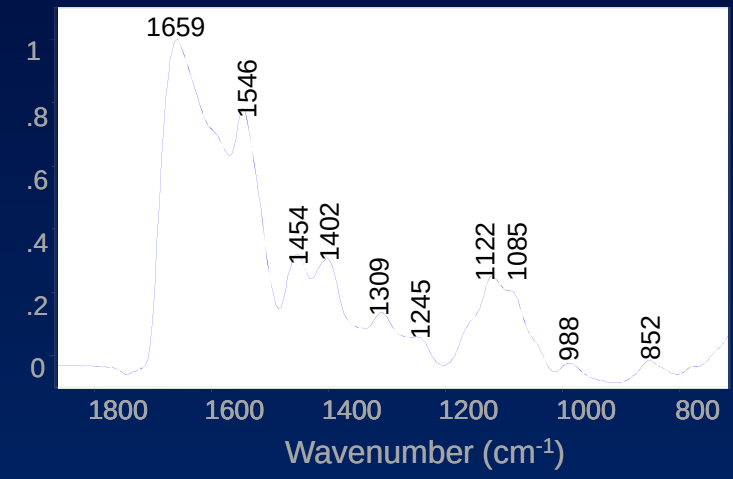

Effluent from an Impaired Healing Wound, Colonized with Acinetobacter

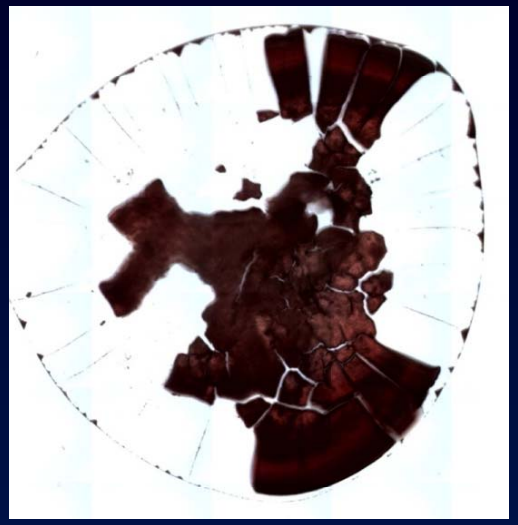

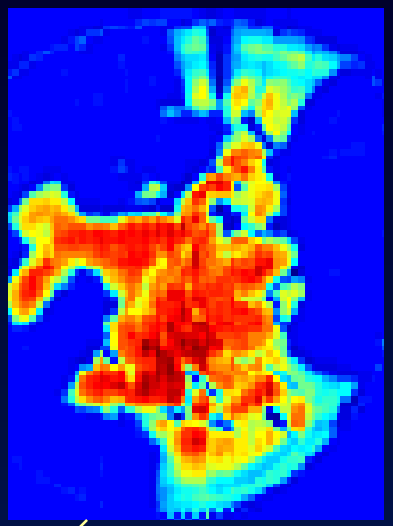

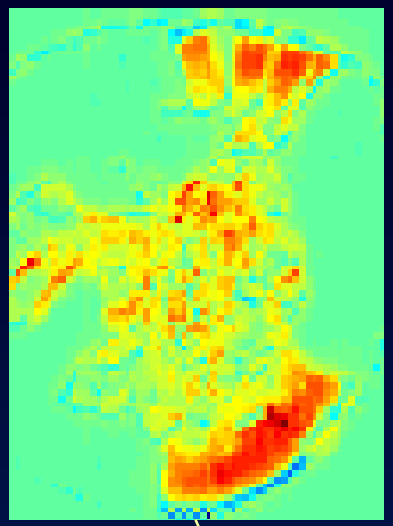

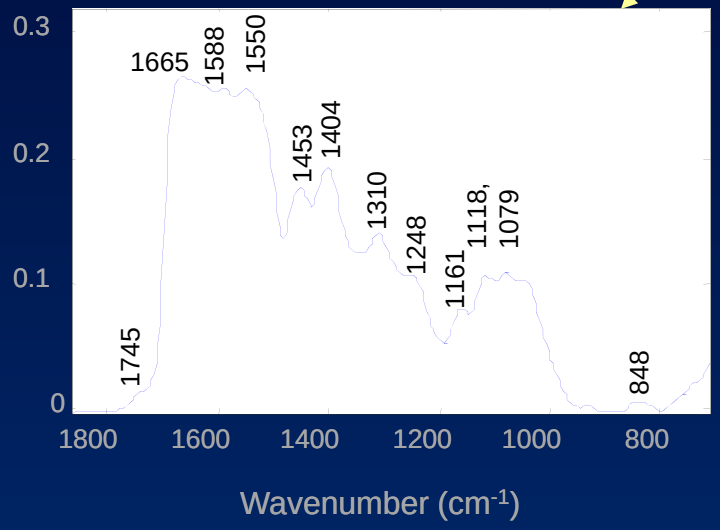

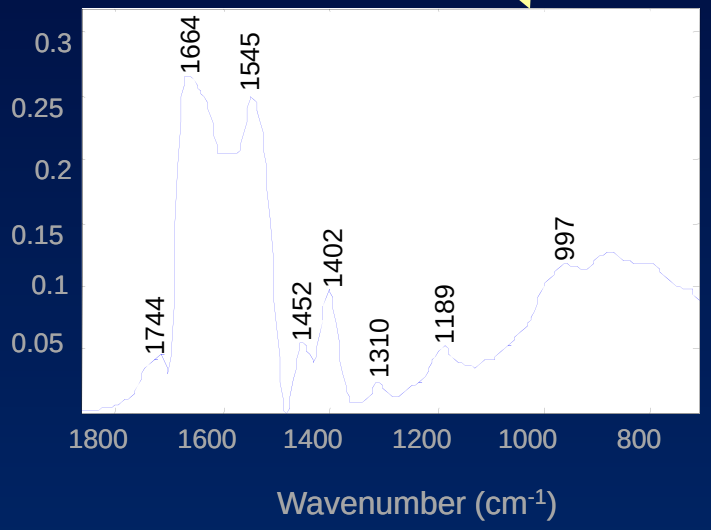

Effluent from Impaired Healing Wound, Colonized with *Acinetobacter*

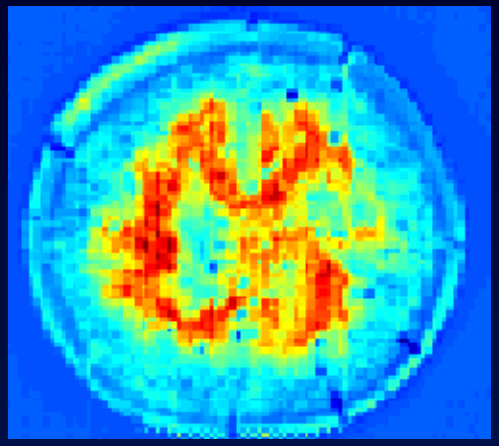

high intensity

low intensity

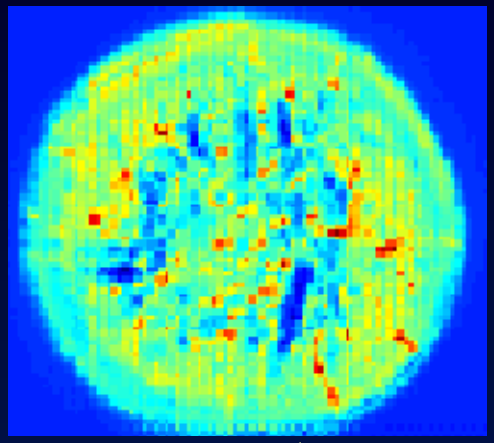

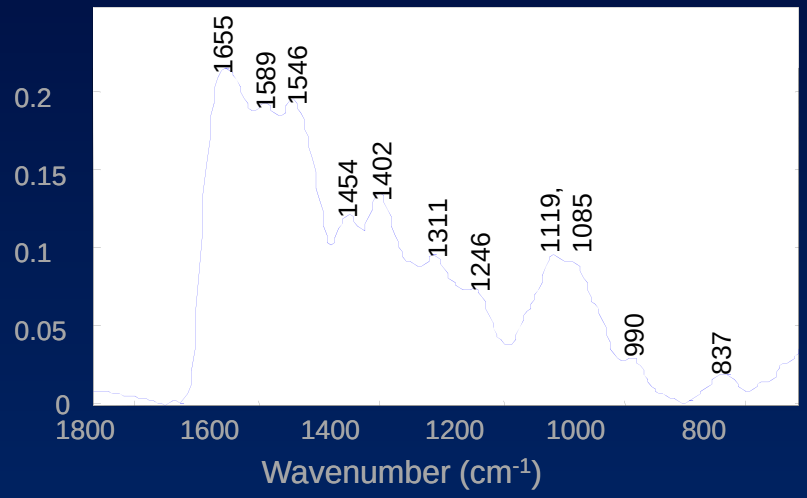

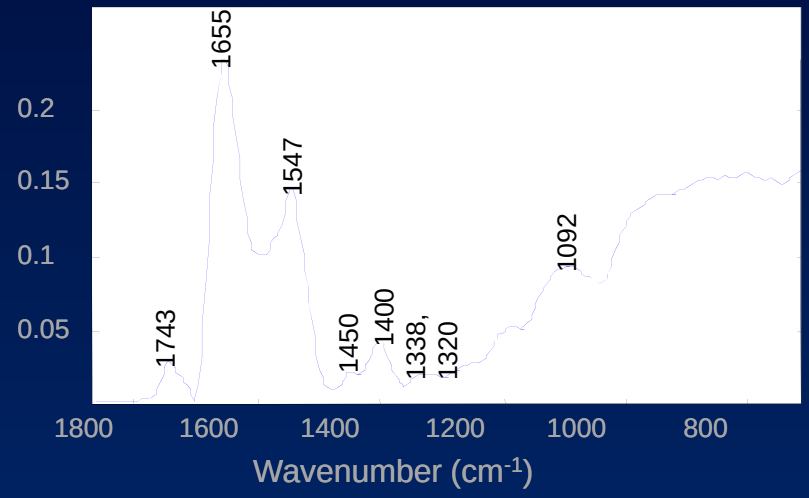

Different Strains of Biofilm-producing *Acinetobacter Baumannii*

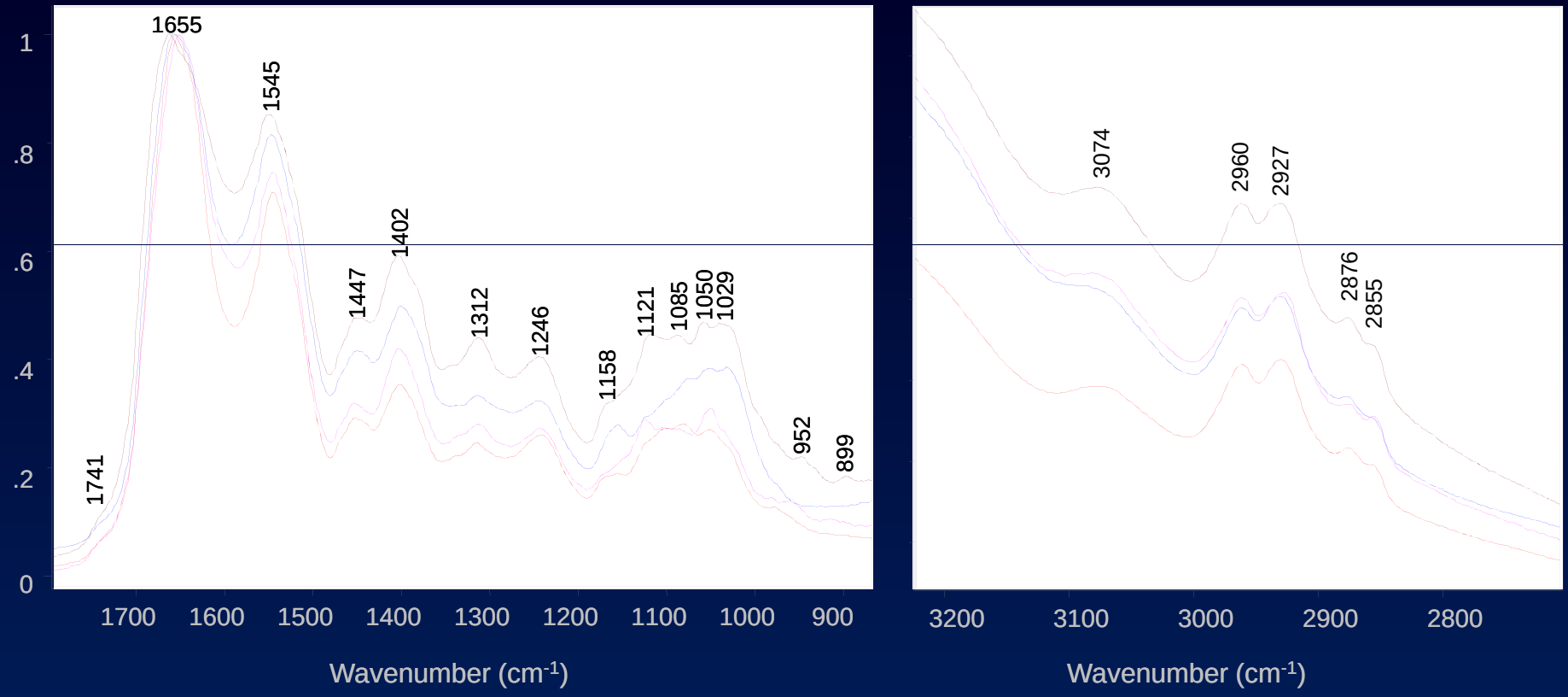

- Four strains of Acinetobacter obtained from WRAIR Infectious Diseases.
- Spectral differences largely observed from 1200-1000 cm^{-1}, attributed to saccharide components.

Comparison of *Acinetobacter* Spectra and the Second Factor

- Likely that the second factor extracted from the FTIR images is Acinetobacter, but likely a different strain from those examined.

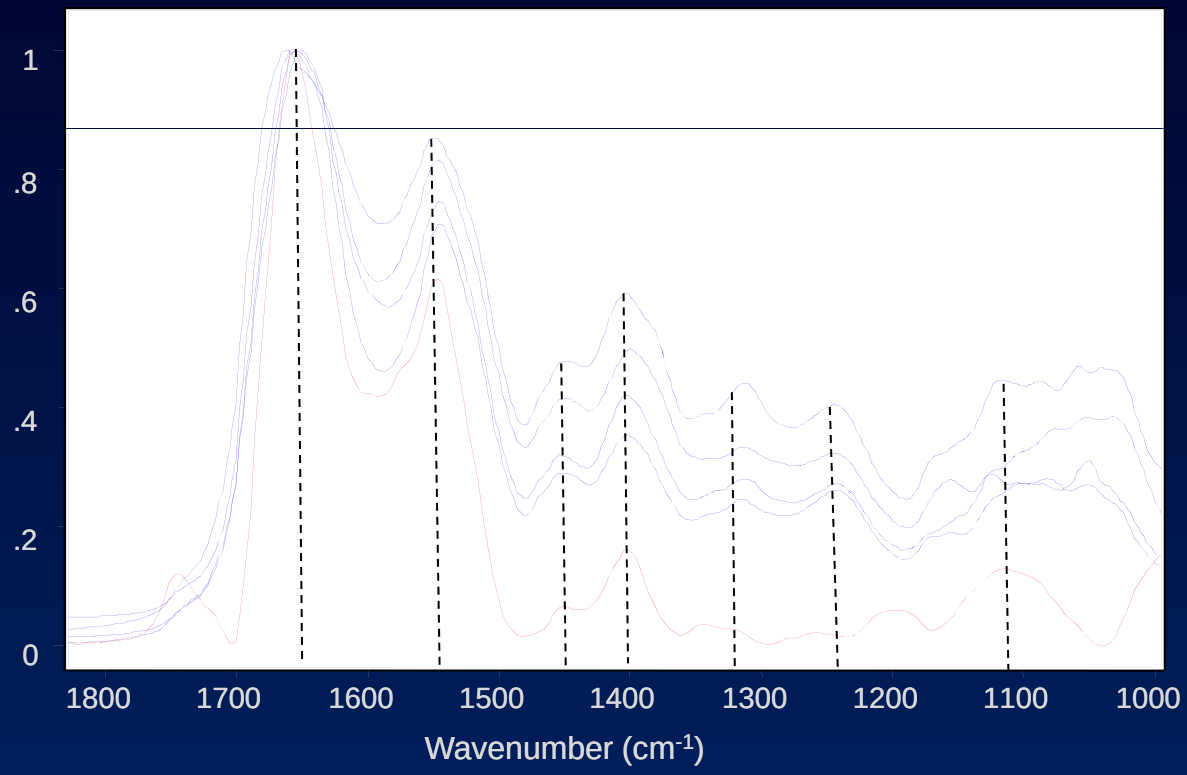

Wound Effluent

- FTIR has been previously used to identify different strains of Acinetobacter (*J Appl Microbiol. 96(2): 328-339, 2004*).
- The use of FTIR imaging has the potential to reduce the time for microbiological processing of effluent samples from 24-48 hours to 1-2 hours.
- Raman spectroscopy has also been used to differentiate Acinetobacter strains (*J Microbiol Methods. 64(1): 126-131, 2006)*; we have yet to explore the use of Raman spectroscopy with our samples.

Disclaimer

- The multidisciplinary care of these patients would not have been possible without the dedicated efforts of everyone at WRAMC and NNMC. Both civilian and military personnel have rendered skilled and compassionate care for these casualties. All of our efforts are dedicated to those who have been placed in harm's way for the good of our nation.
- The views expressed in this manuscript are those of the authors and do not reflect the official policy of the Department of the Army, Department of the Navy, the Department of Defense or the United States Government.

- This effort was supported (in part) by the U.S. Navy Bureau of Medicine and Surgery under the Medical Development Program and Office of Naval Research work unit number (604771N.0933.001.A0604).

- This study was approved by the National Naval Medical Center Institutional Review Board in compliance with all Federal regulations governing the protection of human subjects.

Acknowledgements

Naval Medical Research Center

Dr. Eric Elster
Dr. Trevor Brown
Dr. Doug Tadaki
Dr. Tom Davis
Nancy Porterfield
Frederick Gage
Eric Olsen
Wesley Stepp

National Naval Medical Center

Dr. Jonathan Forsberg
Dr. Benjamin Potter

Walter Reed Army Institute of Research

Dr. Daniel Zurowski

Walter Reed Army Medical Center

Dr. Fred O'Brien

Thermo Scientific

Developing a New Toolbox for Analysis of Warrior Wounds

Nicole J. Crane
Regenerative Medicine Department
Naval Medical Research Center

BSEC – Knoxville, TN
March 16-17th , 2011

Acute Combat Wounds

- The management of modern traumatic war wounds remains a significant challenge for clinicians.
  - Extensive osseous and soft-tissue damage caused by blasts and high-energy projectiles.
- The ensuing inflammatory response ultimately dictates the pace of wound healing and tissue regeneration.
- The timing of wound closure or definitive coverage is subjectively based.
- Despite the use and application of novel wound-specific treatment modalities, some wounds fail to close, or dehisce.
- In addition, some wounds are complicated by wound infection and subsequent biofilm formation , and heterotopic ossification (the pathological mineralization of soft tissues).

Acute Combat Wounds

An understanding of the molecular environment of acute wounds throughout the debridement process can provide valuable insight into the mechanisms associated with the eventual wound outcome.

Current Treatment

Surgical debridements are performed every 2-3 days.

- remove devitalized tissue
- decrease bacterial load

Negative pressure wound therapy (NPWT) is applied between debridements. NPWT promotes wound closure.

Wound assessment involves:

- patient's general condition
- injury location
- adequacy of perfusion
- gross appearance of the wound

The Challenge

Monitor wound healing *in vivo*, i.e. monitor wound healing during surgical debridements.

- Is it the best time to close the wound?
- Is the wound developing HO?
- Is the wound infected? With what?

Develop an objective and predictive model for wound healing.

The Toolbox

Real-time PCR

Multiplex Protein Assay

Raman Spectroscopy

FTIR Imaging

Thermography

Visible Reflectance Imaging

Bayesian Belief Network modeling

Needs and Knowledge Gaps

- Develop assays for enhanced detection and quantification of pathogenic organisms in combat wounds.

- Better understanding of the contribution of the species-specific composition of wound colonization to wound healing.

- Rapid, clinically-relevant assay for wound colonization and the potential risk to patient, wound healing, or heterotopic ossification.

- Objective decision-supportive tools utilizing biomarkers to provide personalized care based on an individual patient's current health condition.

- Record keeping system that includes sample repository tracking, workflow tracking, clinical information, and data storage.

Disclaimer

- The multidisciplinary care of these patients would not have been possible without the dedicated efforts of everyone at WRAMC and NNMC. Both civilian and military personnel have rendered skilled and compassionate care for these casualties. All of our efforts are dedicated to those who have been placed in harm's way for the good of our nation.

- The views expressed in this presentation are those of the authors and do not reflect the official policy of the Department of the Army, Department of the Navy, the Department of Defense or the United States Government.

- This effort was supported (in part) by the U.S. Navy Bureau of Medicine and Surgery under the Medical Development Program and Office of Naval Research work unit number (604771N.0933.001.A0604).

- This study was approved by the National Naval Medical Center Institutional Review Board in compliance with all Federal regulations governing the protection of human subjects.

Acknowledgements

Naval Medical Research Center

Dr. Eric Elster
Dr. Trevor S. Brown
Dr. Doug Tadaki
Dr. Tom Davis
Mr. Frederick Gage
Dr. Jonathan A. Forsberg

National Naval Medical Center

Dr. Jonathan Forsberg
Dr. Benjamin Potter

Walter Reed Army Institute of Research

Dr. Daniel Zurowski

Walter Reed Army Medical Center

Dr. Fred O'Brien
Dr. Jason Hawksworth

Vibrational Spectroscopy: A New Tool for the Analysis of Warfighter Wounds

Nicole J. Crane

Naval Medical Research Center

USUHS
May 19th, 2011

Acute Combat Wounds

Acute Combat Wounds

- The management of modern traumatic war wounds remains a significant challenge for clinicians.
  - Extensive osseous and soft-tissue damage caused by blasts and high-energy projectiles.
- The ensuing inflammatory response ultimately dictates the pace of wound healing and tissue regeneration.
- The timing of wound closure or definitive coverage is subjectively based.
- Despite the use and application of novel wound-specific treatment modalities, some wounds fail to close, or dehisce.
    - wound infection and subsequent biofilm formation
    - heterotopic ossification (the pathological mineralization of soft tissues)

Acute Combat Wounds

An understanding of the molecular environment of acute wounds throughout the debridement process can provide valuable insight into the mechanisms associated with the eventual wound outcome.

Acute Combat Wounds – Current Treatment

Surgical debridements are performed every 2-3 days.

- remove devitalized tissue
- decrease bacterial load

Negative pressure wound therapy (NPWT) is applied between debridements. NPWT promotes wound closure.

Wound assessment involves:

- patient's general condition
- injury location
- adequacy of perfusion
- gross appearance of the wound

Acute Combat Wounds – The Challenge

Monitor wound healing *in vivo*, i.e. monitor wound healing during surgical debridements.

- Is it the best time to close the wound?
- Is the wound developing HO?
- Is the wound infected? With what?

Develop an objective and predictive model for wound healing.

The Toolbox

Our Toolbox

- Real-time PCR
- Multiplex Protein Assay
- Raman Spectroscopy
- FTIR Imaging
- Thermography
- Visible Reflectance Imaging
- Bayesian Belief Network modeling

Vibrational Spectroscopy

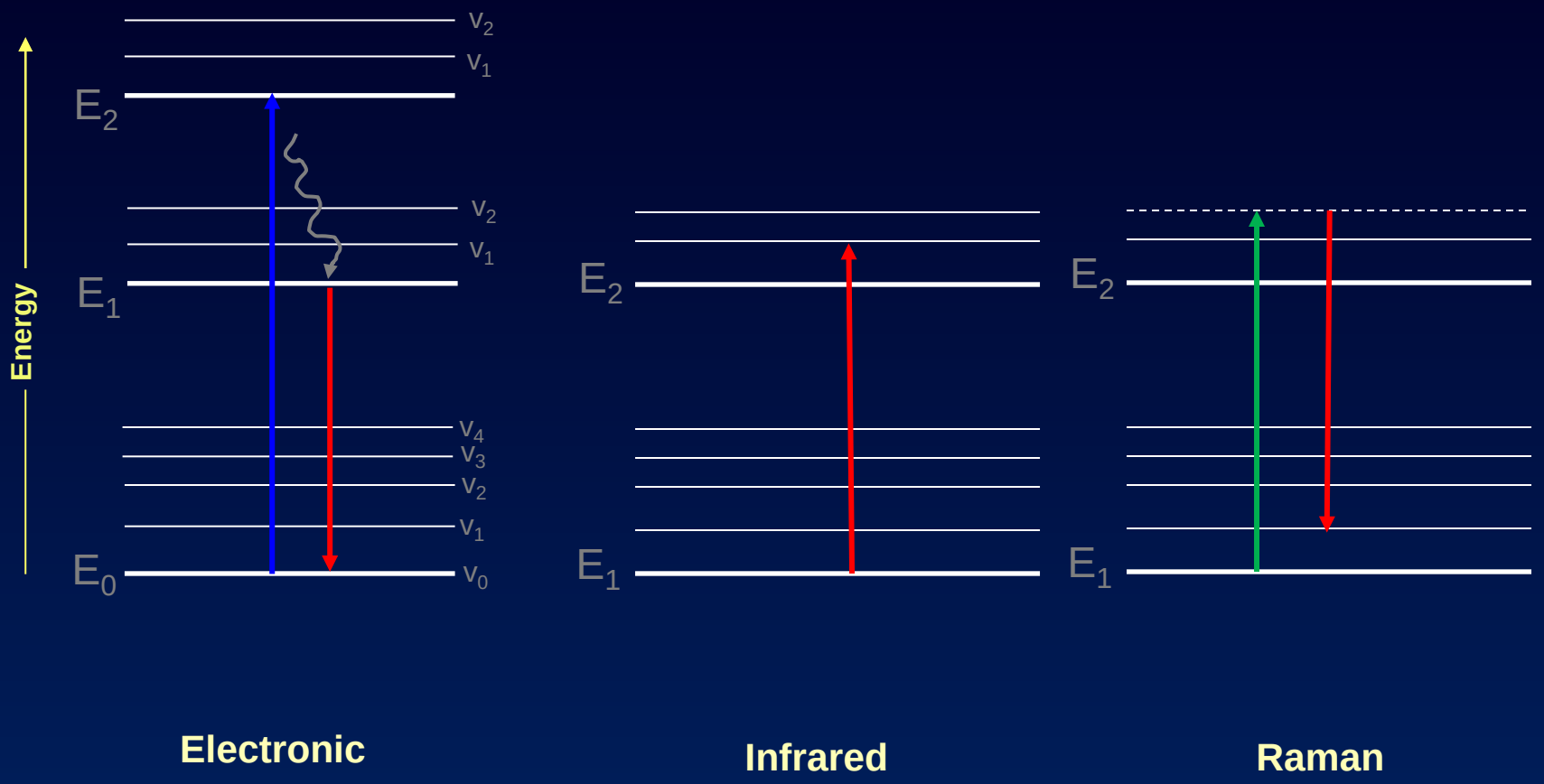

Electronic **Infrared** **Raman**

Vibrational Spectroscopy

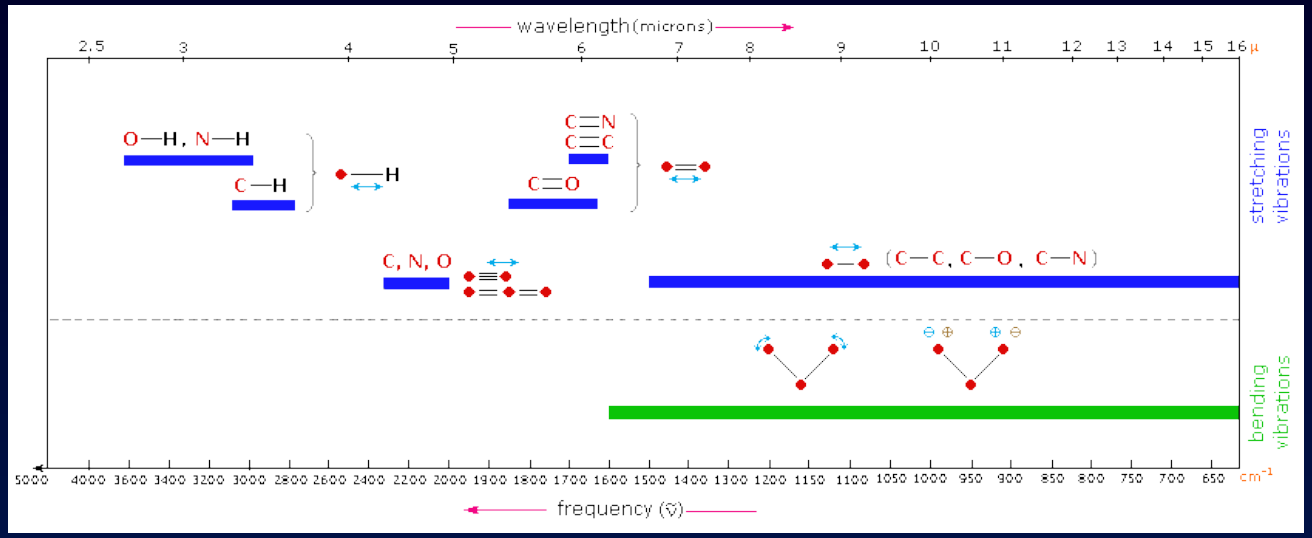

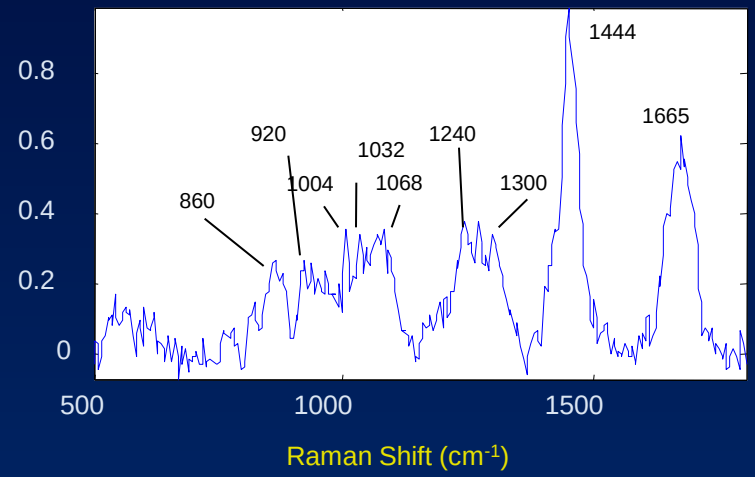

Raman Shift (cm^{-1})	Vibrational Band Assignment	Component
860	ν(C-C)	nucleic acids
920	ν(C-N), ν(C-C)	nucleic acids, keratin
1004	ν(C-C) ring	phenylalanine
1030	ν(C-C) skeletal	nucleic acids, protein
1070	ν(C-C) skeletal	nucleic acids, protein
1240, 1270	ν (C-N) and δ(N-H); Amide III	protein
1300	$\delta(CH_2)$ twisting	nucleic acids, protein
1445	$\delta(CH_3)$ and $\delta(CH_2)$ scissoring	protein
1609		aromatic amino acids
1665	ν(C=O); Amide I	protein

Preliminary Study – Raman Spectroscopic Mapping

Preliminary Study – Raman Mapping

First Debridement

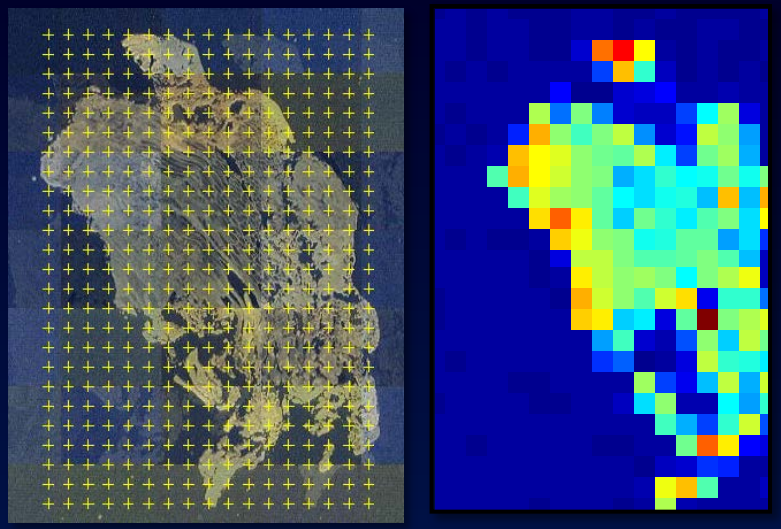

Last Debridement

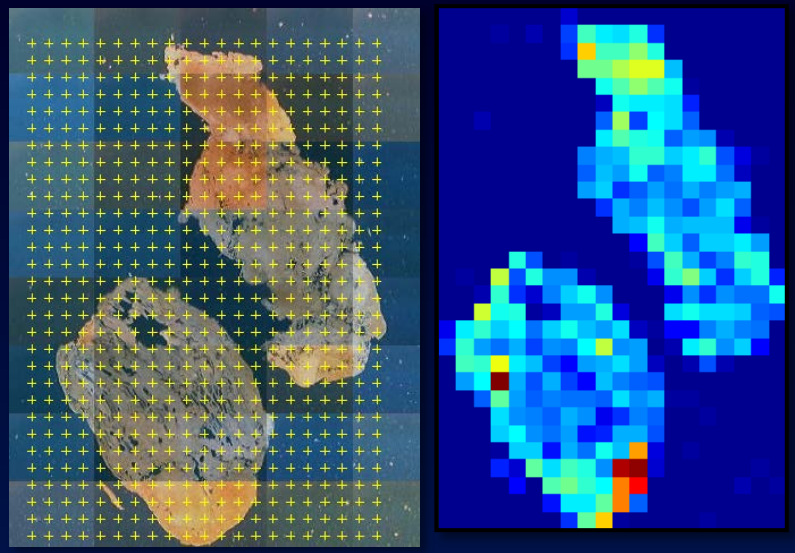

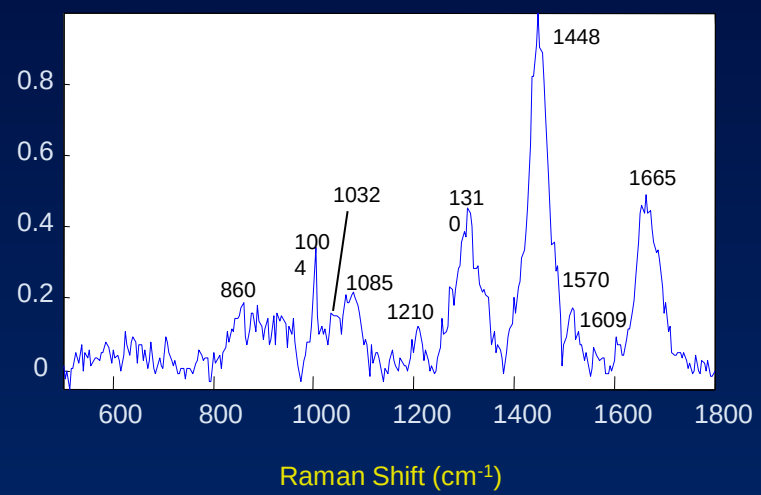

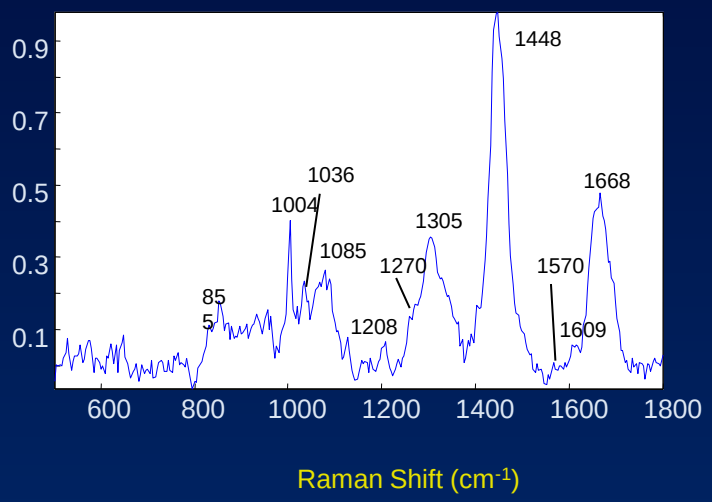

Preliminary Study – Raman Mapping

Intensity	*Area*
1665/1448	**1665/1448**
0.5034	0.4492
0.4525	0.4413

Difference between 1665/1448 cm^{-1} band area ratios:
-1.8%

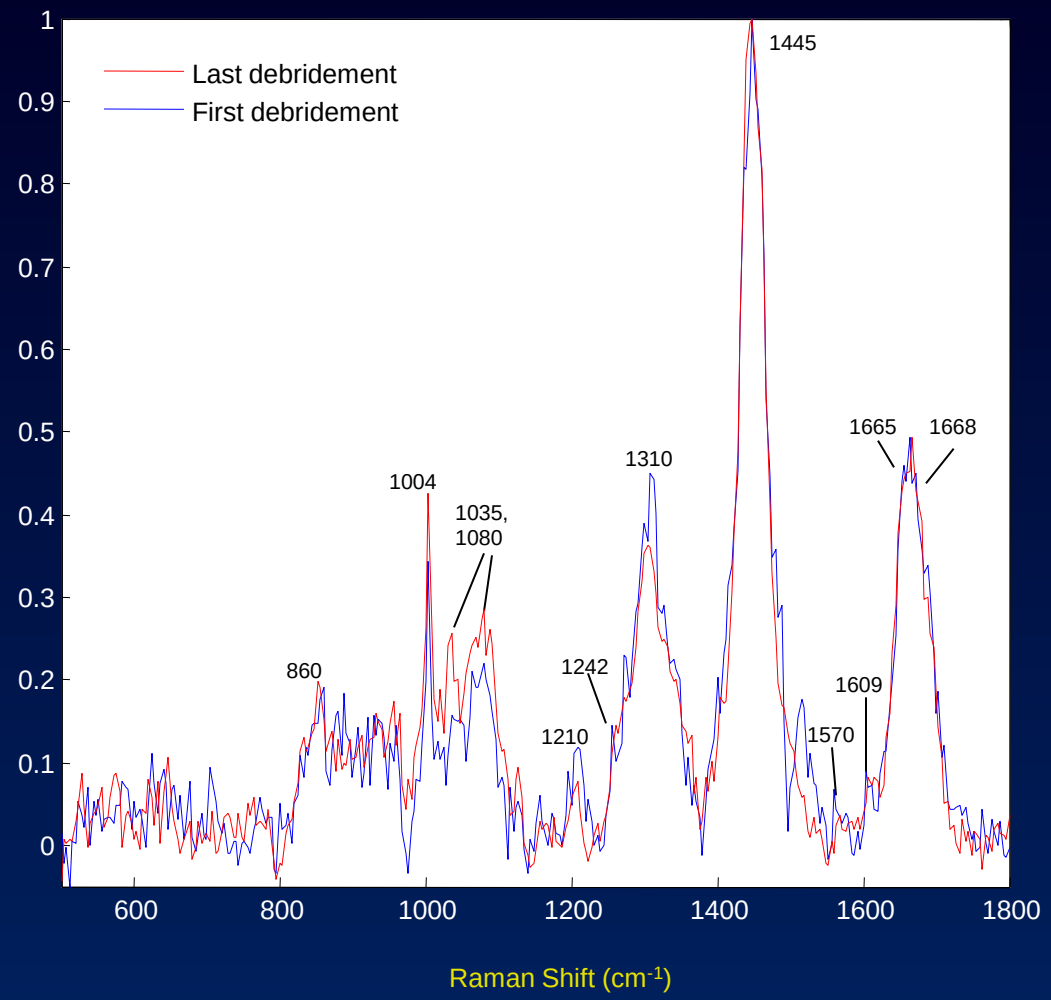

Preliminary Study – Raman Mapping Results

- Previous study demonstrated the potential of Raman spectroscopic analysis of wound biopsies for classification of wounds as normal or impaired healing from changes in the 1665 cm^{-1}/1445 cm^{-1} band area ratio.

Wound Rep Regen. 18(4): 409-416, 2010.

Ann Surg. 250(6):1002-7, 2009.

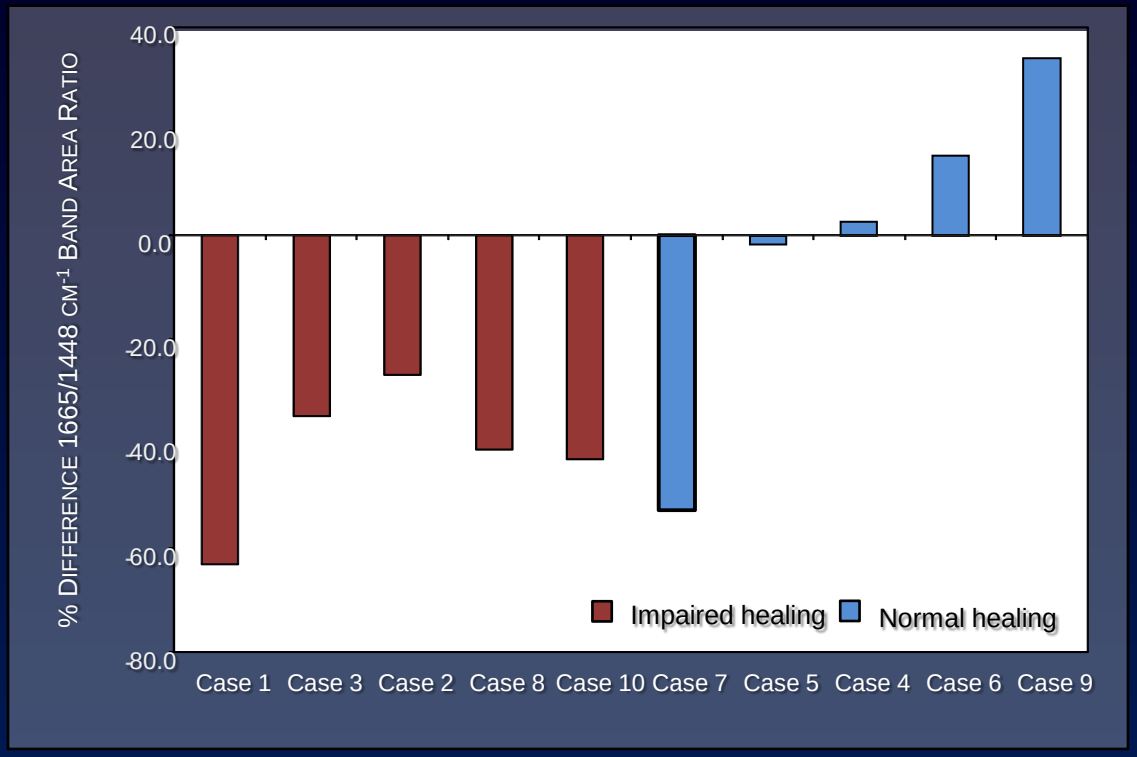

- Impaired healing wounds demonstrate a significant decrease in the 1665/1448 cm^{-1} band area ratio compared to normal healing wounds, as demonstrated by Raman spectroscopic mapping.

Preliminary Study – Real-Time PCR Analysis Results

- Results were corroborated by altered collagen/collagenase gene expression profiles of tissue biopsies.
- Gene expression profiles confirm decreased gene expression of collagen types I and III at the first debridement and collagen type III at the final debridement in impaired wounds.

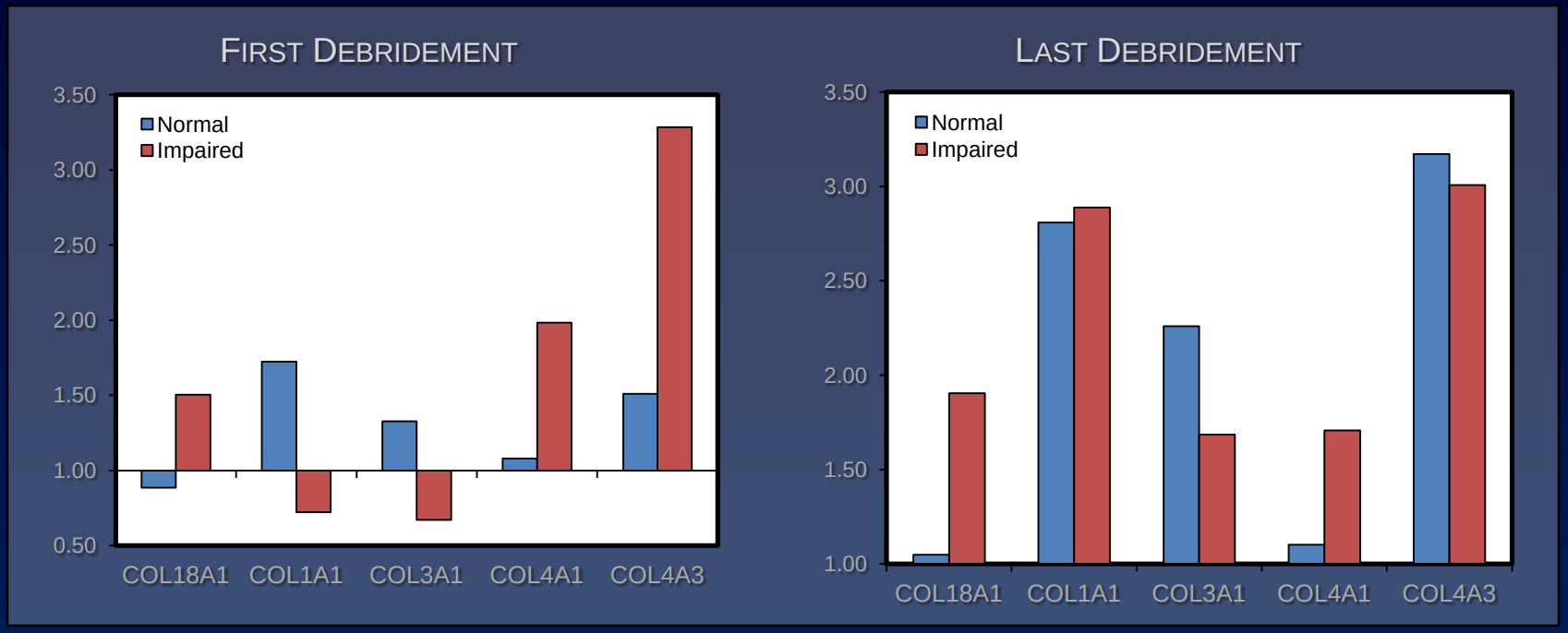

- COL18A1 mRNA expression remains elevated for impaired healing wounds at almost all time points when compared to normal healing wounds. Continued elevation of endostatin would inhibit neovascularization.

Monitoring a Wound Over Time – Normal vs. Impaired Healing

During early wound healing, type III collagen is the most abundant collagen and is gradually replaced by type I collagen.

- *delayed deposition of type III collagen* = *delayed deposition of type I collagen* = *delayed re-epithelialization*

Could this type of analysis be extended to intact wound biopsies and ultimately obviate the need for excisional wound biopsies?

Monitoring a Wound Over Time - Normal vs. Impaired Healing

Raman Fiber Probe Data Collection

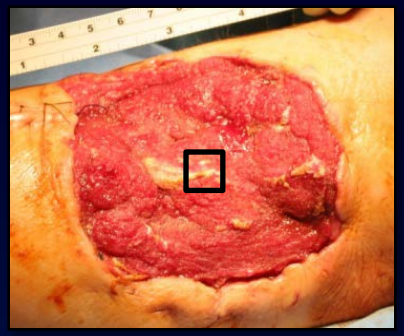

Approximately 1 cm^2 tissue biopsy is excised from the center of the wound bed.

Tissue is fixed in 10% neutral buffered formalin for storage.

Prior to spectral acquisition, samples are rinsed in 0.9% NaCl saline solution.

Examine multiple spots across the tissue.

40 accumulations, 5s spectrum

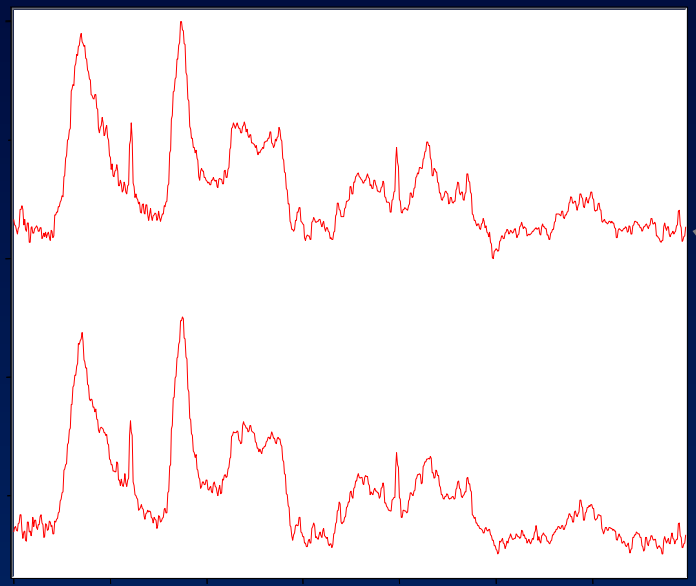

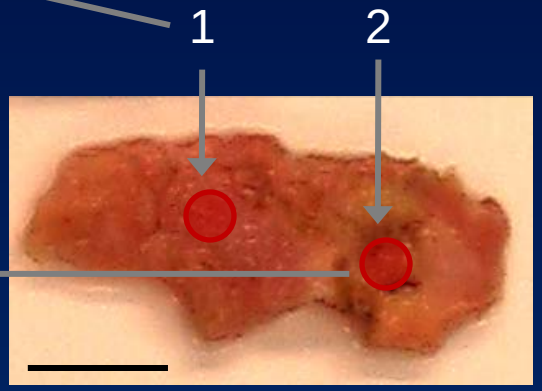

Monitoring a Wound Over Time – Normal vs. Impaired Healing

First Debridement

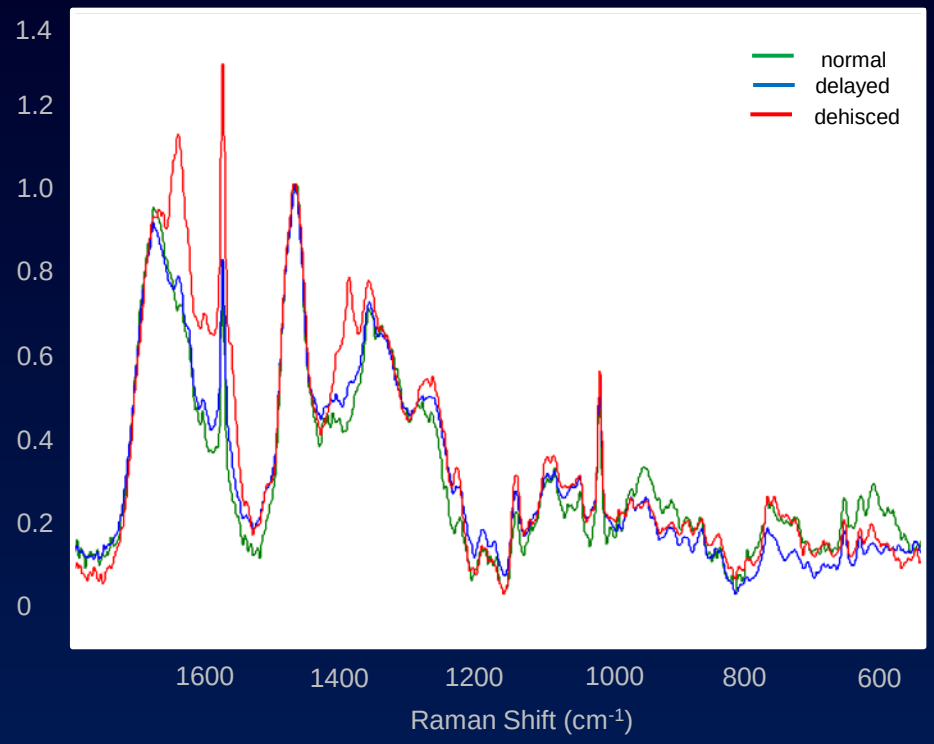

Final Debridement

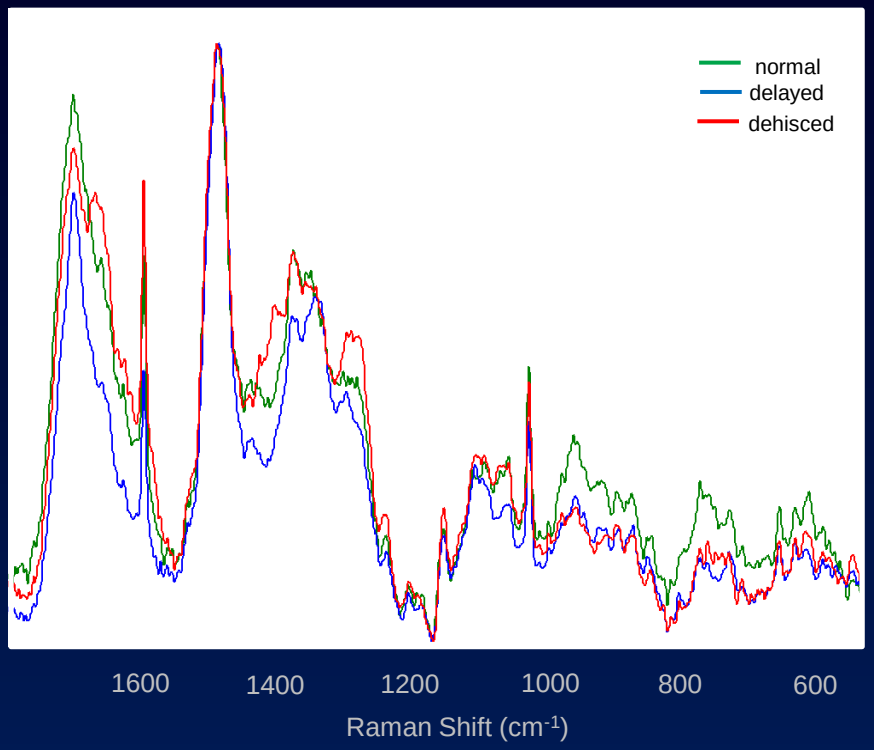

- At the first debridement, the normal and impaired healing biopsy spectra are similar.
- The first debridement the wound biopsy from the dehisced wound already exhibits spectral differences when compared to the normal and impaired healing wounds.
- At the final debridement, there appears to be a decrease in the 1665 cm^{-1}/1445 cm^{-1} band area ratio of the impaired healing wound.

Monitoring a Wound Over Time – Normal vs. Impaired Healing

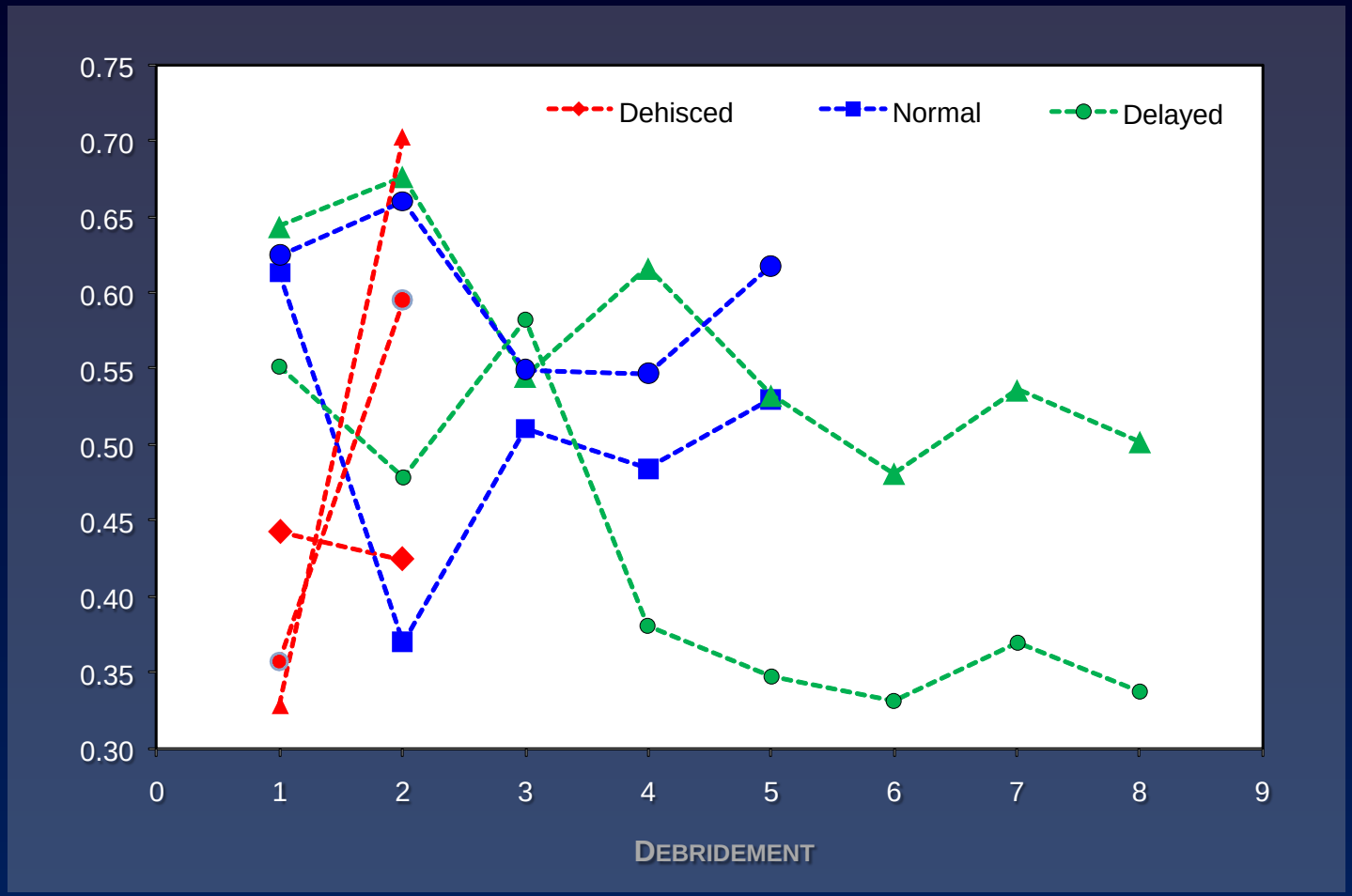

Monitoring a Wound Over Time – Normal vs. Impaired Healing

- Currently, we are building our biopsy database for Bayesian Belief Network modeling.
- We have over 200 tissue biopsies from over 50 patients.
- Peak fitting needs to be performed over the entire spectrum to determine which vibrational bands provide optimal sensitivity and specificity.
- We have an amendment submitted to the IRB for the use of Raman spectroscopy in the operating room during the surgical debridements. Note, at this time the collection of Raman spectra will not alter the course of treatment, i.e. not a clinical diagnostic.

The Development of Heterotopic Ossification

Heterotopic Ossification

- Heterotopic ossification (HO) refers to the aberrant formation of mature, lamellar bone in non-osseous tissues.
- Currently, orthopaedic surgeons faced with treating mature, refractory, symptomatic HO are left with few options other than operative excision. *Potter et al. J Bone Joint Surg Am. 2007;89:476-486.*
- Following most civilian trauma, HO formation is relatively rare in the absence of head injury. Even following traumatic brain or spinal cord injury, it develops in only 20% and 11% of patients. Rates of HO formation exceed 50% only in the setting of femoral shaft fractures with concomitant head injury.

Potter et al. J Bone Joint Surg Am. (In press).

ORTHOPEDICS 2008;31(12):1237.

UPOJ 1998;11:59-66.

Heterotopic Ossification

- In a study evaluating whether the mechanism of injury (blast or non-blast) correlated with either the presence or severity of HO, we found clinically detectable HO in 63% of residual limbs. Combat-related injuries, in general, are associated with higher-than-expected prevalence of HO, when compared to civilian data.

- Some patients with HO remain entirely asymptomatic and no specific treatment is indicated. Many patients, however, develop symptoms directly attributable to their HO which persists indefinitely.

- The most common indications for HO excision in our wounded warrior population is pain with prosthesis wear.

USA Today, February 12, 2006.

Potter et al. J Bone Joint Surg Am. (In press).

Bone

- Bone is 35% organic material and 65% inorganic material

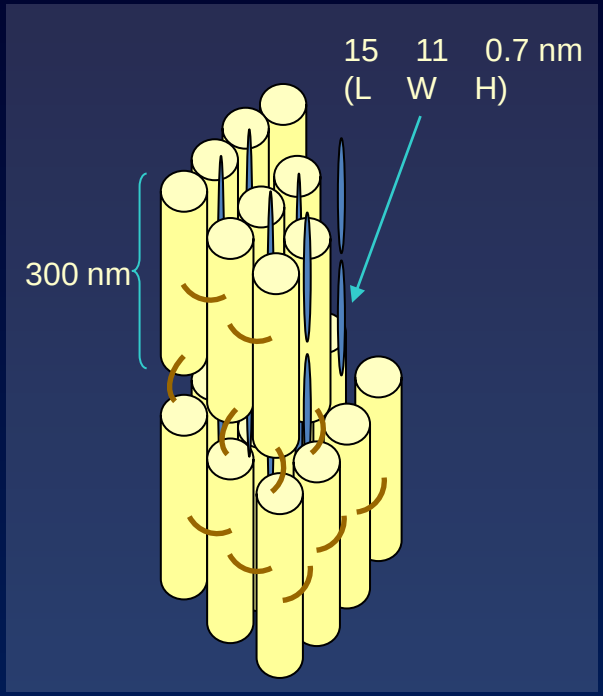

- For organic material
  - 90% of organic material is type I collagen
  - 10% noncollagenous proteins
- For inorganic material
  - commonly assumed to be some form of hydroxyapatite

$$Ca_{10}(PO_4)_2(OH)_6$$

  - more closely resembles a B-type carbonated apatite

$$Ca_{8.3\ \ 1.7}(PO_4)_{4.3}(CO_3)_1(HPO_4)_{0.7}(OH)_{0.3}$$

Raman Spectrum of Bone

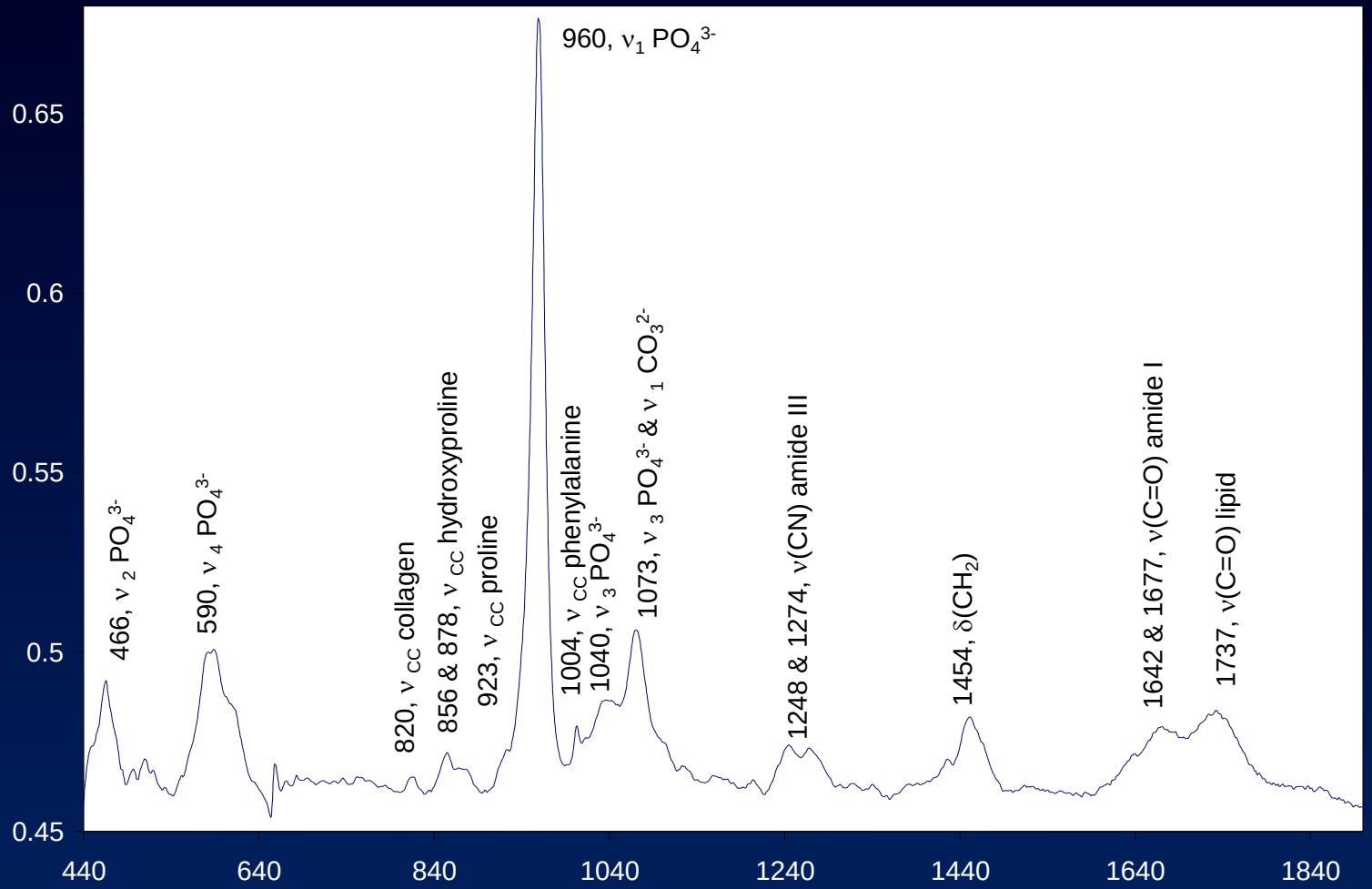

Heterotopic Ossification

- Pre-HO tissue is not necessarily obvious.

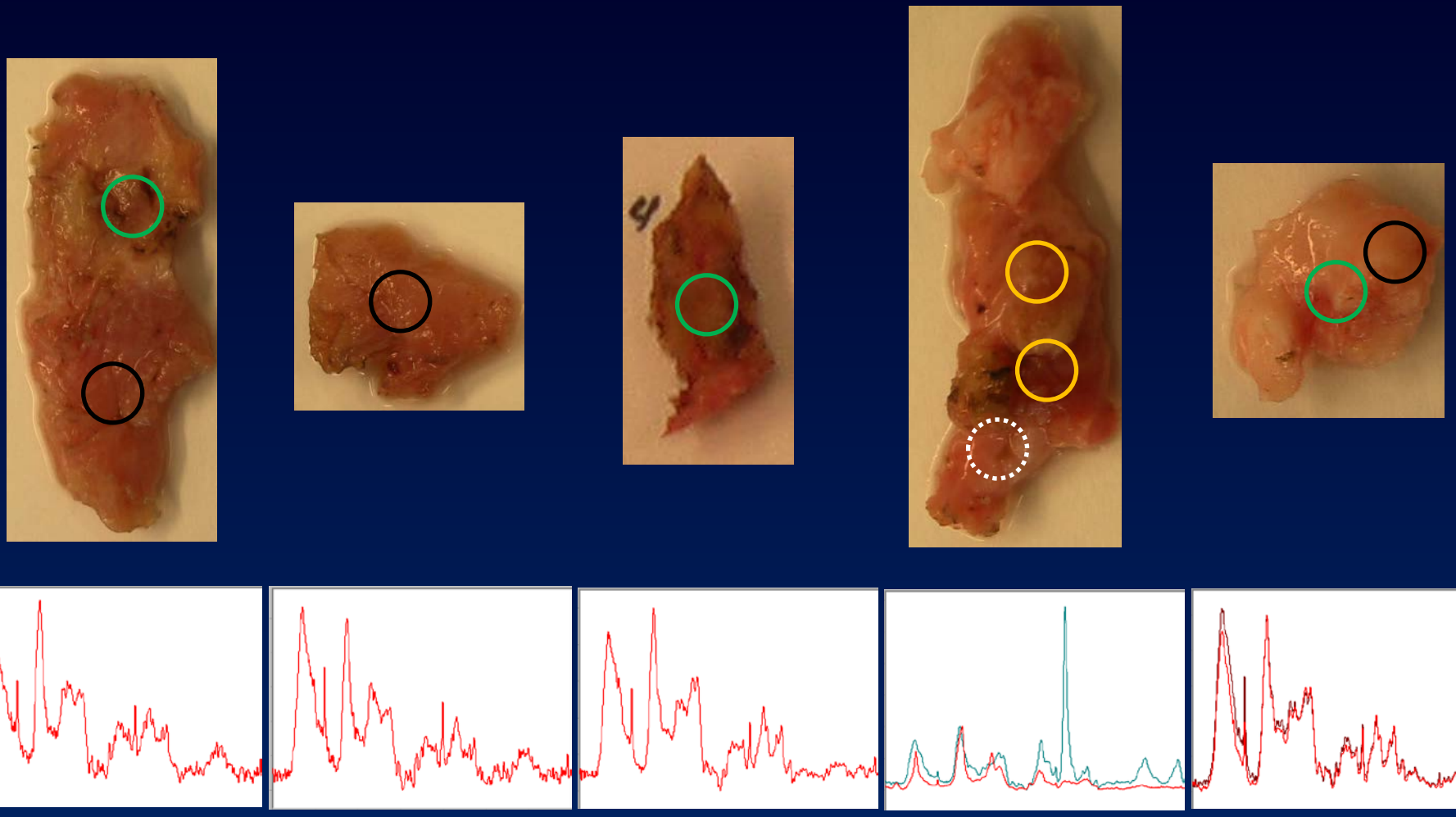

Heterotopic Ossification

- Sometimes HO tissue is incredibly obvious.

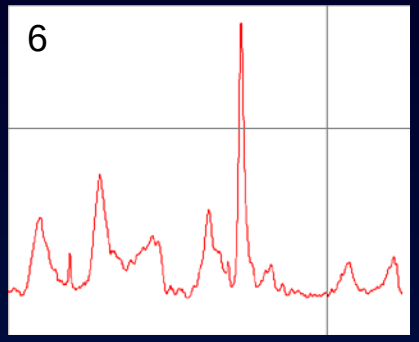

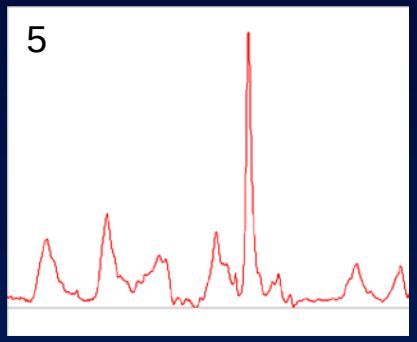

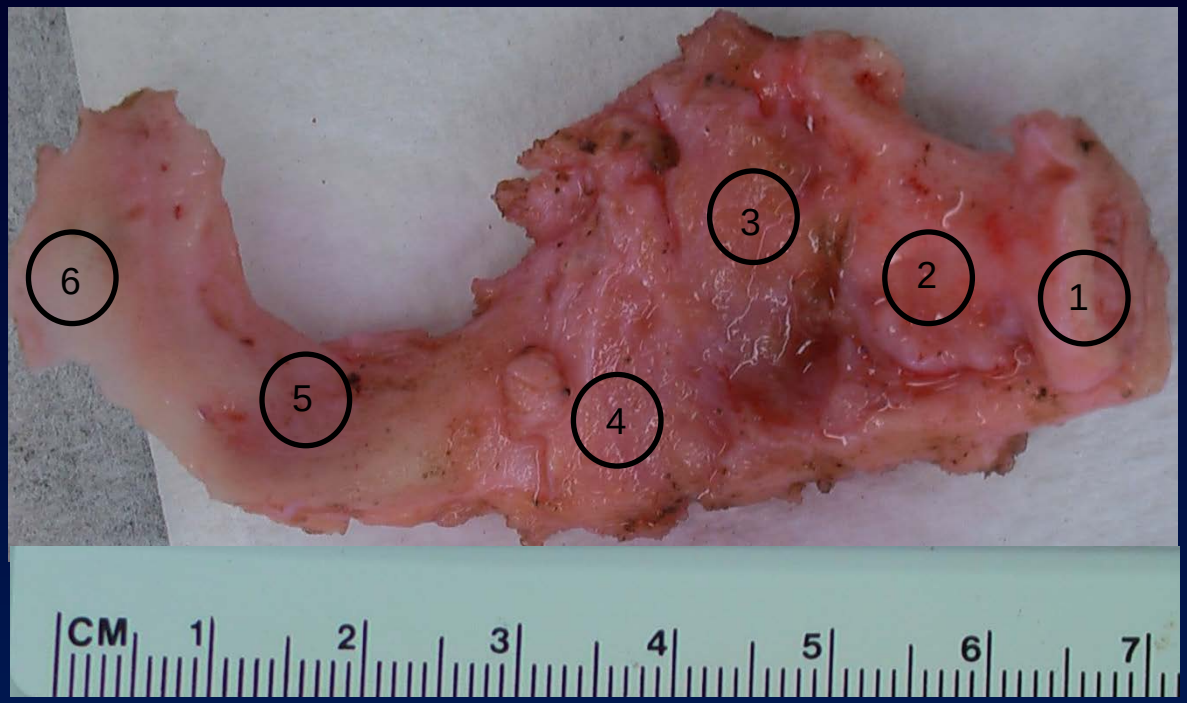

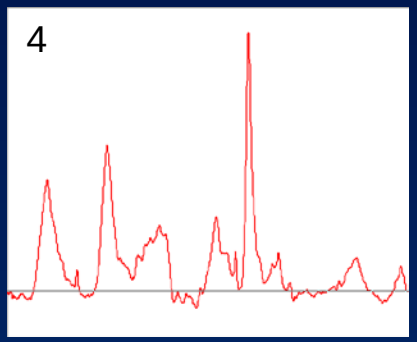

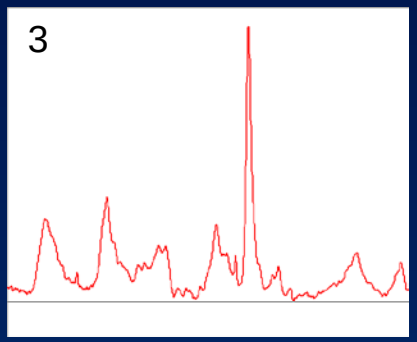

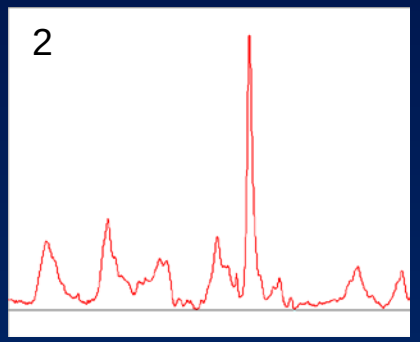

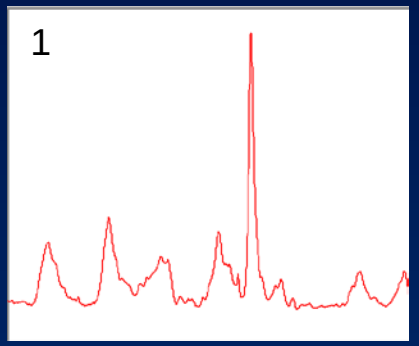

Heterotopic Ossification

Spectral comparison of muscle and collagen.

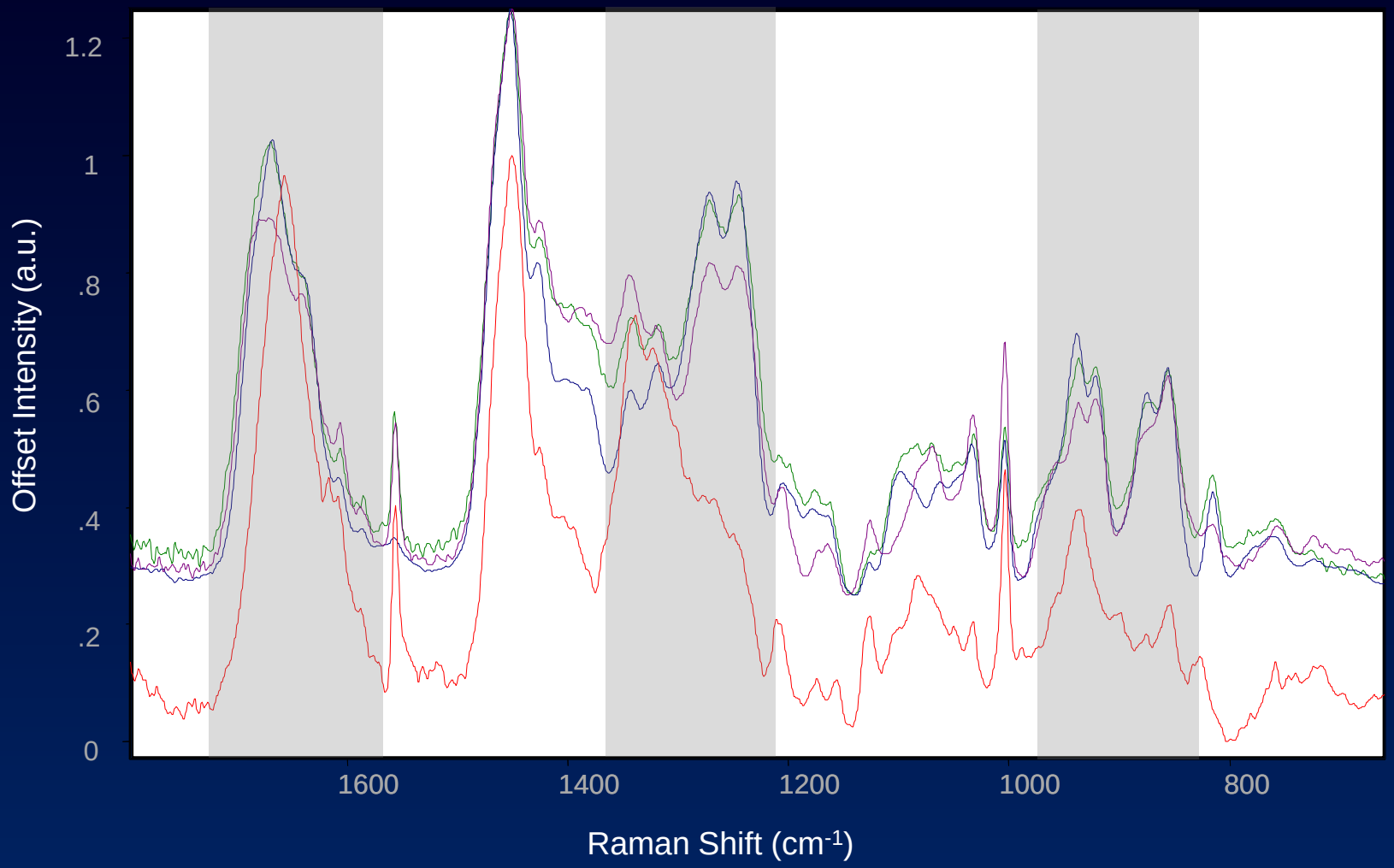

Heterotopic Ossification

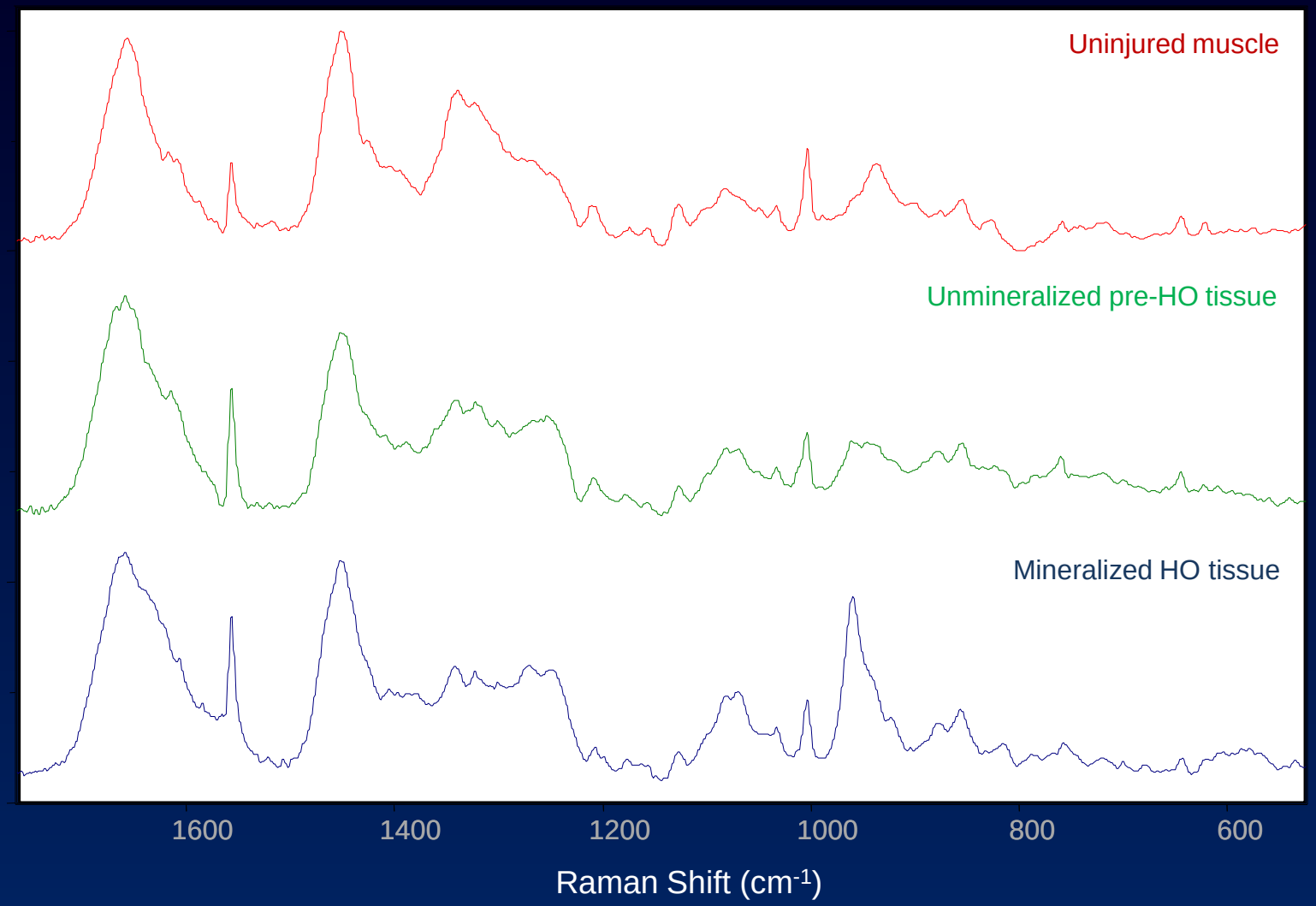

Heterotopic Ossification

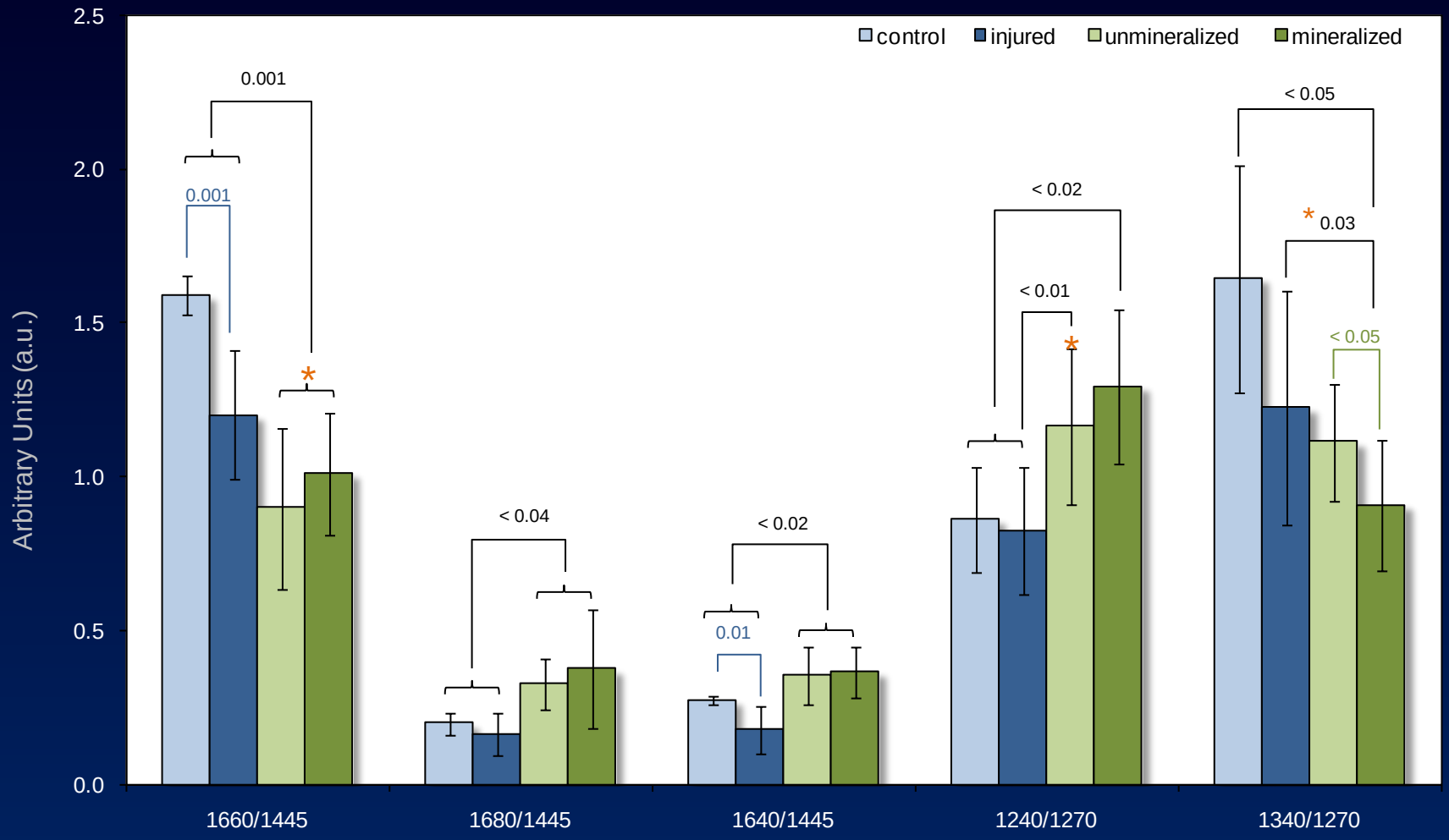

Heterotopic Ossification

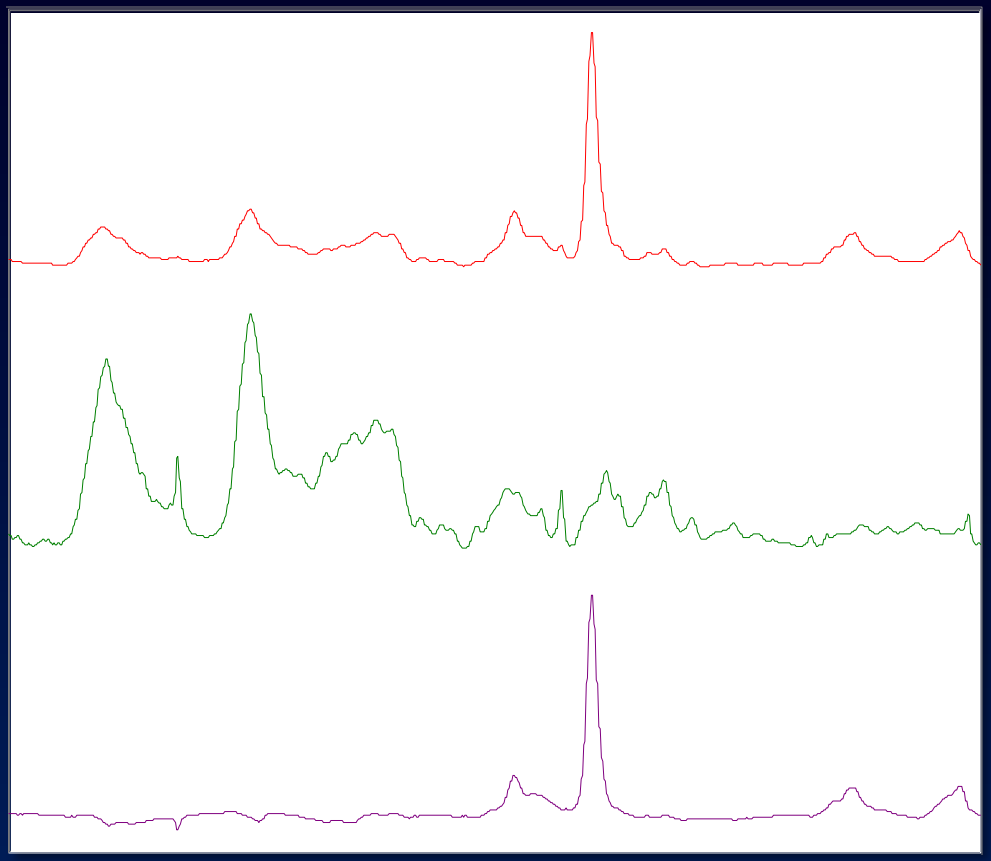

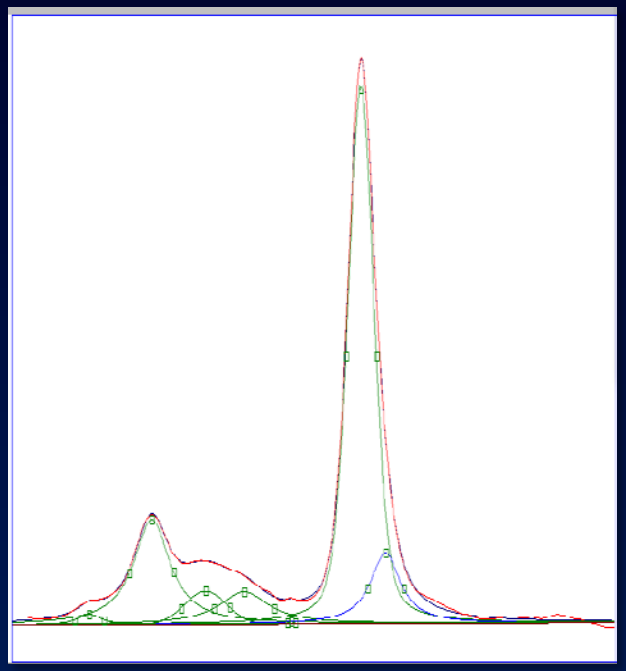

Soft tissue was subtracted from the spectrum to isolate the mineral spectrum.

Normal Bone vs. HO Bone

The adjacent femur is used as a normal bone control.

In normal bone, carbonate content increases with age (1070:960 cm^{-1} BAR), as does crystallinity (945:960 cm^{-1} BAR) and degree of mineralization.

Heterotopic Ossification

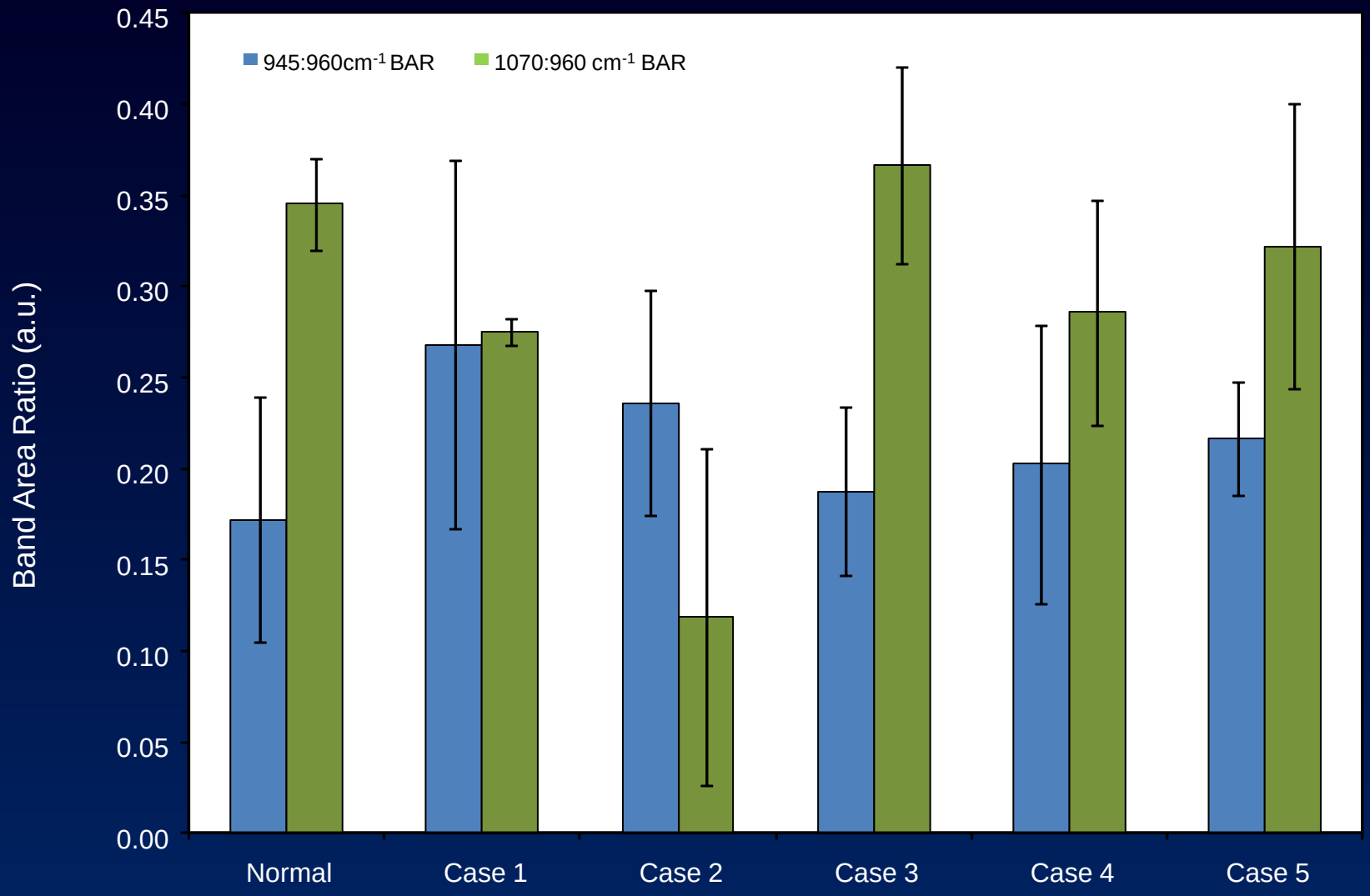

Heterotopic Ossification

- Preliminary results illuminate distinct differences between control muscle and muscle that eventually develops HO.

- HO that develops quickly after injury has lower carbonate content (1070:960 cm^{-1} band area ratio) and an increased 948 cm^{-1} shoulder (945:960 cm^{-1} band area ratio).

- We would like to be able to accurately determine which portions of the tissue are mineralizing – this has significant implications for amputation revisions. Additionally, we may be able to prevent the development of HO by accurately excising pre-HO tissue during the course of the surgical debridements.

- While we only have samples from 5 patients that developed HO, we are continuing to collect samples.

FTIR Images of Wound Effluent

Wound Effluent

- Also called exudate – fluid that filters from the circulatory system into lesions or areas of inflammation.

- Complicated mixture of various fluids, cells, and proteins.
  - *Plasma, lymph fluid, white blood cells, red blood cells, dead tissue, dead cells, cytokines, chemokines, immunoglobulins, growth factors, etc.*

Sample Preparation

- Effluent was collected from WoundVac container
  - *Sample was centrifuged at 12,000-13,000 g*
  - *Supernatant was drawn off with pipette and passed through a 0.65 μm filter*
  - *Samples stored at -20 C*
- 4μL of effluent were deposited onto an aluminized slide and allowed to air dry
- FTIR images were acquired using the Nicolet iN10 FTIR microscope
  - Imaging Parameters:

    8 cm^{-1} spectral resolution

    4000 – 715 cm^{-1} spectral range
  - Factor analysis performed on images over truncated spectral range (1870-715 cm^{-1})

Effluent from a Normal Healing Wound, Not Colonized

high intensity

low intensity

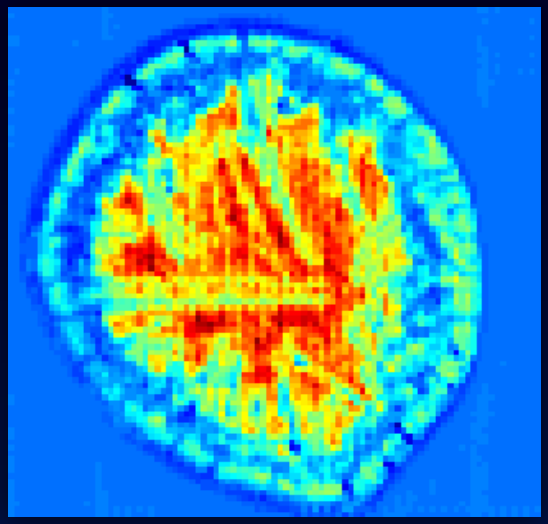

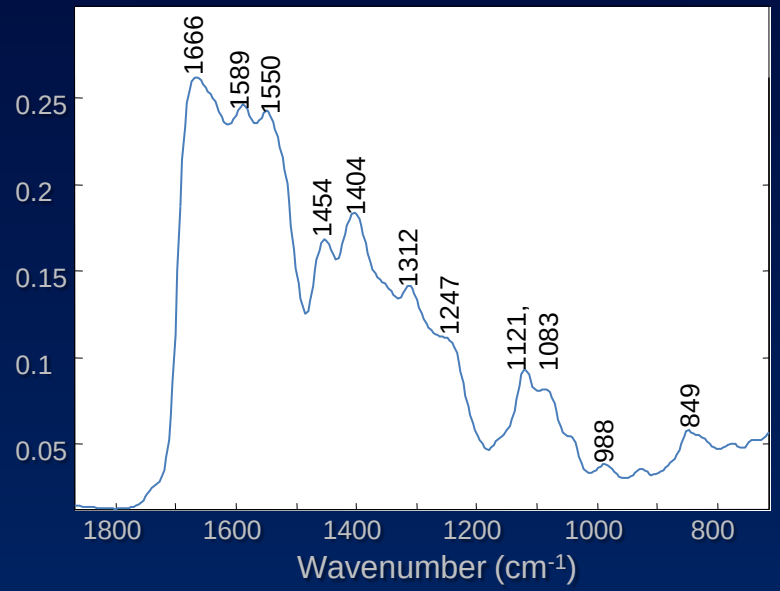

Effluent from a Dehisced Wound, Colonized with *Acinetobacter*

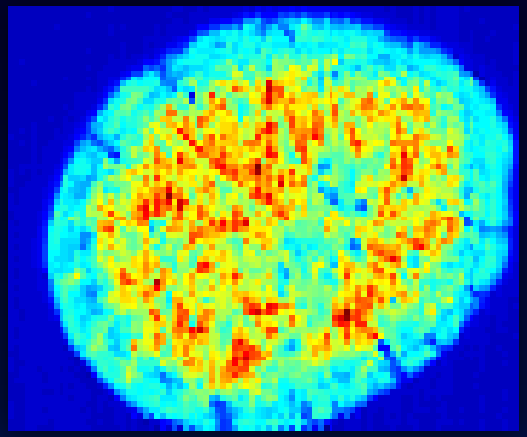

high intensity

low intensity

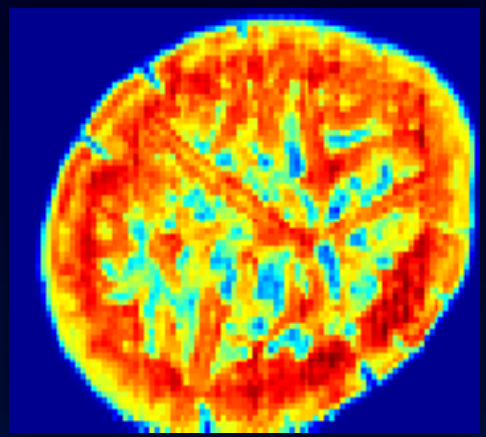

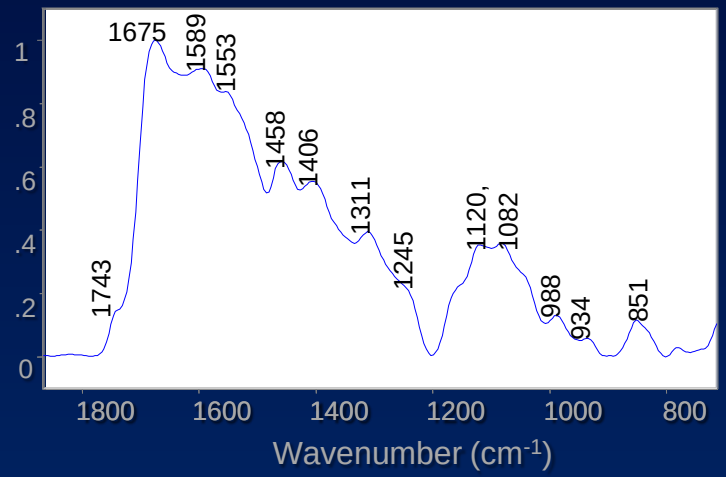

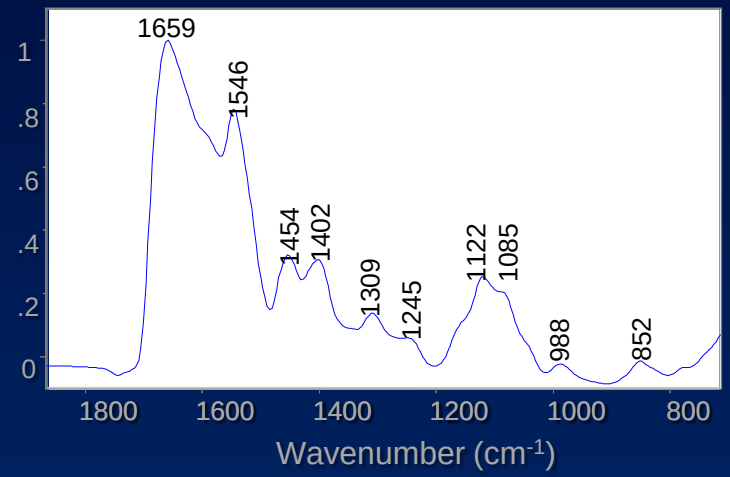

Effluent from an Impaired Healing Wound, Colonized with Acinetobacter

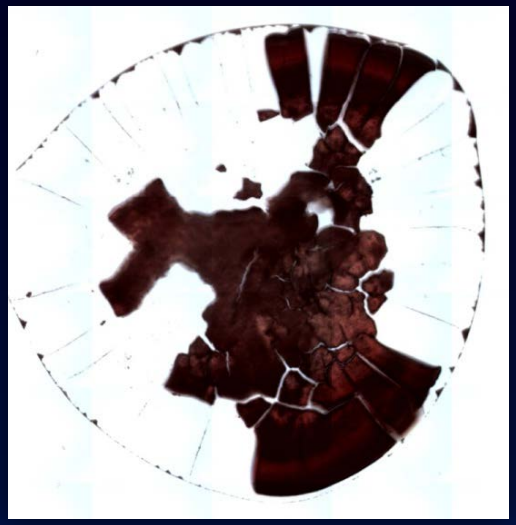

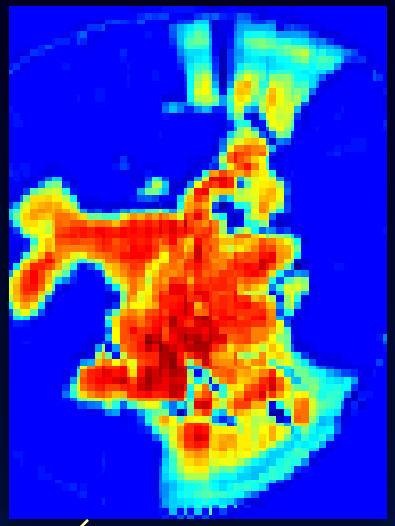

high intensity

low intensity

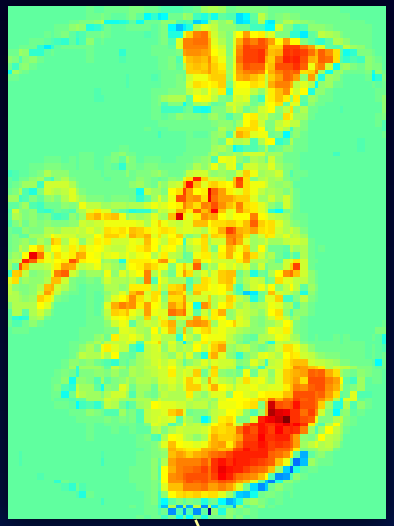

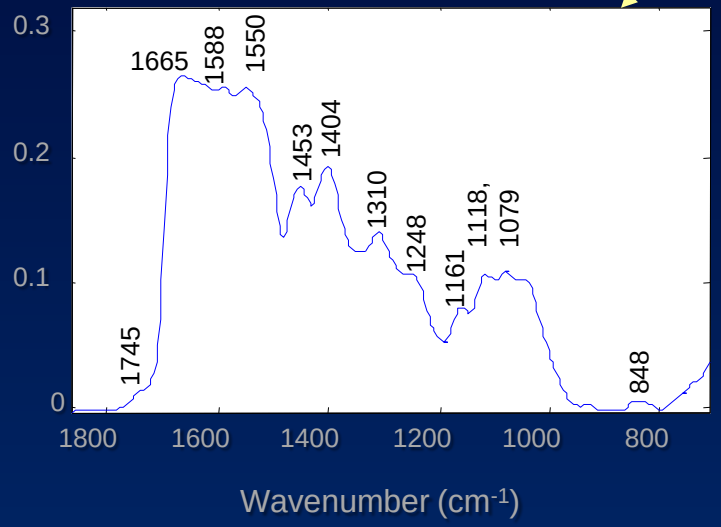

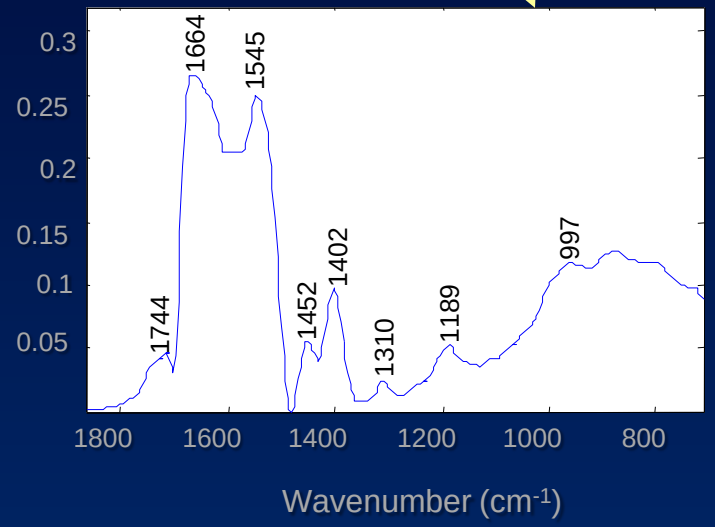

Effluent from Impaired Healing Wound, Colonized with *Acinetobacter*

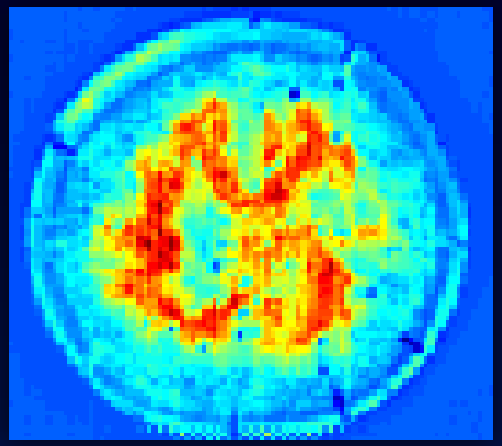

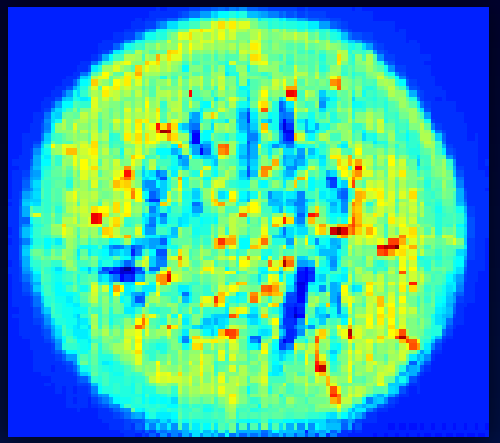

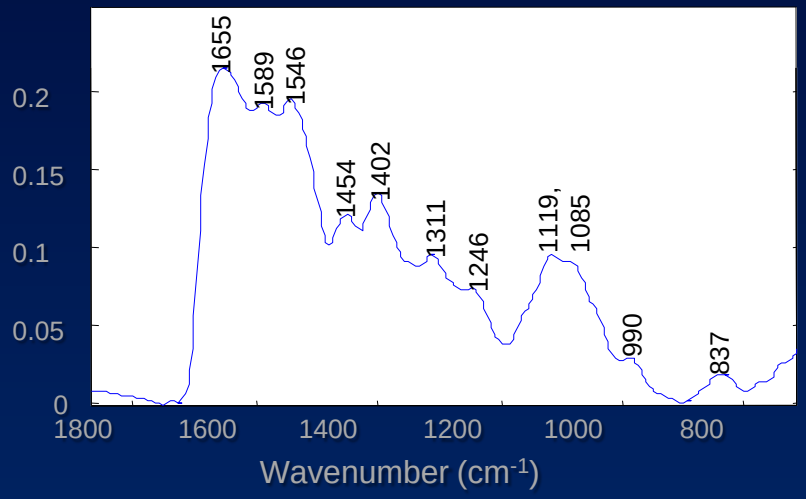

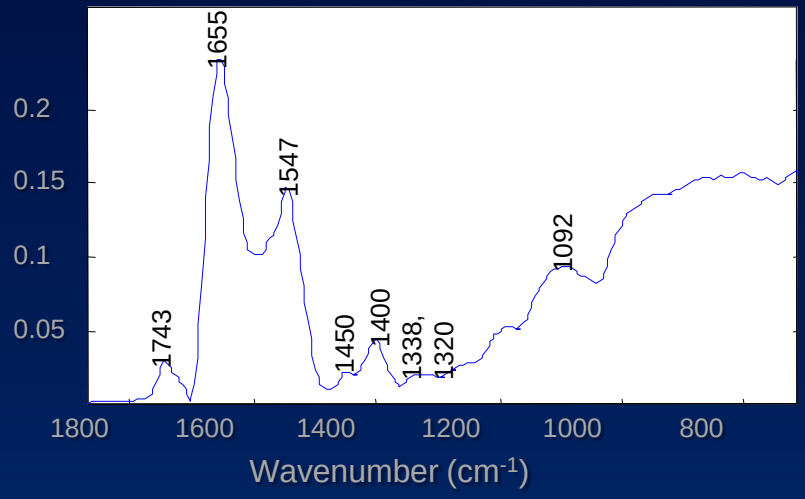

Different Strains of Biofilm-producing *Acinetobacter Baumannii*

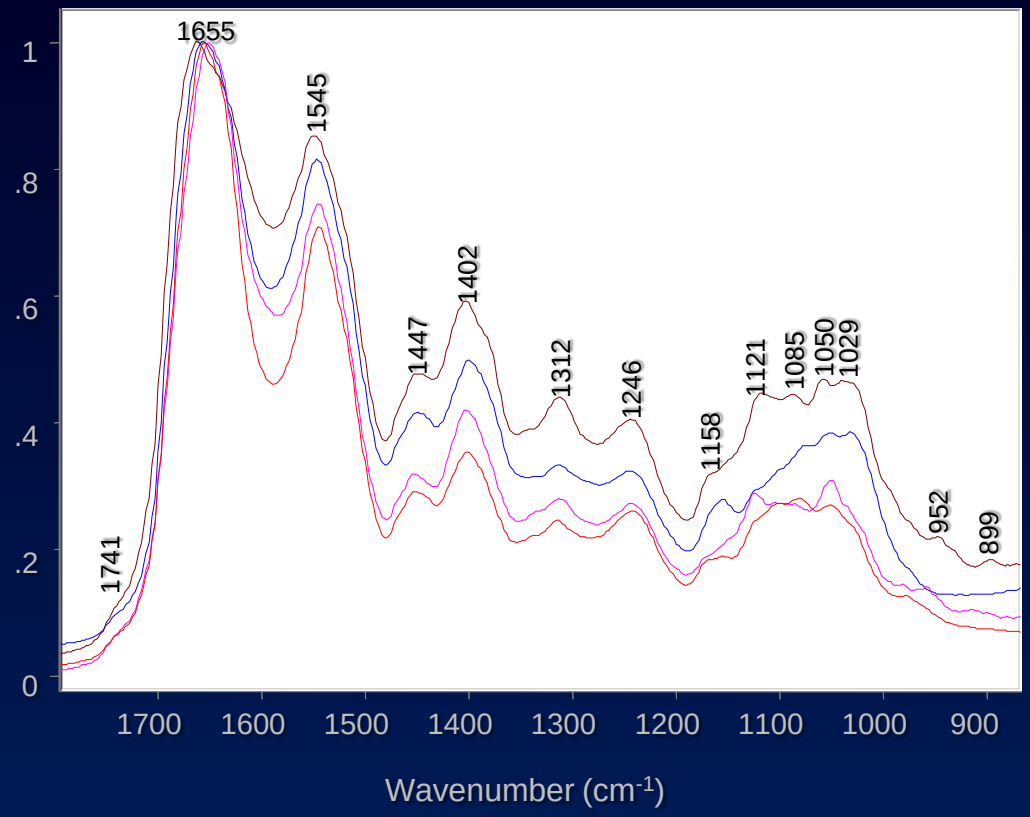

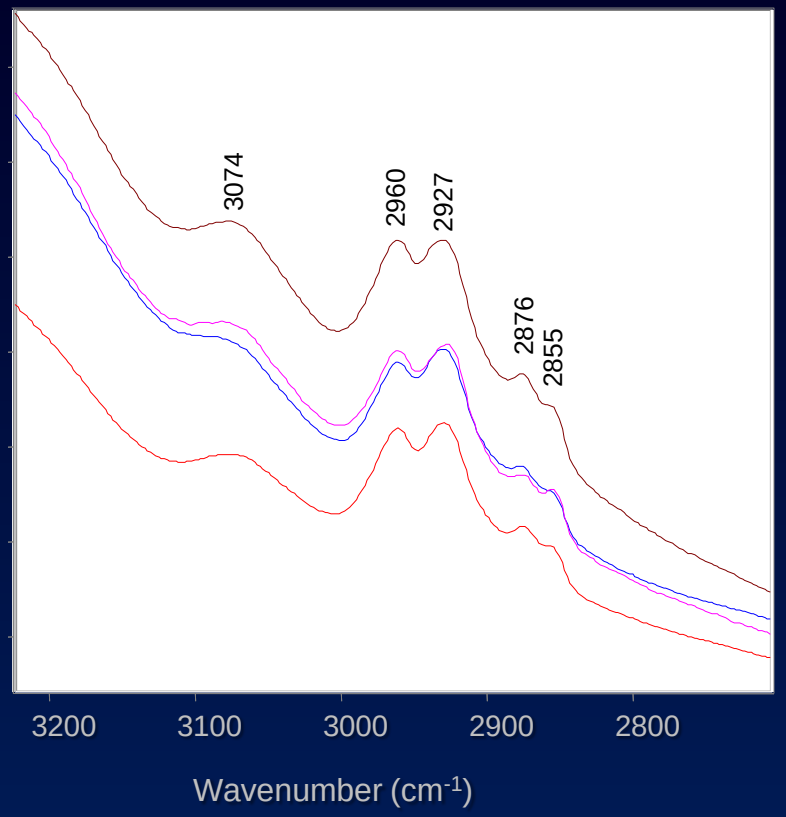

- Four strains of Acinetobacter obtained from WRAIR Infectious Diseases.
- Spectral differences largely observed from 1200-1000 cm^{-1}, attributed to saccharide components.

Comparison of *Acinetobacter* Spectra and the Second Factor

- Likely that the second factor extracted from the FTIR images is Acinetobacter, but likely a different strain from those examined.

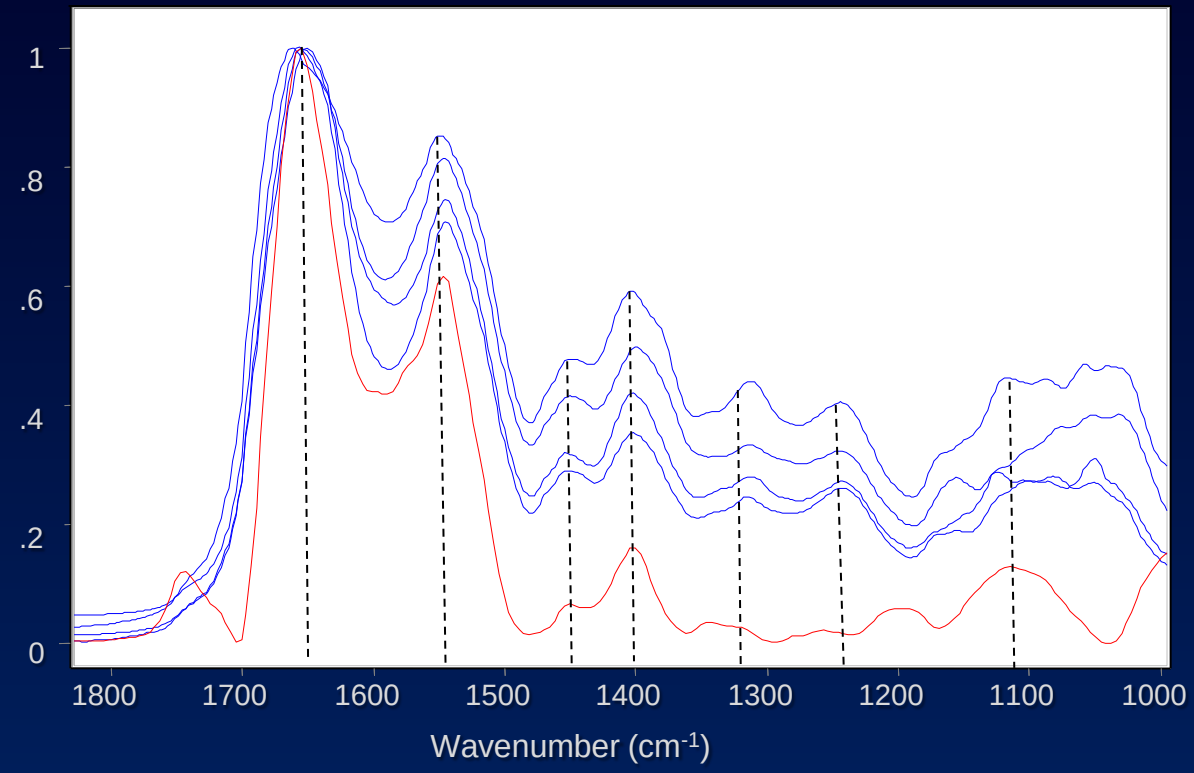

Wound Effluent

- FTIR has been previously used to identify different strains of Acinetobacter (*J Appl Microbiol. 96(2): 328-339, 2004*).
- The use of FTIR imaging has the potential to reduce the time for microbiological processing of effluent samples from 24-48 hours to 1-2 hours.
- Raman spectroscopy has also been used to differentiate Acinetobacter strains (*J Microbiol Methods. 64(1): 126-131, 2006)*; we have yet to explore the use of Raman spectroscopy with our samples.

Disclaimer

- The multidisciplinary care of these patients would not have been possible without the dedicated efforts of everyone at WRAMC and NNMC. Both civilian and military personnel have rendered skilled and compassionate care for these casualties. All of our efforts are dedicated to those who have been placed in harm's way for the good of our nation.
- The views expressed in this manuscript are those of the authors and do not reflect the official policy of the Department of the Army, Department of the Navy, the Department of Defense or the United States Government.

- This effort was supported (in part) by the U.S. Navy Bureau of Medicine and Surgery under the Medical Development Program and Office of Naval Research work unit number (604771N.0933.001.A0604).

- This study was approved by the National Naval Medical Center Institutional Review Board in compliance with all Federal regulations governing the protection of human subjects.

Acknowledgements

Naval Medical Research Center

Dr. Eric Elster
Dr. Doug Tadaki
Dr. Trevor Brown
Dr. Tom Davis
Nancy Porterfield
Frederick Gage
Eric Olsen
Wesley Stepp

National Naval Medical Center

Dr. Jonathan Forsberg
Dr. Benjamin Potter

Walter Reed Army Institute of Research

Dr. Daniel Zurowski

Walter Reed Army Medical Center

Dr. Fred O'Brien

Thermo Scientific

Heterotopic Ossification Following Combat-Related Trauma

By MAJ Benjamin K. Potter, MD, LCDR Jonathan A. Forsberg, MD, Thomas A. Davis, PhD, CPT Korboi N. Evans, MD, MAJ Jason S. Hawksworth, MD, Doug Tadaki, PhD, Trevor S. Brown, PhD, Nicole J. Crane, PhD, MAJ Travis C. Burns, MD, CPT Frederick P. O'Brien, MD, and CDR Eric A. Elster, MD

Introduction

The term *heterotopic ossification* refers to the aberrant formation of mature, lamellar bone in nonosseous tissue. Translated from its Greek (*heteros* and *topos*) and Latin (*ossificatio*) etymologic origins, heterotopic ossification can be literally defined as "bone formation in other location." The first written account of heterotopic ossification describes the treatment of symptomatic lesions. Al-Zahrawi (more commonly known in Western cultures as Albucasis), widely considered the father of surgery, wrote in the year 1000 C.E., "This callus often occurs after the healing of a fracture. . .and sometimes there is limitation of the natural function of the limb. . .if the callus is stony hard and its removal is urgent, incise the place and cut away the superfluous prominence, or pare it away with a scraper until it is gone; and dress the wound until it heals."[1] Currently, orthopaedic surgeons faced with treating mature, refractory, symptomatic heterotopic ossification are left with few options other than operative excision. Although it is remarkable that the treatment of heterotopic ossification has scarcely changed in the last millennium, it is generally accepted that prophylaxis against heterotopic ossification is far preferable than the later treatment of symptomatic lesions. As such, the focus of scientific effort in recent years has been directed toward prophylaxis, not treatment.

The formation of heterotopic ossification has been observed following total hip arthroplasty, acetabular and elbow fracture surgery, electrocution and burn injuries, and traumatic brain injury or spinal cord injury[2]. Following most traumatic injuries in the civilian population, the formation of heterotopic ossification is relatively rare in the absence of head injury. Even following traumatic brain injury or spinal cord injury, heterotopic ossification develops in only 20% and 11% of patients, respectively[3]. Rates of heterotopic ossification formation exceed 50% only in the setting of femoral shaft fractures with concomitant head injury[4], although reported rates following acetabular and elbow fractures vary substantially. Numerous combat-related injury and amputation studies from the latter half of the twentieth century make no specific mention of heterotopic ossification, suggesting that it was not a common occurrence in prior conflicts[5-8]. However, military medical texts from the U.S. Civil War and World War I[9,10] make specific mention of heterotopic ossification as a common problem following amputation, as described by Huntington: ". . .the stumps became conical sooner or later; short stumps sometimes remained well-rounded, long stumps rarely; but when they remained full it was often due to osteophytes, which in time became troublesome."[10]

Thus, since the birth of both surgery and modern warfare, heterotopic ossification has been recognized as a nameless condition that occurs following trauma. Indeed, in the current conflicts in Iraq and Afghanistan, heterotopic ossification has proven to be a frequent occurrence and a common clinical problem. The goals of the present manuscript are to summarize recent findings and the current state of science with regard to combat-related heterotopic ossification as well as to present the preliminary findings of ongoing studies and future directions.

Source of Funding

The aforementioned studies were supported, in part, by research grants from USAMRAA OTRP W81XWH-07-1-0222, the Office of Naval Research and U.S. Navy BUMED Advanced Medical Development 6.4/5 Program 604771N.0933.001.A0604.

Epidemiology of and Risk Factors for Combat-Related Heterotopic Ossification

The trend in modern warfare has shifted toward a higher percentage of extremity injuries[11-18]. This, coupled with the

Disclosure: In support of their research for or preparation of this work, one or more of the authors received, in any one year, outside funding or grants in excess of $10,000 from the U.S. Navy Bureau of Medicine and Surgery under the Medical Development Program and Office of Naval Research work unit number 604771N.0933.001.A0604 and USAMRAA OTRP W81XWH-07-1-0222. Neither they nor a member of their immediate families received payments or other benefits or a commitment or agreement to provide such benefits from a commercial entity.

introduction of improved body armor, the judicious use of tourniquets, and the availability of forward-deployed surgical units, has given rise to highly survivable yet paradoxically devastating extremity injury patterns[19,20]. As a result, the current prevalence of heterotopic ossification has been found to be higher than expected in the combat-wounded patient population[21-23].

We were the first to report this increased prevalence of heterotopic ossification in a cohort of 330 patients with 373 combat-related amputations, which are an important subset of combat casualties[23]. The study evaluated whether the mechanism of injury (blast or nonblast) correlated with either the presence or severity of heterotopic ossification. Surgery-related variables, such as the level of amputation (either within or proximal to the zone of injury), the number of irrigation and debridement procedures, the time from injury to definitive wound closure, and the prevalence of early wound complications following definitive closure, were also evaluated. The study found clinically detectable heterotopic ossification in 63% of residual limbs and, with the use of univariate analysis, identified the following important risk factors for the eventual development of heterotopic ossification: blast mechanism of injury ($p < 0.05$), and amputations performed in the zone of injury ($p < 0.05$). The latter risk factor also correlates with the severity of lesions, with use of the newly described Walter Reed Classification of heterotopic ossification[23] (Figs. 1-A, 1-B, and 1-C). Interestingly, only twenty-five limbs (6.7%) required surgical excision of symptomatic lesions and a variety of prophylactic measures against secondary recurrence were used, including a single fraction of radiation therapy (700 cGy), indomethacin, cyclooxygenase (COX)-2 inhibitors, and other nonsteroidal anti-inflammatory drugs. Importantly, despite the various means of secondary prophylaxis used, the rate of symptomatic recurrence in this subgroup was low at 0%.

We also defined the prevalence of heterotopic ossification in a separate cohort of patients with combat-related extremity trauma requiring orthopaedic intervention[21]. Two hundred and forty-three patients requiring amputation, external fixation, or internal fixation were evaluated. This cohort study compared 157 patients who developed heterotopic ossification (the study group) to eighty-six patients who did not (the control group). This design enabled us to estimate the prevalence of heterotopic ossification not only in amputees (66% of lower-extremity amputees and 30% of upper-extremity amputees), but also in patients undergoing limb salvage (60.1%). The findings from the former study[21] corroborated our earlier findings[23]. The data from the later study[21] suggested that combat-related injuries, in general, are associated with a higher-than-expected prevalence of heterotopic ossification, when compared with civilian data[3,4,24-29].

This study[21] also identified several important risk factors for the development of heterotopic ossification in this patient population. Traumatic brain injury was associated with both the presence ($p = 0.006$) and the severity ($p = 0.003$) of heterotopic ossification on univariate but not multivariate analysis. Regression analysis revealed that the Injury Severity Score (as a continuous variable) and an Injury Severity Score of ≥16 ($p = 0.02$, odds ratio = 2.2) were significant predictors, as was multiple limb trauma requiring orthopaedic intervention ($p = 0.002$, odds ratio = 3.9). The most striking observation, however, was that the presence of an amputation was, itself, independently associated with the development of heterotopic ossification ($p = 0.048$, odds ratio = 2.9).

The association between heterotopic bone growth and the number and method of surgical debridement procedures, including the use of negative-pressure wound therapy, is controversial. We have observed, on univariate analysis, that patients who subsequently developed heterotopic ossification have undergone more debridement procedures ($p < 0.001$) and thus have been exposed to a longer duration of negative-pressure wound therapy ($p < 0.001$)[21]. Nevertheless, these results should be interpreted with caution because the increases in both the number of debridement procedures and the duration of negative-pressure wound therapy are likely more indicative of the severity of injury than they are causal. This is supported by the nonsignificant relationship between the formation of ectopic bone and these wound-care modalities as revealed by multivariate analysis[21]. Although local factors may play a supporting role, current data[21,23] suggest that the development of heterotopic ossification in this patient population is largely due to systemic factors.

Barriers to Primary Prophylaxis

Given the high prevalence of combat-related heterotopic ossification in our war-wounded patients, a primary prophylaxis regimen including radiation therapy, conventional nonsteroidal anti-inflammatory drugs, and/or etidronate (an older, nonselective bisphosphonate and the only medication currently approved by the U.S. Food and Drug Administration for the treatment or prevention of heterotopic ossification) would be extremely appealing. Local radiation therapy, generally administered within twenty-four hours preoperatively to forty-eight hours postoperatively in patients at risk for heterotopic ossification, and nonsteroidal anti-inflammatory drugs have well-documented efficacy in the prevention of primary heterotopic ossification[21,23,30-40]. Recent meta-analyses and reviews have suggested that radiation therapy may be slightly more effective than nonsteroidal anti-inflammatory drugs for this purpose, although most of this difference is thought to be related to patient noncompliance with medication[35,41]. Unfortunately, the vast majority of severely injured combatants have multiple medical contraindications to prophylaxis against heterotopic ossification that make the interventions listed above difficult to accomplish. Commonly encountered relative and absolute contraindications to prophylaxis against heterotopic ossification include severe systemic polytrauma, open and contaminated wounds, concomitant traumatic brain injury and/or long bone fractures or spinal column injuries requiring operative stabilization and fusion, and the need for serial surgical procedures. Additionally, substantial potential for impaired renal function, bleeding, and stress gastritis have precluded widespread use of nonsteroidal anti-inflammatory drugs to date. Logistical limitations at remote, far-forward medical facilities in the theater of war are additional hurdles, particularly for the timely administration of radiation therapy.

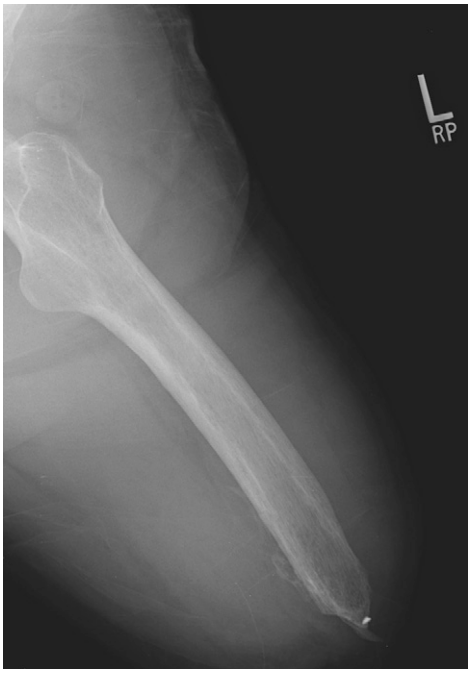

Fig. 1-A

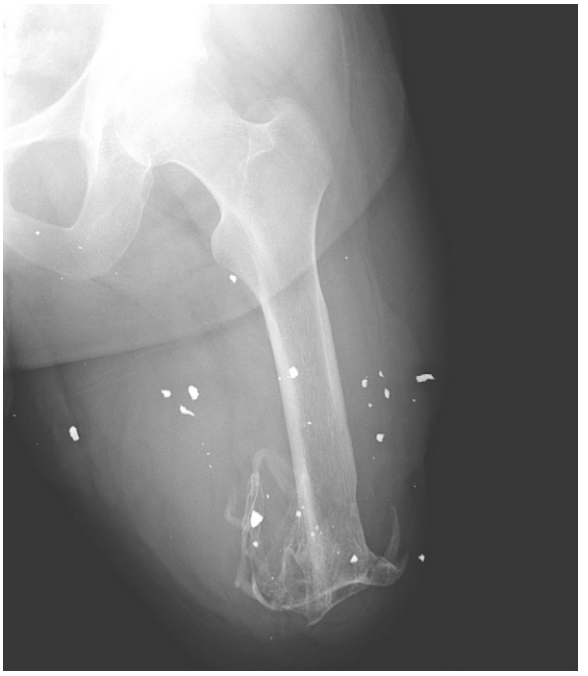

Fig. 1-B

Fig. 1-C

Figs. 1-A, 1-B, and 1-C Representative radiographs depicting the Walter Reed classification system for grading the severity of heterotopic ossification in the residual limbs of amputees. The severity of heterotopic ossification is graded on the basis of the single radiographic projection (either anteroposterior or lateral) that demonstrates the greatest amount of ectopic bone within the soft tissues of the residual limb. The heterotopic ossification is considered to be (Fig. 1-A) Grade I (mild) if it occupies <25% of the cross-sectional area of the residual limb on the radiograph; (Fig. 1-B) Grade II (moderate) if it occupies 25% to 50% of the cross-sectional area; and (Fig. 1-C) Grade III (severe) if it occupies >50% of the cross-sectional area.

Etidronate can be administered later in the period after injury, but there can be problems with late mineralization or formation of heterotopic ossification after the cessation of medication. Thus, the efficacy of etidronate has recently been called into question by, among others, a recent Cochrane Database review[42]. Etidronate is also a relatively nonselective osteoclast inhibitor, potentially owing its limited efficacy to osteoblast inhibition, and may inhibit fracture-healing and spinal fusion. Corticosteroids, colchicine, retinoid agonists, coumarin derivatives, and calcitonin have all been studied for their value with regard to prophylaxis against heterotopic ossification; however, the data on human usage is either limited or absent and these drugs share many of the same medical concerns and contraindications as nonsteroidal anti-inflammatory drugs[23,43-48]. Thus, no

practicable primary prophylactic regimen for combat-related heterotopic ossification has been identified, although a trial of the COX-2 inhibitor celecoxib is in development, as discussed below.

Clinical Sequelae of Combat-Related Heterotopic Ossification

Fortunately, some patients with combat-related heterotopic ossification remain entirely asymptomatic and no specific treatment is indicated. In many others, lesions are transiently painful or bothersome and symptoms subside as adjacent joint motion improves, residual limb "toughening" occurs, and the combat-related heterotopic ossification transitions from its more inflammatory formative phase into a more quiescent maturation phase. Many patients, however, develop symptoms directly attributable to their combat-related heterotopic ossification that persist indefinitely. These symptoms may be localized pain, including, but not limited to, residual limb pain and prosthetic fitting difficulties; ulceration, particularly when the combat-related heterotopic ossification develops beneath an overlying skin graft (Figs. 2-A and 2-B); overt joint ankylosis; secondary arthrofibrosis due to osseous impingement (Figs. 3-A and 3-B); muscle entrapment (Fig. 4); or neurovascular entrapment (Figs. 5-A and 5-B). The treatment of symptomatic combat-related heterotopic ossification is individualized to the patient and the symptoms associated with their combat-related heterotopic ossification.

Management of Symptomatic Combat-Related Heterotopic Ossification

In the absence of overt ulceration causing concomitant deep infection or overt joint ankylosis, the initial management of symptomatic combat-related heterotopic ossification is nonoperative. This generally includes a period of rest, physical therapy, and gentle stretching and splinting to treat secondary contractures. Taking pressure off of symptomatic areas by positioning, pads or prosthetic socket adjustments, and optimizing pain control and medication regimens are also important. Other potentially contributing causes of pain should be investigated and treated appropriately including infection, fracture nonunion, internal derangement of adjacent joints, symptomatic neuromata, phantom pain, and complex regional pain syndrome. When nonoperative measures fail, concurrent procedures in addition to "simple" heterotopic ossification excision are often indicated and appropriate including amputation revision, neuroma excision, quadricepsplasty, contracture release, and/or skin graft excision. The most common indications for excision of combat-related heterotopic ossification in our military patients are pain that is caused by wearing a prosthesis and that has proven to be refractory to multiple socket adjustments, and arthrofibrosis in patients for whom limb salvage will be attempted.

Abundant recent evidence suggests that a prolonged waiting period of twelve to twenty-four months for heterotopic ossification "maturation" prior to excision is not necessary in the post-extremity trauma setting, particularly in the absence of traumatic injury to the brain or spinal cord[23,49-58]. Instead, a waiting period of six months after injury appears to be adequate to permit sufficient bone maturation to ensure the presence of a gross cortical rind to facilitate marginal excision and to permit a diligent trial of nonoperative treatments. Patients with recalcitrant ulcerations or severe secondary joint contractures may become operative candidates as early as three to four months after injury.

Operative Planning and Three-Dimensional Modeling

The operative approach to combat-related heterotopic ossification must account for the local anatomy, the location and severity of the heterotopic ossification, and the patient's prior wounds and incisions. We advocate a direct approach utilizing, when feasible, existing incisions, followed by marginal excision of the symptomatic lesion(s). The entirety of the heterotopic ossification need not be removed when the patient's symptoms are focal, particularly when access to the entire lesion would be difficult and the combat-related heterotopic ossification has a mature cortical shell. Wide excision to prevent recurrence would not be feasible in most patients because of the magnitude of tissue sacrifice that would be required. We have noted infrequent recurrences following excision about the elbow, but no symptomatic recurrences in residual limbs or about the thigh in more than 100 patients (unpublished data). This surgical approach has been coupled with the judicious use of secondary prophylaxis with nonsteroidal anti-inflammatory drugs. The decision was made to incorporate the use of secondary prophylaxis into our treatment protocol because of the high rate of wound complications in our initial series of amputees who were treated with radiation, which is used along with nonsteroidal anti-inflammatory drugs in patients with the most severe conditions[23,38]. However, the prognosis for concomitant excision and quadricepsplasty of the thigh for treatment of combat-related heterotopic ossification is guarded as a result of anecdotally high rates of wound complications, recurrent arthrofibrosis, extensor mechanism compromise, or preexisting arthrosis due to prior fractures, prolonged immobilization, or ankylosis.

Computed tomography-based three-dimensional modeling is very useful in the evaluation and treatment of symptomatic combat-related heterotopic ossification (Figs. 6-A and 6-B). Clinically, it is useful for allowing patients, therapists, and prosthetists to anatomically localize symptomatic areas and take efforts to avoid irritation through the use of activity modification, prosthetic socket relief, or model-assisted stereolithographic socket design. For the patient with symptomatic combat-related heterotopic ossification, resin models are useful for both preoperative planning and intraoperative referencing. The formation of combat-related heterotopic ossification distorts normal anatomy, placing critical neurovascular structures and muscle groups at risk for inadvertent injury. In some instances, major nerves and vessels may pass directly through and be incarcerated in the combat-related heterotopic ossification. The physical resin models serve as intraoperative anatomical guides that are based on heterotopic ossification topography. This is particularly helpful for patients in whom the condition is severe or for patients in whom excision of the focal, symptomatic combat-related

Fig. 2-A

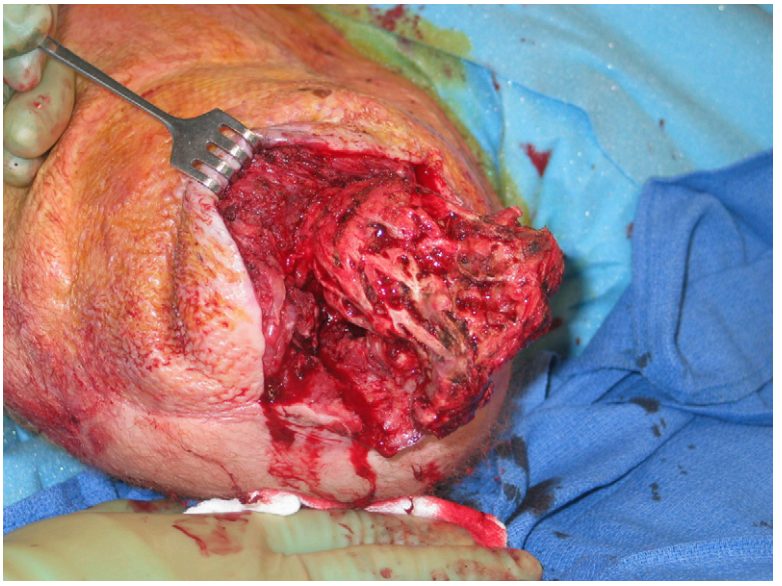

Fig. 2-B

Fig. 2-A Clinical photograph demonstrating overt ulceration of split-thickness skin graft of a transfemoral amputation due to underlying heterotopic ossification.

Fig. 2-B Intraoperative photograph during marginal excision of the heterotopic ossification with concurrent revision of the amputation in the same patient.

heterotopic ossification is attempted in an effort to avoid complete takedown of the myodesis and revision of the amputation stump.

Biochemical Signature of Heterotopic Ossification

It is generally accepted that systemic inflammation is associated with the development of heterotopic ossification. Evans et al.[59] examined the systemic and local wound inflammatory response in twenty-four patients with high-energy, penetrating extremity wounds. In preparation for the development of a prognostic clinical decision model, the goal of this pilot study was to identify whether a particular cytokine and chemokine profile could be identified in those at risk of developing heterotopic ossification. Serum and wound effluent samples were collected prior to each of these procedures in a manner previously described[60,61]. Twenty-two cytokines and chemokines (including interleukin [IL]-1 through 8, 10, 12, 13, and 15; interferon [IFN]-γ; eotaxin; tumor necrosis factor [TNF]-α; monocyte chemotactic protein [MCP]-1; granulocyte colony stimulating factor [GCSF]; macrophage inflammatory protein

Fig. 3-A

Fig. 3-B

Figs. 3-A and 3-B Anteroposterior radiograph (Fig. 3-A) and sagittal computed tomography reconstruction (Fig. 3-B) of a transfemoral amputation with limited hip flexion due to direct impingement of severe heterotopic ossification against the anterior pelvic brim and acetabulum.

[MIP]-1α; the protein regulated on activation, normal T expressed and secreted [RANTES]; and IFN-γ inducible protein-10) were quantified. After a minimum follow-up of two months, subjects were then stratified according to a two-author (K.N.E. and J.A.F.) blinded review of radiographs into a study group and a control group, on the basis of the presence or absence of heterotopic ossification within the wounded extremity.

Serum analysis demonstrated a profound systemic inflammatory response in the study group. Of the twenty-two serum cytokines and chemokines analyzed, only three (IL-6, IL-10, and human MCP-1 [also known as chemokine (C-C motif) ligand 2, or CCL-2]) differed significantly between the two groups (unpublished data). Specifically, IL-6 remained elevated at all time points, as did MCP-1. Both are inflammatory agents and recruit monocytes and macrophages to the site(s) of injury, indicating sustained inflammation throughout the debridement process. MCP-1, however, is also involved in bone remodeling and may be an early indicator of this process. Interestingly, concentrations of IL-10, an anti-inflammatory cytokine that is important in inhibiting the production of pro-inflammatory cytokines, became significantly more concentrated in the study group approximately two weeks after injury, as compared that in the control group. The late upregulation of this anti-inflammatory mediator also signifies the presence of persistent systemic inflammation and supports our previous observation[62] that the systemic inflammatory response in this patient population has aberrant regulation.

An analysis of the local wound effluent during the serial debridement process produced similar findings. Wounds that developed heterotopic ossification expressed significantly higher concentrations of MIP-1α and lower concentrations of IFN-γ-inducible protein-10 in the study group as compared with controls. Although both are considered pro-inflammatory, their prolonged, discordant expression, without a demonstrable compensatory anti-inflammatory component, also appears dysregulated. The change in the regulation of the inflammatory response that was observed systemically also seems to persist within the local wound environment. As such, the association between these biomarkers and heterotopic ossification may not simply be related to the difference in concentration between the two groups, but rather, the relationship between pro-inflammatory and anti-inflammatory mediators as well as their relative time-dependent concentrations as measured throughout the debridement process.

Progenitor Cell Research

The cellular and biochemical etiology and pathophysiology of heterotopic ossification remain unclear. A postulate theory is that heterotopic ossification results from the presence of osteoprogenitors that pathologically are induced by an imbalance of local and/or systemic factors in soft tissue following traumatic injury. It is thought that a systemic increase in the

Fig. 4

Lateral radiograph of the distal part of the femur of a patient with fractures of the femoral shaft and tibial plateau, above a transtibial amputation. The radiograph shows arthrofibrosis of the knee joint secondary to entrapment of the quadriceps muscle by heterotopic ossification at the anterior portion of the femur, extending from the femoral shaft fracture callus. The patient had only 10° of total knee motion (5° to 15°) at eight months after a blast injury. He underwent excision of the heterotopic ossification with concurrent release of the knee and quadricepsplasty and achieved an intraoperative range of motion of 0° to 115°. Following a subsequent manipulation under anesthesia at seven weeks postoperatively, the patient was able to maintain a range of motion of 0° to 105°. In our experience, however, such results are not typical, with frequent recurrence of arthrofibrosis, infection, and/or compromise of the extensor mechanism, generally occurring even in the absence of recurrent heterotopic ossification.

osteogenic potential of endogenous muscle progenitor cells occurs in these severely injured patients in the immediate period after trauma.

Mesenchymal stem cells are multipotent, adult progenitor cells of great interest because of their unique immunologic properties and regenerative potential[63]. Mesenchymal stem cells reside within most adult connective tissues and organs[64]. Muscle-derived mesenchymal progenitor cells have been shown to be inherently plastic, enabling them to differentiate along multiple lineages; they promote wound-healing and regeneration of surrounding tissues by migrating to the site of injury, promoting repair and regeneration of damaged tissue, modulating immune and inflammatory responses, stimulating the proliferation and differentiation of resident progenitor cells, and secreting other trophic factors that are important in wound-healing and tissue remodeling[63,65-68]. Several recent reports describe the isolation and characterization of extensively passaged mesenchymal cell-like progenitor cells (MPCs) isolated from tissue collected following surgical debridement of traumatic orthopaedic extremity wounds[67,69-71]. Yet, the effects of acute and often prolonged aberrant inflammation[62] on muscle-derived mesenchymal cells are unclear.

We speculate that the initiation of heterotopic ossification involves a complex interplay of signaling molecules secreted from the injured tissue. Proliferation and recruitment of local and/or circulating progenitor cells and the aberrant commitment, growth, and differentiation of these cells into bone occur early in the process of wound-healing and repair. In a series of preliminary studies, we have found that wound effluent collected strictly from patients with heterotopic ossification at times of early wound debridement is highly osteogenic, which accelerates the directed in vitro osteogenic differentiation of multipotent bone-derived mesenchymal stem cells in culture (Fig. 7). In contrast, mesenchymal stem-cell cultures treated with wound effluent alone, without exogenous exposure to standard induction media, had no measurable effect on the induction of bone formation. Therefore, there is some strong preliminary evidence that severe trauma leads to the release and delivery of osteogenic factors. The identity of these factors and how they interact with progenitor-cell signaling remain unknown.

Currently, little is known about the precursor cell to heterotopic ossification or the environment that permits formation of heterotopic ossification. Understanding the signaling pathways and the involvement of MPC differentiation is essential for the development of early diagnostic and prognostic tests and the development of novel prophylactic therapies. We have developed a unique cell-isolation process and in vitro culture system to easily quantify functionally assayable multipotent muscle-derived progenitor cells at the clonal level. The multipotent differentiation capacity of individual clonal cell-derived colonies can be easily assessed by their ability to undergo osteogenic, chondrogenic, and adipogenic differentiation when incubated with specific differentiation induction media. Using this system, we tested the hypothesis that endogenous muscle-derived progenitor cells following severe blunt trauma are greater in number and have a stronger osteogenic potential in patients in whom wound-healing is associated with the formation of combat-related heterotopic ossification than in patients whose wounds heal uneventfully. We prospectively collected wound muscle biopsies during debridements of ten active-duty service members who sustained high-energy penetrating injuries of an extremity during combat operations. Ectopic bone formation was determined by follow-up radiographic assessment at various intervals during the recovery period and was compared with culture results. We also collected hamstring muscle as control tissue from five healthy

Fig. 5-A

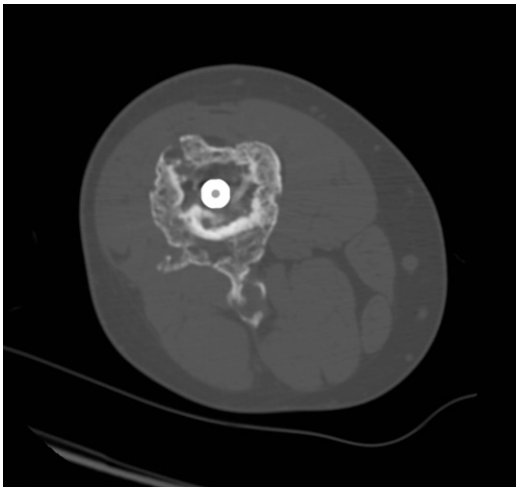

Fig. 5-B

Figs. 5-A and 5-B Lateral radiograph (Fig. 5-A) and axial computed tomography scan (Fig. 5-B) showing a femoral shaft fracture. Fracture-healing was complicated by heterotopic ossification, which caused symptomatic entrapment of the sciatic nerve (i.e., decreased distal motor function and dysesthesia of the foot, exacerbated by deep knee flexion). Partial excision of the heterotopic ossification was performed along with neurolysis and decompression of the sciatic nerve. Distal motor and sensory function were retained, and the patient's symptoms abated.

patients undergoing elective anterior cruciate ligament reconstruction with hamstring autograft. We found that the number of adherent colony-forming progenitor cells that could be isolated per gram of tissue from wartime wounds was profoundly increased (range, thirty-twofold to fiftyfold) compared with the number in the uninjured muscle tissue of the control group (Fig. 8). Quantification of progenitor cells with osteogenic potential showed that the measured 2.3-fold increase in osteogenic progenitors in tissue from patients with combat-related heterotopic ossification compared with that in tissue from patients with noncombat-related heterotopic ossification was significant ($p < 0.007$)[72]. Therefore, these findings suggest that wounds that present with a higher prevalence of resident assayable osteoprogenitors in the tissue, presumably supported through local and/or systemic reactions, correlate with the eventual formation of ectopic bone in traumatized tissue.

Raman Spectroscopy

Raman spectroscopy is a scattering technique that can be used to gain information about the structure and composition of molecules from their vibrational transitions. A Raman spectrum can be thought of as a chemical "fingerprint" and is thought of as a complementary technique to the more widely known infrared spectroscopic techniques. The vibra-

Fig. 6-A

Figs. 6-A and 6-B Digital three-dimensional computed tomography reconstruction (Fig. 6-A) and photograph of the corresponding life-size three-dimensional resin model (Fig. 6-B) of both residual limbs and the pelvis of a blast-injured bilateral transfemoral amputee with severe heterotopic ossification of both residual limbs. The model was a useful reference intraoperatively during the staged surgical procedures to excise the heterotopic ossification and revise the amputation, as it provided a ''roadmap'' of the surface topography of the ectopic bone.

tional (and rotational) bands in a Raman spectrum are specific to the chemical bonds and particular structure of the molecule(s) being investigated. In addition, the band area of a Raman vibrational band is proportional to the amount of analyte present. Thus, Raman spectroscopy can identify the components that are present and quantify the amount of each component.

Over the past fifteen years, Raman spectroscopy has become an attractive technology for probing biomedical samples for several reasons. First, Raman spectroscopy can be used to study both organic and inorganic components (i.e., protein and mineral). Second, Raman spectroscopy can be applied noninvasively. Recent in vivo Raman spectroscopic studies include incorporation of a Raman probe into an endoscope for examination of the esophagus and stomach[73,74], detection of cervical dysplasia[75], diagnosis of nonmelanoma skin cancer[76], characterization of psoriatic skin[77], observation of human-swine coronary xenografts after transplantation[78], measurement of macular carotenoids in the eye[79-82], and transcutaneous monitoring of bone[83]. Third, most biological samples contain water, and unlike infrared spectroscopy, the Raman spectra of biological samples do not suffer from spectral interference of water vibrational bands. Fourth, Raman spectroscopy is a scattering technique, requiring very little, if any, sample preparation. Finally, the technological advances during the past fifteen years, such as holographic notch filters, small-form diode lasers, and thermoelectrically cooled charge-coupled device detectors, have enabled the production of less expensive, compact, and portable Raman spectroscopic systems.

While Raman spectroscopy has been used extensively to study the process of biomineralization[84-98], it has not been previously used to provide insight into the pathologic process of heterotopic ossification. We have collected Raman spectra of uninjured muscle, injured muscle, and combat-injured tissue with pre-heterotopic ossification (defined as palpably firm or "woody" tissue without roentgenographic evidence

Fig. 6-B

of heterotopic ossification) found within high-energy penetrating wounds (Fig. 9). When comparing uninjured to injured muscle, there is an apparent decrease in the 1340 and 1320 cm^{-1} vibrational bands in the injured muscle as well as an increase in the 1266 cm^{-1} vibrational band. This suggests collagen-specific alterations within the tissue, as a result of traumatic injury. In one case, a patient exhibited combat-injured muscle with pre-heterotopic ossification during a debridement procedure. On Raman spectroscopic examination, it was clear that the tissue was indeed mineralized, even in "soft" tissue areas. Mineral vibrational bands at 1070, 960, and 591 cm^{-1}, typical of a carbonated apatite, were prominent in the spectrum. These vibrational bands are attributed to the phosphate and carbonate stretching modes of bone[99]. Thus, Raman spectroscopy can potentially be utilized to identify areas of tissue affected by early combat-related heterotopic ossification as well as areas of tissue that may be predisposed to the formation of combat-related heterotopic ossification.

Small Animal Model

A critical hurdle in our investigation of the etiology, treatment, and prevention of combat-related heterotopic ossification is the absence of a reliable and reproducible small animal model in which to further characterize the formation of combat-related heterotopic ossification, potentially identifying new therapeutic targets, and to test new therapeutic interventions. Currently, several small animal models exist. These models include the forcible passive manipulation of the hindlimbs of paralyzed rabbits[100,101]; implantation of Matrigel (basement membrane/collagen-IV matrix; BD Biosciences, Bedford, Massachusetts) impregnated with recombinant human bone morphogenetic protein (rhBMP)-2[48] or BMP-4[102] in genetically predisposed mice; implantation of genetically engineered, BMP-2-producing human or murine fibroblasts into immunocompromised mice[103]; and crush injury of the quadriceps augmented with syngeneic bone-marrow stem cells in inbred rats[104]. Our current understanding of heterotopic ossification suggests that these models have important limitations that may make them unsuitable proxies for combat-related heterotopic ossification. Specifically, these models all lack the systemic injury (e.g., blast injury and/or traumatic brain injury) components commonly seen in injured military personnel with combat-related heterotopic ossification. Additionally, no induced wound with associated bacterial contamination and resulting bioburden, as is the

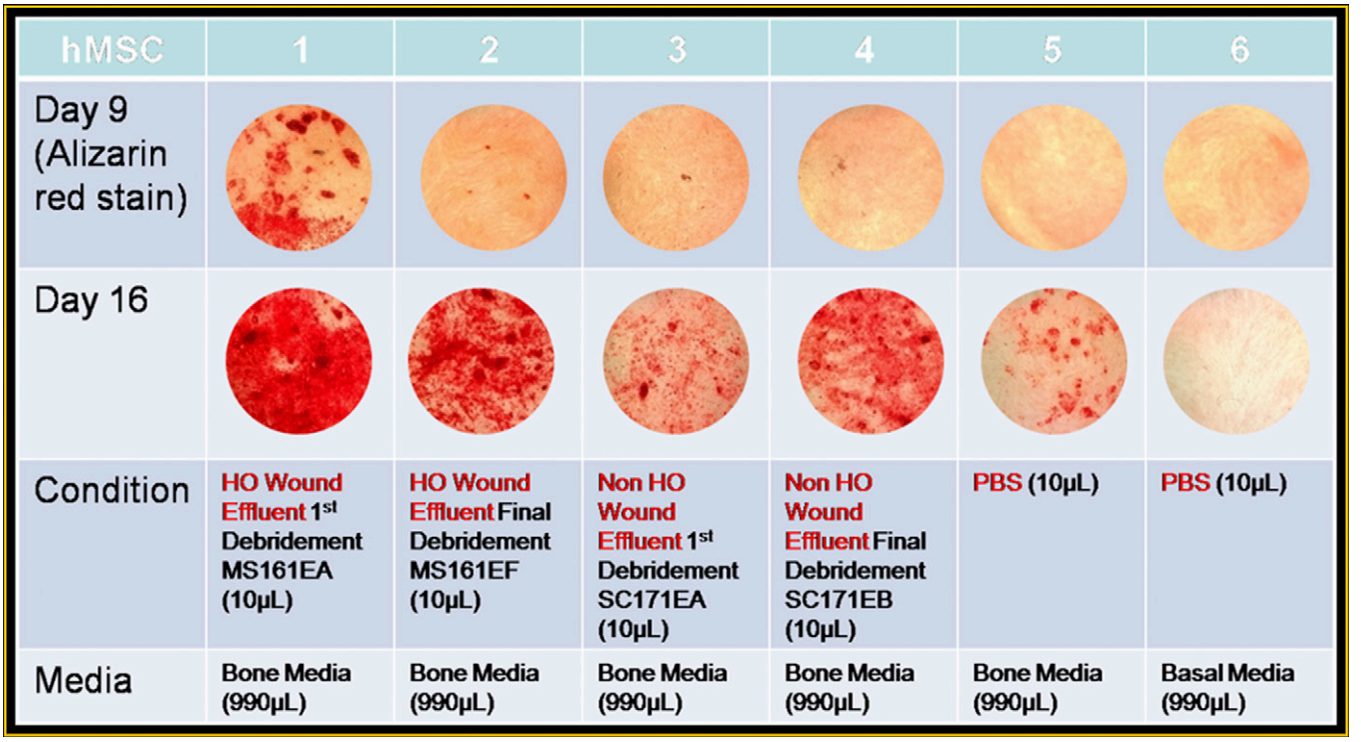

Fig. 7

Microphotographs of commercially available adult mesenchymal stem cells (hMSC) cultured in standard bone or basal media, with the addition of wound effluent from blast-injured patients who developed heterotopic ossification at the same site, blast-injured patients who did not develop ectopic bone, or phosphate-buffered saline solution, at days 9 and 16 of cell culture. Alizarin red (bone) staining (×10 magnification) demonstrated increased osteogenesis in the cells cultured with wound effluent from a patient who developed heterotopic ossification. HO = heterotopic ossification, and PBS = phosphate-buffered saline.

rule rather than the exception for combat injuries, is associated with these models. Moreover, there is a lack of general agreement within the current literature as to whether all inciting events lead to heterotopic ossification via the same cellular mechanisms and even whether all heterotopic ossification occurs via enchondral ossification[2,22,105]. Finally, these models are non-physiologic in that they artificially induce bone growth in the soft tissues of small animals through augmentation or manipulation of cellular signals, genetic predispositions, and/or cell presence. Previously described small-animal models therefore produce ectopic bone growth that may have little, if any, relationship to the clinical heterotopic ossification that is seen in human patients in general or in combat-injured patients in particular.

We have conceived of a physiologic rodent model that we hope will fill this research gap. Our model incorporates blast exposure, soft-tissue crush injury, and bacterial contamination, augmented with one of several additional systemic insults to invoke additional systemic inflammation. The fracture component will be omitted to limit rodent mortality as well as avoid confounding results due to exuberant fracture callus, if it were to occur. It is our hope that this model will reliably produce heterotopic ossification through mechanisms similar to that seen in our combat-wounded patients and that it will allow further characterization of this pathologic process. Once validated, this model may permit future identification of novel therapeutic targets as well as testing of various described and original therapeutic modalities.

Prospective Randomized Trial of Primary Prophylaxis in Combat-Injured Patients

As noted, due to medical contraindications and logistical constraints, no practicable primary prophylaxis regimen has yet been developed, tested, or widely utilized in wounded servicemen despite the exceedingly high rate of heterotopic ossification in this population. Recently, COX-2 inhibitors such as celecoxib have been shown to be safe and efficacious for the prevention of heterotopic ossification following hip and acetabular surgery[106-108] and may be useful in our patient population. COX-2 is required for endochondral bone formation, a mechanism implicated in the development of heterotopic ossification[103]. Although not prescribed as prophylaxis against heterotopic ossification, COX-2 inhibitors are currently used in this institution as part of a comprehensive pain-management regimen and are thought to decrease the patient's opioid requirement. Concerns about COX-2 inhibitors in an orthopaedic population stem from the blunting of "helpful" inflammation necessary for endochondral ossification in early fracture-healing[109-113]. Nevertheless, several studies evaluating COX-2 inhibitors found

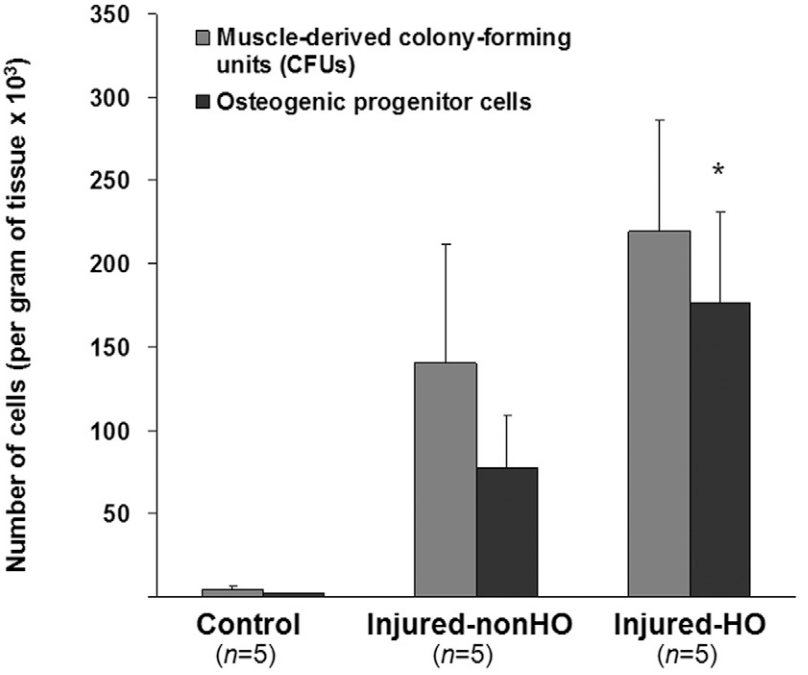

Fig. 8

Graphical depiction of the number of muscle-derived colony-forming units and osteogenic progenitor cells cultured from muscle tissue of normal (control) patients, combat-injured patients who did not develop heterotopic ossification (Injured-nonHO), and combat-injured patients who developed heterotopic ossification (Injured-HO). Even with these preliminary results (n = 5 patients per group) a significant (*, $p < 0.05$) increase in the number of osteogenic progenitor cells is evident in patients who developed heterotopic ossification as compared with patients in the other two groups. (Error bars indicate 95% confidence interval.)

little or no deleterious effect on fracture-healing or osseous healing[99,114-117].

In order to address the safety and efficacy of COX-2 inhibition in combat-related heterotopic ossification, a prospective randomized trial of celecoxib, started within five days after injury for a two-week treatment period (200 mg by mouth twice a day), will begin enrolling patients this year. The study will enroll as many as 100 patients (fifty in the treatment arm and fifty in the control arm), and is powered to detect a 30% relative decrease in the rate of formation of combat-related heterotopic ossification (e.g., a decrease from 60% to 40%). Primary study end points are the overall prevalence and severity of combat-related heterotopic ossification in study patients. This decrease in combat-related prevalence of heterotopic ossification is well below that anticipated on the basis of a putative 56% to 67% reduction in heterotopic ossification rates with use of nonsteroidal anti-inflammatory drugs in other populations[31]. Testing for this lower rate of reduction appears reasonable because the actual effect of nonsteroidal anti-inflammatory drugs may differ in patients with combat-related heterotopic ossification, because treatment cannot practicably be initiated at the point and time of injury, and because testing would serve to ensure adequate power of the trial. Secondary end points include fracture nonunion, time to fracture union, rate of impaired wound-healing, medical and drug-related complications (e.g., gastrointestinal problems and renal dysfunction), and patient pain ratings and opioid requirements.

The concern that celecoxib may delay fracture-healing is an important one. Nevertheless, its effect may be tempered by the timing of fracture fixation in a high-energy penetrating injury of an extremity. In most cases, fracture fixation is not performed until ten to fourteen days after injury, which is the time it takes to debride and prepare the wound for closure or flap coverage. Prophylaxis against heterotopic ossification is started as soon after injury as possible and continued for fourteen days. Ideally, celecoxib dosing for the purpose of prophylaxis against heterotopic ossification will be complete prior to definitive fracture fixation. Goodman and colleagues demonstrated that COX-2 inhibitors, if given within the first fourteen days following fracture, did not result in appreciable impairment of fracture-healing[118]. There is also no evidence to suggest that celecoxib significantly affects fracture-healing in our combat-wounded patient population. Nevertheless, "nonunion" and "time to union" will be reported as secondary outcomes in this study. Of note, short-term use of celecoxib in patients without fractures, including amputees, has not been associated with any negative effects.

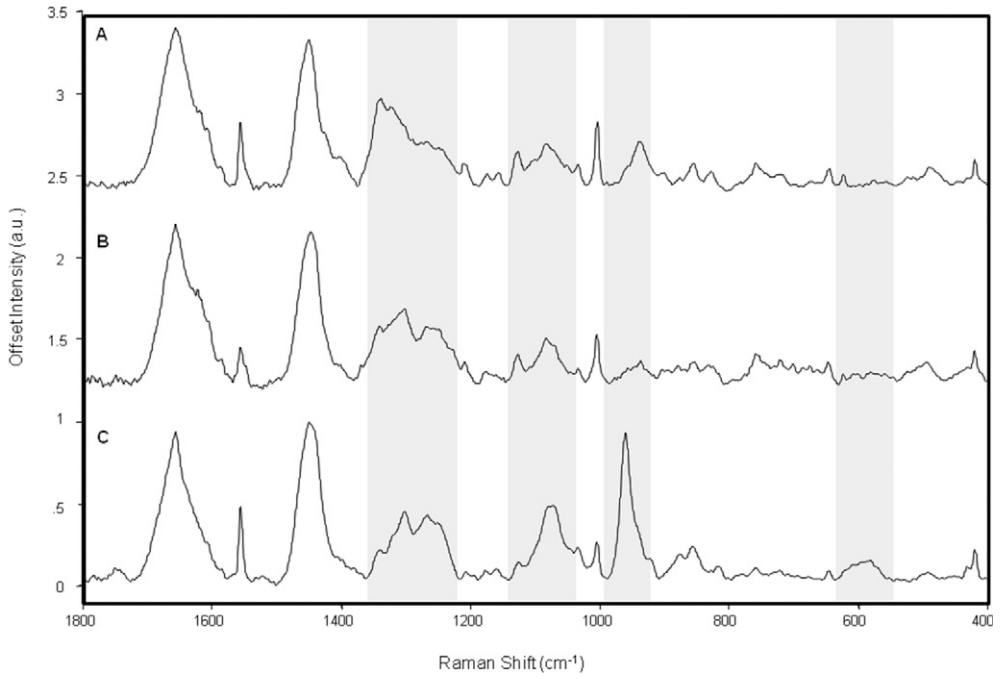

Fig. 9

Raman spectra of (A) uninjured muscle (control tissue), (B) combat-injured muscle, and (C) combat-injured muscle with pre-heterotopic ossification. The gray bands highlight spectral changes in the amide-III envelope (1340-1240 cm^{-1}) and the appearance of mineral vibrational bands at 1070, 960, and 591 cm^{-1}.

Conclusions and Future Directions

Combat-related heterotopic ossification is exceptionally common and is often a harbinger of a complex and difficult clinical course. Operative excision of symptomatic combat-related heterotopic ossification lesions is generally successful and associated with low rates of recurrence but can be technically demanding and fraught with complications, particularly about the knee when concurrent quadricepsplasty is required. We have identified numerous clinical factors and biological markers that are predictive of eventual formation of combat-related heterotopic ossification. Through ongoing and future research efforts by our consortium, we hope to further elucidate the biochemical and cellular basis for the formation of combat-related heterotopic ossification, further define the relative roles of local and systemic inflammation, continue to develop new means of early diagnosis and prognostication, and test and validate both conventional and novel practicable primary prophylactic treatment modalities. It is our hope that, through a combination of new diagnostic and therapeutic interventions, we can affect both the incidence and clinical management of combat-related heterotopic ossification. ■

NOTE: The authors acknowledge the research and/or clinical support of the following individuals: Fred Gage; Wesley Stepp, MS; Steve Ahlers, PhD; COL James Ficke, MD; COL(ret) William Doukas, MD; LTC(P) Romney Andersen, MD; LTC(P) Dan White, MD; LTC Scott Shawen, MD; CDR John Keeling, MD; MAJ Wade Gordon, MD; Stephen Rouse, PhD; Peter Liacouras, PhD; LTC(P) Tad Gerlinger, MD; LTC(P) Donald Gajewski, MD; MAJ(P) Joseph Hsu; and H. Michael Frisch, MD.

MAJ Benjamin K. Potter, MD
LCDR Jonathan A. Forsberg, MD
CPT Korboi N. Evans, MD
MAJ Jason S. Hawksworth, MD
CPT Frederick P. O'Brien, MD
Walter Reed National Military Medical Center,
6900 Georgia Avenue N.W., Bldg 2, Clinic 5A, Washington, DC 20307.
E-mail address for B.K. Potter: kyle.potter@us.army.mil

Thomas A. Davis, PhD
Doug Tadaki, PhD
Trevor S. Brown, PhD
Nicole J. Crane, PhD
CDR Eric A. Elster, MD
Naval Medical Research Center,
503 Robert Grant Avenue, Silver Spring, MD 20910

MAJ Travis C. Burns, MD
San Antonio Military Medical Center,
3851 Roger Brooke Drive, Fort Sam Houston, Texas 78234

References

1. Al-Zahrawi AQK. Albucasis on surgery and instruments. Berkeley: University of California Press; 1972.

2. Kaplan FS, Glaser DL, Hebela N, Shore EM. Heterotopic ossification. J Am Acad Orthop Surg. 2004;12:116-25.

3. Garland DE. Clinical observations on fractures and heterotopic ossification in the spinal cord and traumatic brain injured populations. Clin Orthop Relat Res. 1988; 233:86-101.

4. Garland DE, O'Hollaren RM. Fractures and dislocations about the elbow in the head-injured adult. Clin Orthop Relat Res. 1982;168:38-41.

5. Dougherty PJ. Long-term follow-up study of bilateral above-the-knee amputees from the Vietnam War. J Bone Joint Surg Am. 1999;81:1384-90.

6. Dougherty PJ. Transtibial amputees from the Vietnam War. Twenty-eight-year follow-up. J Bone Joint Surg Am. 2001;83:383-9.

7. Hull JB. Traumatic amputation by explosive blast: pattern of injury in survivors. Br J Surg. 1992;79:1303-6.

8. Johnson DE, Fleming A, Wongrukmitr B, Traverso LW. Combat casualties in northern Thailand: emphasis on land mine injuries and levels of amputation. Mil Med. 1981;146:682-5.

9. Brackett EG. Care of the amputated in the United States. In: The medical department of the United States army in the world war. Vol. 2. Washington, DC: US Government Printing Office; 1927. p 713-48.

10. Otis GA, Huntington DL. Wounds and complications. In: The medical and surgical history of the civil war. Vol. 2, pt. 3. Washington, DC: US Government Printing Office; 1883. p 880.

11. Covey DC. Blast and fragment injuries of the musculoskeletal system. J Bone Joint Surg Am. 2002;84:1221-34.

12. Covey DC. Combat orthopaedics: a view from the trenches. J Am Acad Orthop Surg. 2006;14(10 Spec No.):S10-7.

13. Gofrit ON, Leibovici D, Shapira SC, Shemer J, Stein M, Michaelson M. The trimodal death distribution of trauma victims: military experience from the Lebanon War. Mil Med. 1997;162:24-6.

14. Islinger RB, Kuklo TR, McHale KA. A review of orthopedic injuries in three recent U.S. military conflicts. Mil Med. 2000;165:463-5.

15. Lin DL, Kirk KL, Murphy KP, McHale KA, Doukas WC. Evaluation of orthopaedic injuries in Operation Enduring Freedom. J Orthop Trauma. 2004;18(8 Suppl): S48-53.

16. London PS. Medical lessons from the Falkland Islands' Campaign. Report of a meeting of the United Services Section of the Royal Society of Medicine held at the Royal College of Surgeons on February 17 and 18, 1983. J Bone Joint Surg Br. 1983;65:507-10.

17. Mabry RL, Holcomb JB, Baker AM, Cloonan CC, Uhorchak JM, Perkins DE, Canfield AJ, Hagmann JH. United States Army Rangers in Somalia: an analysis of combat casualties on an urban battlefield. J Trauma. 2000;49:515-29.

18. Mazurek MT, Ficke JR. The scope of wounds encountered in casualties from the global war on terrorism: from the battlefield to the tertiary treatment facility. J Am Acad Orthop Surg. 2006;14(10 Spec No.):S18-23.

19. Fox CJ, Gillespie DL, Cox ED, Kragh JF Jr, Mehta SG, Salinas J, Holcomb JB. Damage control resuscitation for vascular surgery in a combat support hospital. J Trauma. 2008;65:1-9.

20. Kragh JF Jr, Walters TJ, Baer DG, Fox CJ, Wade CE, Salinas J, Holcomb JB. Survival with emergency tourniquet use to stop bleeding in major limb trauma. Ann Surg. 2009;249:1-7.

21. Forsberg JA, Pepek JM, Wagner S, Wilson K, Flint J, Andersen RC, Tadaki D, Gage FA, Stojadinovic A, Elster EA. Heterotopic ossification in high-energy wartime extremity injuries: prevalence and risk factors. J Bone Joint Surg Am. 2009;91:1084-91.

22. Forsberg JA, Potter BK. Heterotopic ossification in wartime wounds. J Surg Orthop Adv. 2010;19:54-61.

23. Potter BK, Burns TC, Lacap AP, Granville RR, Gajewski DA. Heterotopic ossification following traumatic and combat-related amputations. Prevalence, risk factors, and preliminary results of excision. J Bone Joint Surg Am. 2007;89:476-86.

24. Garland DE. A clinical perspective on common forms of acquired heterotopic ossification. Clin Orthop Relat Res. 1991;263:13-29.

25. Garland DE, Blum CE, Waters RL. Periarticular heterotopic ossification in head-injured adults. Incidence and location. J Bone Joint Surg Am. 1980;62:1143-6.

26. Garland DE, Dowling V. Forearm fractures in the head-injured adult. Clin Orthop Relat Res. 1983;176:190-6.

27. Giannoudis PV, Mushtaq S, Harwood P, Kambhampati S, Dimoutsos M, Stavrou Z, Pape HC. Accelerated bone healing and excessive callus formation in patients with femoral fracture and head injury. Injury. 2006;37 Suppl 3:S18-24.

28. Spencer RF. The effect of head injury on fracture healing. A quantitative assessment. J Bone Joint Surg Br. 1987;69:525-8.

29. Steinberg GG, Hubbard C. Heterotopic ossification after femoral intramedullary rodding. J Orthop Trauma. 1993;7:536-42.

30. Burd TA, Lowry KJ, Anglen JO. Indomethacin compared with localized irradiation for the prevention of heterotopic ossification following surgical treatment of acetabular fractures. J Bone Joint Surg Am. 2001;83:1783-8.

31. Fransen M, Neal B. Non-steroidal anti-inflammatory drugs for preventing heterotopic bone formation after hip arthroplasty. Cochrane Database Syst Rev. 2004; 3:CD001160.

32. Gregoritch SJ, Chadha M, Pelligrini VD, Rubin P, Kantorowitz DA. Randomized trial comparing preoperative versus postoperative irradiation for prevention of heterotopic ossification following prosthetic total hip replacement: preliminary results. Int J Radiat Oncol Biol Phys. 1994;30:55-62.

33. Matta JM, Siebenrock KA. Does indomethacin reduce heterotopic bone formation after operations for acetabular fractures? A prospective randomised study. J Bone Joint Surg Br. 1997;79:959-63.

34. Moore KD, Goss K, Anglen JO. Indomethacin versus radiation therapy for prophylaxis against heterotopic ossification in acetabular fractures: a randomised, prospective study. J Bone Joint Surg Br. 1998;80:259-63.

35. Pakos EE, Ioannidis JP. Radiotherapy vs. nonsteroidal anti-inflammatory drugs for the prevention of heterotopic ossification after major hip procedures: a meta-analysis of randomized trials. Int J Radiat Oncol Biol Phys. 2004;60:888-95.

36. Pellegrini VD Jr, Konski AA, Gastel JA, Rubin P, Evarts CM. Prevention of heterotopic ossification with irradiation after total hip arthroplasty. Radiation therapy with a single dose of eight hundred centigray administered to a limited field. J Bone Joint Surg Am. 1992;74:186-200.

37. Koelbl O, Seufert J, Pohl F, Tauscher A, Lehmann H, Springorum HW, Flentje M. Preoperative irradiation for prevention of heterotopic ossification following prosthetic total hip replacement results of a prospective study in 462 hips. Strahlenther Onkol. 2003;179:767-73.

38. Moed BR, Letournel E. Low-dose irradiation and indomethacin prevent heterotopic ossification after acetabular fracture surgery. J Bone Joint Surg Br. 1994;76: 895-900.

39. Seegenschmiedt MH, Goldmann AR, Martus P, Wölfel R, Hohmann D, Sauer R. Prophylactic radiation therapy for prevention of heterotopic ossification after hip arthroplasty: results in 141 high-risk hips. Radiology. 1993;188:257-64.

40. Seegenschmiedt MH, Goldmann AR, Wölfel R, Hohmann D, Beck H, Sauer R. Prevention of heterotopic ossification (HO) after total hip replacement: randomized high versus low dose radiotherapy. Radiother Oncol. 1993;26:271-4.

41. Blokhuis TJ, Frölke JP. Is radiation superior to indomethacin to prevent heterotopic ossification in acetabular fractures?: a systematic review. Clin Orthop Relat Res. 2009;467:526-30.

42. Haran M, Bhuta T, Lee B. Pharmacological interventions for treating acute heterotopic ossification. Cochrane Database Syst Rev. 2004;18:CD003321.

43. Buschbacher R, McKinley W, Buschbacher L, Devaney CW, Coplin B. Warfarin in prevention of heterotopic ossification. Am J Phys Med Rehabil. 1992;71:86-91.

44. Guillemin F, Mainard D, Rolland H, Delagoutte JP. Antivitamin K prevents heterotopic ossification after hip arthroplasty in diffuse idiopathic skeletal hyperostosis. A retrospective study in 67 patients. Acta Orthop Scand. 1995;66:123-6.

45. Günal I, Hazer B, Seber S, Göktürk E, Turgut A, Köse N. Prevention of heterotopic ossification after total hip replacement: a prospective comparison of indomethacin and salmon calcitonin in 60 patients. Acta Orthop Scand. 2001;72:467-9.

46. Moed BR, Karges DE. Prophylactic indomethacin for the prevention of heterotopic ossification after acetabular fracture surgery in high-risk patients. J Orthop Trauma. 1994;8:34-9.

47. Salai M, Langevitz P, Blankstein A, Zemmer D, Chechick A, Pras M, Horoszowski H. Total hip replacement in familial Mediterranean fever. Bull Hosp Jt Dis. 1993;53: 25-8.

48. Shimono K, Morrison TN, Tung WE, Chandraratna RA, Williams JA, Iwamoto M, Pacifici M. Inhibition of ectopic bone formation by a selective retinoic acid receptor alpha-agonist: a new therapy for heterotopic ossification? J Orthop Res. 2010;28: 271-7.

49. Beingessner DM, Patterson SD, King GJ. Early excision of heterotopic bone in the forearm. J Hand Surg Am. 2000;25:483-8.

50. Freebourn TM, Barber DB, Able AC. The treatment of immature heterotopic ossification in spinal cord injury with combination surgery, radiation therapy and NSAID. Spinal Cord. 1999;37:50-3.

51. Garland DE, Hanscom DA, Keenan MA, Smith C, Moore T. Resection of heterotopic ossification in the adult with head trauma. J Bone Joint Surg Am. 1985;67: 1261-9.

52. Garland DE, Orwin JF. Resection of heterotopic ossification in patients with spinal cord injuries. Clin Orthop Relat Res. 1989;242:169-76.

53. McAuliffe JA, Wolfson AH. Early excision of heterotopic ossification about the elbow followed by radiation therapy. J Bone Joint Surg Am. 1997;79:749-55.

54. Moritomo H, Tada K, Yoshida T. Early, wide excision of heterotopic ossification in the medial elbow. J Shoulder Elbow Surg. 2001;10:164-8.

55. Shehab D, Elgazzar AH, Collier BD. Heterotopic ossification. J Nucl Med. 2002; 43:346-53.

56. Tsionos I, Leclercq C, Rochet JM. Heterotopic ossification of the elbow in patients with burns. Results after early excision. J Bone Joint Surg Br. 2004;86:396-403.

57. VanLaeken N, Snelling CF, Meek RN, Warren RJ, Foley B. Heterotopic bone formation in the patient with burn injuries. A retrospective assessment of contributing factors and methods of investigation. J Burn Care Rehabil. 1989;10:331-5.

58. Viola RW, Hanel DP. Early "simple" release of posttraumatic elbow contracture associated with heterotopic ossification. J Hand Surg Am. 1999;24:370-80.

59. Evans KN, Forsberg JA, Potter BK, Hawksworth JS, Brown TS, Andersen RC, Dunne JR, Stojadinovic A, Tadaki D, Elster EA. Inflammatory cytokine and chemokine expression is associated with heterotopic ossification in high-energy penetrating war injuries. Read at the Annual Uniformed Services University Surgical Associates Day; 2009 Mar 23; Bethesda, MD.

60. Forsberg JA, Elster EA, Andersen RC, Nylen E, Brown TS, Rose MW, Stojadinovic A, Becker KL, McGuigan FX. Correlation of procalcitonin and cytokine expression with dehiscence of wartime extremity wounds. J Bone Joint Surg Am. 2008;90:580-8.

61. Utz ER, Elster EA, Tadaki DK, Gage F, Perdue PW, Forsberg JA, Stojadinovic A, Hawksworth JS, Brown TS. Metalloproteinase expression is associated with traumatic wound failure. J Surg Res. 2010;159:633-9.

62. Hawksworth JS, Stojadinovic A, Gage FA, Tadaki DK, Perdue PW, Forsberg J, Davis TA, Dunne JR, Denobile JW, Brown TS, Elster EA. Inflammatory biomarkers in combat wound healing. Ann Surg. 2009;250:1002-7.

63. Uccelli A, Moretta L, Pistoia V. Mesenchymal stem cells in health and disease. Nat Rev Immunol. 2008;8:726-36.

64. da Silva Meirelles L, Chagastelles PC, Nardi NB. Mesenchymal stem cells reside in virtually all post-natal organs and tissues. J Cell Sci. 2006;119:2204-13.

65. Caplan AI. Adult mesenchymal stem cells for tissue engineering versus regenerative medicine. J Cell Physiol. 2007;213:341-7.

66. Chamberlain G, Fox J, Ashton B, Middleton J. Concise review: mesenchymal stem cells: their phenotype, differentiation capacity, immunological features, and potential for homing. Stem Cells. 2007;25:2739-49.

67. Jackson WM, Nesti LJ, Tuan RS. Potential therapeutic applications of muscle-derived mesenchymal stem and progenitor cells. Expert Opin Biol Ther. 2010;10: 505-17.

68. Phinney DG, Prockop DJ. Concise review: mesenchymal stem/multipotent stromal cells: the state of transdifferentiation and modes of tissue repair—current views. Stem Cells. 2007;25:2896-902.

69. Jackson WM, Aragon AB, Bulken-Hoover JD, Nesti LJ, Tuan RS. Putative heterotopic ossification progenitor cells derived from traumatized muscle. J Orthop Res. 2009;27:1645-51.

70. Jackson WM, Aragon AB, Djouad F, Song Y, Koehler SM, Nesti LJ, Tuan RS. Mesenchymal progenitor cells derived from traumatized human muscle. J Tissue Eng Regen Med. 2009;3:129-38.

71. Nesti LJ, Jackson WM, Shanti RM, Koehler SM, Aragon AB, Bailey JR, Sracic MK, Freedman BA, Giuliani JR, Tuan RS. Differentiation potential of multipotent progenitor cells derived from war-traumatized muscle tissue. J Bone Joint Surg Am. 2008; 90:2390-8.

72. O'Brien FP, Anam K, Potter BK, Tadaki D, Forsberg JA, Elster EA, Davis TA. Heterotopic ossification formation in complex orthopedic combat wounds:quantification and characterization of mesenchymal stem/progenitor cell activity in traumatized muscle. Read at the Robert A Phillips Resident Research Competition; 2010 Apr 16; Bethesda, MD.

73. Hattori Y, Komachi Y, Asakura T, Shimosegawa T, Kanai G, Tashiro H, Sato H. In vivo Raman study of the living rat esophagus and stomach using a micro-Raman probe under an endoscope. Appl Spectrosc. 2007;61:579-84.

74. Shim MG, Song LM, Marcon NE, Wilson BC. In vivo near-infrared Raman spectroscopy: demonstration of feasibility during clinical gastrointestinal endoscopy. Photochem Photobiol. 2000;72:146-50.

75. Robichaux-Viehoever A, Kanter E, Shappell H, Billheimer D, Jones H 3rd, Mahadevan-Jansen A. Characterization of Raman spectra measured in vivo for the detection of cervical dysplasia. Appl Spectrosc. 2007;61:986-93.

76. Lieber CA, Majumder SK, Ellis DL, Billheimer DD, Mahadevan-Jansen A. In vivo nonmelanoma skin cancer diagnosis using Raman microspectroscopy. Lasers Surg Med. 2008;40:461-7.

77. Egawa M, Kunizawa N, Hirao T, Yamamoto T, Sakamoto K, Terui T, Tagami H. In vivo characterization of the structure and components of lesional psoriatic skin from the observation with Raman spectroscopy and optical coherence tomography: a pilot study. J Dermatol Sci. 2010;57:66-9.

78. Chau AH, Motz JT, Gardecki JA, Waxman S, Bouma BE, Tearney GJ. Fingerprint and high-wavenumber Raman spectroscopy in a human-swine coronary xenograft in vivo. J Biomed Opt. 2008;13:040501.

79. Bernstein PS, Zhao DY, Sharifzadeh M, Ermakov IV, Gellermann W. Resonance Raman measurement of macular carotenoids in the living human eye. Arch Biochem Biophys. 2004;430:163-9.

80. Bernstein PS, Zhao DY, Wintch SW, Ermakov IV, McClane RW, Gellermann W. Resonance Raman measurement of macular carotenoids in normal subjects and in age-related macular degeneration patients. Ophthalmology. 2002;109:1780-7.

81. Gellermann W, Bernstein PS. Noninvasive detection of macular pigments in the human eye. J Biomed Opt. 2004;9:75-85.

82. Zhao DY, Wintch SW, Ermakov IV, Gellermann W, Bernstein PS. Resonance Raman measurement of macular carotenoids in retinal, choroidal, and macular dystrophies. Arch Ophthalmol. 2003;121:967-72.

83. Schulmerich MV, Cole JH, Kreider JM, Esmonde-White F, Dooley KA, Goldstein SA, Morris MD. Transcutaneous Raman spectroscopy of murine bone in vivo. Appl Spectrosc. 2009;63:286-95.

84. Akkus O, Adar F, Schaffler MB. Age-related changes in physicochemical properties of mineral crystals are related to impaired mechanical function of cortical bone. Bone. 2004;34:443-53.

85. Crane NJ, Popescu V, Morris MD, Steenhuis P, Ignelzi MA Jr. Raman spectroscopic evidence for octacalcium phosphate and other transient mineral species deposited during intramembranous mineralization. Bone. 2006;39:434-42.

86. Gajjeraman S, Narayanan K, Hao J, Qin C, George A. Matrix macromolecules in hard tissues control the nucleation and hierarchical assembly of hydroxyapatite. J Biol Chem. 2007;282:1193-204.

87. Kohn DH. Ultrastructural changes during the fatigue of bone. JOM J Miner Metals Mater Soc. 2006;58:46-50.

88. Kozloff KM, Carden A, Bergwitz C, Forlino A, Uveges TE, Morris MD, Marini JC, Goldstein SA. Brittle IV mouse model for osteogenesis imperfecta IV demonstrates postpubertal adaptations to improve whole bone strength. J Bone Miner Res. 2004; 19:614-22.

89. Lakshmi RJ, Alexander M, Kurien J, Mahato KK, Kartha VB. Osteoradionecrosis (ORN) of the mandible: a laser Raman spectroscopic study. Appl Spectrosc. 2003; 57:1100-16.

90. McCreadie BR, Morris MD, Chen TC, Sudhaker Rao D, Finney WF, Widjaja E, Goldstein SA. Bone tissue compositional differences in women with and without osteoporotic fracture. Bone. 2006;39:1190-5.

91. Morris MD, Finney WF, Rajachar RM, Kohn DH. Bone tissue ultrastructural response to elastic deformation probed by Raman spectroscopy. Faraday Discuss. 2004;126:159-83.

92. Nalla RK, Kruzic JJ, Kinney JH, Balooch M, Ager JW III, Ritchie RO. Role of microstructure in the aging-related deterioration of the toughness of human cortical bone. Mater Sci Eng C. 2006;26:1251-60.

93. Penel G, Leroy G, Rey C, Bres E. MicroRaman spectral study of the PO4 and CO3 vibrational modes in synthetic and biological apatites. Calcif Tissue Int. 1998;63: 475-81.

94. Rehman I, Smith R, Hench LL, Bonfield W. Structural evaluation of human and sheep bone and comparison with synthetic hydroxyapatite by FT-Raman spectroscopy. J Biomed Mater Res. 1995;29:1287-94.

95. Smith R, Rehman I. Fourier transform Raman spectroscopic studies of human bone. J Mater Sci. 1994;5:775-8.

96. Tarnowski CP, Ignelzi MA Jr, Morris MD. Mineralization of developing mouse calvaria as revealed by Raman microspectroscopy. J Bone Miner Res. 2002;17: 1118-26.

97. Wopenka B, Kent A, Pasteris JD, Yoon Y, Thomopoulos S. The tendon-to-bone transition of the rotator cuff: a preliminary Raman spectroscopic study documenting the gradual mineralization across the insertion in rat tissue samples. Appl Spectrosc. 2008;62:1285-94.

98. Yerramshetty JS, Lind C, Akkus O. The compositional and physicochemical homogeneity of male femoral cortex increases after the sixth decade. Bone. 2006; 39:1236-43.

99. Persson PE, Sisask G, Nilsson O. Indomethacin inhibits bone formation in inductive allografts but not in autografts: studies in rat. Acta Orthop. 2005;76:465-9.

100. Vanden Bossche LC, Van Maele G, Wojtowicz I, De Cock K, Vertriest S, De Muynck M, Rimbaut S, Vanderstraeten GG. Free radical scavengers are more effective than indomethacin in the prevention of experimentally induced heterotopic ossification. J Orthop Res. 2006;25:267-72.

101. Izumi K. Study of ectopic bone formation in experimental spinal cord injured rabbits. Paraplegia. 1983;21:351-63.

102. Glaser DL, Economides AN, Wang L, Liu X, Kimble RD, Fandl JP, Wilson JM, Stahl N, Kaplan FS, Shore EM. In vivo somatic cell gene transfer of an engineered Noggin mutein prevents BMP4-induced heterotopic ossification. J Bone Joint Surg Am. 2003;85:2332-42.

103. Olmsted-Davis E, Gannon FH, Ozen M, Ittmann MM, Gugala Z, Hipp JA, Moran KM, Fouletier-Dilling CM, Schumara-Martin S, Lindsey RW, Heggeness MH, Brenner MK, Davis AR. Hypoxic adipocytes pattern early heterotopic bone formation. Am J Pathol. 2007;170:620-32.

104. Rapuano BE, Boursiquot R, Tomin E, Macdonald DE, Maddula S, Raghavan D, Lane JM, Helfet DL. The effects of COX-1 and COX-2 inhibitors on prostaglandin synthesis and the formation of heterotopic bone in a rat model. Arch Orthop Trauma Surg. 2008;128:333-44.

105. Cipriano CA, Pill SG, Keenan MA. Heterotopic ossification following traumatic brain injury and spinal cord injury. J Am Acad Orthop Surg. 2009;17:689-97.

106. Macfarlane RJ, Ng BH, Gamie Z, El Masry MA, Velonis S, Schizas C, Tsiridis E. Pharmacological treatment of heterotopic ossification following hip and acetabular surgery. Expert Opin Pharmacother. 2008;9:767-86.

107. Saudan M, Saudan P, Perneger T, Riand N, Keller A, Hoffmeyer P. Celecoxib versus ibuprofen in the prevention of heterotopic ossification following total hip replacement: a prospective randomised trial. J Bone Joint Surg Br. 2007;89:155-9.

108. Xue D, Zheng Q, Li H, Qian S, Zhang B, Pan Z. Selective COX-2 inhibitor versus nonselective COX-1 and COX-2 inhibitor in the prevention of heterotopic ossification after total hip arthroplasty: a meta-analysis of randomised trials. Int Orthop. 2009 Oct 15 [Epub ahead of print].

109. Bergenstock M, Min W, Simon AM, Sabatino C, O'Connor JP. A comparison between the effects of acetaminophen and celecoxib on bone fracture healing in rats. J Orthop Trauma. 2005;19:717-23.

110. Herbenick MA, Sprott D, Stills H, Lawless M. Effects of a cyclooxygenase 2 inhibitor on fracture healing in a rat model. Am J Orthop (Belle Mead NJ). 2008;37:E133-7.

111. Mullis BH, Copland ST, Weinhold PS, Miclau T, Lester GE, Bos GD. Effect of COX-2 inhibitors and non-steroidal anti-inflammatory drugs on a mouse fracture model. Injury. 2006;37:827-37.

112. Simon AM, Manigrasso MB, O'Connor JP. Cyclo-oxygenase 2 function is essential for bone fracture healing. J Bone Miner Res. 2002;17:963-76.

113. Simon AM, O'Connor JP. Dose and time-dependent effects of cyclooxygenase-2 inhibition on fracture-healing. J Bone Joint Surg Am. 2007;89:500-11.

114. Brown KM, Saunders MM, Kirsch T, Donahue HJ, Reid JS. Effect of COX-2-specific inhibition on fracture-healing in the rat femur. J Bone Joint Surg Am. 2004;86:116-23.

115. Gerstenfeld LC, Thiede M, Seibert K, Mielke C, Phippard D, Svagr B, Cullinane D, Einhorn TA. Differential inhibition of fracture healing by non-selective and cyclooxygenase-2 selective non-steroidal anti-inflammatory drugs. J Orthop Res. 2003;21:670-5.

116. Keller J. Effects of indomethacin and local prostaglandin E2 on fracture healing in rabbits. Dan Med Bull. 1996;43:317-29.

117. Reikeraas O, Engebretsen L. Effects of ketoralac tromethamine and indomethacin on primary and secondary bone healing. An experimental study in rats. Arch Orthop Trauma Surg. 1998;118:50-2.

118. Goodman SB, Ma T, Mitsunaga L, Miyanishi K, Genovese MC, Smith RL. Temporal effects of a COX-2-selective NSAID on bone ingrowth. J Biomed Mater Res A. 2005;72:279-87.

Developing a toolbox for analysis of warrior wound biopsies: vibrational spectroscopy

Nicole J. Crane*[a], Frederick P. O'Brien[b], Jonathan A. Forsberg[b,c], Benjamin K. Potter[b,c], Eric A. Elster[a,c,d]

[a]Department of Regenerative Medicine, Operational and Undersea Medicine Directorate, Naval Medical Research Center, Silver Spring, Maryland
[b]Department of Orthopaedics and Rehabilitation, Walter Reed National Military Medical Center, Washington, District of Columbia
[c]Department of Surgery, Uniformed Services University of Health Sciences, Bethesda, Maryland
[b]Department of Surgery, Walter Reed National Military Medical Center, Bethesda, Maryland

ABSTRACT

The management of modern traumatic war wounds remains a significant challenge for clinicians. This is a reflection of the extensive osseous and soft-tissue damage caused by blasts and high-energy projectiles. The ensuing inflammatory response ultimately dictates the pace of wound healing and tissue regeneration. Consequently, the eventual timing of wound closure or definitive coverage is often subjectively based. Some wounds require an extended period of time to close or fail to remain closed, despite the use and application of novel wound-specific treatment modalities. Aside from impaired wound healing, additional wound complications include wound infection and heterotopic ossification (the pathological mineralization of soft tissues). An understanding of the molecular environment of acute wounds throughout the debridement process can provide valuable insight into the mechanisms associated with the eventual wound outcome. The analysis of Raman spectra of *ex vivo* wound biopsy tissue obtained from serial traumatic wound debridements reveals a decreased 1665 cm^{-1}/1445 cm^{-1} band area ratio in impaired healing wounds, indicative of an impaired remodeling process, in addition to a decreased 1240 cm^{-1}/1270 cm^{-1} band area ratio. The examination of debrided tissue exhibits mineralization during the early development of heterotopic ossification. Finally, preliminary results suggest that Fourier transform infrared (FT-IR) images of wound effluent may be able to provide early microbiological information about the wound.

Keywords: combat wounds; biopsies; wound effluent; Raman spectroscopy; FT-IR imaging

1. INTRODUCTION

Extremity wounds have become the most common injuries sustained in modern warfare. These wounds, caused predominately by blasts, are characterized by high-energy fractures, often with bacterial and environmental contamination, thermal injury, and soft tissue loss. The result is a devastating life- and limb-threatening injury pattern that demands considerable time, effort, and resources throughout all phases of treatment. Thus, the management of modern combat extremity wounds is challenging, and complications such as infection and heterotopic ossification are all too common.[1-3] Accurate assessment of these wounds is necessary to guide both surgical decision-making and prophylactic medical therapy.

Wound healing is the result of complex cellular and molecular signals, ultimately leading to closure of the wound gap and the formation of scar tissue. As such, much remains to be learned about the structure and composition of the tissue itself during the wound healing process. Complicating the process of wound healing even more is the general heterogeneity of tissue, specifically skin and the underlying soft tissues. Current methods for monitoring wound healing rely largely on physician observations and are subjective, regardless of physician experience.

Raman vibrational spectroscopy is a modality that offers the capability to accurately detect and identify various molecules that comprise the extracellular matrix during wound healing in their native state. It is a spectroscopic technique in which the precise biochemical composition of biologic samples can be obtained via noninvasive and nondestructive means. It has been proven effective in assessing tissues at the molecular level with diverse clinical and diagnostic applications to include the analysis of cellular structure and the determination of tumor grade and type.[4-20] Pathologic alterations of wounds are accompanied by fundamental changes in the molecular environment that can be analyzed by vibrational spectroscopy.[9, 21] The identified changes might provide the objective markers of acute wound healing which can then be integrated with clinical characteristics to guide the management of traumatic wounds. For instance, changes in collagen vibrational bands could be correlated with alterations in collagen deposition and re-epithelialization of the wound bed. In addition, mineralization associated with pre-clinical and pre-radiographic heterotopic ossification could be easily monitored with Raman spectroscopy.[8, 22-35]

Also, because of vibrational spectroscopy's molecular specificity, it can also be used to evaluate the bioburden of wounds. There have been numerous Raman spectroscopic studies of microorganisms, many focusing on rapid identification of the microorganisms.[36-44] FT-IR spectroscopy can afford spectral information similar to that provided by Raman spectroscopy. There are several studies that focus on the use of FT-IR spectroscopy to detect and accurately classify microbiological organisms, such as *Acinetobacter*.[38, 45-48]

We hypothesized that vibrational spectroscopy could predict whether or not a wound will heal normally, whether or not a wound will develop heterotopic ossification, and whether or not wound effluent is colonized.

2. MATERIALS AND METHODS

2.1 Clinical Studies

The clinical studies were approved by the institutional review boards of the National Naval Medical Center (NNMC) and the Walter Reed Army Medical Center (WRAMC). All study participants were recruited from wounded Operation Iraqi Freedom and Operation Enduring Freedom U.S. service members evacuated to the National Capital Area. Age-matched control subjects were enrolled to provide untraumatized muscle for comparison. Patients in the control group were scheduled to undergo an elective ACL reconstruction using hamstring autograft and were recruited from the outpatient orthopaedic clinic. Informed consent was obtained from all participating patients.

For the treatment of combat wounds, surgical debridement and pulse lavage were performed in the operating room every 48-72 hours until definitive wound closure or coverage. Negative pressure wound therapy (NPWT) was applied to the wounds between surgical debridements, as per current standard practice at NNMC.[49] All wounds were examined once daily following wound closure or coverage until the sutures were removed. All patients were followed clinically for 30 days. Successful wound healing was defined as definitive wound closure or coverage. Impaired wound healing included a delayed wound closure or subsequent wound dehiscence. Delayed wound closure was defined as definitive closure occurring two standard deviations outside of the normal wound closure time period, which, in this case, was greater than or equal to 21 days after injury. Dehiscence was defined as loss after skin grafting. Thus, wounds that progressed to healing by thirty days after injury and did not necessitate a return to the operating room were considered healed. The timing of the wound closure was at the discretion of the attending surgeon.

2.2 Sample Collection

Control muscle samples (n=3) were collected from excess, discarded muscle tissue harvested during hamstring autograft preparation following routine, elective anterior cruciate ligament reconstruction and stored in 0.9% NaCl saline solution for transport. For injured muscle and wound biopsies (n=25), a 1 cm^3 wound tissue sample was obtained from the center of the wound bed at each debridement (Figure 1A) and fixed in 10% neutral buffered formalin for at least 48 hours. Samples were stored at -20˚F until analysis. Prior to Raman spectral acquisition, samples were thawed in 0.9% NaCl saline solution. Additionally, both soft and hard tissue heterotopic ossification

samples (n=25) were collected during the surgical removal of heterotopic ossification (Figures 1B and 1C, respectively) and stored in 0.9% NaCl solution for transport.

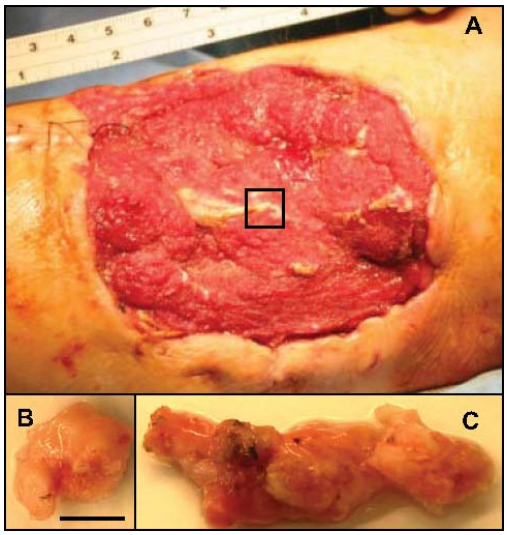

Figure 1. A) Picture taken of a wound bed at the time of surgical debridement. The black box indicates the typical biopsy size. B) Unmineralized tissue biopsy collected during excision of heterotopic ossification. Scale bar = 1 cm. C) Partially mineralized tissue biopsy collected during excision of heterotopic ossification.

Wound effluent, the exudate that filters from the circulatory system into a wound bed, was collected from the NPWT canister (without gel pack; Kinetic Concepts, Inc., San Antonio, TX) two hours following the first surgical debridement and over a 12 hour period prior to each subsequent wound debridement. Samples (n=4) were centrifuged at 12,000-13,000g. The supernatant was drawn off with a pipette and passed through a 0.65 μm filter.

2.3 Raman Spectroscopy

Tissue samples were placed on an aluminum foil covered weighing dish prior to spectral acquisition. A 785 nm Raman PhAT system (Kaiser Optical Systems, Inc., Ann Arbor, MI) was used to collect spectra of the tissue biopsies. Final spectra were the accumulation of forty 15 second spectra, acquired using the 3 mm spot size. At least three dark-subtracted, illumination-corrected spectra were obtained for each biopsy/sample. All spectral preprocessing was performed in GRAMS/AI software (Thermo Fisher Scientific, Madison, WI). Raman spectra were truncated to 1800-400 cm^{-1} and baseline corrected with a sixth degree polynomial. Spectral subtraction of blood was performed if spectral interference of blood was noted. All spectra were intensity normalized to the CH_2 scissoring band at 1445 cm^{-1}. Subsequently, curve fitting was performed over two spectral regions, 1730-1500 cm^{-1} and 1525-1185 cm^{-1}. All Raman bands were fit with mixed Gaussian/Lorentzian bands. The fit was considered good when the R^2 value reached at least 0.99.

2.4 FTIR Imaging

Approximately 4 μL of wound effluent was pipette onto an aluminized slide (Thermo Fisher Scientific, Madison, WI) and allowed to air dry. The Nicolet iN10 (Thermo Fisher Scientific, Madison, WI) was used to collect FT-IR images of the deposited effluent with 8 cm^{-1} spectral resolution from 4000 to 715 cm^{-1}. Total acquisition time for the image was approximately 15 minutes. Factor analysis was performed on truncated data cubes (1800 to 715 cm^{-1}). Briefly, all FT-IR image cubes were imported into MATLAB® (Mathworks, Natick, MA), where they were subjected to multivariate analysis. Singular value decomposition was applied to all data sets. A Scree plot was used to determine the necessary number of loadings such that 99% of the variance in the data set was described by the chosen loadings. Loadings used for factor analysis were extracted with band target entropy minimization (BTEM)[50-52] and then manually rotated until all factors were non-negative and their associated score images were non-

negative. Non-negative factors closely resemble real FT-IR spectra. Non-negative score images ensure orthogonality of factors and a unique basis set.

2.5 Statistical Analysis

Differences in band area ratios were assessed using a Mann-Whitney *U*-test. Analyses were performed using SPSS software (SPSS 18.0, SPSS Inc., Chicago, IL). Differences in values were considered statistically significant with a two-tailed *p*-value less than 0.05.

3. RESULTS

3.1 Raman spectral comparison of wound biopsies

The spectral profiles of *ex vivo* wound biopsies were compared for a normal healing wound, a delayed healing wound, and a dehisced wound. Raman spectra of wound biopsies collected during the first surgical debridement are contrasted with Raman spectra of wound biopsies collected during the final surgical debridement in Figure 2. Major bands exhibited in the spectra are shown in Table 1.

Table 1. Raman vibrational band assignments.[38, 53-60] (Phe - phenylalanine; Pyr – pyrrole; Tyr - tyrosine; Hb - hemoglobin; Trp - tryptophan).

Raman Shift (cm^{-1})	Vibrational Band Assignment	Component
938	ν(CC) residues	protein
1004	ν(CC) aromatic ring	Phe; protein
1035	ν(CC) skeletal; C-O stretch	mostly lipid with minor protein contribution; protein
1070, 1080		
1128	ν(CC) and ν(CN) skeletal; ν(Pyr half ring)	mostly lipid with minor protein contribution; Hb
1213		Tyr; Phe
1245	ν(CN) Amide III - β-sheet	protein
1270	ν(CN) Amide III - α-helix	protein
1340	δ(CH_2); ν(Pyr half ring)	protein; Trp; Hb
1371	ν(Pyr half ring)	Hb
1405		
1450	CH_2 scissoring	protein
1557	ν(CC) ring stretching	protein; Trp; Hb
1622	ν(C=C)	Hb; Tyr; Phe
1657	ν(C=O) Amide I	protein

When examining the Raman spectra of the first debridement wound biopsies (Figure 2A), the profiles of the normal healing and delayed healing wounds overlap extensively. The Raman spectrum of the wound biopsy from the dehisced wound, however, demonstrates several differences. The intensities of the Raman vibrational bands at 1622 cm^{-1}, 1557 cm^{-1}, and 1371 cm^{-1} are significantly increased for the wound biopsy from the dehisced wound compared to the normal and delayed healing wounds. The 1270 cm^{-1} and 1240 cm^{-1} amide III bands also appear to be more intense in the dehisced wound than in the normal or delayed healing wounds. Finally, the intensity of the 938 cm^{-1} vibrational band in the Raman spectrum of the normal healing wound biopsy is increased when compared to the band intensities of the delayed healing or dehisced wound biopsy spectra. Additionally, differences in the spectral profiles of the wound biopsies from the final debridement are evident (Figure 2B). The overall intensity of the amide I band in both the dehisced and delayed healing wounds is decreased when compared to the intensity of the normal healing wound. The intensities of the Raman vibrational bands at 1622 cm^{-1}, 1557 cm^{-1}, 1371 cm^{-1}, 1270 cm^{-1}, and 1240 cm^{-1} remain significantly increased for the wound biopsy from the dehisced wound compared to the normal and delayed healing wounds. The amide III bands, including the 1340 cm^{-1} Raman vibrational band, are also decreased for the delayed healing wound compared to the normal healing wound, unlike at the first surgical debridement. The intensity of the 938 cm^{-1} vibrational band in the Raman spectrum of the normal healing wound

biopsy also remains increased when compared to the band intensities of the delayed healing or dehisced wound biopsy spectra. Finally, the Raman vibrational band at 1405 cm^{-1} is apparently decreased for the dehisced wound biopsy when compared to the normal and delayed healing wounds, at both the first and final surgical debridements.

Band area ratios were calculated for the normal and delayed healing wounds for wound biopsies collected at each surgical debridement. As expected, there are three additional time points presented for the delayed healing wound. The plot of the 1665 cm^{-1}/1445 cm^{-1} band area ratios shows an initial decrease followed by an increase for the normal healing wound biopsies. The band area ratio for the delayed wound continues to decrease over time, unlike the normal healing wound biopsies. A similar trend is observed for the 1240 cm^{-1}/1270 cm^{-1} band area ratios; the band area ratio increases for the normal healing wound but continually decreases for the delayed healing wound.

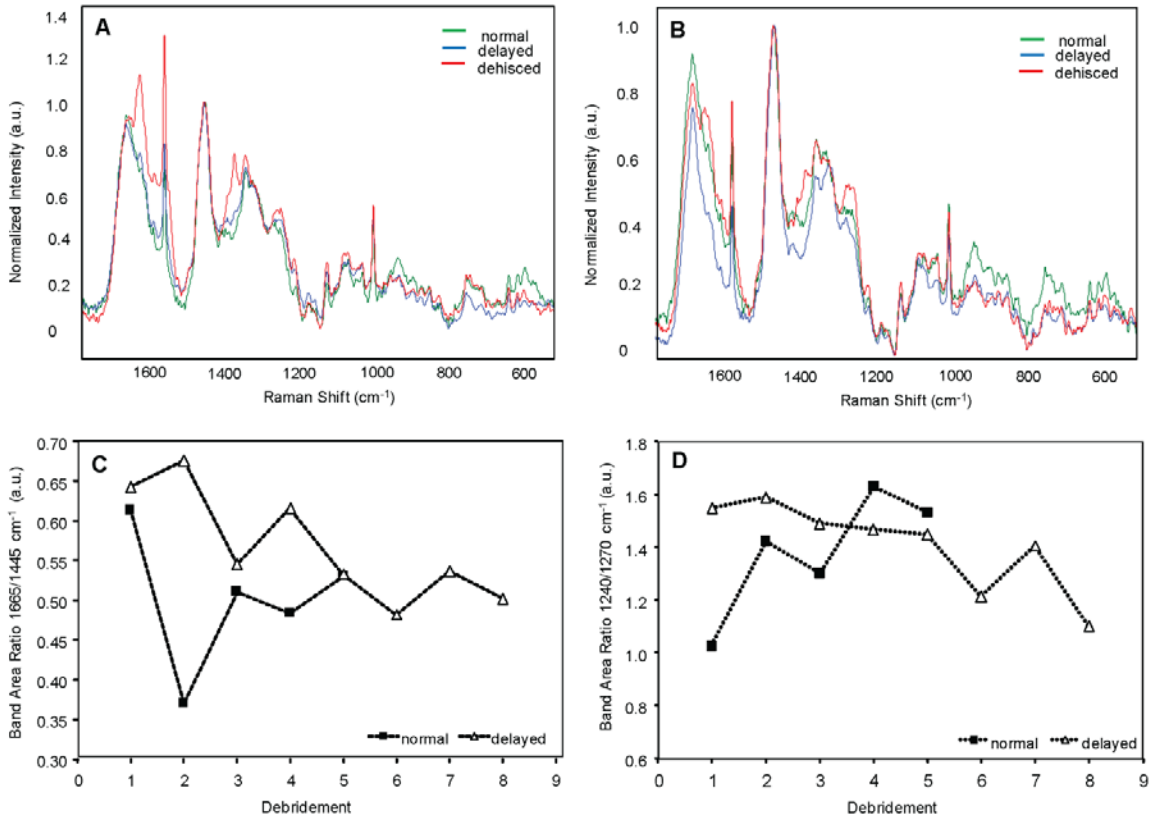

Figure 2. A) Comparison of Raman spectra for first debridement biopsies from three different wounds. B) Comparison of Raman spectra for final debridement biopsies from three different wounds. C) Profile of 1665 cm^{-1}/1445 cm^{-1} band area ratio over time for biopsies from two different wounds. D) Profile of 1240 cm^{-1}/1270 cm^{-1} band area ratio over time for biopsies from the same two wounds.

3.2 Raman spectral comparison of muscle tissue and heterotopic ossification tissue

Raman spectra of *ex vivo* samples of uninjured (or control) muscle, injured muscle, and excised tissue from heterotopic ossification surgical removal were also compared. Figure 3A shows the offset spectra of a control muscle sample, a sample of unmineralized HO tissue, and a sample of mineralized HO tissue. The gray boxes highlight regions of spectral difference. The mean band center for the amide I band of uninjured muscle is 1655 cm^{-1}. For the HO tissue, whether unmineralized or mineralized, the amide I band shifts to a higher frequency and is centered at 1662-1663 cm^{-1}. Differences are also apparent in the amide III envelope of the spectra. The intensity of the 1340 cm^{-1} Raman vibrational band is decreased in the spectra of the HO tissue compared to the uninjured muscle tissue. The 1270 cm^{-1} and 1240 cm^{-1} Raman vibrational bands are increased in the spectra of the HO tissue compared to the uninjured muscle. The most notable difference in the spectrum of the mineralized HO tissue is the presence of the 960 cm^{-1} band, a ν_1 P-O stretching mode. This is a typical Raman vibrational band observed for

hydroxyapatite, and in this case, for the carbonated hydroxyapatite in bone mineral. Finally, the intensities of the 921 cm^{-1}, 876 cm^{-1}, and 855 cm^{-1} bands are more intense in the spectra of the HO tissue than in the spectrum of the uninjured muscle. The bands at 921 cm^{-1}, 876 cm^{-1}, and 855 cm^{-1} are ν(CC) stretching backbone modes, assigned to proline and hydroxyproline in collagen.

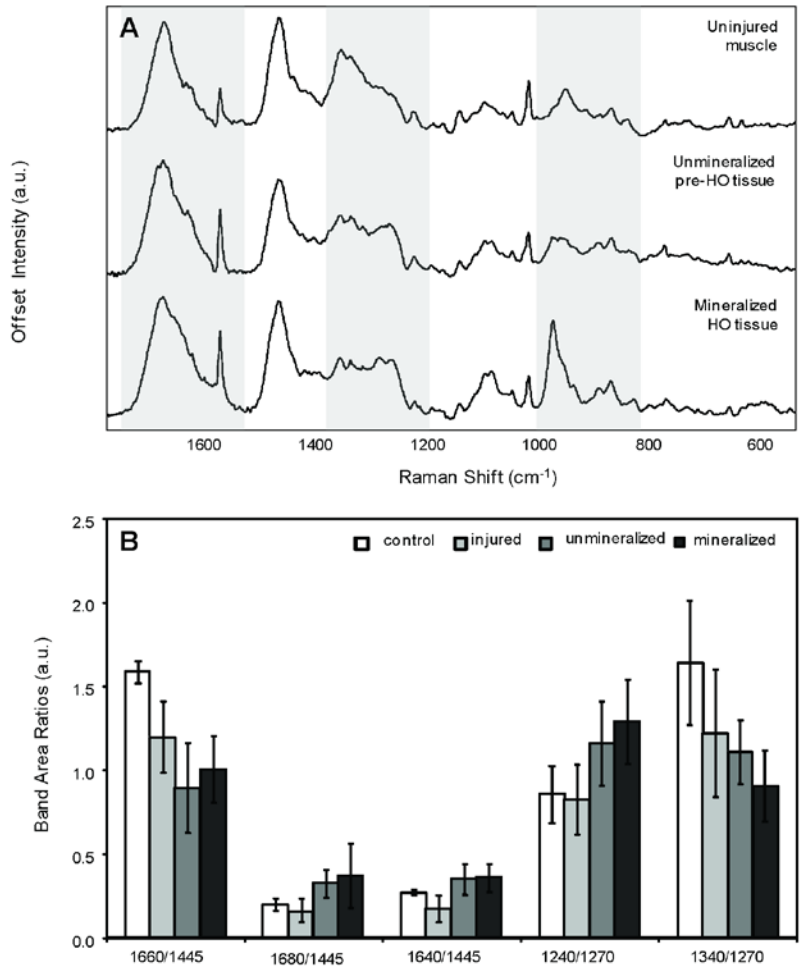

Figure 3. A) Comparison of Raman spectra collected of a control muscle (top) sample, an unmineralized tissue sample from a patient that develops HO (middle), and a mineralized tissue sample from a patient with radiographically confirmed HO (bottom). The gray boxes indicate spectral regions with significantly different profiles. B) Band area ratios calculated from spectra of control muscle, injured muscle, unmineralized HO tissue, and mineralized HO tissue. Error bars = ± standard deviation.

Figure 3B displays calculated band area ratios for the Raman spectra of control muscle (n=3), injured muscle (n=8), unmineralized HO tissue (n=13), and mineralized HO tissue (n=12). There is a statistically significant difference between the 1660 cm^{-1}/1445 cm^{-1} band area ratio when comparing uninjured muscle to injured muscle, as well as when comparing muscle tissue and HO tissue ($p < 0.001$). There is also a significant difference between the 1680 cm^{-1}/1445 cm^{-1} and 1640 cm^{-1}/1445 cm^{-1} band area ratios, when comparing muscle tissue and HO tissue ($p < 0.04$ and $p < 0.02$, respectively). Band area ratios for the amide III envelope also indicate significant differences between the tissue types. The *p*-values calculated for the 1240 cm^{-1}/1270 cm^{-1} band area ratios are < 0.01 for the comparison of muscle tissue and unmineralized HO tissue and < 0.02 for the comparison of muscle tissue and mineralized HO tissue. Notable differences are also demonstrated for the comparison of the 1340 cm^{-1}/1270 cm^{-1} band area ratios calculated for muscle tissue and HO tissue, as well as for unmineralized and mineralized HO tissue ($p < 0.05$).

3.3 FT-IR imaging of wound effluent

A visible light image of a dried, non-colonized effluent sample is displayed in Figure 4A. The corresponding score image (Figure 4B) and major factor (Figure 4C) are also shown. The score image indicates that the presence of this factor is contained primarily within the center of the effluent drop, not the ring of the effluent drop. The factor, which is representative of the major component in the effluent, exhibits vibrational bands that can be mostly attributed to various proteinaceous components – plasma, hemoglobin, cells. The 1666 cm^{-1} and 1550 cm^{-1} vibrational bands are assigned to the amide I and amide II bands, respectively, and are evident in the spectrum of proteins.[38, 61] The vibrational band at 1589 cm^{-1} has been observed the FT-IR spectrum of plasma.[62] The band at 1454 cm^{-1} has the same vibrational band assignment for Raman and FT-IR spectroscopy (C-H deformation of CH_2).[38] The vibrational band at 1404 cm^{-1} is assigned to a C=O stretching band (carbohydrates, amino acids) while the 1312 cm^{-1} and 1247 cm^{-1} bands are assigned to the amide III N-H deformation (proteins). The 1247 cm^{-1} band also overlaps with a P=O stretching band, often observed in phospholipids.[38] The bands displayed between 1200-900 cm^{-1} are generally attributed to the C-O stretching modes of saccharides, glucose, lactate, and glycerol.[61]

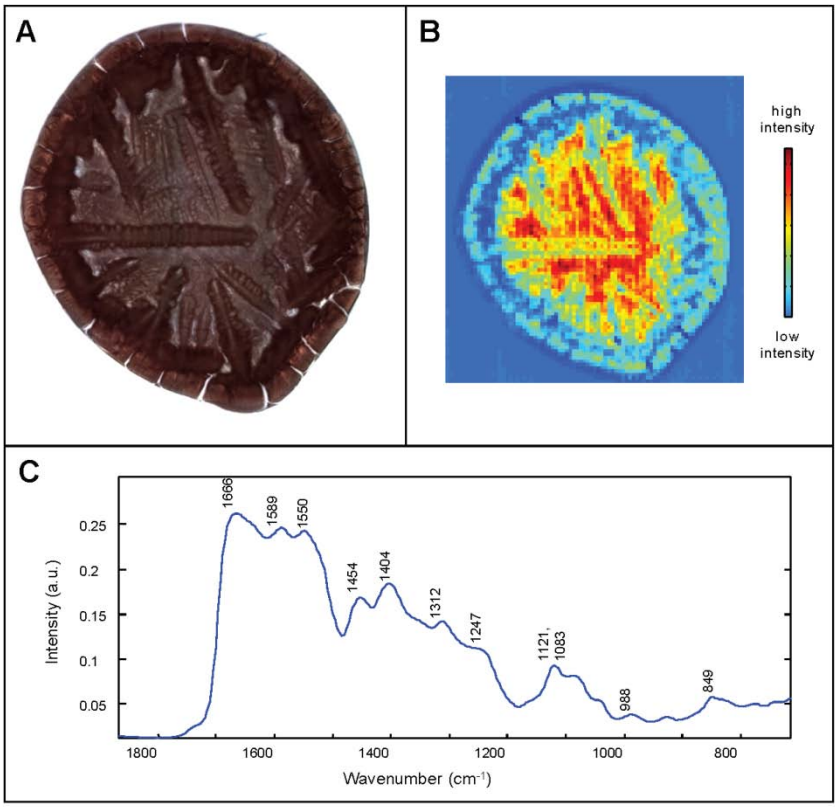

Figure 4. A) Visible light image of non-colonized wound effluent deposited onto aluminized slide. The FT-IR score image (B) and corresponding factor (C) are also shown.

Similar results were obtained for a sample of colonized effluent (Figure 5). Bacterial colonization for this study is defined as a bacterial load $\geq 10^5$ colony forming units.[63] The dried effluent appears visibly similar (Figure 5A) to the sample shown in Figure 4. The score image in Figure 5B and the factor in Figure 5D also resemble the score image and factor obtained for the previously mentioned sample. There is, however, a second factor (Figure 5E) and corresponding score image. The score image in Figure 5C indicates that the second factor is present in the ring of the effluent drop, as well as the center of the effluent drop. The factor in Figure 5E is also proteinaceous in nature, but contains bands that are shifted and have different intensities from the factor shown in Figure 5D.

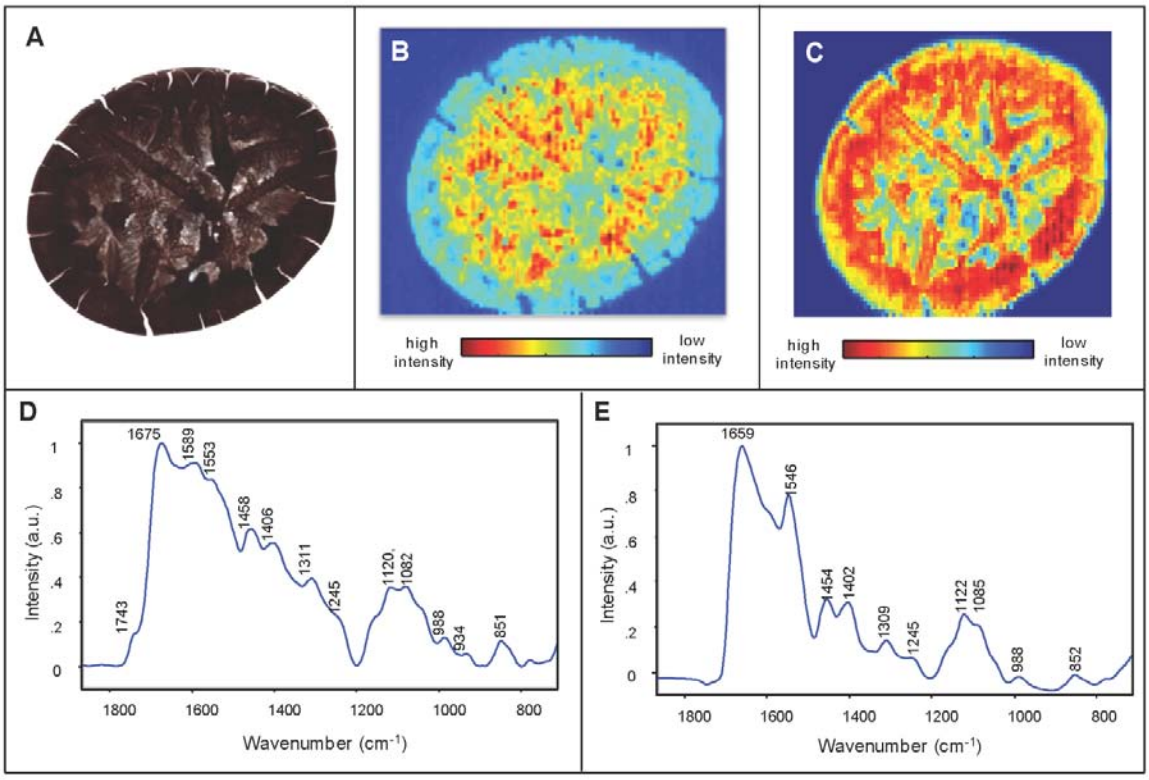

Figure 5. A) Visible light image of colonized wound effluent deposited onto aluminized slide. The FT-IR score images, (B) and (C), and the corresponding major factors, (D) and (E), are also shown.

For this preliminary study, images from three colonized effluent samples (n=3) and one non-colonized effluent sample (n=1) were examined. Microbiological tests of the effluent reported colonization with *Acinetobacter baumannii* for three of the samples. Analysis of each of the colonized samples revealed a second factor, similar to that shown in Figure 5E. Subsequently, the spectral profile of the second factor was compared to FT-IR spectra of several biofilm producing *Acinetobacter baumanni* strains (Figure 6). The spectra overlay closely, suggesting the possibility that the second factor is representative of bacteria, and more specifically *Acinetobacter baumannii*. Differences in the spectral profiles for the *Acinetobacter baumannii* strains are found primarily in the vibrational bands between 1350 cm^{-1} and 900 cm^{-1}. These vibrational bands are of mixed origin, including carbohydrates, proteins, phospholipids, and nucleic acids.

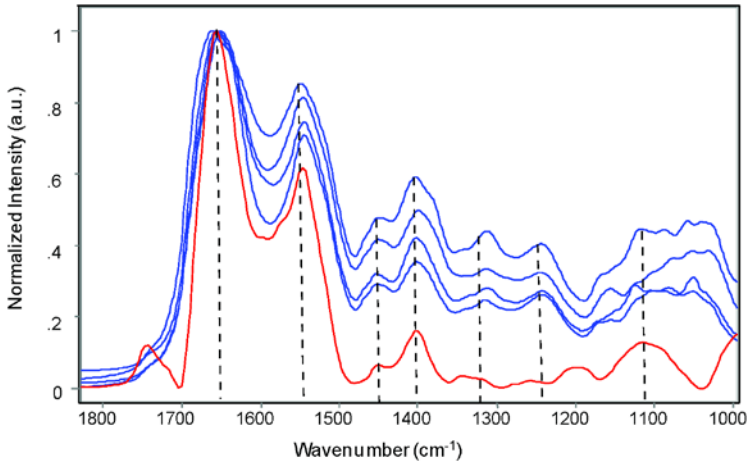

Figure 6. Comparison of FT-IR spectral profiles of second colonized wound effluent factor (red) and reference spectra of different biofilm forming *Acinetobacter baumannii* strains (blue).

4. DISCUSSION

Wounds are currently evaluated using parameters such as location of injury, crude adequacy of perfusion, gross appearance of the wound, wound tensile strength, and the patient's general condition. Parameters like location of injury, gross appearance of the wound, and the patient's general condition are quite obvious and reasonably assessed; however, parameters such as adequacy of perfusion and tensile strength are not readily quantifiable during surgery. It has been previously demonstrated that there is a greater incidence of associated vascular injury in delayed healing wounds when compared to normal healing wounds.[3] It is also well established that tensile strength of the wound is dependent on collagen deposition.[64] Confounding these issues is the development of heterotopic ossification (HO) in over 60% our patient population.[1, 65] Heterotopic ossification is the spontaneous mineralization of soft tissue, which once formed, can only be managed surgically, as spontaneous resolution is infrequent.[66] Because of this, prophylaxis is much preferred to the treatment. Thus, there exists a need for technologies that can non-invasively and objectively assess these challenging wounds in an effort to better guide surgical decision-making in the setting of delayed wound healing, and/or prophylactic therapy in cases of early mineralization (heterotopic ossification).

In this preliminary study, Raman spectroscopic profiling of *ex vivo* wound biopsies collected during wound surgical debridements demonstrates a decrease in the 1665 cm^{-1}/1445 cm^{-1} band area ratio of an impaired healing wound over the course of treatment compared to a normal healing wound. Using the CH_2 scissoring band area (1445 cm^{-1}) as an indicator of overall proteinaceous content and the amide I band area (1665 cm^{-1}) as a measure of collagen content, one can monitor collagen deposition in the wound biopsies, utilizing the 1665 cm^{-1}/1445 cm^{-1} band area ratio. Thus, the decrease in the 1665 cm^{-1}/1445 cm^{-1} band area ratios could be an indication of impaired collagen deposition in wounds that are classified as delayed healing wounds. Additionally, the delayed healing wound exhibits a chronological decrease in the 1240 cm^{-1}/1270 cm^{-1} band area ratio compared to the normal healing wound. The Raman spectral profile of muscle differs from collagen, especially in the amide III envelope. Specifically, muscle tissue exhibits a reduced 1240 cm^{-1}/1270cm^{-1} band area ratio compared to collagen. Thus, an increase in the 1240 cm^{-1}/1270 cm^{-1} band area ratio could also be reflective of collagen deposition within the site of injury. In a response to muscle injury, collagen is formed and deposited within the site of the injury.[67] These results corroborate an earlier study, in which wound biopsies were mapped with Raman spectroscopy at two time points during the healing process – first surgical debridement and last surgical debridement.[68]

Raman spectroscopy was also utilized to discern molecular changes that precursor the development of heterotopic ossification (HO). The molecular etiology of heterotopic ossification is complex and not well understood.[2, 65-66, 69] In this preliminary study, we compared normal muscle tissue to injured muscle tissue, unmineralized HO tissue, and mineralized HO tissue. While mature HO tissue is generally apparent upon physical examination, radiologic studies, or Raman spectroscopic probing, immature and largely unmineralized HO tissue is not as obvious. The Raman spectra of various tissues demonstrate that there are clear differences in the amide I and amide III spectral regions of HO tissue compared to normal tissue, which may provide clues as to whether or not muscle tissue will develop HO. These differences include a significant shift in the location of the amide I band and an increase in the 1240 cm^{-1}/1270 cm^{-1} band area ratio. In fact, the Raman spectrum of unmineralized HO tissue closely resembles the Raman spectrum of collagen. Type I collagen not only plays an important role in the process of wound healing, but also in the formation of osseous tissue, such as HO tissue. Osteoblasts secrete and deposit type I collagen, which comprises 90% of bone matrix, prior to mineralization.[70] In some cases, the collagen that serves as an initiator of wound healing may also act as the scaffold for the deposition of bone mineral.

As we have demonstrated, vibrational spectroscopy can also be utilized to examine wound effluent, in addition to the wound tissue itself. Wound effluent is a complex mixture of fluids, cells, and proteins, containing plasma, lymph fluid, white blood cells, red blood cells, dead tissue and cells, cytokines, chemokines, and growth factors. In some cases, the wound effluent is colonized with bacteria. The most common isolate observed in our patient population is *Acinetobacter baumannii*.[63] Current microbiological techniques require a 24-48 culture period following sample collection. Here, we were able to extract a spectroscopic factor that closely resembles the FT-IR spectrum of *Acinetobacter baumannii* in less than an hour. FT-IR spectra of individual *Acinetobacter baumannii* strains exhibited spectral differences from 1350-900 cm^{-1}. While the band assignments over this spectral region are mixed, other studies have found subsets of that spectral region optimal for discriminating *Brucella* species[71], Gram

negative bacteria[45], and *Bordetella pertussis*[47]. This kind of rapid assessment may eventually help to direct antibiotic therapy and prevent over- or under-treatment of bacterial infection.

Raman spectra of wound tissue was collected and analyzed, to compare the chemical compositions of normal healing wound tissue, impaired healing wound tissue, and HO wound tissue. While all data acquisition and analysis was performed outside of the surgical arena, it is possible to incorporate the Raman spectroscopic equipment into the operating room. One advantage of Raman spectroscopy is that it can be employed in a non-invasive manner, such as a fiber probe-coupled system. Another advantage of Raman spectroscopy, and particularly the fiber-coupled probe used in this study, is the probe design itself. The Raman spectroscopic system utilized here could sample a tissue volume of up to ~60 mm^3, or greater; a standard punch biopsy samples approximately 140 mm^3 of tissue. Though the number of samples examined here was small and preliminary, the results are encouraging and certainly deserving of further study.

5. CONCLUSIONS

This study demonstrates the potential of vibrational spectroscopy as a technique capable of affording an objective measurement regarding wound effluent colonization, wound healing, and wound HO in the operating room. Such a capability would allow for real-time point of care analysis of wounds, allowing subjective decisions to be supplanted by objective data. This is a critical need as constraints on surgical education reduce operative exposure and clinical decision-making is moved from the subjective arena to personalized, data driven decisions. The use of such methodologies as presented herein, may allow for fewer debridement procedures, reduced costs, and faster rehabilitation in patients with traumatic wounds. In order to reach this potential, future work must to expand the number of patients in the study to better delineate Raman spectroscopic trends during the wound healing process and to explore and develop a classification model for wound infection.

6. ACKNOWLEDGEMENTS

The authors would like to thank Frederick Gage for the collection of tissue samples examined in these studies. The authors would also like to thank Dr. Daniel Zurowski for providing the reference bacterial strains presented in this study. This work was prepared as part of the authors' official duties. Title 17 U.S.C. §105 provides that 'Copyright protection under this title is not available for any work of the United States Government.' Title 17 U.S.C. §101 defines a U.S. Government work as a work prepared by a military service member or employee of the U.S. Government as part of that person's official duties. The views expressed in this article are those of the author and do not necessarily reflect the official policy or position of the Department of the Navy, Department of Defense, nor the U.S. Government. This work was supported by funded by work unit number 604771N.0933.001.A0604.

7. REFERENCES

[1] B. K. Potter, T. C. Burns, A. P. Lacap *et al.*, "Heterotopic ossification following traumatic and combat-related amputations. Prevalence, risk factors, and preliminary results of excision," J Bone Joint Surg Am, 89(3), 476-86 (2007).

[2] J. A. Forsberg, J. M. Pepek, S. Wagner *et al.*, "Heterotopic ossification in high-energy wartime extremity injuries: prevalence and risk factors," J Bone Joint Surg Am, 91(5), 1084-91 (2009).

[3] J. S. Hawksworth, A. Stojadinovic, F. A. Gage *et al.*, "Inflammatory biomarkers in combat wound healing," Ann Surg, 250(6), 1002-7 (2009).

[4] H. Wills, R. Kast, C. Stewart *et al.*, "Raman spectroscopy detects and distinguishes neuroblastoma and related tissues in fresh and (banked) frozen specimens," J Pediatr Surg, 44(2), 386-91 (2009).

[5] T. J. Harvey, E. C. Faria, A. Henderson *et al.*, "Spectral discrimination of live prostate and bladder cancer cell lines using Raman optical tweezers," J Biomed Opt, 13(6), 064004 (2008).

[6] P. O. Andrade, R. A. Bitar, K. Yassoyama *et al.*, "Study of normal colorectal tissue by FT-Raman spectroscopy," Anal Bioanal Chem, 387(5), 1643-8 (2007).

[7] H. P. Buschman, G. Deinum, J. T. Motz *et al.*, "Raman microspectroscopy of human coronary atherosclerosis: biochemical assessment of cellular and extracellular morphologic structures in situ," Cardiovasc Pathol, 10, 69-82 (2001).
[8] A. Carden, R. M. Rajachar, M. D. Morris *et al.*, "Ultrastructural changes accompanying the mechanical deformation of bone tissue: a Raman imaging study," Calcified Tissue Int, 72, 166-175 (2003).
[9] K. L. Chan, G. Zhang, M. Tomic-Canic *et al.*, "A Coordinated Approach to Cutaneous Wound Healing: Vibrational Microscopy and Molecular Biology," J Cell Mol Med, (2008).
[10] M. V. Chowdary, K. K. Kumar, K. Thakur *et al.*, "Discrimination of normal and malignant mucosal tissues of the colon by Raman spectroscopy," Photomed Laser Surg, 25(4), 269-74 (2007).
[11] N. J. Crane, V. Popescu, M. D. Morris *et al.*, "Raman spectroscopic evidence for octacalcium phosphate and other transient mineral species deposited during intramembraneous mineralization," Bone, 39, 434-442 (2006).
[12] A. S. Haka, Z. Volynskaya, J. A. Gardecki *et al.*, "In vivo margin assessment during partial mastectomy breast surgery using raman spectroscopy," Cancer Res, 66(6), 3317-22 (2006).
[13] P. R. Jess, D. D. Smith, M. Mazilu *et al.*, "Early detection of cervical neoplasia by Raman spectroscopy," Int J Cancer, 121(12), 2723-8 (2007).
[14] S. Koljenovic, T. C. Schut, R. Wolthuis *et al.*, "Raman spectroscopic characterization of porcine brain tissue using a single fiber-optic probe," Anal Chem, 79(2), 557-64 (2007).
[15] G. Leroy, G. Penel, N. Leroy *et al.*, "Human tooth ename: a Raman polarized approach," Appl Spectrosc, 56(8), 1030-1034 (2002).
[16] N. McGill, P. A. Dieppe, M. Bowden *et al.*, "Identification of pathological mineral deposits by Raman microscopy," Lancet, 337, 77-78 (1991).
[17] A. Robichaux-Viehoever, E. Kanter, H. Shappell *et al.*, "Characterization of Raman spectra measured in vivo for the detection of cervical dysplasia," Appl Spectrosc, 61(9), 986-93 (2007).
[18] G. Shetty, C. Kendall, N. Shepherd *et al.*, "Raman spectroscopy: elucidation of biochemical changes in carcinogenesis of oesophagus," Br J Cancer, 94(10), 1460-4 (2006).
[19] M. G. Shim, B. C. Wilson, E. Marple *et al.*, "Study of fiber-optic orobes for *in vivo* medical Raman spectroscopy," Appl Spectrosc, 53(6), 619-627 (1999).
[20] T. D. Wang, and J. Van Dam, "Optical biopsy: a new frontier in endoscopic detection and diagnosis," Clin Gastroenterol Hepatol, 2(9), 744-53 (2004).
[21] G. Chen, J. Chen, S. Zhuo *et al.*, "Nonlinear spectral imaging of human hypertrophic scar based on two-photon excited fluorescence and second-harmonic generation," Br J Dermatol, 161(1), 48-55 (2009).
[22] A. Carden, and M. D. Morris, "Application of vibrational spectroscopy to the study of mineralized tissues," J Biomed Optics, 5(3), 259-268 (2000).
[23] A. Carden, T. J. A. Morris, C. M. Edwards *et al.*, "Raman imaging of bone mineral and matrix: composition and function," Proc SPIE, 3608, 132-138 (1999).
[24] C. J. de Grauw, J. D. de Bruijn, C. Otto *et al.*, "Investigation of bone and calcium phospahte coatings and crystallinity determination using Raman micrrospectroscopy," Cell Mater, 6(1-3), 57-62 (1996).
[25] M. D. Morris, A. Carden, R. M. Rajachar *et al.*, "Bone microstructure deformation observed by Raman microscopy," Proc SPIE, 4254, 81-89 (2001).
[26] M. D. Morris, and W. F. Finney, "Recent developments in Raman and infrared spectroscopy and imaging of bone tissue," Spectroscopy, 18(2), 155-159 (2004).
[27] M. D. Morris, S. Stewart, C. Tarnowski *et al.*, "Raman spectroscopy of early mineralization of normal and pathological calvaria," Proc SPIE, 4614, 28-39 (2002).
[28] M. D. Morris, C. Tarnowski, J. L. Dreier *et al.*, "Raman microscopy of *de novo* woven bone tissue," Proc. SPIE, 4254, (2001).
[29] G. Penel, N. Leroy, P. van Lanuyt *et al.*, "Raman microspectrometry studies of brushite cement: *In vivo* evolution in a sheep model," Bone, 25(2), 81S-84S (1999).
[30] G. Pezzotti, and S. Sakakura, "Study of the toughening mechanisms in bone and biomimetic hydroxyapatite materials using Raman microprobe spectroscopy," J Biomed Mater Res, 65A, 229-236 (2003).
[31] J. A. Pezzuti, M. D. Morris, J. F. Bonadio *et al.*, "Hyperspectral Raman Imaging of Bone Growth and Regrowth Chemistry," Proc SPIE, 3261, 270 - 276 (1998).
[32] Smith, and I. Rehman, "Fourier transform Raman spectroscopic studies of human bone," J Mater Sci: Mater Med, 5, 775-778 (1995).

[33] C. P. Tarnowski, M. A. Ignelzi, and M. D. Morris, "Mineralization of developing mouse calvaria as revealed by Raman microspectroscopy," J Bone Miner Res, 17(6), 1118-1126 (2003).
[34] J. Timlin, A. Carden, M. D. Morris *et al.*, "Raman spectroscopic imaging markers for fatigue-related microdamage in bovine bone," Anal Chem, 72(10), 2229-2236 (2000).
[35] J. A. Timlin, A. Carden, M. D. Morris *et al.*, "Spatial distribution of phosphate species in mature and newly generated mammalian bone by hyperspectral Raman imaging," J Biomed Opt, 4(1), 28-34 (1999).
[36] P. C. Buijtels, H. F. Willemse-Erix, P. L. Petit *et al.*, "Rapid identification of mycobacteria by Raman spectroscopy," J Clin Microbiol, 46(3), 961-5 (2008).
[37] M. F. Escoriza, J. M. VanBriesen, S. Stewart *et al.*, "Raman spectroscopy and chemical imaging for quantification of filtered waterborne bacteria," J Microbiol Methods, 66(1), 63-72 (2006).
[38] K. Maquelin, C. Kirschner, L. P. Choo-Smith *et al.*, "Identification of medically relevant microorganisms by vibrational spectroscopy," J Microbiol Methods, 51(3), 255-71 (2002).
[39] Q. Wu, W. H. Nelson, S. Elliot *et al.*, "Intensities of E. coli nucleic acid Raman spectra excited selectively from whole cells with 251-nm light," Anal Chem, 72(13), 2981-6 (2000).
[40] L. Zeiri, B. V. Bronk, Y. Shabtai *et al.*, "Surface-enhanced Raman spectroscopy as a tool for probing specific biochemical components in bacteria," Appl Spectrosc, 58(1), 33-40 (2004).
[41] K. Maquelin, L. Dijkshoorn, T. J. van der Reijden *et al.*, "Rapid epidemiological analysis of Acinetobacter strains by Raman spectroscopy," J Microbiol Methods, 64(1), 126-31 (2006).
[42] K. Maquelin, L. P. Choo-Smith, T. van Vreeswijk *et al.*, "Raman spectroscopic method for identification of clinically relevant microorganisms growing on solid culture medium," Anal Chem, 72(1), 12-9 (2000).
[43] K. S. Kalasinsky, T. Hadfield, A. A. Shea *et al.*, "Raman chemical imaging spectroscopy reagentless detection and identification of pathogens: signature development and evaluation," Anal Chem, 79(7), 2658-73 (2007).
[44] L. Zeiri, B. V. Bronk, Y. Shabtai *et al.*, "Silver metal induced surface enhanced Raman of bacteria," Colloid Surface A, 208, 357-362 (2002).
[45] A. Bosch, A. Minan, C. Vescina *et al.*, "Fourier transform infrared spectroscopy for rapid identification of nonfermenting gram-negative bacteria isolated from sputum samples from cystic fibrosis patients," J Clin Microbiol, 46(8), 2535-46 (2008).
[46] K. Maquelin, C. Kirschner, L. P. Choo-Smith *et al.*, "Prospective study of the performance of vibrational spectroscopies for rapid identification of bacterial and fungal pathogens recovered from blood cultures," J Clin Microbiol, 41(1), 324-9 (2003).
[47] D. O. Serra, G. Lucking, F. Weiland *et al.*, "Proteome approaches combined with Fourier transform infrared spectroscopy revealed a distinctive biofilm physiology in Bordetella pertussis," Proteomics, 8(23-24), 4995-5010 (2008).
[48] C. L. Winder, E. Carr, R. Goodacre *et al.*, "The rapid identification of Acinetobacter species using Fourier transform infrared spectroscopy," J Appl Microbiol, 96(2), 328-39 (2004).
[49] J. S. Hawksworth, A. Stojadinovic, F. A. Gage *et al.*, "Inflammatory Biomarkers in Combat Wound Healing," Ann Surg, 250(6), 1002-7 (2009).
[50] E. Widjaja, C. Li, W. Chew *et al.*, "Band-Target Entropy Minimization. A robust algorithm for pure component spectra recovery. Application to complex randomized mixtures of six components," Anal Chem, 75, 4499-4507 (2003).
[51] E. Widjaja, N. Crane, T. Chen *et al.*, "Band-Target Entropy Minimization (BTEM) Applied to Hyperspectral Raman Image Data," Appl Spectrosc, 57(11), 1353-1362 (2003).
[52] L. R. Ong, E. Widjaja, R. Stanforth *et al.*, "Fourier transform Raman spectral reconstruction of inorganic lead mixtures using a novel band-target entropy minimization (BTEM) method," J Raman Spectrosc, 34, 282-289 (2003).
[53] B. R. Wood, and D. McNaughton, "Raman excitation wavelength investigation of single red blood cells in vivo," J Raman Spectrosc, 33(7), 517-523 (2002).
[54] S. U. Sane, S. M. Cramer, and T. M. Przybycien, "A holistic approach to protein secondary structure characterization using amide I band Raman spectroscopy," Anal Biochem, 269(2), 255-72 (1999).
[55] J. L. Lippert, D. Tyminski, and P. J. Desmeules, "Determination of the secondary structure of proteins by laser Raman spectroscopy," J Am Chem Soc, 98(22), 7075-80 (1976).
[56] N. C. Maiti, M. M. Apetri, M. G. Zagorski *et al.*, "Raman spectroscopic characterization of secondary structure in natively unfolded proteins: alpha-synuclein," J Am Chem Soc, 126(8), 2399-408 (2004).

[57] M. Pezolet, M. Pigeon, D. Menard *et al.*, "Raman spectroscopy of cytoplasmic muscle fiber proteins. Orientational order," Biophys J, 53(3), 319-25 (1988).
[58] J. Wohlrab, A. Vollmann, S. Wartewig *et al.*, "Noninvasive characterization of human stratum corneum of undiseased skin of patients with atopic dermatitis and psoriasis as studied by Fourier transform Raman spectroscopy," Biopolymers, 62(3), 141-6 (2001).
[59] B. G. Frushour, and J. L. Koenig, "Raman scattering of collagen, gelatin, and elastin," Biopolymers, 14, 379-391 (1975).
[60] L. Chrit, C. Hadjur, S. Morel *et al.*, "In vivo chemical investigation of human skin using a confocal Raman fiber optic microprobe," J Biomed Opt, 10(4), 44007 (2005).
[61] G. Deleris, and C. Petibois, "Applications of FT-IR spectrometry to plasma contents analysis and monitoring," Vib Spectrosc, 32(1), 129-136 (2003).
[62] J. Mordehai, J. Ramesh, M. Huleihel *et al.*, [Health status prediction using FTIR microspectroscopy of blood components and cluster analysis], (2003).
[63] F. R. Sheppard, P. Keiser, D. W. Craft *et al.*, "The majority of US combat casualty soft-tissue wounds are not infected or colonized upon arrival or during treatment at a continental US military medical facility," Am J Surg, 200(4), 489-95 (2010).
[64] F. C. Brunicardi, D. Andersen, T. Billiar *et al.*, [Schwartz's Manual of Surgery] The McGraw-Hill Companies, New York, NY(2006).
[65] M. B. K. Potter, L. J. A. Forsberg, T. A. Davis *et al.*, "Heterotopic Ossification Following Combat-Related Trauma," J Bone Joint Surg Am, 92(Supplement_2), 74-89 (2010).
[66] J. L. Hunt, B. D. Arnoldo, K. Kowalske *et al.*, "Heterotopic ossification revisited: a 21-year surgical experience," J Burn Care Res, 27(4), 535-40 (2006).
[67] J. L. Kaar, Y. Li, H. C. Blair *et al.*, "Matrix metalloproteinase-1 treatment of muscle fibrosis," Acta Biomater, 4(5), 1411-20 (2008).
[68] N. J. Crane, T. S. Brown, K. N. Evans *et al.*, "Monitoring the healing of combat wounds using Raman spectroscopic mapping," Wound Repair Regen, 18(4), 409-16 (2010).
[69] K. Liu, S. Tripp, and L. J. Layfield, "Heterotopic ossification: review of histologic findings and tissue distribution in a 10-year experience," Pathol Res Pract, 203(9), 633-40 (2007).
[70] F. S. Kaplan, W. C. Hayes, T. M. Keaveny *et al.*, [Form and Function of Bone] American Academy of Orthopaedic Surgeons, Rosemont, IL(1994).
[71] M. A. M. Gomez, M. A. B. Perez, F. J. M. Gil *et al.*, "Identification of species of Brucella using fourier transform infrared spectroscopy," J Microbiol Meth, 55(1), 121-131 (2003).

8

Use of Optical Imaging and Spectroscopy in Assessment of Organ Perfusion

Samuel Phinney[1], Nicole J. Crane[2], Frederick A. Gage[2], Alexander M. Gorbach[3], and Eric A. Elster[2, 4]

[1]Department of Surgery, Walter Reed Army Medical Center, Washington, D.C.
[2]Department of Regenerative Medicine, Operational and Undersea Medicine Directorate, Naval Medical Research Center, Silver Spring, MD
[3]Bioengineering and Physical Science, National Institute of Biomedical Imaging and Bioengineering, National Institutes of Health, Bethesda, MD
[4]Department of Surgery, Uniformed Services University of the Health Sciences, Bethesda, MD

Corresponding author: Eric A. Elster
Department of Regenerative Medicine, Operational and Undersea Medicine Directorate, Naval Medical Research Center, 503 Robert Grant Avenue, Silver Spring MD 20910, Phone: 301 319 8632,
E-mail: eric.elster1@med.navy.mil

Abstract

We present procedures to use imaging to assess organ perfusion in an ischemia/reperfusion injury model in the intraoperative and organ procurement setting, in particular, on pump perfusion. These technologies, namely 3-CCD, IR, and VRIS imaging, use the spectral signatures of kidneys to determine tissue oxygenation and perfusion. This information not only correlates directly with the physiology of organ perfusion but can be provided in a clinically useful, real-time format. Utilization of the technologies in tandem for quantitative assessment of organ viability is discussed.

Key terms: imaging, infrared imaging (IR), organ perfusion, 3-charged couple devices (3-CCD), visible reflectance imaging system (VRIS), ischemia/reperfusion injury, renal transplantation, pump perfusion

8.1 Introduction

Given the tremendous shortage of available organs, there is great interest in using donor kidneys from extended criteria donors that may include underlying disease and prolonged ischemic time. One of the methods employed for this purpose is pump perfusion, also referred to as machine perfusion-preservation. Advantages of pump perfusion include:

1. Extending cold ischemic time without detriment to graft function;
2. Diagnosing segmental or global problems with flow and resistance [1];
3. Limiting delayed graft function [2].

As one of the available kidney perfusion modalities, normothermic pulsatile perfusion is of special interest, as it may have the capability to maintain some metabolic processes, deliver oxygen, remove oxygen free radicals, and preserve cellular adenosine triphosphate (ATP). Normothermic pulsatile perfusion may improve early graft function and possibly graft survival [3].

The major issue that arises with the use of nonideal donor organs is the assessment of the condition of the organ, since it becomes necessary to avoid using those that are damaged significantly and will likely result in graft failure. However, conventional methods of assessing organ perfusion and viability often lack immediate real-time information and organ specificity. In the preoperative setting, there may be surrogate information such as donor comorbidities, creatinine, and glomerular filtration rate, in addition to ischemic time. Intraoperatively or in the organ procurement setting, there is the appearance of the organ, and in the case of pulsatile perfusion pump, pressure, flow, and resistance. Postoperatively, with the return of urine output, labs tests such as creatinine, glomerular filtration rate (GFR), and biopsy, or imaging studies such as CT (computed tomography) scans and radionucleotide perfusion studies are possible though each have significant disadvantages. However, none of these parameters provide direct, comprehensive, and conclusive information about vital factors in ischemia/reperfusion injury. There is a need for real-time, relevant, and objective information to assist in the diagnosis of ischemia and to estimate the extent of ischemic damage and organ resilience. Current clinical measures of ischemia, such as physical exam, intraoperative urine output, and pump resistance and flow, can certainly be improved upon.

Advances in imaging using a variety of spectroscopic technologies hold promise for specific, objective measurements in organ perfusion, particularly in intraoperative and organ procurement settings. Such imaging technologies can be generally categorized into systems which gather a detailed look at a focal area of tissue or globally assess an entire surface of an organ. Using an enhanced understanding of the way light is emitted by tissue (infrared), or reflected by tissue (e.g., a charged coupled device or 3-CCD, and visible reflectance imaging system), we can begin to quantify the information gathered to describe conditions at the cellular or molecular level. Many of these technologies are emerging, some of which hold tremendous promise for an enhanced objective assessment of organ perfusion in real time.

The characteristics of an ideal monitoring system for the assessment of intraoperative organ oxygenation and perfusion would be noninvasive, reproducible, real-time, cost-effective, and easily incorporated into the operating arena and organ procurement lab, as well as capable of directly measuring tissue oxygenation and perfusion.

These imaging techniques should ideally be capable of performing both point spectroscopy, providing detailed information about a small area of tissue, (e.g., a cubic millimeter, equivalent to a biopsy specimen) and global imaging, which can more accurately estimate the health of the entire organ by examining the entire surface or any specific region of interest.

There are two characteristics of the kidney which are particularly relevant when considering different technologies to monitor tissue oxygenation and perfusion. First, the kidney is an end organ entirely without collateral circulation in the parenchyma. Second, the region of the kidney most sensitive to ischemia is the tubular epithelium, abundant superficially beneath the renal capsule [4]. Therefore it is possible to capture the ischemic state of the organ with high fidelity even if the imaging method has limited depth of penetration.

In this chapter, we describe imaging methods to accurately assess kidney perfusion and oxygenation in the intraoperative and organ procurement setting in ischemia/reperfusion injury models, which provides information directly correlated with the physiology of organ perfusion and can be obtained in a clinically useful, real-time format. Both point spectroscopy and global imaging technologies are described. In combination, these spectroscopic modalities have the potential to assess donor kidney viability thoroughly, and therefore enable the use of many currently discarded organs.

8.1.1 Spectral Imaging Technologies Overview

We employ three alternative technologies to assess perfusion and oxygenation state of ischemic kidneys. These technologies provide alternatives to each other with different types of information, strengths, and weaknesses, which when used in tandem can enable accurate and thorough assessment of the level of ischemia in a kidney and ultimately enable real-time evaluation of its viability before, during, and after transplantation. Below, an overview of each technology in context of ischemic kidney evaluation methodology is provided.

8.1.1.1 Three-Charged Coupled Device (3-CCD)

This relatively ubiquitous imaging technology provides chemically specific information in oxygenated/deoxygenated hemoglobin along with a large field of view and real-time in vivo detection simultaneously. It is present in commonly used surgical laparoscopic equipment and a variety of handheld video cameras, hence rendering it an accessible first option for assessing global oxygenation levels. Applications of 3-CCD technology include not only quantification of oxygenation in parenchymal tissue, but also identification of vascular structures in laparoscopic surgery.

3-CCD use in ischemia/reperfusion injury assessment relies on hemoglobin (Hb), which exhibits well established spectroscopic characteristics in both oxygenated and deoxygenated states. Oxygenated Hb has major absorption bands and 416, 541, and 577 nm and deoxygenated Hb has major absorption bands at 430, 556 nm; hence, tissue oxygenation can be readily assessed spectroscopically via Hb. Briefly, a color image is reconstructed and recorded using red, green, and blue bandpass filters in front of three separate monochrome charge coupled devices (CCDs). 3-CCD cameras are widely used in operating room (OR) suites due to better color sensitivity and increased color palette range. The individual colors can be combined, subtracted, and otherwise manipulated

to enhance the contrast of an image so that detection is sensitive to molecules of interest, which for our purposes is hemoglobin.

Enhanced images are prepared by separating the filtered responses (see Figure 8.1) and then by subtracting blue CCD channel absorbance from the red CCD channel absorbance. The enhancement images are plotted using a red-blue color map, where red corresponds to small differences between the signal intensity of the red and blue channels and blue corresponds to large differences between the signal intensity of the red and blue channels. 3-CCD enhancement arises directly from the absorption properties of hemoglobin (Hb). While the red channel total absorbance for deoxygenated Hb (556-nm band) and oxygenated Hb (541-nm and 577-nm bands) are very similar, the difference between deoxygenated Hb (430-nm band) and oxygenated Hb (416-nm band) is much larger in the blue CCD channel. The intensity difference between red and blue channels (ΔS) has a linear relationship with the degree of oxygenation in Hb.

$$S\lambda \cong \int_b^b f(\lambda)A(\lambda)d(\lambda)$$

S, the absorbance signal over a particular wavelength range (λ), is evaluated as an integral of the measured absorbance [A(λ)] over the wavelength (a to b) convoluted with filter attenuation [f(λ)] over the same wavelength range. The contrast between the two different filters is simply the difference of the two integrals:

$$\Delta S_{red-blue} = S_{red} - S_{blue}$$

Deoxygenated Hb exhibits 20% more absorbance relative to oxygenated Hb in the blue channel, when compared to the red channel.

When evaluating tissue in vivo, as in the studies described below, still images of the kidneys are analyzed for glare-free regions of interest (ROIs) to demonstrate relative intensity values, which may be compared to either a control kidney (baseline), or to healthy nonischemic surrounding tissue, or to oxygen saturation of blood (sO_2), as described in Section 8.5.

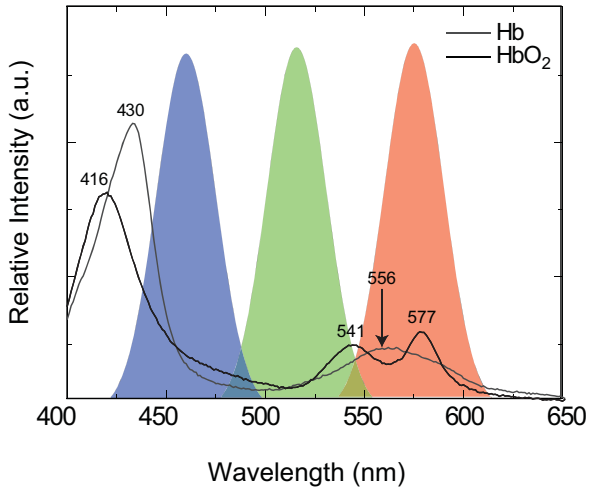

Figure 8.1 The spectral properties of hemoglobin as detected by a 3-CCD camera.

8.1.1.2 Infrared (IR) Imaging

Infrared imaging is based on two-dimensional mapping of temperature differences by detecting natural emissions from the tissue that are warmer (or cooler) than surrounding structures. The relationship of radiation emitted (E) to temperature (T) is exponential (i.e., small changes in temperature lead to large changes in radiation) as expressed by the Stefan-Boltzmann law:

$$E = \sigma T^4$$

This relationship is best demonstrated within the infrared spectrum from approximately 3–5 microns, necessitating specialized equipment. The IR signal is used to assess the degree to which renal surface temperature reflects underlying renal ischemia. There are multiple medical and surgical applications for infrared imaging, which include identification of biliary and ureteral structures and inadvertent injury [5, 6], as well as organ perfusion/viability in transplant and general surgery [7]. In Figure 8.2, perfusion of a live donor kidney is clearly demonstrated with infrared imaging. Prior to unclamping, the kidney is dark; as the kidney reperfuses, the temperature of the kidney increases, resulting in a bright kidney. Additionally, reperfusion of various regions of the kidney can be profiled.

Work with IR on hypothermic pulsatile perfusion has demonstrated a strong correlation with flow and resistance with IR readings, and increased homogeneity of flow after

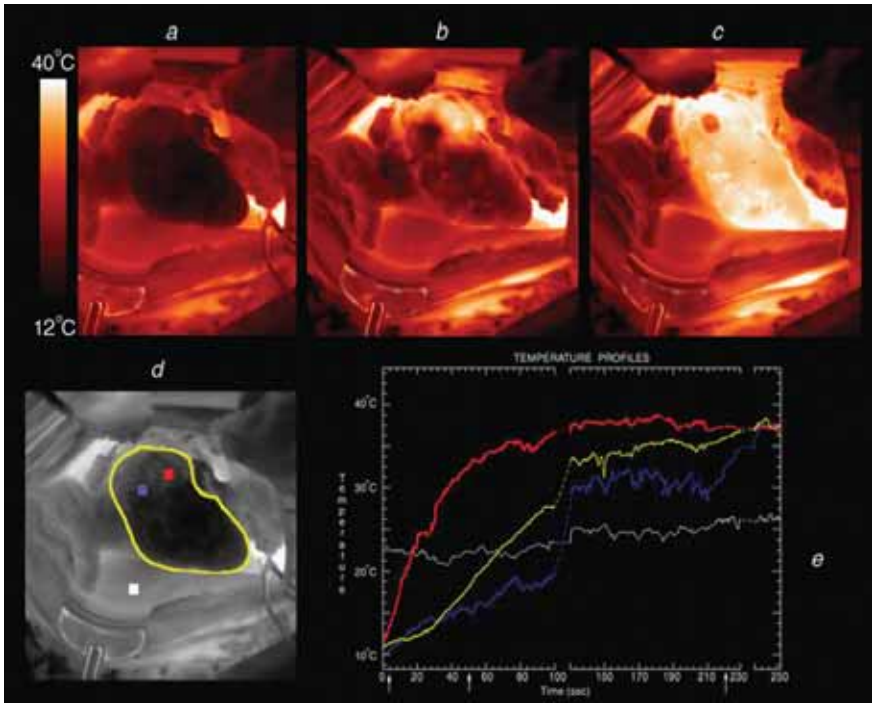

Figure 8.2 Intraoperative thermal profiles from a live donor kidney: (a) kidney immediately prior to unclamping vascular pedicle; (b) after 48 seconds of reperfusion; (c) after 220 seconds of reperfusion and; (d) a grayscale version of (a) with the kidney edges outlined. The blue square in image (d) is a ROI with the lowest signal, where the red square ROI has the highest signal. The graph (e) shows the thermal profiles of each ROI over 250 seconds. Note the degree of heterogeneity in image (b) which has resolved by 170 seconds later in image (c).

pump perfusion both in small and large animal models. Temperature is directly proportional to resistance and is inversely proportional to flow [8, 9].

In intraoperative studies, temperature profiles undergo spectral (frequency) analysis to assess their relationship with well-described oscillations of microcirculation. Two kinds of oscillations in particular are noted: tubuloglomerular feedback (TGF) and very slow oscillations (VSO), at 0.02–0.05 Hz and 0.01 Hz, respectively. While the magnitudes of both oscillations diminish with decreasing blood flow, becoming absent with sufficient ischemia and the returning in a time dependent manner, VSO is more sensitive to ischemia and reperfusion [10]. The intrinsic low frequency oscillations seen in viable tissues in the kidney may represent autoregulation in the form of tubuloglomerular feedback [11]. However, the origin of the low frequency oscillations has not been established. To be able to register such oscillations, the infrared camera should be able to identify small (~0.02–0.04ºC) temperature gradients between perfused vasculature and tissue.

Care should be taken to account the heat emitted from the OR spot lights. These problems may be solved with the use of surgical light that incorporates light-emitting diodes (LED) or a strobe light mechanism. In the organ procurement setting, however, this is less of a problem; the IR camera is positioned above the organ while on the pulsatile perfusion pump (Figure 8.3). IR imaging of kidneys preserved at 5°C on pulsatile perfusion still retains enough temperature contrast to be clinically useful [9]. Likewise, use of cold/room temperature normal saline or use of ice intra-operatively can increase the background temperature gradient and highlight ischemic portions in a reproducible fashion.

8.1.1.3 Visible Reflectance Imaging System (VRIS)

VRIS uses the spectral signature of reflected light in the visible spectrum to infer chemical information from the illuminated sample. Herein we specifically focus on

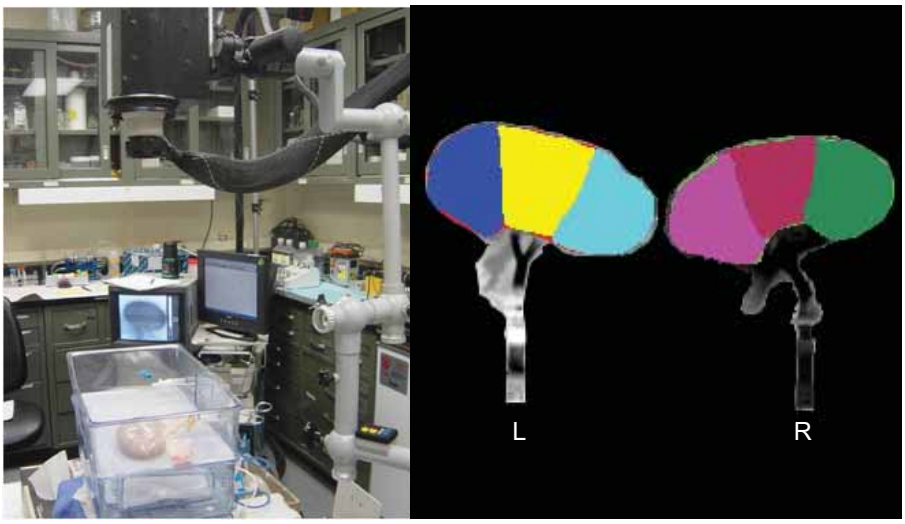

Figure 8.3 (a) The infrared imaging system is positioned over a porcine kidney on a perfusion pump. (b) Representative vascular segments are outlined on the anterior surface of the kidney.

oxygenated and deoxygenated hemoglobin [12] although other autofluroscent molecules such as NADH are also possible targets. Briefly, a quartz-tungsten halogen lamp, emitting 100 watts of light, is used as the broadband white light source to illuminate the kidney. The light is then reflected by mirrors to pass through a liquid crystal tunable filter (LCTF), which can be set to filter specific wavelengths of light. While the filter can function over the wavelength range of 420–700 nm, here an abbreviated wavelength range is employed that focuses just on hemoglobin specific bands (520–645 nm). Once passed through the LCTF, the light is then focused by a camera lens onto a CCD for data collection. Once data collection is finished, image analysis is performed on a personal computer. In Figure 8.4, the index finger of the hand was made ischemic by occlusion with a rubber band. The VRIS image shows a clear difference between the ischemic finger and the rest of the hand. The spectral profile of the perfused finger exhibits oxygenated Hb bands (544 nm and 577 nm), while the spectral profile of the ischemic finger indicates the presence of predominately deoxygenated Hb (565 nm).

Reflectance spectroscopy, either in the visible or near-infrared (NIR) range, is becoming a popular technology for obtaining noninvasive real-time chemical information from tissue. NIR illumination provides a greater depth of penetration below the surface compared to visible illumination, whereas visible illumination is able to reliably and quickly gain spectral information, though from a smaller volume of tissue. Because the difference in Hb oxygenation is greater in the blue region of the visible light spectrum and its depth of penetration is reduced, VRIS can obtain saturated oxygen measurements (sO_2) more rapidly and from a smaller more shallow tissue sample [13]. These characteristics allow for its use in smaller probes, even becoming incorporated into an endoscope/laparoscope. Reflectance spectroscopy has found applications in continuous

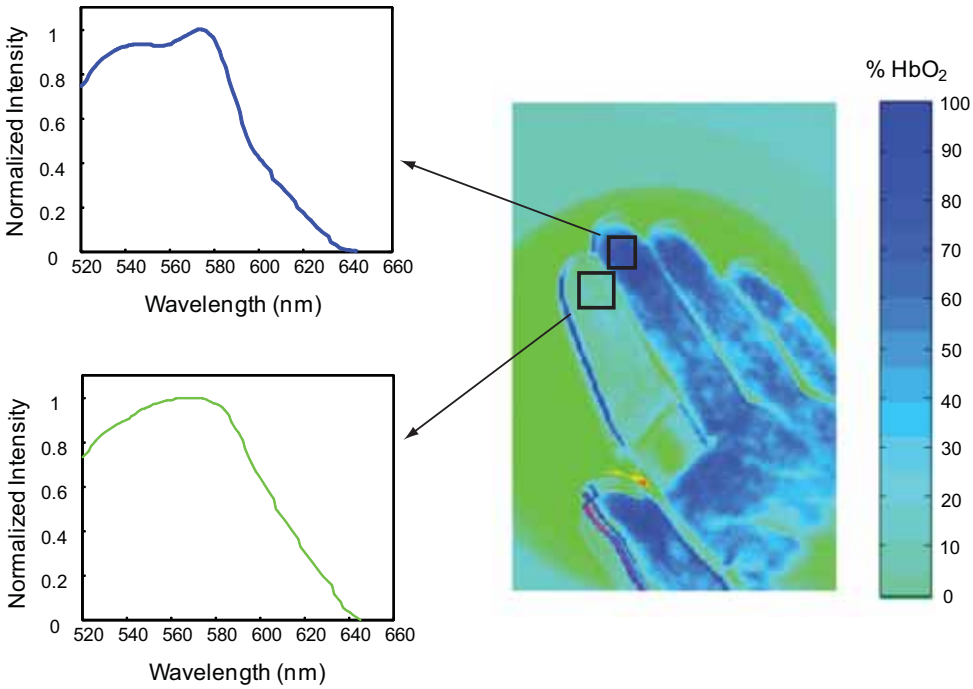

Figure 8.4 Human hand with focal ischemia to the index finger as visualized by VRIS.

peripheral tissue oximetry for identification of multiple organ failure vulnerability in trauma patients [14], to quantify cardiac myoglobin oxygenation/hypoxia and its contribution to supplying mitochondria in increased cardiac workload [15], and assessing the viability of skin flaps [16].

8.1.1.4 Technology Summary

Each of the imaging technologies has strengths and weaknesses in the operative or procurement setting. 3-CCD cameras can provide global tissue oxygenation information during pump perfusion and postanastomosis. 3-CCD cameras are widely used in the operating room and therefore less expensive, and the software for real-time analysis is quickly becoming a reality. However, the depth of penetration for the image analysis is superficial and essentially limited to an exposed organ surface. IR complements 3-CCD by providing enhanced penetration depth, approximately 1–2 cm. The enhanced penetration depth allows IR imaging to monitor tissue temperature and circulation during machine perfusion or in vivo post anastomosis, including assessment of the heterogeneity of tissue microcirculation, particularly relevant in normothermic perfusion of ischemically damaged organs. Further, IR is capable of detecting and quantifying potentially metabolic and regulatory information in the oscillations within the microcirculation. Finally, VRIS further complements 3-CCD and IR by providing an entire spectrum of light over a given range, offering very specific chemical information beyond 3CCD images, for instance tissue NADH levels as an indicator of energy levels during/after ischemia. VRIS is able to measure small volumes of tissue quickly, as part of a probe or endoscope [13, 17–21] or more conventionally for a more global picture of organ perfusion [22–25]. It remains capable of, though further from, real-time assessment than the other technologies and it is not currently commercially available.

In tandem, the three imaging modalities can provide detailed information about the ischemic status of the organ at all stages of organ recovery, preservation, and transplantation. Figure 8.5 summarizes each technology and shows how they might be integrated into a single platform. Ultimately, we envision that the information provided by these imaging methods can be employed to assess the viability of the organ in an objective, quantitative, and accurate fashion such that the decision to transplant can be done accurately with minimal waste of donor organs.

8.2 Experimental Design

Below we describe the equipment, materials, and methods necessary to perform combined imaging with 3-CCD, IR, and VRIS techniques to evaluate ischemia in kidneys. In order to assist in visualizing the experiments, the design is presented as a hypothetical study evaluation viability of porcine kidneys after preservation in Figure 8.6, where an autotransplant model (a Maastricht 1-2 renal autotransplantation/nephrectomy model with 24 hours of interposed storage/pump time) is employed to compare the data and results obtained by imaging modalities described with short term clinical outcomes (urine output, serum creatinine, and histology). However, note that typical results are exemplified in only some of these experimental scenarios. Specifically, the experimental data presented demonstrates the use of IR on hypothermic and normothermic perfu-

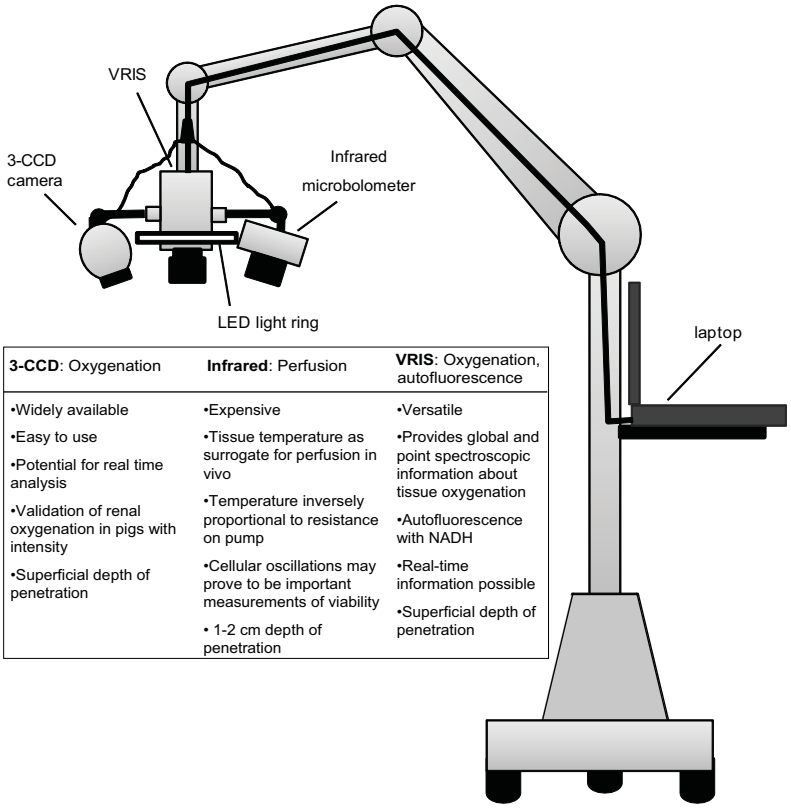

Figure 8.5 Summary of the optical and spectroscopic technologies with an operating microscope platform incorporating each of the technologies.

sion, as well as ischemia reperfusion injury models in large and small animals. 3-CCD and VRIS have been studied in large animals without perfusion in an ischemic reperfusion injury model. Clinical utility has been demonstrated with both 3-CCD and VRIS in normothermic perfusion-preservation.

8.3 Materials

- Pigs—either sex, any age, size 20–40 kg, 8 pigs per arm, 24 total (Animal Biotech Industries, Inc. Danboro, Pennsylvania).
- Anesthetic medications: IV Ketamine, Buprenorphine, Cefazolin/Ceftriaxone, Beuthanasia (www.henryschein.com, Melville, New York).
- Operative suite–standard halogen spot lights, laparotomy set, drapes, suction.
- 3-CCD camera—laparoscopic camera without laparoscopic lens mounted on OR lights, above pump during normothermic perfusion. Options for 3-CCD equipment include:
  - Conmed Linvatec (Goleta, California) laparoscopic tower includes: HD 3-CCD camera head, 300W Xenon light source, fiber optic light guide;

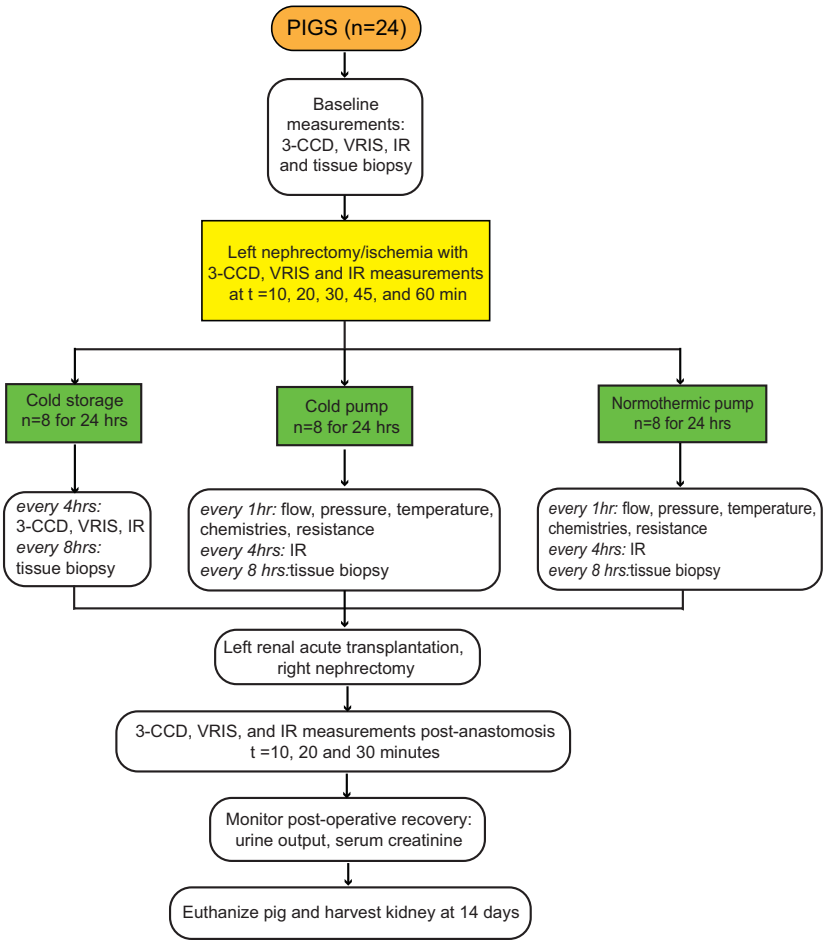

Figure 8.6 Proposed experimental design.

- Stryker (San Jose, California) laparoscopic tower includes: camera head and coupler kit, three-chip camera head, Xenon light source (100W), fiber optic light cable;
- Storz (El Segundo, California) laparoscopic tower includes: camera head and coupler kit, 3-chip camera head, Xenon light source (100W), fiber optic light cable.

- Infrared advanced digital camera (Santa Barbara Focal Plan Array, California) on Zeiss operating microscopic stand with conventional surgical drapes. The camera (14 bits, 0.02°C thermal resolution, 320 × 256 pixels per image, 1–2.0 Hz acquisition rate) is sensitive to the passive emission of IR photons over the wavelength range of 3–5 microns. Intraoperative motion artifacts may be managed with a plastic holder. Non-heat-producing LED OR spot lights are recommended; however, conventional OR lights can be used with a strobe mechanism. Ten-minute collection intervals are needed for acquisition of oscillations. It is possible that the camera will be sensitive enough to detect temperature differences despite the heat generated by conventional OR lights. The camera is mounted above cold and normothermic pumps on either a Zeiss operating stand or another mounting bracket.

- VRIS—intermittent collection intervals lasting 1.5 minutes, dual mounting on Zeiss operating stand with sterile drapes. This system requires a white light source during data acquisition:
  - Output ~100W, 66890 Series Q quartz-tungsten-halogen lamp (Newport-Oriel, Stratford, Connecticut);
  - LCTF, 400–720 nm, 10-nm bandwidth (Cri Inc., Woburn, Massachusetts);
  - Sensys, 768 × 512 pixel charge-coupled device detector (Photometrics, Tucson, Arizona).
- Waters RM3 renal preservation system perfusion pump (Minneapolis, Minnesota)—Cold storage and cold pump solution is Belzer machine preservative solution, while the normothermic perfusion pump should have Lifor organ preservation medium (Adelphia, New Jersey).
- Viaspan (also called University of Wisconsin, UW) solution for organ cold storage from Cardinal Health (Dublin, Ohio); Belzer (UW pump) from Transmed Corporation (Elk River, Minnesota); Lifor solution from Lifeblood Medical (Adelphia, New Jersey, www.lifebloodmedical.com).
- Video screen for intraoperative results.
- Computer and MATLAB software for analysis.
- Cold storage—wet ice.

8.4 Methods

8.4.1 Room Setup

The surgical suite should have adequate illumination with a standard surgical spot light. A 3-CCD camera should be fixed to the arm of the spot light with an adequate view of the surgical field. The VRIS equipment should be positioned on the pig's left side with appropriate operating microscope and surgical draping. This array should be positioned above the exposed left kidney for a complete view of the anterior surface. The IR camera should be on the pig's right side, positioned 50–60 centimeters above the exposed left kidney.

8.4.2 Preparation for Kidney Harvest

1. An 18-gauge core needle biopsy device should be kept close at hand. Be prepared to place a figure-of-eight stitch into the biopsy wounds if they bleed.
2. Sedate and anesthetize the animal with isoflurane.
3. Position the pig on its right side down. Prep and drape with standard surgical drapes.
4. Perform a cut down over the external jugular (EJ), tunnel the catheter to the back, cannulate the EJ by modified Seldinger technique, secure catheter with heavy silk suture, and close the cut down incision.
5. Reposition the pig into supine position, prep and drape abdomen in standard surgical fashion.
6. Make a midline abdominal incision with left renal mobilization, hilar dissection and identification of all renal vessels.

7. Position your Debakey vascular (or intestinal) clamps around the renal arteries.

8.4.3 Left Kidney Harvest, Preservation, and Data Collection

1. Obtain baseline measurements with 3-CCD, IR, and VRIS systems. IR data collection for 20 minutes with OR lights off, VRIS data collection for 1.5 minutes with OR lights on; harvest punch biopsy.
2. Clamp left renal artery, begin timing, and proceed with left renal harvest.
3. At ischemia for 10, 20, 30, 45, ands 60 minutes, gather IR images without the OR spot light for 10-minute intervals, then VRIS for 1.5 minutes.
4. While waiting for the imaging to be completed the Waters RM3 (Waters Medical, Rochester, Minnesota) renal preservation system should be set up and primed with corresponding perfusate for arm 2 or arm 3. The Waters RM3 was chosen for this experiment because it is the only FDA-approved renal perfusion system that uses true pulsatile pressure and has a built-in oxygenator.
5. After the kidney has been imaged, transect the kidney from the swine.
6. Take the kidney to the back table.
7. Dissect the renal artery and vein and remove the adipose tissue from the renal vascular structure.
8. Insert the appropriate sized straight renal cannula (Waters Medical, Rochester, Minnesota) into the renal artery.
9. Tie the cannula in place with a 2-0 silk tie; if there are multiple renal arteries each artery should be individually cannulated and then placed onto a multiple artery adapter (Waters Medical, Rochester, Minnesota).
10. Place the cannula onto the perfusion circuit at approximately a 45° angle until all the air is removed from the renal artery and the cannula.
11. The initial perfusion pressure should be set for a systolic pressure of 40 to 45 mmHg, the flow and the temperature will fluctuate as the renal vascular system dilates. As the renal vascular system dilates, the systolic pressure will decrease and the perfusion pressure will need to be adjusted over the initial hour of perfusion to maintain the systolic pressure at 40 to 45 mmHg; then the systolic pressure will be maintained over the perfusion run at 40 to 45 mmHg until the kidney is taken off the perfusion circuit for transplantation.
12. The three arms are separated into cold storage, cold pump, and normothermic pump:

    a. Cold storage: flush kidney with Viaspan solution, and place on ice. Perform 3-CCD, VRIS, and IR image collection every 4 hours as above. Punch biopsy harvested every 8 hours.

    b. Cold pump: flush kidney with Belzer solution and place in ice and on pump. Record pump pressure, flow, resistance, and chemistries every hour[1], with intermittent IR measurements every 4 hours. A punch biopsy is harvested from the posterior surface of the organ every 8 hours. Perform 3-CCD, VRIS and IR image collection every 4 hours as above. Punch biopsy harvested every 8 hours.

    c. Normothermic pump: flush with Lifor perfusilate solution, place on pump. Record pump pressure, flow, resistance, and chemistries every hour. Punch

[1] Perfusate pH, PO_2, PCO_2, Na, K+, ionized calcium, lactate, glucose, calculated bicarb, osmolality.

biopsy harvested every 8 hours. Perform 3-CCD, IR, VRIS data collection every 4 hours as above.

8.4.4 Autotransplantation

1. Return pig to OR after 24 hours on pump/in storage; anesthetize and prepare for surgery in standard fashion.
2. Using the same midline incision, perform right nephrectomy. Keep the kidney on the perfusion circuit until the right iliac fossa is prepared for implantation.
3. Remove the perfused kidney from the perfusion circuit and flush with cold lactated ringers (both Belzer and Lifor have potassium, which could potentially cause cardiac problems).
4. After right iliac fossa has been prepared for autotransplantation, finish venous anastomosis, and begin timing at reanastomosis of renal artery.

8.4.5 Reanastomosis

3-CCD, VRIS, IR data collection performed at reanastomosis, and again after 10, 15, and 30 minutes. Punch biopsy harvested at 30 minutes after arterial reanastomosis.

8.4.6 Completion of Surgery, Recovery, and Euthanasia

1. Complete reanastomosis of ureter, close abdomen.
2. Recover animal from anesthesia and surgery with appropriate postoperative management.
3. Analgesia can be provided with Buprenex 0.5–1.0 mg/kg IM every 12 hours for the first 3 days.
4. Record urine output and serum creatinine every 24 hours.
5. Euthanize at 14–21 days as creatinine stabilizes. Routine euthanasia: Ketamine (33 mg/kg) followed by Beuthanasia 100 mg/kg IV. Alternate euthanasia: Ketamine (12–20 mg/kg) plus Xylazin (2.2 mg/kg) IM, followed by Euthasol 6 100 mg/kg IV.

8.5 Data Acquisition, Anticipated Results, and Interpretation

Outcomes for the three arms (cold storage, cold pump, and normothermic pump) can be divided into traditional and experimental outcomes. Traditional clinical measures include serum creatinine, primary nonfunction, and delayed graft function[2]. Our method seeks to add more direct measurements of oxygenation and cellular respiration (3-CCD, VRIS, and IR) to enable better assessment of organ viability.

8.5.1 3-CCD

Using appropriate imaging software (such as MATLAB), regions of interest (ROIs) should be selected on the surface of the kidney from each stage of the experiment, as illustrated in Figure 8.7. Each ROI should be at least 10 pixels (usually on the order of 50 × 50) and

[2] Defined as failure of creatinine to improve by greater than or equal to 25% of baseline in 24 hours.

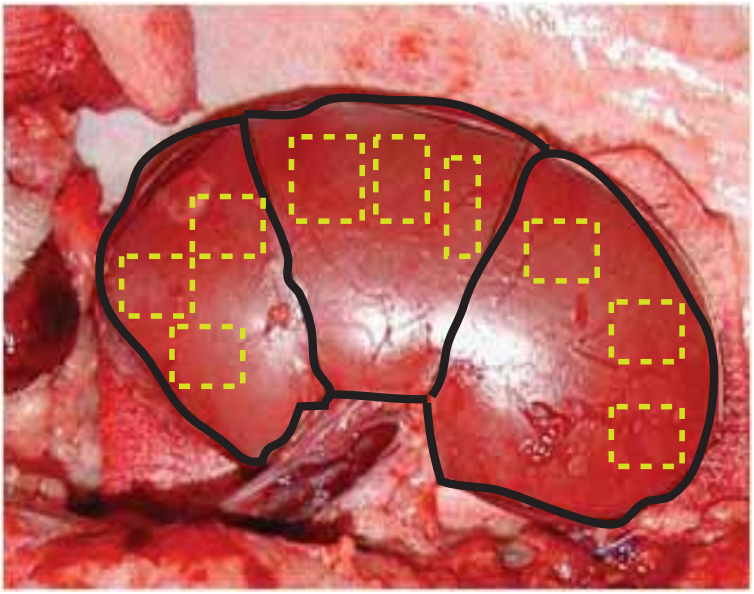

Figure 8.7 The anterior surface of porcine kidney with approximate vascular segments (solid lines). Note the glare on middle and inferior segments that should be avoided when creating ROIs (dotted boxes).

free from blood or obvious fat/connective tissue. A mean value is generated per ROI. The ROIs from each segment are then averaged together to form a mean intensity value for each segment.

Next, the intensity value is then converted to sO_2 using calibration data. Figure 8.8 provides an example of a calibration data set. For the calibration experiment, 3-CCD measurements were made as FiO_2 was decreased from 100% to 2%. As sO_2 stabilized at each FiO_2, renal venous blood draws provided direct sO_2 measurements. Plotting the mean ROI intensity values of the kidney parenchyma versus renal blood oxygenation yields a linear relationship. Using the equations derived from the trendlines of the calibration data, the mean ROI intensity value can be converted to sO_2.

3-CCD intensity values have been compared with postoperative renal function. In a series of nine living donor renal transplants, mobilized by laparoscopic nephrectomy under 3-CCD visualization, intraoperative 3-CCD intensity values were compared to serum creatinine before and after surgery (Table 8.1). Table 8.1 shows the mean intensity normalized ROI values of human kidneys from both the start and end of each transplant with recipient serum creatinine levels, pre- and post-operative (all donor creatinine levels were normal). Normal serum creatinine levels are =1.6mg/mL [26]. In nine patients, there were no significant differences in ROI intensity from the beginning to end of the donor nephrectomy, indicating that mobilization of the donor kidney was performed without a significant measurable ischemic event (p-values were calculated using a two-tailed paired Student's T-test). All graft recipients demonstrated immediate graft function with eight of nine patients' serum creatinine returning to normal. Note that comparison between cases in this series is not performed due to variability in illumination and duration of pneumoperitoneum [26].

Measuring the standard deviation within each ROI denotes how homogenous the sample area is or is not—factors that can attribute to reduced homogeneity are glare

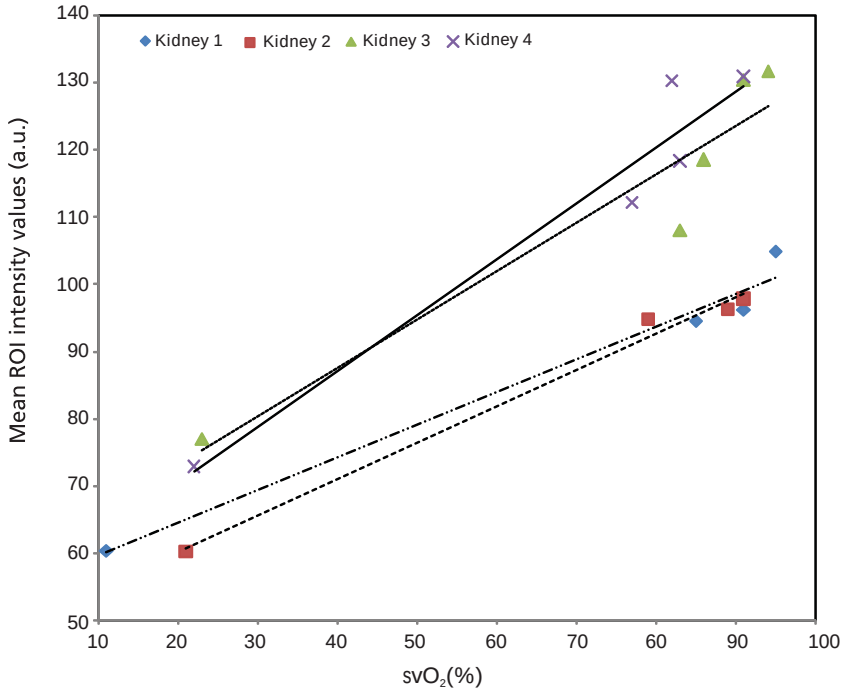

Figure 8.8 A graph demonstrating the correlation of mean ROI intensity values and venous sO_2 in four kidneys. R^2 = 0.977 (◆), 0.990 (■), 0.909 (▲) and 0.945 (×).

Table 8.1 Comparison of 3-CCD Mean ROI Intensity Values and Recipient Serum Creatinine

Case	Recipient Serum Creatinine (mg/dl)			Mean ROI	Mean ROI	p-value
	Postop day 1	Postop day 5	Postop day 10	Starting point	End point	
A	5.1	1.5	1.7	48.40	44.48	0.13
B	5.1	1.7	1.6	54.88	65.02	0.56
C	7.9	1.8	1.6	72.42	61.17	0.16
D	5.6	1.2	1.0	84.27	75.58	0.14
E	4.1	1.1	0.9	79.78	68.64	0.21
F	3.6	1.3	1.3	81.17	75.98	0.38
G	4.1	1.4	1.6	75.50	78.96	0.60
H	7.9	2.4	1.7	62.41	60.29	0.79
I	3.8	1.9	2.0	73.09	67.74	0.07

and superficial fat. In addition, heterogeneity of the tissue (as indicated by mean ROI values with large standard deviations) may become clinically relevant with a segmental vasospasm or thrombosis.

To date, 3-CCD imaging has not been studied during pulsatile pump perfusion, but, its clinical applicability should extend to normothermic pulsatile perfusion, due in large part to the presence of bovine hemoglobin in the Lifor perfusate solution.

8.5.2 Infrared

Infrared data consists of global and segmental regions of interest with mean temperature profiles and localized oscillations. Data is collected for a given collection time in segments of 4 minutes. Image alignment between data measurements is accomplished using three or more landmark points on each kidney (i.e., points of maximal curvature of blood vessels or kidney edges or blood spots). Several software tools (ENVI imaging registration tool, validated by a performance algorithm) exist to help minimize pixel frame shift to a goal of 3–5 per image. Temperature profiles (IR intensity versus time) are obtained for the established ROIs both globally and in segmental fashion, ultimately providing a temporal aspect to thermal change (i.e., mean temperature changes over time and localized oscillations for each ROI) (Figure 8.9).

Spectral analysis of the oscillation frequency range for temperature profiles is performed for the global and segmental ROIs for living organs in the ischemia and reperfusion phases. Figure 8.10 shows a correlation between oscillation and infrared thermography in the setting of focal renal ischemia. During experiments, the presence

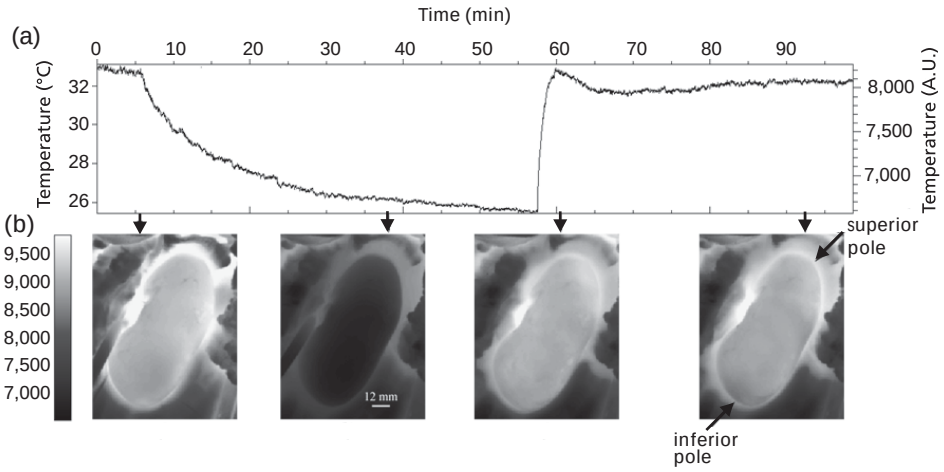

Figure 8.9 Corresponding IR images with thermal profile in an ischemia reperfusion model.

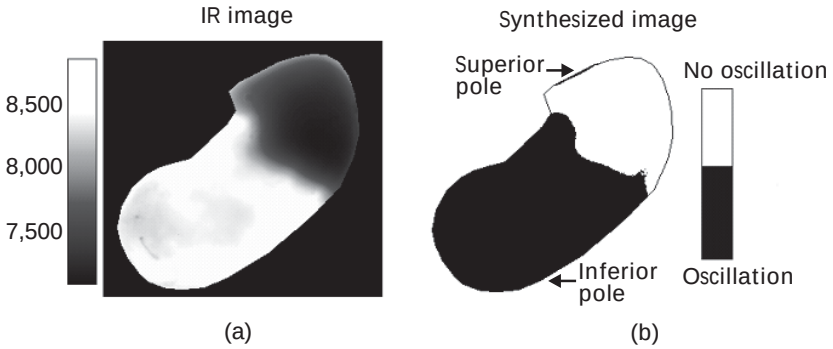

Figure 8.10 (a) Thermal and (b) oscillation images of the same kidney in which the superior pole vessel was ligated produce an ischemic segment. Note that the ischemic area is not perfused and colder and the dominant frequency is not present.

of oscillations likely will not be found during cold storage or cold pump; however, it may be present during use of the normothermic pump. Consequently, the 10-minute data collection intervals should continue in the pump phase of the experiment. Our group has already validated the presence of these oscillations against white noise in small animals [8] and further research is planned in a large animal model. A first-order polymonial detrending algorithm (ENVI/IDL, California) removes trends that might be present across successive trends (such as room temperature changes). A power spectrum is calculated by applying a fast Fourier transformation (FFT) to the data points in each thermal profile (Figure 8.11).

The anticipated results from infrared analysis in this experiment should be thought of as intraoperative and on-pump. Intraoperatively, thermal profiles and the very slow oscillations (VSO) at 0.01 Hz should have a direct relationship with blood flow (Figure 8.12). Accordingly, as the length of warm ischemic time progresses, one can expect to see both the temperature and VSO diminish. Of great interest is the length of ischemic time that the kidney can tolerate and recover to normal function. The expected result off-pump is an attenuated or possibly absent post occlusive reactive hyperemia (PORH).

While IR imaging can prove valuable for assessment even with static cold storage perfusion as quantitative measure of ischemia, it is during machine perfusion—either with cold or normothermic—that its true value is observed; IR imaging during machine perfusion enables diagnosing segmental areas of poor flow—perhaps corresponding to vasospasm. Table 8.2 shows a proportional relationship between colder thermal profiles and flow (inversely proportional to resistance) in porcine and human kidneys. Colder infrared thermal profiles have a direct relationship with flow (V) and inversely to resistance (R) during hypothermic pulsatile perfusion. Heterogeneous perfusion that improved over time with pulsatile perfusion would not have been seen without IR views. Evaluating the hetereogeneity of flow through an organ is only possible via IR imaging. Further, if such heterogeneity is observed, it is then possible to reverse the vasospasm, for instance with nitrates, thus treating focal areas of poor flow in the higher risk donor kidneys [27].

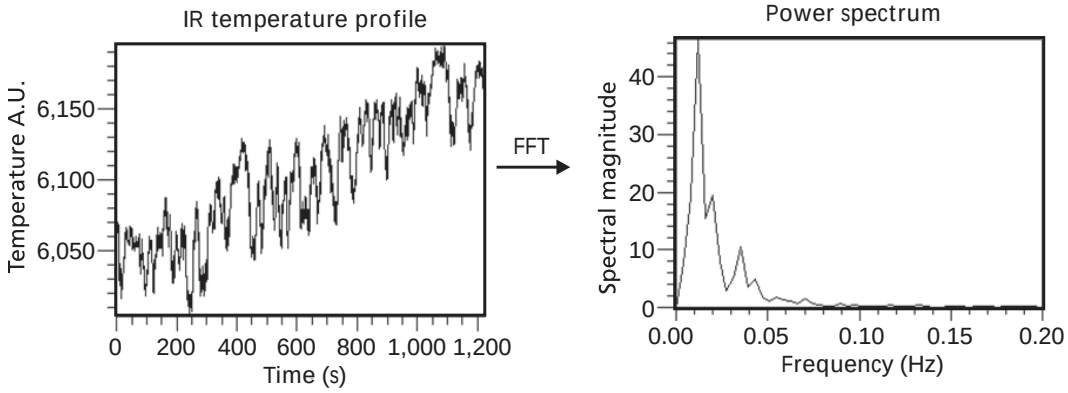

Figure 8.11 Using fast Fourier transform analysis translated thermal profiles into a power spectrum to assess whether the low-frequency oscillations were present in the model. Tubuloglomerular feedback (TGF) and very slow oscillations (VSO) at 0.02–0.05 Hz and 0.01 Hz can be seen on the right.

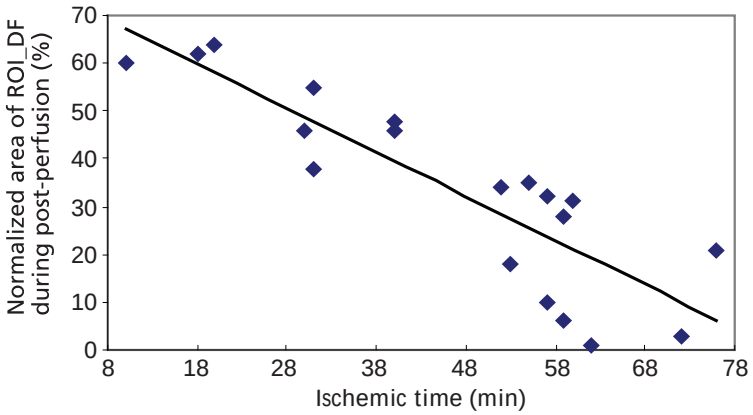

Figure 8.12 The percentage of the kidney recovering dominant frequency (VSO) after 30 minutes of reperfusion. The recovery of the DF was inversely proportional to the length of the warm ischemia period. Therefore, a kidney with 15 minutes of warm ischemia had 60% of the organ with the DF while a kidney with 60 minutes of warm ischemia had 0% to 30% of the kidney with the DF.

Table 8.2 Relationships of Thermal Profiles with Flow (V) and Resistance (R)

Human Kidneys	Mean V	Mean R	Porcine Kidneys	Mean V	Mean R
Cool (T = 5.02)	88.3	0.24	Cool (T = 5.02)	78	0.46
Warm (T = 5.84)	69	0.42	Warm (T = 5.84)	38	0.91
P value	0.0044	0.0085	P value	0.008	0.0016

8.5.3 VRIS

VRIS performs global imaging. This means that an entire image (two dimensional) is collected at each specified wavelength, creating a three dimensional image cube. The CCD detects an image (768 × 512 pixels) at each wavelength, over the range of 520–645 nm. To increase the signal intensity and reduce the effect of aberrant photons, three neighboring pixels are added together; this process is called binning. Each 768 × 512 pixel image becomes a 256 × 170 pixel image, allowing for faster data acquisition and reducing the analysis time by compressing the data. Individual reflectance spectra can be extracted from each pixel in the image.

The measured reflectance spectra are converted to apparent absorbance (A) by creating a ratio of reflected sample radiation (R) from a reflectance standard (R_0) at given wavelength (λ).

$$A(\lambda) = \log \frac{R_0(\lambda)}{R(\lambda)}$$

Once all spectra are apparent absorbance spectra, percent oxygenated Hb is determined by deconvoluting the measured spectra into its HbO_2 and Hb components; deconvoluting the spectra via classic least squares fit is shown in Figure 8.13. By performing a classic least squares regression for all of the spectra in the image cube, $\%HbO_2$ is calculated for each binned pixel. Thus, spectral measurements using VRIS provide a direct relationship between the absorbance of oxygenated hemoglobin (HbO_2) and actual tissue oxygenation (sO_2). In Figure 8.14(a–c), a kidney is monitored via every 5

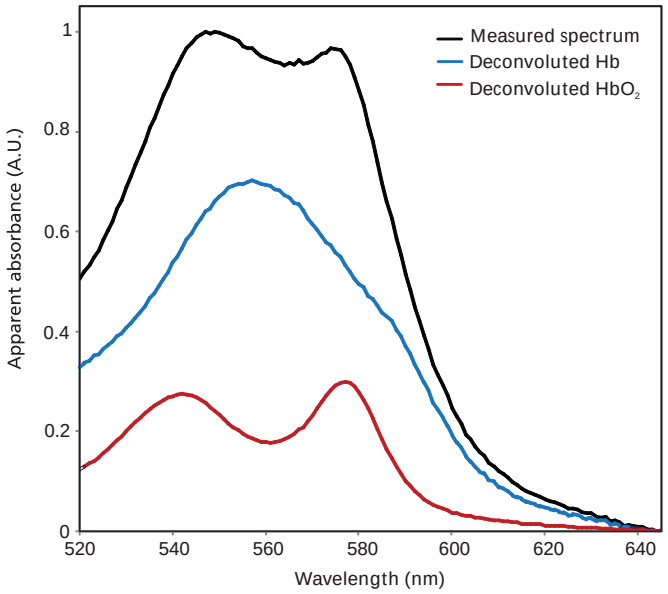

Figure 8.13 Classic least squares regression of Hb and HbO_2 spectra from a measured spectrum. Deconvolution indicates approximately 30% HbO_2 and 70% Hb.

minutes during 30 minutes of cold ischemia (ice slush) and 30 minutes of reperfusion. The relative concentration of HbO_2 drops slightly as ice slush is added to the abdomen and then decreases significantly during ischemia. Following the unclamping of the renal artery, reperfusion demonstrates hyperemia before returning to a baseline value of HbO_2 [Figure 8.14(d)].

In the ischemia reperfusion model, expected results include a dose-dependent decline in oxygenation within the tissue with a predictable hyperemia with reperfusion and return to baseline provided the ischemic injury is not irreversible. We anticipate that VRIS images collected during cold storage without pump perfusion will not provide useful images due to the absence of hemoglobin in the perfusate solution.

8.6 Discussion and Commentary

The transplant community is increasingly relying on expanded criteria donors (ECD) and donation after cardiac death (DCD) to meet the escalating need for organs. In this light, there is a recognized need for better ways to assess the viability of cadaveric kidneys prior to transplantation. The development of pulsatile perfusion for organ preservation in ECD and DCD kidneys allows for some measure of salvage for these nonideal grafts. The use of flow and resistance during perfusion continues to be the most important variables during machine perfusion-preservation of kidneys.

In this context, the normothermic perfusion approach is particularly exciting because it may actually meet the metabolic needs of the kidney while on pump, continue to supply oxygen via oxygen carriers, and scavenge oxygen radicals. It is conceivable that delayed graft function might be prevented in more of these nonideal donor

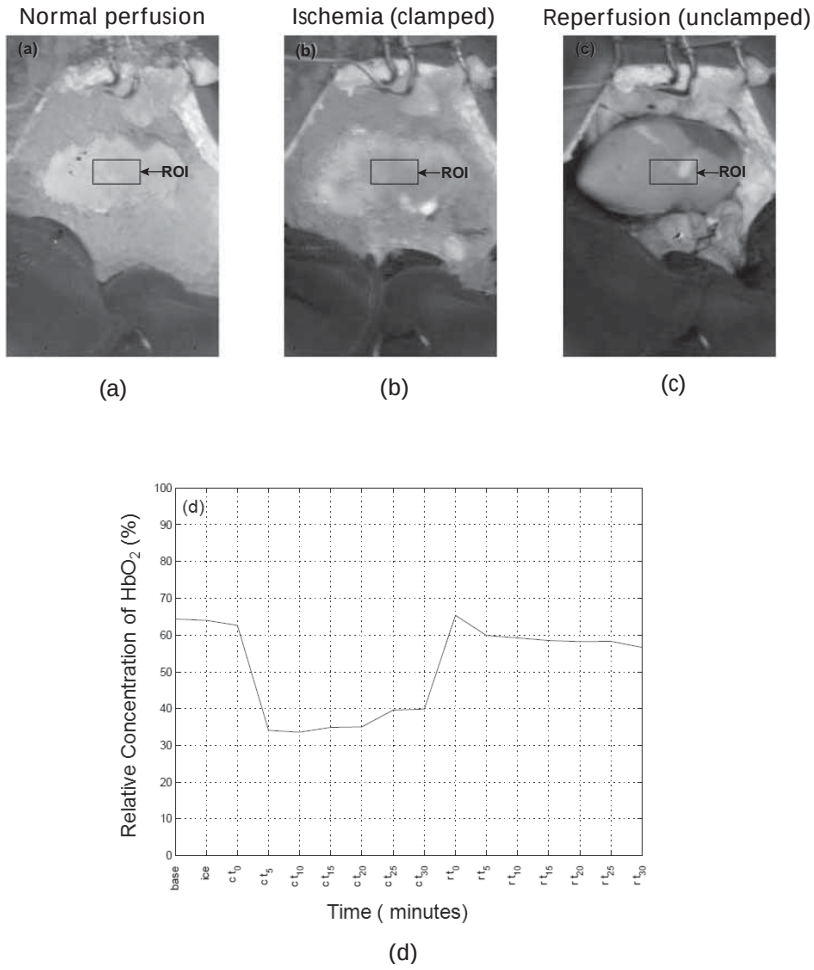

Figure 8.14 Intraoperative VRIS images showing a kidney during (a) normal perfusion, (b) ischemia, and (c) reperfusion. (d) Changes in relative HbO2 concentration, using the same ROI, are plotted during 30 minutes of ischemia and reperfusion.

kidneys, potentially improving graft survival. Assessment of organ viability is especially critical in this scenario.

The methodology described here demonstrates the viability of introducing imaging and spectroscopic technologies to the perfusion system to assess the extent of ischemia. The information gathered provides insight into the segmental vasculature via assessment of heterogeneity of perfusion, tissue oxygenation via the oxygenation of hemoglobin intraoperatively and on pump, and a rudimentary understanding of microcirculatory regulation with the very slow oscillations (VSO) that appear to have an inverse relationship with ischemia in living tissue. Ultimately an index of donor allograft viability may be constructed from either the degree of image heterogeneity on pump, percentage of graft with VSO after reperfusion, or time at a given tissue oxygenation level, allowing for an accurate and quantitative prognosis before the kidney is transplanted, hence removing the guesswork involved in marginal donor organ transplantation.

Each of the imaging technologies brings complementary information to this clinical scenario. Compared individually to renal biopsy, or in combination, the imaging and spectroscopic modalities of 3-CCD, IR, and VRIS hold a great deal of promise for accurate monitoring of renal allograft perfusion in the intraoperative and organ preservation settings. Accurate real-time information about tissue oxygenation is also critical with the transplantation of other organs. In the bowel, a global analysis with 3-CCD or VRIS of the surfaces of relatively large amounts of tissue would be important. In particular, the use of 3-CCD intraoperatively to assess bowel viability in necrotizing enterocolitis or a mid-gut volvulus might keep a patient from the morbidity and mortality associated with a small bowel transplant. Infrared imaging with its greater depth of penetration could be useful for pancreas or liver. Cardiac transplantation might well benefit from 3-CCD, VRIS, and particularly IR if motion artifact can be accounted for.

Troubleshooting Table

Complication	Solution
Standard deviation >20 on 3-CCD intensity, ROIs including glare.	Change ROI to avoid glare.
Poor illumination on 3-CCD image.	Perform white balance.
Too much motion artifact intraoperatively.	Fashion plastic holder/surgical towels to immobilize organ.
Bleeding after punch biopsy.	Figure of 8 stitch.
High flow, low diastolic pressure.	Branch artery leak or artery leak, or leak around cannula.
High systolic pressure, low flow.	Twisted artery.
High systolic pressure.	Kinked artery, partially occluded artery with plaque/cannula.
No visual hilar pulse, reasonable pressure, low to moderate flows.	Partially twisted artery, partially blocked artery by cannula/plaque.

8.8 Summary Points

- The increasing demand for expanded criteria donors (ECD) and donors after cardiac death (DCD) highlights the need to have accurate, specific methods of assessing organ viability.
- Infrared (IR) imaging can add to organ preservation on pulsatile perfusion pump with hypothermic perfusate the ability to assess segmental flow and resistance, and, in living tissue, oscillations that may be related to microcirculatory regulation.
- 3-CCD and VRIS can add to organ preservation the ability to record tissue oxygenation, even while on pulsatile perfusion pump with normothermic perfusate.
- Intraoperatively, 3-CCD, IR, and VRIS can diagnose focal ischemia and measure tissue response to reperfusion.
- Each of these technologies individually or in combination adds relevant clinical information to renal transplantation in the intraoperative and organ procurement settings.

Acknowledgments

Many thanks to the staff in the Department of Regenerative Medicine at NMRC for all their help.

Disclaimer

The views expressed in this manuscript are those of the authors and do not reflect the official policy of the Department of the Army, Department of the Navy, the Department of Defense or the United States Government.

This effort was supported (in part) by the U.S. Navy Bureau of Medicine and Surgery under the Medical Development Program (PE 0604771N) and Office of Naval Research work unit number: 602227D0483.01.A0518 (MFEL).

We are a military service members (or employees of the U.S. government). This work was prepared as part of our official duties. Title 17 U.S.C. 105 provides the "Copyright protection under this title is not available for any work of the United States Government." Title 17 U.S.C. 101 defines a U.S. Government work as a work prepared by a military service member or employee of the U.S. Government as part of that person's official duties.

The experiments reported herein where conducted in compliance with the Animal Welfare Act and in accordance with principles set forth in the "Guide for the Care and Use of Laboratory Animals," Institute of Laboratory Animals Resources, National Resource Council, National Academy Press, 1996.

I/we certify that all individuals who qualify as authors have been listed; each has participated in the conception and design of this work, the analysis of data (when applicable), the writing of the document, and the approval of the submission of this version; that the document represents valid work; that if we used information derived from another source, we obtained all necessary approvals to use it and made appropriate acknowledgements in the document; and that each takes public responsibility for it.

References

[1] Henry, M. L., B. G. Sommer, and R. M. Ferguson, "Improved Immediate Function of Renal Allografts with Belzer Perfusate," *Transplantation*, Vol. 45, No. 1, 1988, pp. 73–75.

[2] Moers, C., et al., "Machine Perfusion or Cold Storage in Deceased-Donor Kidney Transplantation," *N. Engl. J. Med.*, Vol. 360, No. 1, 2009, pp. 7–19.

[3] Gage, F., et al., "Room Temperature Pulsatile Perfusion of Renal Allografts with Lifor Compared with Hypothermic Machine Pump Solution," *Transplant Proc.*, Vol. 41, No. 9, 2009, pp. 3571–3574.

[4] Hattori, R., et al., "Direct Visualization of Cortical Peritubular Capillary of Transplanted Human Kidney with Reperfusion Injury Using a Magnifying Endoscopy," *Transplantation*, Vol. 79, No. 9, 2005, pp. 1190–1194.

[5] Roberts, W. W., et al., "Laparoscopic Infrared Imaging," *Surgical Endoscopy*, Vol. 11, No. 12, 1997, pp. 1221–1223.

[6] Hanna, B. V., et al., "Intraoperative Assessment of Critical Biliary Structures with Visible Range/Infrared Image Fusion," *J. Am. Coll. Surg.*, Vol. 206, No. 3, 2008, pp. 1227–1231.

[7] Akbari, H., et al., "Hyperspectral Imaging and Diagnosis of Intestinal Ischemia," *Conf. Proc. IEEE Eng. Med. Biol. Soc.*, 2008, pp. 1238–1241.

[8] Gorbach, A. M., H. Wang, and E. Elster, "Thermal Oscillations in Rat Kidneys: An Infrared Imaging Study," *Philos. Trans. A Math Phys. Eng. Sci.*, Vol. 366, No. 1880, 2008, pp. 3633–3647.

[9] Gorbach, A. M., et al., "Assessment of Cadaveric Organ Viability During Pulsatile Perfusion Using Infrared Imaging," *Transplantation*, Vol. 87, No. 8, 2009, pp. 1163–1166.

[10] Gorbach, A. M., et al., "Assessment of Critical Renal Ischemia with Real-Time Infrared Imaging," *J. Surg. Res.*, Vol. 149, No. 2, 2008, pp. 310–318.

[11] Siu, K. L., et al., "Detection of Low-Frequency Oscillations in Renal Blood Flow," *Am. J. Physiol. Renal Physiol.*, Vol. 297, No. 1, 2009, pp. F155–F162.

[12] Zuzak, K. J., et al., "Visible Reflectance Hyperspectral Imaging: Characterization of a Noninvasive, In Vivo System for Determining Tissue Perfusion," *Analytical Chemistry*, Vol. 74, 2002, pp. 2021–2028.

[13] Benaron, D. A., et al., "Design of a Visible-Light Spectroscopy Clinical Tissue Oximeter," *Journal of Biomedical Optics*, Vol. 10, No. 4, 2005, p. 044005.

[14] Cohn, S. M., et al., "Tissue Oxygen Saturation Predicts the Development of Organ Dysfunction During Traumatic Shock Resuscitation," *J. Trauma*, Vol. 62, No. 1, 2007, pp. 44–54.

[15] de Groot, B., C. J. Zuurbier, and J. H. van Beek, "Dynamics of Tissue Oxygenation in Isolated Rabbit Heart as Measured with Near-Infrared Spectroscopy," *Am. J. Physiol.*, Vol. 276, No. 5, 1999, pp. H1616–H1624.

[16] Payette, J. R., et al., "Assessment of Skin Flaps Using Optically Based Methods for Measuring Blood Flow and Oxygenation," *Plastic Reconstructive Surgery*, Vol. 15, 2005, pp. 539–546.

[17] Karliczek, A., et al, "Intraoperative Assessment of Microperfusion with Visible Light Spectroscopy in Esophageal and Colorectal Anastomoses," *Eur. Surg. Res.*, Vol. 41, No. 3, 2008, pp. 303–311.

[18] Zuzak, K. J., et al., "Characterization of a Near-Infrared Laparoscopic Hyperspectral Imaging System for Minimally Invasive Surgery," *Anal. Chem.*, Vol. 79, No. 12, 2007, pp. 4709–4715.

[19] Feather, J. W., et al., "A Portable Scanning Reflectance Spectrophotometer Using Visible Wavelengths for the Rapid Measurement of Skin Pigments," *Physics in Medicine and Biology*, Vol. 7, 1989, p. 807.

[20] Stratonnikov, A. A., and V. B. Loschenov, "Evaluation of Blood Oxygen Saturation In Vivo from Diffuse Reflectance Spectra," *Journal of Biomedical Optics*, Vol. 6, No. 4, 2001, pp. 457–467.

[21] Finlay, J. C., and T. H. Foster, "Hemoglobin Oxygen Saturations in Phantoms and In Vivo from Measurements of Steady-State Diffuse Reflectance at a Single, Short Source-Detector Separation," *Medical Physics*, Vol. 31, No. 7, 2004, pp. 1949–1959.

[22] Zuzak, K. J., et al., "Imaging Hemoglobin Oxygen Saturation in Sickle Cell Disease Patients Using Noninvasive Visible Reflectance Hyperspectral Techniques: Effects of Nitric Oxide," *American Journal of Physiology: Heart and Circulation Physiology*, Vol. 285, 2003, pp. H1183–H1189.

[23] Zuzak, K. J., et al., "Noninvasive Determination of Spatially Resolved and Time-Resolved Tissue Perfusion in Humans During Nitric Oxide Inhibition and Inhalation by Use of a Visible-Reflectance Hyperspectral Imaging Technique," *Circulation*, Vol. 104, 2001, pp. 2905–2910.

[24] Tracy, C. R., et al., "Characterization of Renal Ischemia Using Dlp® Hyperspectral Imaging: A Pilot Study Comparing Artery-Only Occlusion Versus Artery and Vein Occlusion," *Journal of Endourology*, Vol. 24, No. 3, March 2010, pp. 321–325.

[25] Arai, A. E., et al, "Myocardial Oxygenation In Vivo: Optical Spectroscopy of Cytoplasmic Myoglobin and Mitochondrial Cytochromes," *Am. J. Physiol. Heart Circ. Physiol.*, Vol. 277, No. 2, 1999, pp. H683–H697.

[26] Crane, N. J., et al., "Non-Invasive Monitoring of Tissue Oxygenation During Laparoscopic Donor Nephrectomy," *BMC Surg.*, Vol. 8, 2008, p. 8.

[27] Gage, F., et al., "Assessment of Pharmacologic Resuscitation During Pulsatile Perfusion," *American Journal of Transplantation*, Vol. 6, No. S2, 2006, p. 913.